Enhanced Geothermal System Testing and Development at the Milford, Utah FORGE Site

Table of Contents

Enhanced Geothermal System Testing and Development at the Milford, Utah FORGE Site

Executive Summary

This submission describes and documents the attributes of the Utah FORGE site, located in southwest Utah, that fulfill DOE needs for establishing a dedicated EGS laboratory. It encompasses site characterization data, a 3D conceptual geologic model, and a wide range of research and development and environmental management plans.

The Utah FORGE site is located within the Milford Renewable Energy Corridor that currently hosts 2 geothermal plants, a wind farm, a solar field and a biogas facility. The site is accessible year round and receives little snow or rain. It is adjacent to a major paved road, an airport, graded dirt roads and a rail line. The closest residences are in Milford, located 16 km away. Lodging and eating establishments are available in Milford, or the larger community in Beaver, located 35 km further adjacent to Interstate I -15. The population of Milford is 1409 people.

The Utah FORGE site is data-rich. Data from more than 80 thermal gradient wells, 20 deep exploration and development wells, one drilled to 3.8 km (12,650 ft), a catalogue of seismic events dating back to 1981, the results of geophysical surveys, and a pump test of a groundwater supply well provide unambiguous evidence that the temperature, rock type, stress regime, and depth required by DOE exist at the Utah FORGE site. Furthermore the data show that thermal gradients beneath the Utah FORGE deep drill site are conductive, demonstrating the site is outside the boundaries of any existing hydrothermal system and that permeabilities are low.

The reservoir will be developed in Precambrian gneiss and Tertiary granitic plutons beneath private land owned by Murphy Brown LLC and the State Institutional Trust Land Administration (SITLA). These rocks were penetrated in wells east and west of the Utah Forge deep drill site and form the core of the Mineral Mountains to the east. Evidence of fracturing at the surface is widespread and veins representing past zones of weakness are common in the rocks at depth. These features represent critical targets for reservoir creation and long term sustainability.

Sufficient water rights have been obtained for drilling, stimulation and reservoir management activities. The water, which will be obtained from shallow aquifers, represents mixtures of cold groundwater and thermal water that flows outward through the alluvium from the Roosevelt Hot Springs geothermal system to the east. The groundwater is chemically benign and suitable for stimulation and EGS circulation experiments. It is non potable, is not used for agriculture or human consumption, and does not compete for water used for other purposes. Consequently, the groundwater system is currently underutilized.

Seismic activity at the Utah FORGE site has been monitored by the University of Utah Seismic Station since 1981. The seismic station is capable of recording events greater than M 1.5. No seismic events have been detected at the Utah FORGE site, and despite more than 3 decades of electric production and injection into the gneiss and granite at Roosevelt Hot Springs (production began in 1984), few seismic events are spatially associated with the geothermal field. These events show no apparent relationship to injection volume. Circulation rates through the fracture network created at the Utah FORGE site will be ten times lower than the injection rates at

Roosevelt Hot Springs, implying the risk of induced seismicity at the Utah FORGE site is minimal.

Multiple sources of stress data yield a consistent indicator of stress direction. These sources include borehole breakouts, focal mechanisms from seismicity, and the integrated geologic history of stress evident from the attitude of joints, dikes and younger normal faults exposed in hydrothermal opal mounds formed by modern geothermal activity. These constraints all indicate a consistent maximum horizontal compressive stress, SHmax, primarily directed N-S (170-180°) to NNE-SSW (035°). Based on these data, the most likely direction of hydrofracturing, assuming isotropic strength properties of the basement rock is N-S to NNE-SSW, and wells should be deviated at right angles to this direction (E-W, 080-090°; to ESE-WNW, 125°) to optimize the stimulation.

Although major activities will be conducted on private and Utah state property, a utilities corridor will cross approximately 3.3 km (2.1 miles) of the adjoining BLM land. This corridor will be used for light vehicle access, a pipeline connecting ground water supply wells on private land to the deep well site and for electric lines. Cultural and biological clearances will be required. However, the area has been extensively developed, and the BLM and other landowners have indicated they do not anticipate any environmental constraints that would impacts the project. Correspondence received from the BLM describing the work that is required to obtain permits for geophysical and geological surveys and infrastructure enhancement is attached in Appendix Environmental Information Synopsis.

Outreach activities have been a significant component of Phase 1. A Utah FORGE website provides information on the site, team, outreach activities and links to other useful websites. Interactive maps showing seismicity, the 3-D conceptual model and other data can be accessed through the website. A video highlighting Utah FORGE was prepared and is being used by DOE as part of their communications program. We have received enthusiastic support for the project from the landowners, federal and state regulators, state and county government officials, and the local high school. Additionally, the Paiute Indian tribe has been informed about the project and did not raise any objections. Outreach will remain an important component of the project in Phases 2 and 3.

A team from the geothermal and oil and gas industries with practical expertise in the geosciences, drilling, reservoir engineering and management, EGS development, rock mechanics, and data handling will conduct the project. EGI at the University of Utah will serve as the Prime Contractor. The Utah Geological Survey, universities, national laboratories, oil and gas service organizations, and private consultants are major partners in the project.

In Phase 2, we will achieve full NEPA compliance, conduct non-invasive surveys, drill thermal gradient wells and a deep well into the granite to obtain in-situ data required for the deep wells and stimulation in Phase 3. Seismic and ground deformation monitoring networks will be installed. The Science and Technology Advisory Board will be convened.

Phase 3 will involve full implementation of Utah FORGE, including drilling, stimulation, flow testing and reservoir analysis to achieve step-changing improvements over earlier field demonstrations. R&D projects will be selected and tested, with emphasis on the development of

tools capable of withstanding elevated temperatures for long periods of time, new stimulation techniques, smart tracers to improve estimates of heat sweep efficiency, and reservoir monitoring and modeling.

Preface

A large team has compiled the data and interpretations of the characteristics of the FORGE site near Milford, Utah over the last year. This report which is a multi-author effort integrates a large amount of material, reflecting the depth and richness of the legacy datasets. These supply an important foundation for Phase 2 investigations, and many of the topics will be subject to further detailed study and analysis.

Reviews of much of the Phase 1 work were presented at the Stanford Geothermal Workshop in February, 2016 as three papers:

EGS Concept Testing and Development at the Milford, Utah FORGE Site. Proceedings, 41st Workshop on Geothermal Reservoir Engineering, Stanford University, Stanford, CA., 2016 (authors: Allis, R.G., Moore, J.N., Davatzes, N., Gwynn, M., Hardwick, C., Kirby, S., Pankow, K., Potter, S., and Simmons, S.F.)

The Geology, Geochemistry, and Hydrology of the EGS FORGE Site, Milford Utah. Proceedings, 41st Workshop on Geothermal Reservoir Engineering, Stanford University, Stanford, CA., 2016 (authors: Simmons, S., Kirby, S., Jones, C., Moore, J., and Allis, R.)

Geophysical Signatures of the Milford, Utah FORGE Site. Proceedings, 41st Workshop on Geothermal Reservoir Engineering, Stanford University, Stanford, CA., 2016 (authors: Hardwick C.L., Gwynn, M., Allis, R., Wannamaker, P., and Moore, J.)

The following is a list of people who have provided input to this report, arranged by organization.

Energy & Geoscience Institute, University of Utah
Joseph Moore, Stuart Simmons, John McLennan, Phil Wannamaker, Clay Jones, Gosia Skowron,

Utah Geological Survey
Rick Allis, Christian Hardwick, Mark Gwynn, Stefan Kirby, Peter Nielson, Mike Lowe, Mark Milligan, Lance Weaver, Jay Hill.

University of Utah Seismograph Stations
Kris Pankow, Stephen Potter

Add with affiliations Bill Rickard, Ben Barker, DuaneWinkler

Temple University
Nick Davatzes

The large volume of data and its diversity available at the proposed Milford FORGE site is already too large to be completely demonstrated in a written report such as this. Reviewers are therefore encouraged to also look at the site website (http://www.forgeutah.com/) where there is

an interactive map allowing display of well data (raster images) by clicking on well locations (under "Site Advantages" tab), and a 3-D visualization application derived from the ArcGIS™ software that is supporting this project (http://arcg.is/23sy8ro). The visualization allows the viewer to move around the granite that underlies the north Milford basin, and regime where temperatures are greater than 175°C (the 3-D surfaces and some other features can be turned on and off with the layers menu on the right side; and movement with the cursor can be controlled by the symbols on the lower left of the screen). The ultimate goal is to have the ArcGIS system accessible through the web so that viewers can choose which of the numerous geoscientific data layers they wish to view or overlay. The interactive GIS system is only accessible to project participants at the moment. Opening this up to a broader audience will have license and cost implications, and this will be investigated as part of a Phase 2 outreach initiative.

Task numbers correspond to those specified in the Statement of Project Objectives.

TASK 1.1

Compile and Analyze Existing Site Characterization Data

TASK 1.1 COMPILATION AND ANALYSIS OF EXISTING SITE CHARACTERIZATION DATA

Table of Contents

A. SUMMARY

The Milford FORGE deep well site is located 350 km south of Salt Lake City and 16 km north northeast of Milford, Utah. The prospective site covers 4.9 km^2 (1.9 mi^2), and it is situated on a west sloping alluvial fan in the north Milford valley, roughly halfway between the crest of the Mineral Mountains to the east and the Beaver River to the west. A large amount of geoscientific data has been acquired over 40-year period, starting with intensive geothermal exploration during the late 1970s. The work included geological mapping, gravity and magnetotelluric surveys, and the drilling, logging, sampling, and study of numerous shallow (~80) and deep (> 20) wells, including Acord-1, a 3.8 km deep well in the middle of north Milford Valley, west of the FORGE deep drill site. The FORGE deep well site is situated centrally between three, deep, non-productive wells which had thermally conductive gradients and temperatures of more than 175°C at less than 3 km depth.

Based on surrounding wells, the main rock types beneath the FORGE deep well site likely comprise crystalline basement rocks made up of Precambrian gneiss and Tertiary plutons, Tertiary basin-fill composed of volcanic strata, and Quaternary basin fill made of fluvial-lacustrine sedimentary deposits. The Precambrian gneiss was mostly intruded by young igneous rocks, but some contacts between these units are represented by faults and zones of cataclasis. The gneiss is made up of biotite, hornblende, K-feldspar, plagioclase, quartz, and sillimanite, and isotopic dating indicates Proterozoic metamorphism ~1720 Ma. The plutonic rocks include diorite, granodiorite, quartz monzonite, syenite, and granite, which contain variable amounts of biotite, clinopyroxene, hornblende, K-feldspar, magnetite-ilmenite, plagioclase, and quartz. The oldest intrusion was emplaced ~25 Ma followed by younger intrusion events at ~18 Ma and 11 to 8 Ma. Laboratory measurements of a small set of drill core plugs indicate these crystalline rocks have very high compressive strength, a porosity of 0.13%, and a matrix permeability of 0.3 microdarcies. High temperatures in the upper crust beneath this region may be related to the source of the Quaternary rhyolite domes and flows in the adjacent Milford Mountains.

Hydrothermal alteration is widespread, but weak, and it is made up of quartz, illite, chlorite, mixed-layered clays, epidote, leucoxene, hematite, calcite, anhydrite, and K-feldspar, which partly replace precursor minerals or deposited into open spaces. Temperature-sensitive phases lack well-defined depth zonation, which suggest that most of the alteration formed during earlier periods of hydrothermal activity associated with Tertiary magmatism. Modern hydrothermal activity is responsible for steam-heated, acid alteration in the vicinity of fumaroles and steaming ground north of the Negro Mag fault, and silica sinter deposition along the Opal Mound fault.

Three separate types of faults exist, and they are products of two distinct tectonic events that include late Mesozoic-early Cenozoic compression during the Sevier orogeny and middle Tertiary to Recent extension. The younger faulting episode is related to ongoing east-west Basin and Range extension, which dates back at least ~17 Ma, producing predominantly north-south trending fault zones that bound basins and range fronts. The Opal Mound fault is a prominent high-angle fault along the west side of Roosevelt Hot Springs that dips east and offsets surficial deposits of alluvium and silica sinter; additional north-south trending normal faults are likely to occur in basement rocks to the west beneath the alluvial cover but are blind to the surface. The Negro Mag fault is a high-angle east-west trending fault, cutting across the Mineral Mountains.

Lineament analysis shows that the crystalline rocks exposed in the Mineral Mountains have dense joint spacing and azimuths in all compass directions. This suggests the existence of a complex mesh of fractures beneath the FORGE deep drill site, which will respond favorably to stimulation, and support development of a distributed, connected permeability structure.

The 3D understanding of heat flow and temperature gradients is based on analysis of temperature profiles from approximately 100 wells drilled from 200 to 4000 m depth. A large area of anomalously high conductive heat flow, covering over 100 km^2, surrounds the FORGE deep well site. At 2000 and 4000 m depth beneath the FORGE deep well site, the rocks are expected to be hot, ranging from 175 to more than 250°C. The volume of crystalline basement rock having a temperature of more than 175ºC down to 4 km depth exceeds 100 km^3. The Opal Mound fault forms the eastern boundary to this large conductive thermal regime, separating it from Roosevelt Hot Springs to the east where convective hydrothermal heat flow prevails and covers a smaller area of ~10 km^2.

Gravity and magnetotelluric data constrain the basement surface and the depth to crystalline rock, and reflect a basin within a basin-type geometry. The center is steep walled and V-shaped, and the axis is oriented north-south, perpendicular to Basin and Range extension. Outward and upward, the basement contact flattens to form a gently dipping surface that extends beneath the FORGE deep drill site, where the depth to crystalline basement ranges from over 1000 m on the western side to about 500 m on the eastern side.

Lab testing indicates crystalline basement rocks are very strong, and they have very low porosity and very low permeability. The compressive strength was measured at three separate confining pressures, 0, 2800, 8000 psi, giving average values of $2.8x10^4$, $6.0 x10^4$, and $9.0 x10^4$ psi, respectively. The porosity is 0.13% and the permeability, measured with state of the art equipment used for shales and mudstones, is 0.3 microdarcies. It is likely that the porosity and permeability at field-scale will be controlled by the presence or absence of fractures.

Natural seismicity in the Milford region over the period 1965-2012 is relatively quiet in the vicinity of the FORGE deep wells site, with regional events associated with tectonic movements; there is no evidence of injection-induced seismicity in the nearby Roosevelt Hot Springs reservoir. Most natural seismicity is clustered near Milford (0.46 to 3.87 M), which is the site of the 4.1M earthquake in 1908, and diffuse low magnitude activity occurs beneath the Mineral Mountains. Based on borehole breakouts, earthquake focal mechanisms, and the orientations of faults and joints, the maximum compressive stress is oriented NNE-SSW (~000-010°) and the minimum compressive stress is oriented WNW-ESE (~090-100°), consistent with regional patterns of Basin and Range extension.

Hot deep reservoir fluid (240-270 ºC) from Roosevelt Hot Springs is made of near neutral pH sodium chloride water, containing 3000-4500 mg/kg Cl and less than 1000 mg/kg dissolved CO_2. A recent survey of production fluid chemistry indicates that the reservoir water compositions are largely unchanged since 1984, except for effects of steam-loss and mixing with injectate. Preliminary geochemical modeling shows these waters are close to equilibrium with respect to Na and K-bearing feldspars, quartz, chlorite, illite, calcite, and anhydrite.

Pre-production pressure profiles for deep wells in the Roosevelt Hot Springs (RHS) system east of the Opal Mound fault are uniform indicating a hydrostatic pressure head that is 3 MPa higher than wells on the west side of the Opal Mound fault. This means there are two distinct pressure regimes separated by the Opal Mound fault, with faulted, high-permeability rock associated with the RHS to the east, and relatively impermeable rock to the west. The groundwater regime across the FORGE deep well site is controlled by the west sloping potentiometric surface and an unconfined aquifer hosted in alluvial gravels. Geochemical data trace shallow hydrothermal outflow to the northwest and west, consistent with temperature profiles in gradient wells. Groundwater at pump rates of more than 100 gal/min is available from shallow wells towards the center of the north Milford valley. This groundwater is chemically benign, non-potable, and suitable for EGS heat transfer experiments. The Milford FORGE deep well site meets the DOE geoscientific criteria for development of an EGS laboratory.

B. INTRODUCTION

The Milford FORGE deep well site (Fig. 1) is located 350 km south of Salt Lake City and 16 km north northeast of Milford, Utah, in an unpopulated area that is predominantly used for renewable energy (wind, solar, geothermal). It is situated on a west sloping alluvial fan in the North Milford valley, roughly halfway between the crest of the Mineral Mountains to the east and the Beaver River to the west. The deep well site covers 4.9 km^2 (1.9 mi^2) and it is located 5 km west-northwest of the Blundell geothermal power plant, which produces 35 MWe from flash and binary units.

This report provides an overview of the setting of the FORGE deep drill site and the surrounding region. It is based on a compilation of a large amount of geological, geophysical, and geochemical data, which has been acquired over a period spanning 40 years. Much of this work was the product of exploration and development of the Roosevelt Hot Springs KGRA. However, Roosevelt Hot Springs represents only a small part of a large area associated with anomalous heat flow, and the area to the west of the Opal Mound fault has long attracted interest in terms of EGS research and development (e.g. East, 1981; Goff and Decker, 1983). As a result, data are available from numerous field surveys and the drilling, logging, and study of many shallow and deep wells, including Acord-1, a 3.8 km deep well (e.g., Allis et al., 2015, 2016; Hardwick et al, 2016; Simmons et al., 2016). These form the foundation for a 3D understanding of the rock types, fault-fracture patterns, thermal structure, stress regime, hydrology, and fluid types that make up the reservoir of the proposed FORGE laboratory. These elements are summarized here and again in Task 1.2 report where the 3D model is described and uncertainties of reservoir parameters (temperature, rock type, hydrothermal alteration, fluid content, thermal conductivity, permeability, porosity, structure, stress regime, seismic activity, groundwater availability) are discussed.

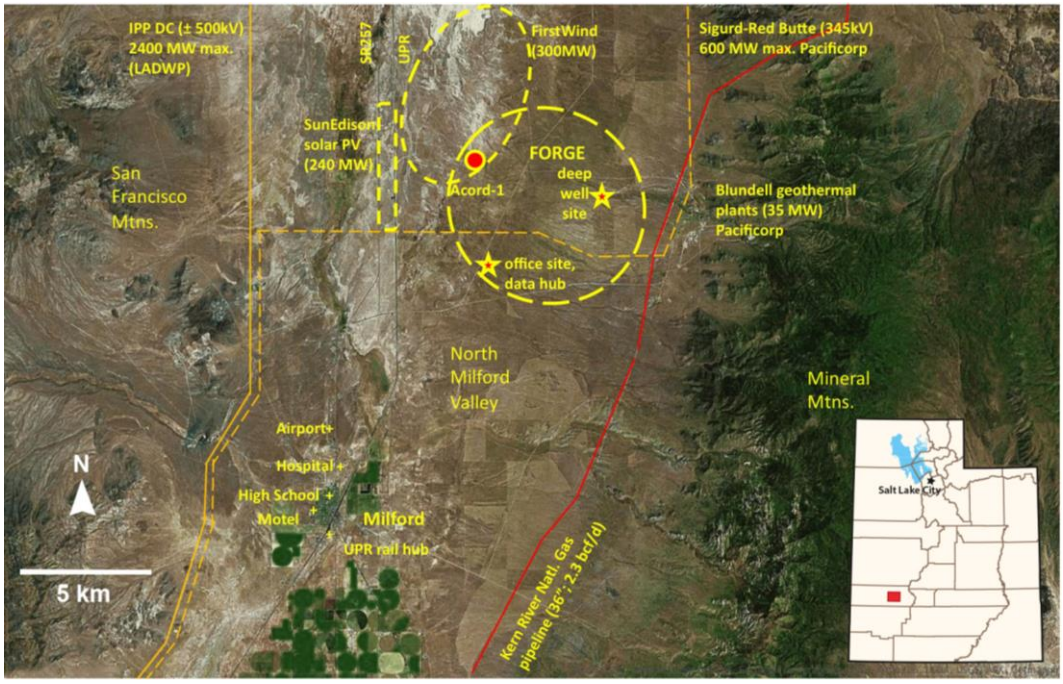

Figure C. 1: *Location of the FORGE deep well site near Milford, Utah, showing infrastructure and physiography.*

C. GEOLOGY

The Milford FORGE site (Fig. C.1) is located within a geologically complex zone that lies inside the southeast margin of the Great Basin and abuts the western edge of the Colorado Plateau (e.g., Wannamaker et al., 2001). Regional features include folded and imbricated Paleozoic-Mesozoic strata of the late Jurassic through Eocene Sevier orogeny, volcanic and intrusive centers resulting from Tertiary arc magmatism, detachment faulting associated with regional extension, tilting and exhumation of core complexes, and north-south trending normal faults resulting from Basin and Range extension (e.g., Dickinson, 2006; Anders et al., 2012). The zone also includes three producing geothermal fields, Cove Fort-Sulphurdale, Roosevelt Hot Springs, and Thermo Hot Springs, which are associated with young extensional faults, centers of Quaternary basalt-rhyolite magmatism, and large areas of anomalous heat flow covering >100 km^2 (e.g., Mabey and Budding, 1987; Blackett, 2007; Kirby, 2012; Simmons et al., 2015; Wannamaker et al., 2015).

C.1 Lithology and Mineralogy

The main rock types associated with the FORGE deep well site are crystalline basement rocks made up of Precambrian gneiss and Tertiary plutons, Tertiary basin-fill composed of volcanic strata, and Quaternary basin fill made of fluvial-lacustrine sedimentary deposits. The occurrence and distribution of these units is known from field mapping and petrographic studies of cuttings and cores mainly from four wells, 14-2, 52-2, 9-1, and Acord-1 (Figs. C2, C3 and C4; Glen and Hulen, 1978; Glenn et al., 1980; Sweeny, 1980; Welsh, 1980; Nielson et al., 1986; Coleman and Walker, 1992; Coleman et al., 1997; Hintze and Davis, 2003; Task 1.1.2). Gravity data (described below) constrain the west sloping contact that separates underlying crystalline rocks, gneiss and granite, from overlying volcanic deposits and fluvial-lacustrine basin fill (Fig. C3; Hardwick et al., 2016). There is no evidence of any Paleozoic-Mesozoic strata in the vicinity of the deep well site, despite being a major component of the regional stratigraphy and exposed in the southern and northern parts of the Mineral Mountains (Nielson et al., 1986).

Precambrian gneiss is the oldest rock type, and outcrops occur sporadically at lowest elevations in the western Mineral Mountains, and it was penetrated in wells (Figs. C2 and C4). Both banded and massive varieties of gneiss exist. Segregations of quartz-K-feldspar form the light bands, whereas biotite-plagioclase-quartz-hornblende-K-feldspar form the dark bands (Glenn et al., 1980). Sillimanite occurs in outcrops. These minerals form an interlocking texture, and planes or zones of weakness, appear to be absent. U-Pb dating of accessory zircons gives an age of 1720 Ma, consistent with a model Rb/Sr whole-rock isochron of 1750 Ma, indicating early Proterozoic metamorphism (Aleinikoff et al., 1987).

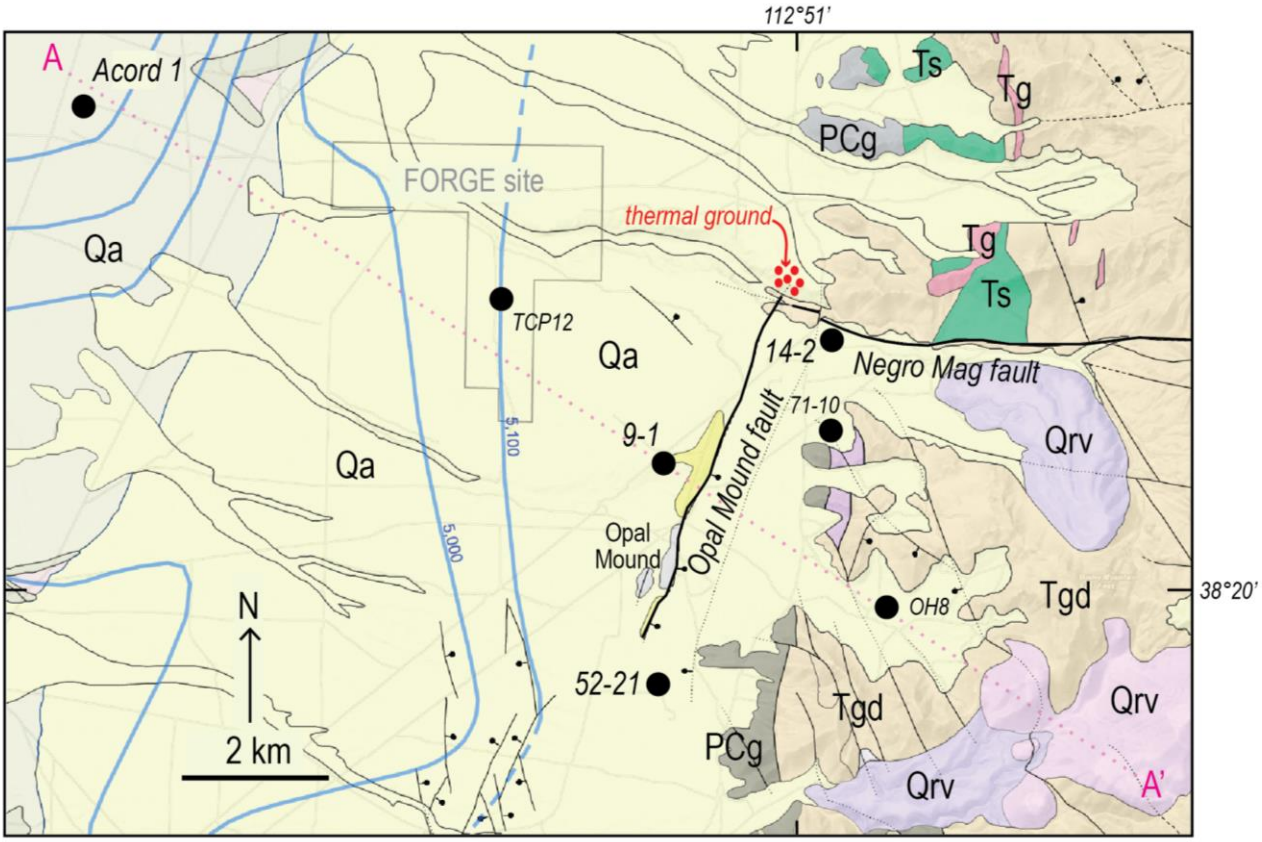

Figure C.2: *Geologic map of the FORGE deep well site, Milford, Utah (Hintze et al., 2003; Rowley et al., 2005; Kirby, 2012). For clarity, only a few of the many wells are shown; these are described later. Blue lines represent the elevation (feet above sea level) of the groundwater potentiometric surface (contour interval variable; the potentiometric head near Acord-1 is at 4950 feet. Abbreviations for map units: Qa=Quaternary alluvium and claystone; Qrv=Quaternary rhyolite volcanic rock; Tgd=Tertiary granodiorite; Tg=Tertiary granite dike; Ts=Tertiary syenite; PCg=Precambrian gneiss.*

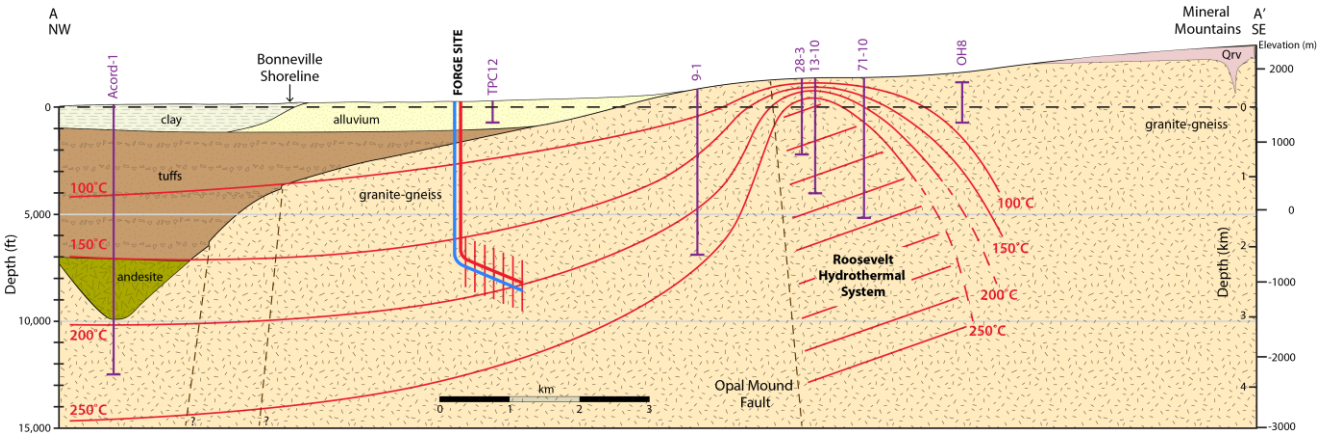

Figure C3: *Geologic cross section A-A' from Figure C2, showing the stratigraphy, structure, and the FORGE deep well site. The zero datum for the depth axes is at 1524 m asl (5000 ft asl). Precambrian gneiss and Tertiary plutonic rocks are undifferentiated. The Roosevelt Hot Springs hydrothermal system lies east of the Opal Mound fault. Isotherms are interpreted from well measurements, and the contact between granite-gneiss and overlying basin fill is interpreted from gravity measurements (Allis et al., 2016; Hardwick et al., 2016). The trajectories of the FORGE deep wells deviate towards the southeast from the western side of the deep-well site. Final decisions on the best location and deviation direction for the deep wells will await the characterization research in Phase 2 of this project. The lower part of the basin fill is shown as having close to 1 km of andesite based on Hintze and Davis (2003). Subsequent logging of the cuttings suggests the andesite could be much thinner and interlayered with volcaniclastics and tuffs.*

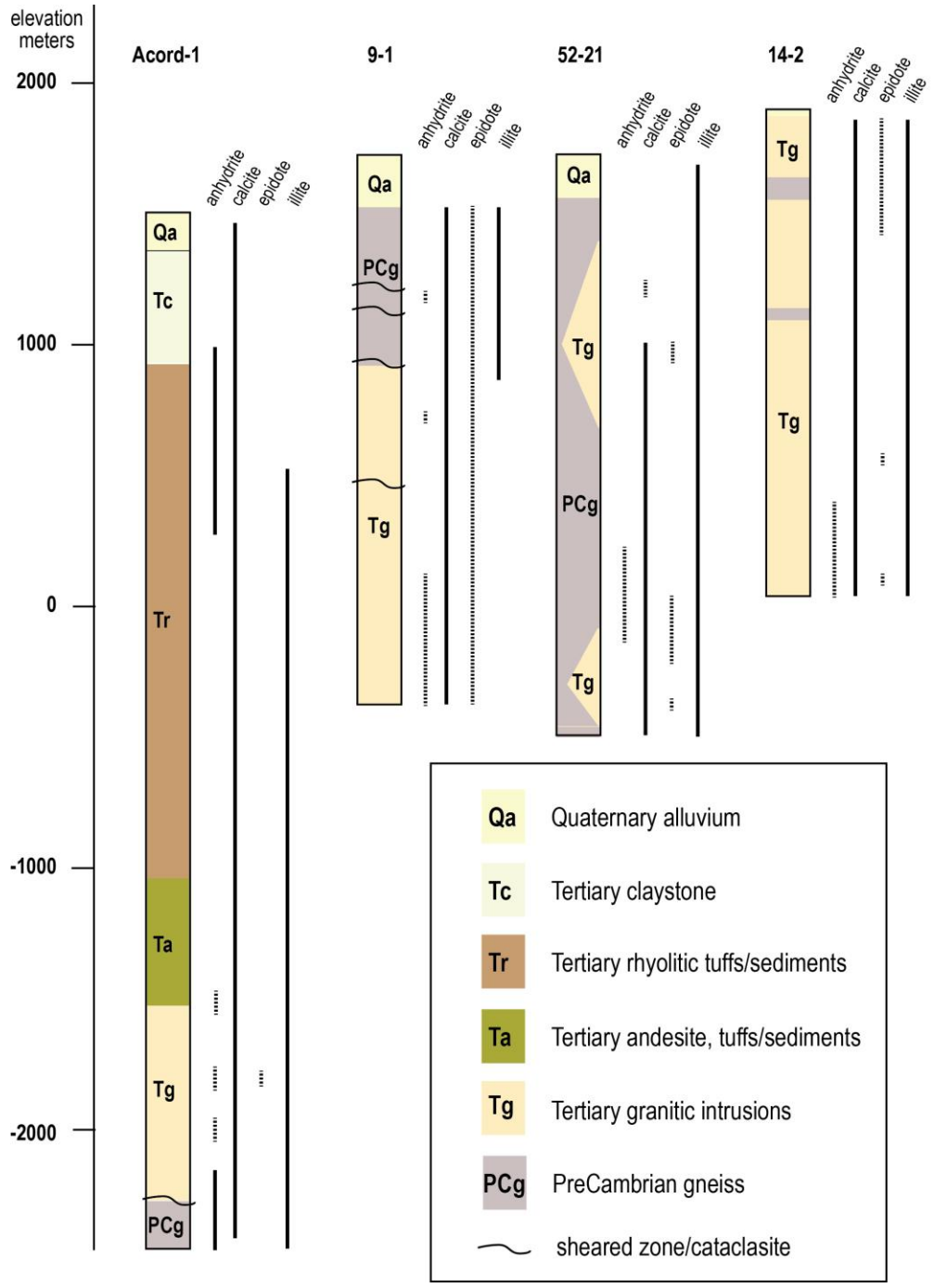

Figure C4: *Stratigraphic logs for four deep wells in the study area surrounding the FORGE deep well site, Milford, Utah. Vertical intervals of hydrothermal anhydrite, calcite, epidote and illite (sericite) are based on petrography and XRD analyses; hydrothermal alteration is weak intensity. Sources of data: Acord-1 (Sweeney, 1980; Welch, 1980; Hintze and Davis, 2003; Task 1.1.2); 9-1 (Glenn et al., 1980; Capuano and Cole 1982); 52-21 and 14-2 (Glenn and Hulen, 1979; Capuano and Cole 1982). Precambrian gneiss and Tertiary plutons are separated by contacts resulting from magmatic intrusion and faulting. All of the other major breaks in rock types are marked by unconformities.*

Plutonic rocks of Oligocene-Miocene age form the core of the Mineral Mountains and the reservoir host rock in the Roosevelt Hot Springs system (Nielson et al., 1986), and these rocks extend to the west beneath the basin fill to the Acord-1 well (Figs. C2 and C4). The plutonic rocks range from intermediate to felsic composition, but the outcrops east of the Roosevelt Hot Springs area mainly expose medium to coarse-grained hornblende granodiorite (Nielson et al., 1986; Coleman and Walker, 1992). Drill cuttings from well 9-1 confirm a spectrum of plutonic rock-types, including diorite, granodiorite, quartz monzonite, syenite, and granite; these phases are made up of variable amounts of plagioclase, hornblende, biotite, clinopyroxene, quartz, K-feldspar, magnetite-ilmenite, and accessory titanite, rutile, apatite, and zircon (Glenn et al., 1980). The oldest intrusion is associated with crystallization and emplacement of the hornblende diorite, and it has a U-Pb zircon date of 25±4 Ma (Aleinikoff et al., 1987); younger intrusion events followed at ~18 Ma and 11 to 8 Ma (Nielson et al., 1986; Coleman and Walker, 1992; Walker et al., 1997).

Tertiary volcanic rocks crop out sporadically through the Mineral Mountains and cover large areas in the adjacent ranges well outside the study area, including the Tushar Mountains to the east and the Star Range to the west (e.g., Nielson et al., 1986; Coleman et al., 1997; Hintze and Davis, 2003). The thick sequence of volcanic strata (~1500 m) penetrated by the Acord-1 well (Fig. C4) is divided into a thick upper group made of felsic tuffs and flows, and a lower group made of andesite lavas, tuffs and volcaniclastic sedimentary deposits (Sweeney, 1980; Welch, 1980; Task 1.1.2). Quaternary volcanic rocks occur in the central part of the Mineral Mountains, representing small volume eruptions, obsidian flows and pyroclastic deposits (0.8-0.5 Ma), including the prominent Bailey Ridge flow (~6 km^2) near Roosevelt Hot Springs (Lipman et al., 1978).

Young unconsolidated basin fill covers the floor of Milford Valley. These deposits consist of alluvial and lacustrine deposits that contain interbedded sand, silt, gravel, and clay (Hintze and Davis, 2003). In Acord-1, unconsolidated basin fill has a thickness of ~500 m and spans from Recent to late Tertiary in age. Within the vicinity of the FORGE deep well site, these deposits are at least 200 m thick, poorly consolidated, and made up of quartzo-feldspathic alluvial fans shed off the Mineral Mountains. Point bar deposits to the west lap on to the fan deposits and mark the high-stand of Lake Bonneville 18,000 years ago.

Petrographic and XRD analysis of drill cutting indicate widespread occurrences of minor amounts of hydrothermal minerals (Fig. 4), comprising quartz, illite, chlorite, mixed-layered clays, epidote, leucoxene, hematite, calcite, anhydrite, and K-feldspar (Glenn and Hulen, 1978; Glenn et al., 1980; Sweeney, 1980; Nielson et al., 1986; Task 1.1.2). Locally, hydrothermal alteration is concentrated around narrow zones of cataclasis, characterized by comminuted rock flour, streaky foliation, and micro-veining (e.g., well 9-1; Glenn et al., 1980). Quartz, chlorite, illite, calcite, epidote and anhydrite, replace precursor phases and fill open spaces, but they lack well-defined depth zonation (Fig. C4; Capuano and Cole, 1982). A number of small prospect pits expose weakly developed hydrothermal Cu-Mo-W mineralization in granitic rocks of the central Mineral Mountains (Nielson et al., 1986). These occurrences suggest that most of the alteration formed during ancient periods of hydrothermal activity, associated with episodes of magmatism, that date back to the Miocene. New results of petrographic and XRD analyses of cuttings from Acord-1 are described in Task 1.1.2.

Mineralogical products of modern hydrothermal activity occur along and east of the Opal Mound fault. In the northern part of the Roosevelt Hot Springs area, quartz, alunite, kaolinite, and hematite are products of steam-heated acid alteration in the vicinity of fumaroles and steaming ground (Parry et al., 1980). In the south, a thick deposit (>3 m) of colloform banded sinter makes up the Opal Mound. A subvertical north-south trending fissure (~0.5 m wide) filled with banded silica forms the main vent and marks the Opal Mound fault. Two radiocarbon dates indicate the sinter deposited between 1600 and 1900 years BP (Lynne et al., 2005). Although the site is no longer thermally active, a significant volume of hot near neutral pH chloride water discharged here, similar in composition to modern produced reservoir waters that feed the Blundell-Roosevelt geothermal plant. The hot water flow to the surface likely ceased due to silica deposition in combination with lowering of the water table. Today the Opal Mound Fault represents the western edge of the hydrothermal system and mineral sealing may have played a role in creating a lateral barrier to horizontal fluid flow.

C.2 Faults and Lineaments

Three separate types of faults have been identified in the study area, and they are products of two distinct tectonic events that include late Mesozoic-early Cenozoic compression during the Sevier orogeny and middle Tertiary to Recent extension. The Sevier orogeny produced large-scale horizontal displacements and low angle thrust faults (e.g., Hintze and Davis, 2003). Examples of these are exposed in the northern and eastern part of the Mineral Mountains. The original dip of these structures may have been steepened through rotation associated with uplift and exhumation of the Miocene plutonic complex (Nielson et al., 1986).

The younger faulting episode is related to ongoing east-west Basin and Range extension, which dates back at least ~17 Ma, producing predominantly north-south trending fault zones that bound basins and range fronts (e.g., Hintze and Davis, 2003; Dickinson, 2006). In the region surrounding the FORGE deep well site and the Mineral Mountains, both older low-angle faults and younger high-angle faults exist (Nielson et al., 1986; Hintze and Davis, 2003). The Cave Creek fault in the southern part of the Mineral Mountains dips 20° west, and it is associated with a 200 m thick zone of cataclasite, which is developed mainly in the underlying 18 Ma pluton (Nielson et al., 1986; Coleman and Walker, 1994; Coleman et al., 1997; Anders et al., 2001). Evidence of early ductile deformation and foliation is crosscut by subvertical fractures and breccias that represent a transition to brittle deformation over time (Nielson et al., 1986). Another low-angle fault, dipping 15° west and named the Wildhorse Canyon fault, is identified in the western Mineral Mountains, directly east of Roosevelt Hot Springs (Nielson et al., 1986). This fault may extend to the west below the surface based on cataclasite intervals intersected in well 9-1 (Fig. C4). The presence of a continuous listric detachment surface, however, is difficult to verify since there are few drill holes with cored intervals to make reliable stratigraphic correlations. Coleman et al (1997) suggest that rather than being the original dip of displacement, the low-angle structures started out as high angle normal faults, which were tilted as the fault zone evolved (e.g., Buck, 1988), consistent with the dip and north-south strike orientation of the youngest faults in the foothills of the Mineral Mountains (Nielson et al., 1986).

The Opal Mound fault (Fig. C2) dips steeply to the east and offsets surficial deposits of alluvium and silica sinter, with a total down-dip displacement of at least 15 m (Nielson et al., 1986). Other young north-south trending faults form a narrow graben in the fan deposits 5 km south of

the FORGE deep well site (Fig. C2). The offset on these faults is small and less than 3 m. We expect that there are additional north-south trending normal faults in the crystalline basement rocks, which are blind to the surface. Buried faults near the deepest part of the basin are inferred from the gravity profile and westward thickening basin fill (Fig. C3; Nielson, et al., 1986; Allis et al., 2016; Hardwick et al., 2016).

The Negro Mag fault is the other major steeply dipping fault, but it trends east-west (Fig. C2). The fault cuts across the Mineral Mountains for ~6 km, however the direction and amount of displacement are unknown due to the absence of markers within the plutonic rocks (Nielson et al., 1986). An east-west trending structure 2 km to the south of Negro Mag fault was the site of micro-seismicity in the late 1970s (Zandt et al., 1982; Nielson et al., 1986; Nielson, 1989; Allis et al., 2016), described below (Chapter 5). East-west trending faults also occur at Cove Fort-Sulphurdale and Thermo Hot Springs. These faults may reflect arc-parallel structures, which formed during southward migrating magmatism in the Eocene-Oligocene, and, or Proterozoic structures in deep-seated basement (e.g., Dickinson, 2006; Wannamaker et al., 2015).

From mineralogical investigations, the crystalline basement rocks appear to be strong, even though they vary in rock composition and mineralogy (i.e., granitic to gneissic); they are massive and banded, and they are locally sheared due to cataclasis. Nonetheless, pre-existing fractures and joints are likely to play the most important role in stimulating new permeability beneath the FORGE deep well site. The range of fracture density and orientations in crystalline rocks beneath the FORGE drill well site were studied by identifying and mapping the orientations and lengths of lineaments in the Mineral Mountains using high-resolution aerial images.

A zone covering 9x9 km^2 directly east of Roosevelt Hot Springs was studied and gridded into 1x1 km^2 sections (Fig. C5). Overall, more than over 4450 lineaments were mapped, ranging from 10s to 100s of meters in length and having orientations in all compass directions, with a predominant west northwest-east southeast trend (Figs. C5 and C6). A finer scale representation of the distributions and orientations of lineaments in two adjacent sections is shown in Figure C7. Three major joint sets were documented in earlier field mapping (Faulder, 1991), two having subvertical dips and azimuth bearings of north-south and east-west and a third having a low-angle dip to the west. These joints are spaced <1 to ~30 m apart (Faulder, 1991).

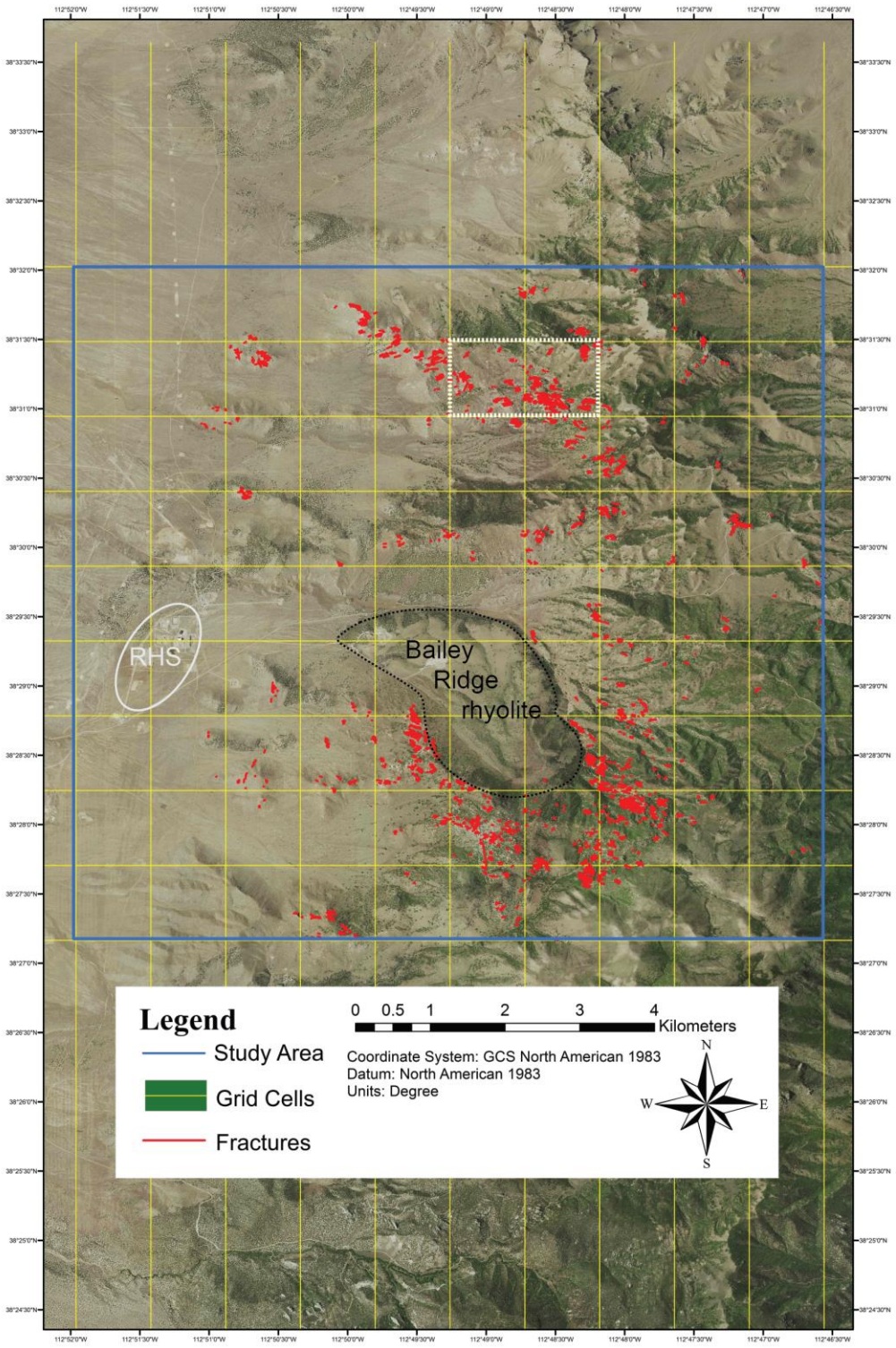

Figure C5: *Lineaments (n=4452) in granitic basement rock in the Mineral Mountains over a 9x9 km^2 area. Dashed white line outlines the area shown in Figure C7. The Bailey Ridge rhyolite (0.5-0.8 Ma) is the youngest rock-type, in the study area. RHS=Roosevelt Hot Springs production steam-field.*

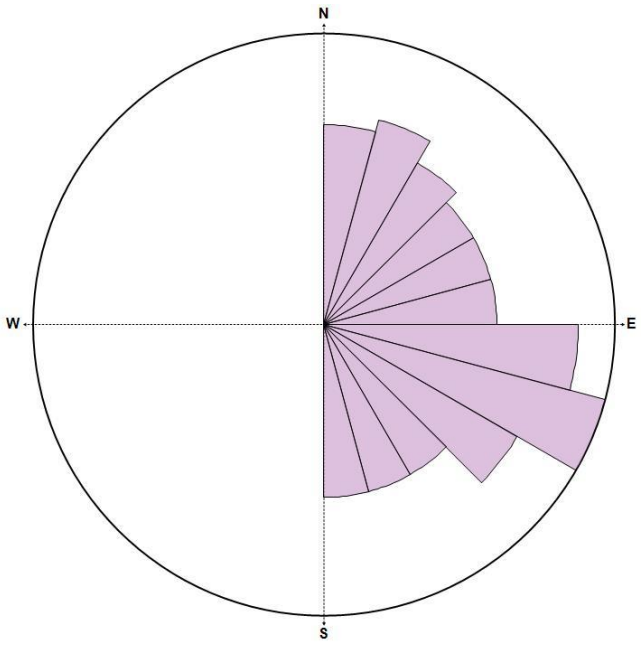

Figure C6: *Summary of lineament orientations (n=4452) in granitic basement rock in the Mineral Mountains over a 9x9 km^2 area.*

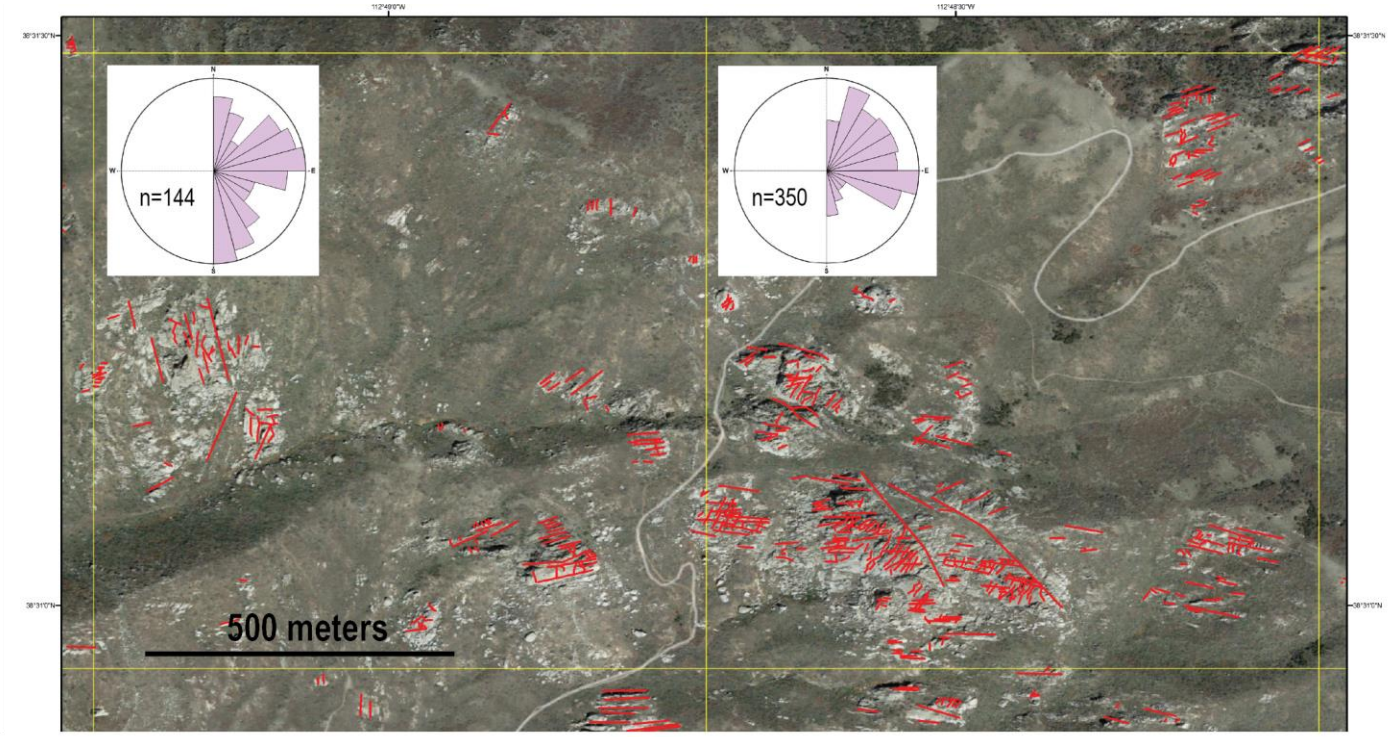

Figure C7: *Illustration of lineaments in granitic basement rock in the Mineral Mountains, ~5 km northeast of Roosevelt Hot Springs. Rose diagrams show how azimuths vary within a 2 km^2 area. The location of the study area is shown in Figure C2.*

D. THERMAL CHARACTERISTICS

Since the late 1970s over 80 shallow thermal gradient wells and 20 deep wells have been drilled and logged (Fig. D1). Analysis of the thermal gradient data shows that the shallow thermal anomaly extends over most of north Milford Valley (Fig. D2). Peripheral wells around north Milford Valley suggest temperatures at 200 m depth are about 20°C, whereas beneath the Mineral Mountains temperatures range between 5 and 12°C. The area with temperatures above 40°C at 200 m depth covers about 100 km^2 and includes the FORGE deep well site. Ward et al. (1978) showed that the highest heat flow area occurs in and around Roosevelt Hot Springs, east of the Opal Mound fault, where convective heat transfer and hydrothermal flow produce about 60 MWth. They also showed that the lobe of elevated heat flow extending north and northwest of the Opal Mound fault, encircled by the 80°C contour (Fig. D2), is an outflow feature. The new analysis of thermal gradients and heat flow are consistent with this basic model, as described below. More importantly, the new analysis demonstrates a very large area of anomalously high conductive heat flow surrounds the area of the FORGE deep well site, which is isolated from the Roosevelt Hot Springs hydrothermal system by the Opal Mound fault.

The volume of well data is such that an interactive map on the project's public website was considered essential to allow rapid location and checking of well data. The interactive map can be found at http://www.forgeutah.com/site/ . The site contains temperature gradient graphs, water levels, and chemical analysis data. Examples of the interactive map are shown in Figure D3. This data has also been submitted to the National Geothermal Data System.

D.1 Acord-1

Acord-1 was drilled to 3.8 km depth in 1979 by McCullough Oil Company. No fluid was produced and the well was plugged and suspended because of lack of production. Mud temperatures while drilling indicate a steady increase with increasing depth (Fig. D4). Correction of bottom-hole temperatures at logging intervals confirms a temperature of 230 ± 5°C at total depth. When combined with the temperature gradient observed in the nearby groundwater supply well for the drilling of Acord-1, a geotherm can be fitted to all the data, which allows the increase in thermal conductivity with increasing depth to be calibrated (k values in Fig. D3). The geotherm implies a heat flow of 120 ± 20 mW/m^2, with most of the uncertainty originating from thermal conductivity determinations.

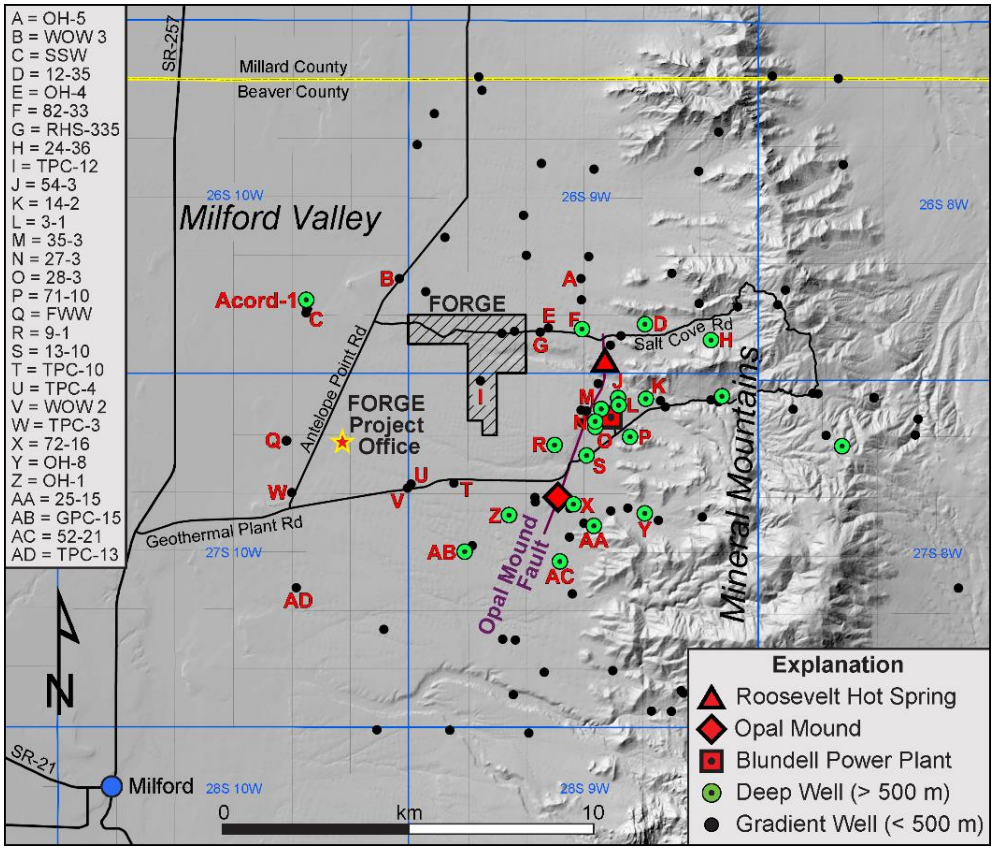

Figure D1. *Location of the FORGE drill site and office area, Acord-1 well, and other wells drilled in the area. Wells referred to in the text are labeled alphabetically.*

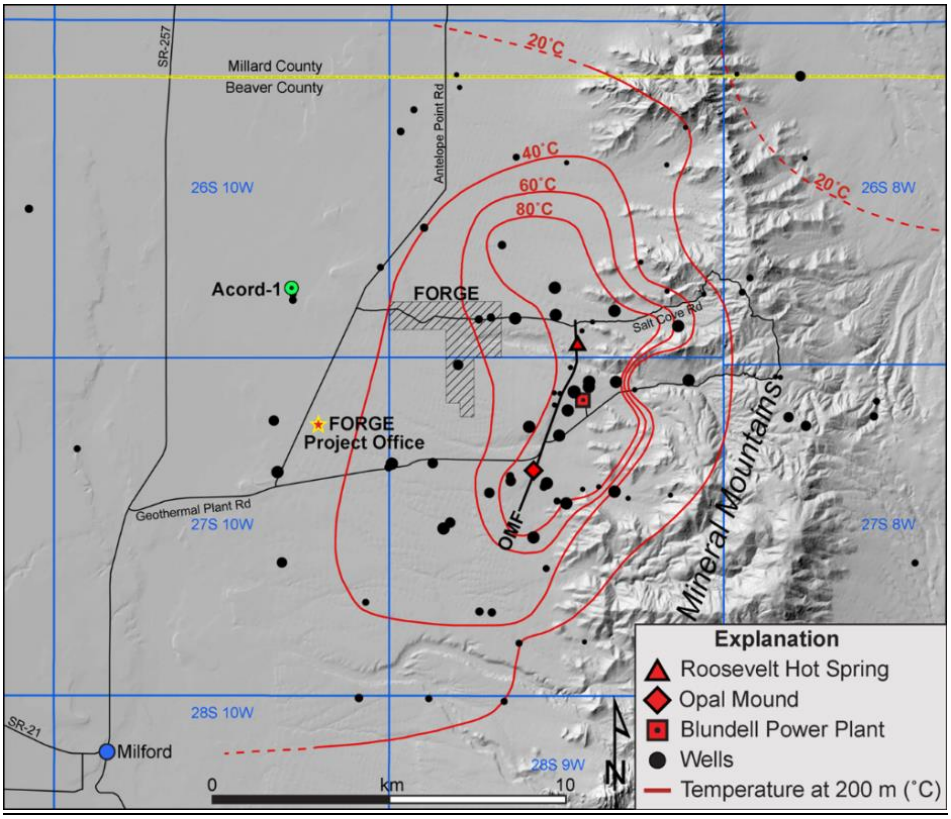

Figure D2. *Temperature at 200 m depth beneath and in the vicinity of the FORGE deep drill site. The size of the filled circle at each well location represents the degree of certainty of the temperature data, which constrain the geometry and positions of isotherms. The largest diameter circle represents wells greater than 200 m depth where the temperature was measured. The smallest diameter circle represents wells about 50 m deep where the temperature had to be extrapolated to depth. On the east side, the contours represent the temperature at 200 m below the 1830 m above sea level (6000 ft asl) datum, which is the elevation of the alluvial fan near to where it laps against the Mineral Mountains. This allows the contours to be smoothed across the ridges and valleys, but requires that higher-elevation wells be extrapolated to greater depths (up to 405 m from the surface). Farther to the west, the contours are at 200 m depth from the surface, and near SR-257 in the middle of the valley this is at about 1325 m asl (4345 ft asl; ground surface about 5000 ft asl or 1525 m asl). OMF is the Opal Mound fault.*

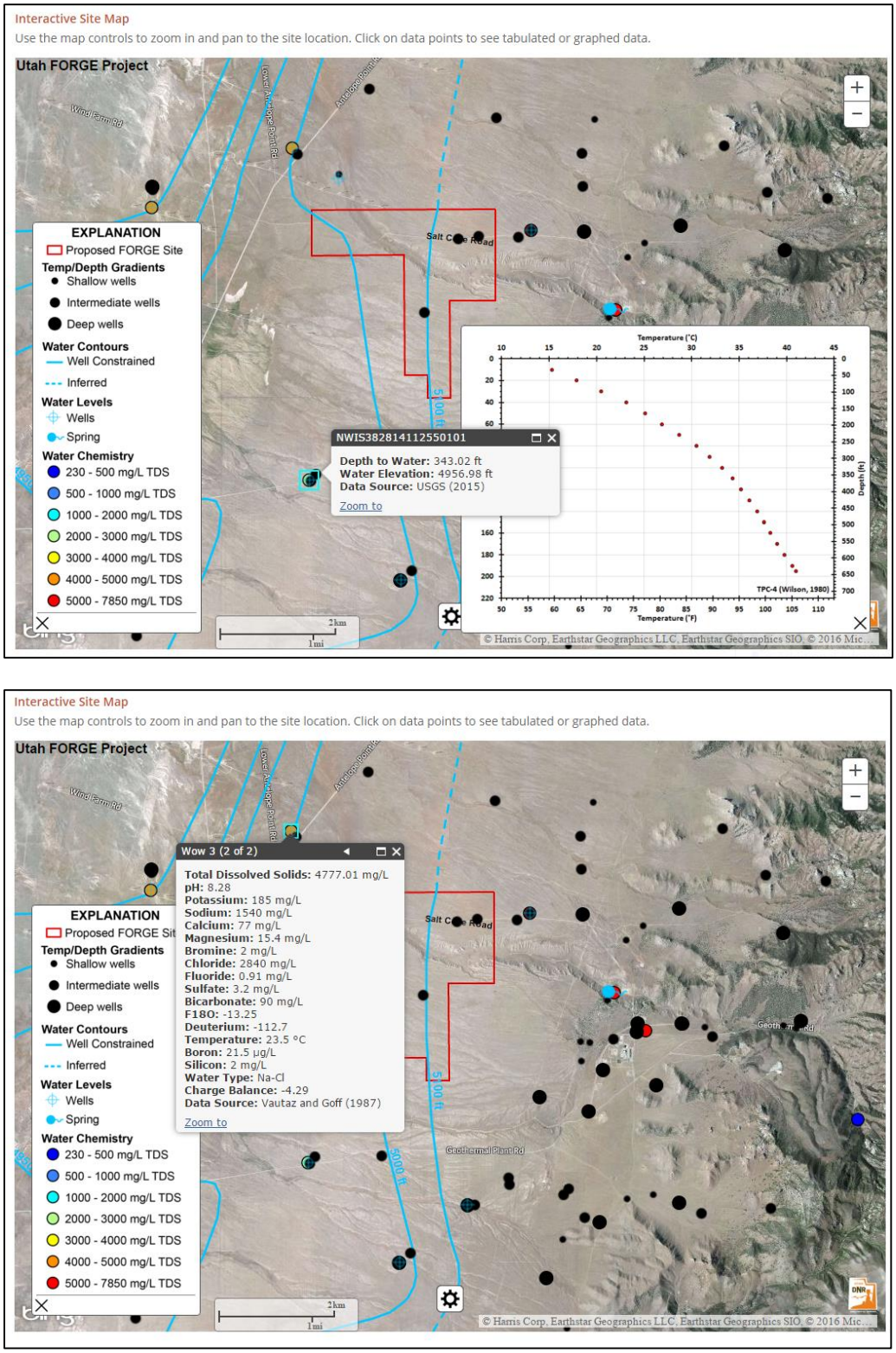

Figure D3. *Examples of the types of well data accessible through the interactive map on the project website.*

D.2 Shallow Temperature Gradients

A selection of shallow temperature profiles from wells between the central Milford Valley and the Opal Mound fault (Fig. D5) shows that the heat flow ranges from 120 to 200 mW/m^2. In the vicinity of the FORGE deep well site (TPC-12, TPC-4, TPC-10), the heat flows are typically in the range 180 ± 40 mW/m^2. In the east, the heat flows are significantly higher at depths less than about 500 m. However, comparison with the deep wells 9-1 and 82-33, both west of the Opal Mound fault, suggests the shallow temperatures are affected by outflow from the Roosevelt Hot Springs. The near-surface gradients exceed 150°C/km and heat flows range from 300 to >1000 mW/m^2 (for example, well RHS-335; Fig. D4). These gradients cannot be extrapolated much below 500 m depth, and when RHS-335 is compared to 9-1, the gradients are clearly decreasing with increasing depth (Figs. D4 and D5). To the north around the county line temperature gradients in shallow wells indicate heat flows of 70 ± 20 mW/m^2 (Fig. D6).

East of the Opal Mound fault, many of the shallow temperature profiles exhibit boiling-point-for-depth profiles, indicative of hydrothermal upflow. Although conductive heat flows can be calculated, the total heat flow is convective and the temperature profiles are controlled by steam-water saturation conditions and hydrostatic pressure gradients.

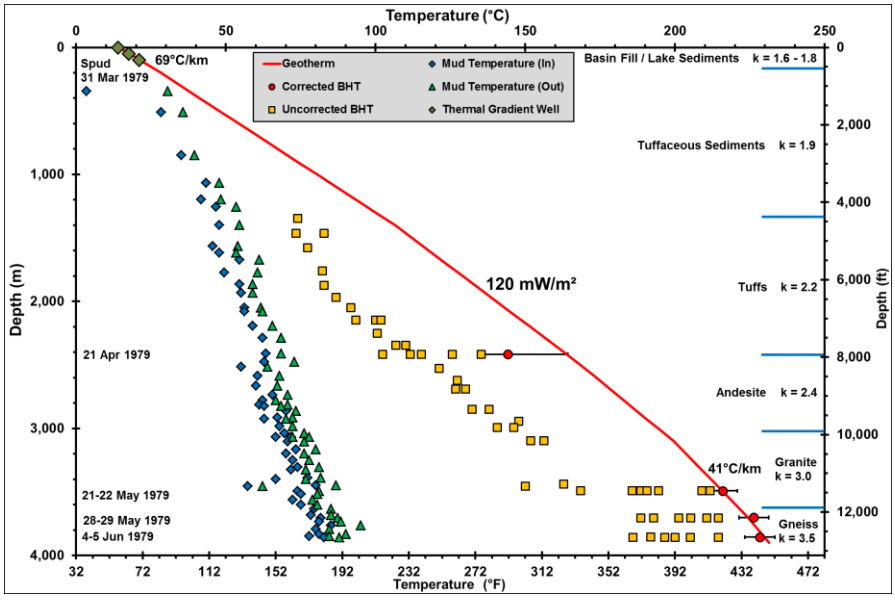

Figure D4. *Temperature data from Acord-1. The bottom hole temperatures (BHTs) are consistent with a conductive profile, with the best-fit geotherm having a heat flow of 120 ± 20 mW/m^2 (uncertainty due to thermal conductivity [k] assumptions; geotherm fits both the observed shallow thermal gradient at the site and the deep, corrected BHTs.) The temperature gradient in the granite is 41°C/km. The thermal conductivity variation with increasing depth is used to calculate geotherms from other thermal gradient wells in the north Milford Valley.*

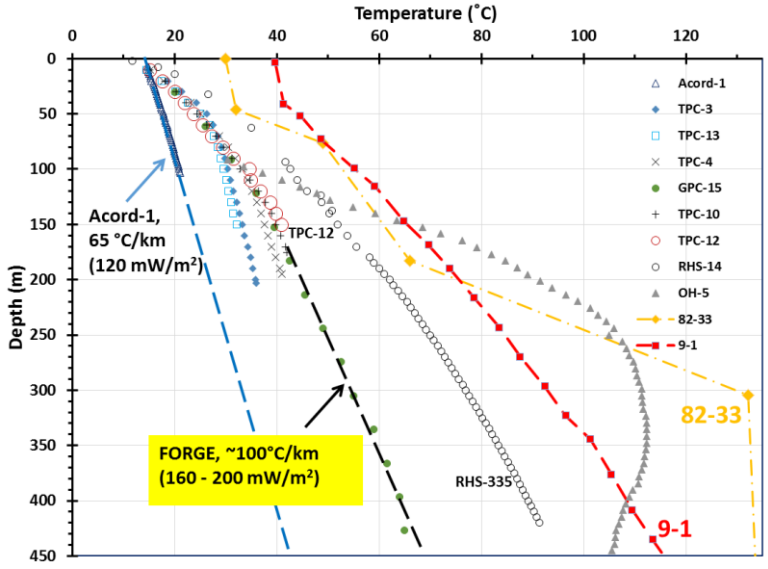

Figure D5. *The thermal regime in selected geothermal gradient wells, together with the upper portion of thermal profiles from the three deep wells west of the Opal Mound fault zone. The thermal gradients vary from 50–65 °C/km in the central valley and increase east towards the Opal Mound fault zone. TPC-12 is within the FORGE deep drilling site and indicates a deeper gradient of close to 100°C/km. Well RHS-335 indicates higher temperatures and is located 300 m east of the western boundary of the FORGE deep drilling site. The profiles for 82-33 and 9-1 are from Faulder (1994).*

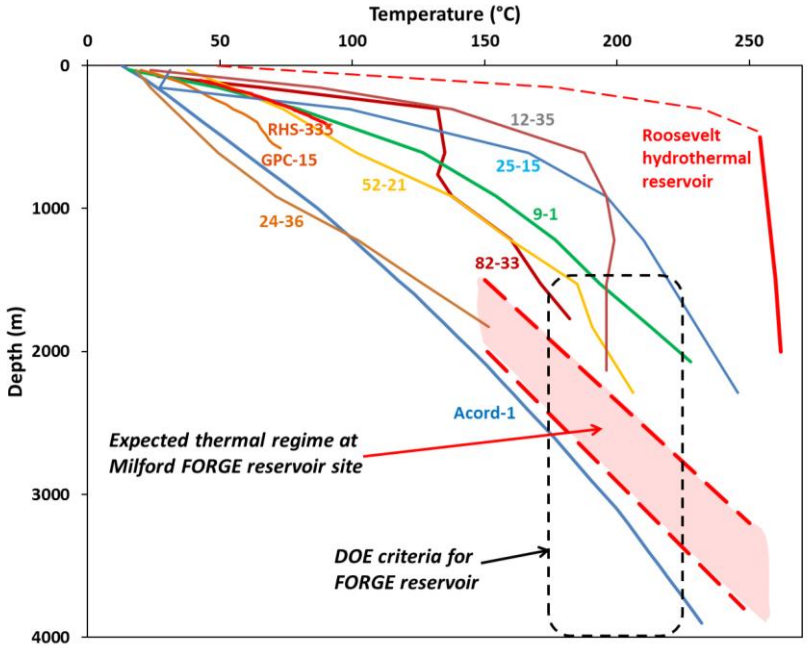

Figure D6. *Likely thermal regime at the FORGE deep drill site based on profiles in surrounding deep wells, and the thermal gradients in shallow wells (Fig. D4). The expected thermal regime beneath the site lies centrally within the bounding constraints specified by DOE. The two red dashed lines bound the likely uncertainties. The nearest wells to the site are 9-1 and 82-33, and*

are mostly in granite; the only wells mostly in basin fill are Acord-1, GPC-15 and RHS-335. Productive wells tapping the Roosevelt hydrothermal system lie east of the Opal Mound fault with near-surface temperature profiles that follow boiling-point-for-depth conditions. The hydrothermal well profiles represent pre-development conditions; subsequent fluid production has lowered some of these profiles by more than 300 m (Allis and Larsen, 2012).

D.3 Deep Thermal Regime

Figure D5 shows temperature profiles of several non-productive deep wells drilled around the Roosevelt Hot Spring system in comparison to profiles from production wells and from wells west of the Opal Mound fault (Fig. D1). With the exception of Acord-1, all deep wells are in granite or gneiss with less than 100 m of alluvium on top. Intermediate depth wells RHS-335 and GPC-15 did not reach granite basement. The trend of decreasing temperature gradient with increasing depth in the upper kilometer in wells near the Opal Mound fault highlights the potential error in extrapolating shallow gradients to greater depth. Below about 1 km depth, the profiles trend towards gradients of 50 - 70°C/km, indicating temperatures of 150°C to more than 200°C at 2 km depth, and 200°C to more than 250°C at 3 km depth. Associated deep conductive heat flows range from 150 to > 200 mW/m^2. Well 12-35 is near the northern end of the Opal Mound fault and the temperature gradient could reflect vertical fluid movement at 190 - 200°C. Well 82-33 lies northwest of the Opal Mound fault; at less than 1000 m depth the temperature profile represents the effects of shallow outflow from Roosevelt Hot Springs, but below this level the thermal gradient is conductive reaching a maximum of 180°C at 1900 m (Fig. D2). Well 24-36 is the easternmost deep well near the northern end of the hydrothermal system, and it has a distinctive concave-upwards temperature profile. This trend is seen in other wells in the Mineral Mountains, and it represents cold meteoric recharge depressing the near-surface temperatures. Production wells inside the Roosevelt Hot Springs hydrothermal system have temperature profiles that match boiling point for depth down to about 500 m depth, below which they steepen sharply and increase linearly to a maximum reservoir temperature of about 270°C (Fig. D5; Faulder, 1994).

D.4 The FORGE Deep Drill Site

The modeling of the deep thermal regime is based on calculating heat flows and fitting geotherms to temperature profiles from wells having reliable data. The trend of increasing thermal conductivity with increasing depth, which was required to best fit a geotherm through the basin fill for Acord-1, has been assumed to apply to all wells. This implicitly assumes the alluvium and lake sediments have uniform physical characteristics and a similar compaction trend with increasing depth. Where the geotherms extend below the granite surface, a thermal conductivity of 3 W/m°C is assumed for the crystalline basement rocks (granite and gneiss).

The heat flow map of the north Milford Valley (Fig. D7) is based largely on the thermal gradient data from wells less than 200 m depth supplemented by thermal gradient data from wells west of Roosevelt Hot Springs, and the very detailed thermal data extending to almost 4 km depth in Acord-1. The uncertainties in each heat flow value depends on whether the measured profile had attained thermal equilibrium, the variation in the gradient with increasing depth, the depth of the well, and assumptions regarding the thermal conductivity. The uncertainties are estimated to be about ± 30% for most data points. In Acord-1, the heat flow has an estimated uncertainty of ± 20

mW/m^2, but the deep temperatures within the interval of crystalline basement is known accurately (± 10°C) because numerous temperatures logs attained thermal equilibrium.

The heat flow map indicates that the undisturbed Roosevelt Hot Springs hydrothermal system had a natural northwest outflow, north of the tip of the Opal Mound fault. The Mineral Mountains have very low heat flow at higher elevations (20 mW/m^2), indicating cool meteoric recharge into the mountains. There are several wells in central valley north of the FORGE deep well site where gradients of about 30°C/km occur over the depth range of 50 – 100 m depth. This implies a heat flow of 50 – 60 mW/m^2, which is low for a typical Great Basin value (90 – 100 mW/m^2). These low heat flows have been used to calculate deep temperatures (Fig. D8), but we suspect that the temperatures are hotter. In the case of the low heat flow in the Mineral Mountains, the shallow gradients are used for temperature calculations at 1 km depth, but temperatures are not extrapolated to greater depth because of the large uncertainty.

A 3-D thermal model down to 4 km depth (Fig. D8) is based on the heat flows derived from the thermal gradient wells in combination with temperature profiles from deep exploration wells in and near Roosevelt Hot Springs. Geotherms for each thermal gradient well were constructed using the depth to granite obtained from the gravity modeling (see below), and the thermal conductivity variations with depth obtained from the Acord-1 well (Fig. D4). The maximum temperature of 270°C in the vicinity of Roosevelt Hot Springs is limited by measured gradients (Fig. D6), but as thermal equilibrium may not have been reached, the errors could be as high as ± 10%. For the rest of the subsurface volume, contours were fitted using ESRI's ArcMap geostatistical kriging, and the mean (geostatistical) error in the contouring ranges ±12 to 14°C.

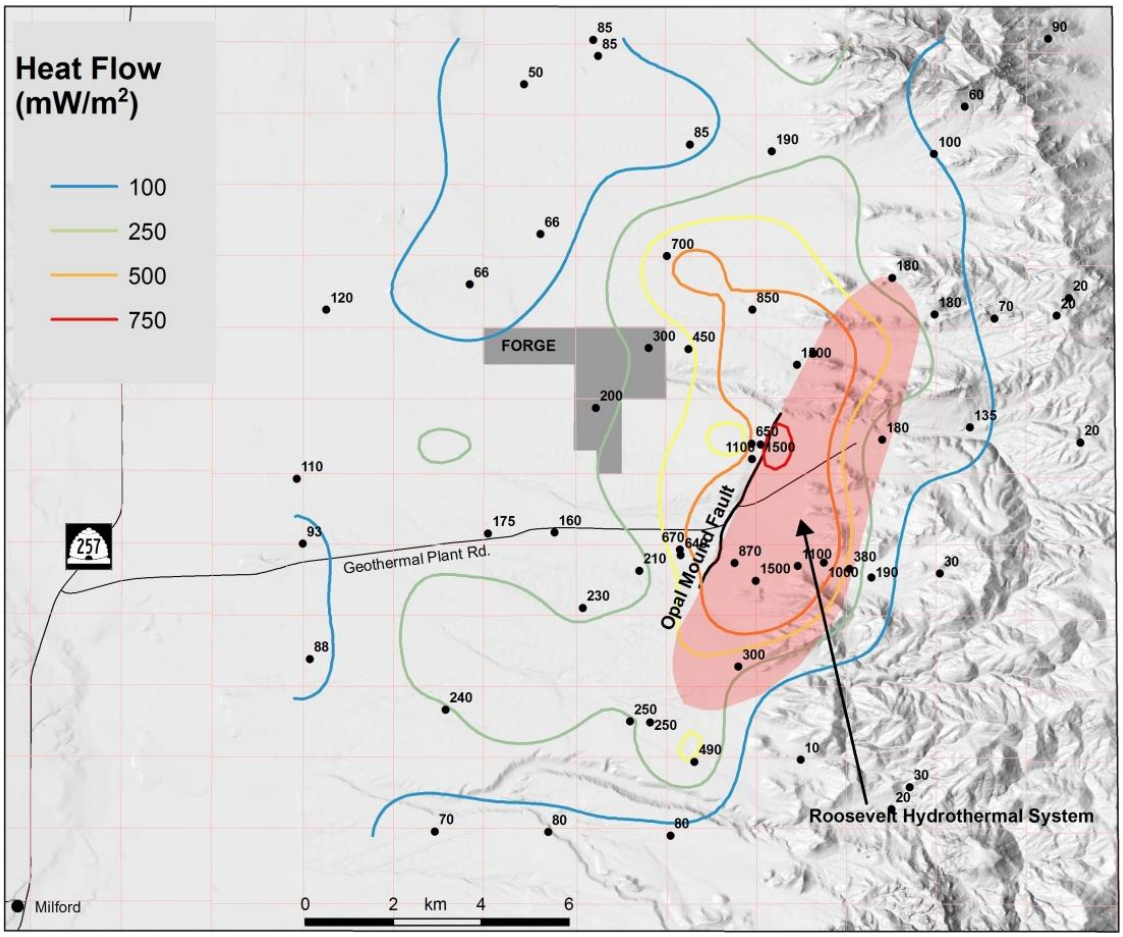

Figure D7. *Contours in conductive heat flow derived from wells around the Roosevelt Hydrothermal System (mW/m^2). Most values are from the gradients in wells less than 200 m deep. Very high heat flows over the hydrothermal system reflect high temperature gradients overlying upflowing hot water, which at shallow depth is constrained by boiling-point-for-depth conditions. West of the hydrothermal system (the Opal Mound fault) the thermal regime is conductive at depth and follows a pattern of decreasing heat flow towards the west.*

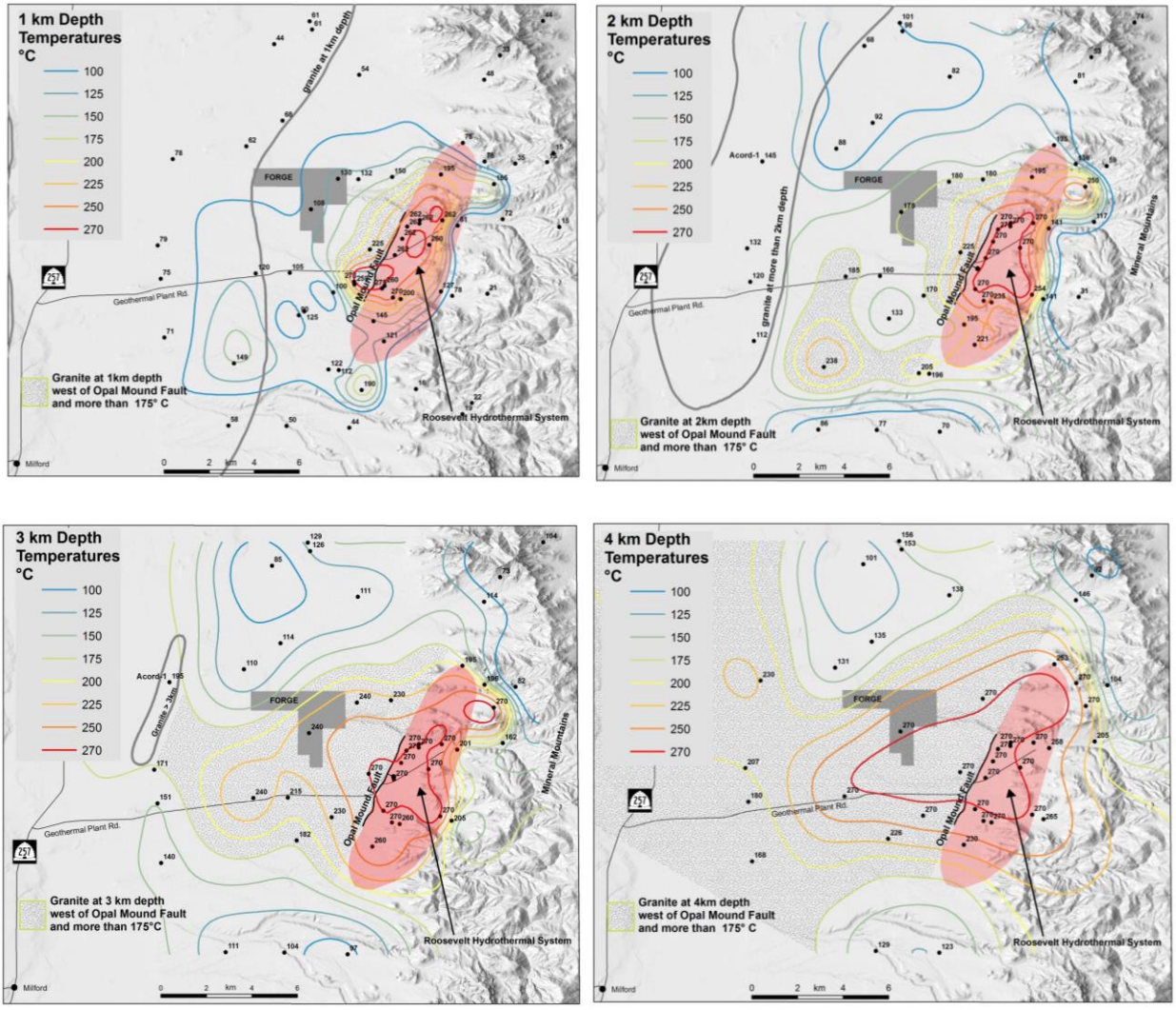

Figure D8. *Contours of temperature at 1, 2, 3, and 4 km depth derived from observations in deep wells and geotherms fitted to thermal gradient wells. Temperature contours have been smoothed using kriging options in ESRI's ArcMap software, and typically have a geostatistical mean uncertainty of ± 13°C depending on adjacent well data. The stipple highlights where granite at that depth is hotter than the minimum reservoir temperature constraint of 175ºC. On the 3 km map, granite hotter than 175ºC extends significantly west and north of Acord-1, but has not been shown because of inadequate well control. The red shading shows the extent of the Roosevelt Hydrothermal System based on pressure measurements in deep wells.*

Integration of all temperature gradient data shows that a large area of anomalously high conductive heat flow, covering about 100 km^2, surrounds the FORGE deep well site (Figs. D7 and D8). The total volume of crystalline basement rock having temperature >175ºC down to 4 km depth is more than 100 km^3. The Opal Mound fault forms the eastern boundary this thermal regime and, as discussed below, marks the transition to theRoosevelt Hot Springs where convective heat flow prevails and covers a much smaller area of ~10 km^2.

E. GEOPHYSICS

Gravity and magnetotelluric data were collected and compiled using stations shown in Figure D8. Aeromagnetic data, teleseismic data, and geophysical well logs (52-21, GPC15, and Acord-1) are part of the legacy datasets.

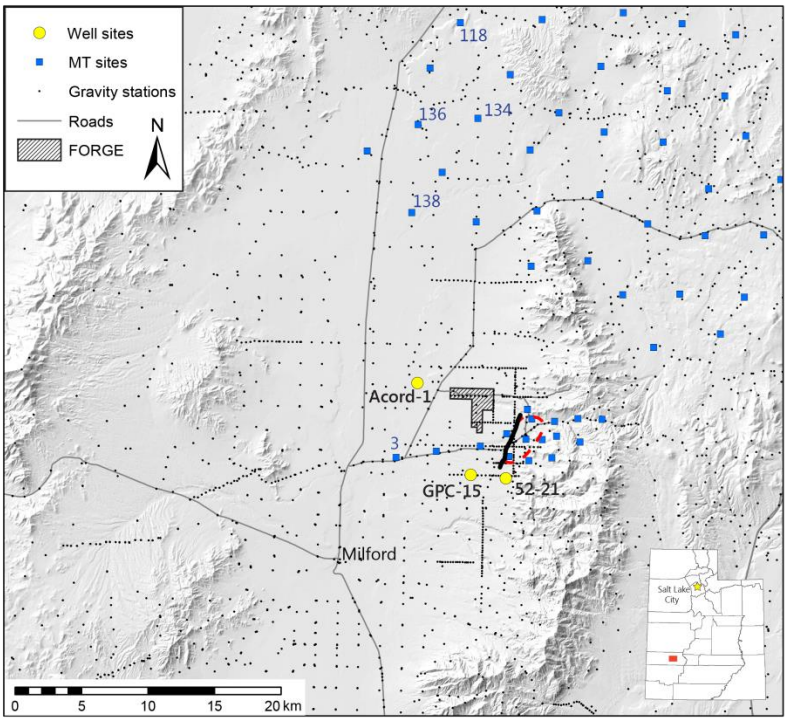

Figure D9. *Map showing sites of gravity and MT stations*

E.1 Gravity Data

New gravity measurements in the vicinity of the FORGE site were previously reported by Hardwick and Chapman (2012) and Hardwick (2013). The complete gravity dataset for this area represents a combination of data collected by the Utah Geological Survey (UGS) and legacy data from the national data repository. All data were reprocessed for terrain corrections and a Complete Bouguer gravity anomaly (CBGA) was calculated according to the methods of Hinze et al. (2005), see Hardwick (2013). A 20 mGal low in the CBGA is located in the central part of the Milford valley, which indicates that there is a significant thickness of low-density basin-fill material (Fig. E1).

The large gravity low in the southeast corner of Figure E1 has a regional effect on the local gravity field. The amplitude is sufficient to mask local gravity anomalies and signatures in the Mineral Mountains, as well as shift the inferred center/axis of the basin to the southeast. The wavelength suggests this regional anomaly is associated with a large structure deep in the crust/upper mantle beneath the transition zone between the physiographic provinces of the Basin and Range and the Colorado Plateau (Wannamaker et al., 2008). After computing regional

isostatic gravity corrections for the area (a function of crustal root thickness based on surface elevation), the deep anomaly requires additional compensation. For example, Becker and Blackwell (1993) used a low-density body representing a pluton at a depth of 5 km below the surface in their model. We believe that the structure is a regional feature of the transition zone, requiring a deeper, and larger, low-density body on the eastern boundary of our study area.

The basin gravity is shown in four east-west profiles (A, B, C, and D; Fig. E1) spanning from exposed bedrock on opposite sides of the valley. From these transects we approximated a linear correction of the gravity data and proceed to 2-dimensional (2D) modelling using the Semi-Automated Marquardt Inversion code (SAKI) (Webring, 1985). Milford basin is primarily trough-shaped, with the northern end being wider than the southern end.

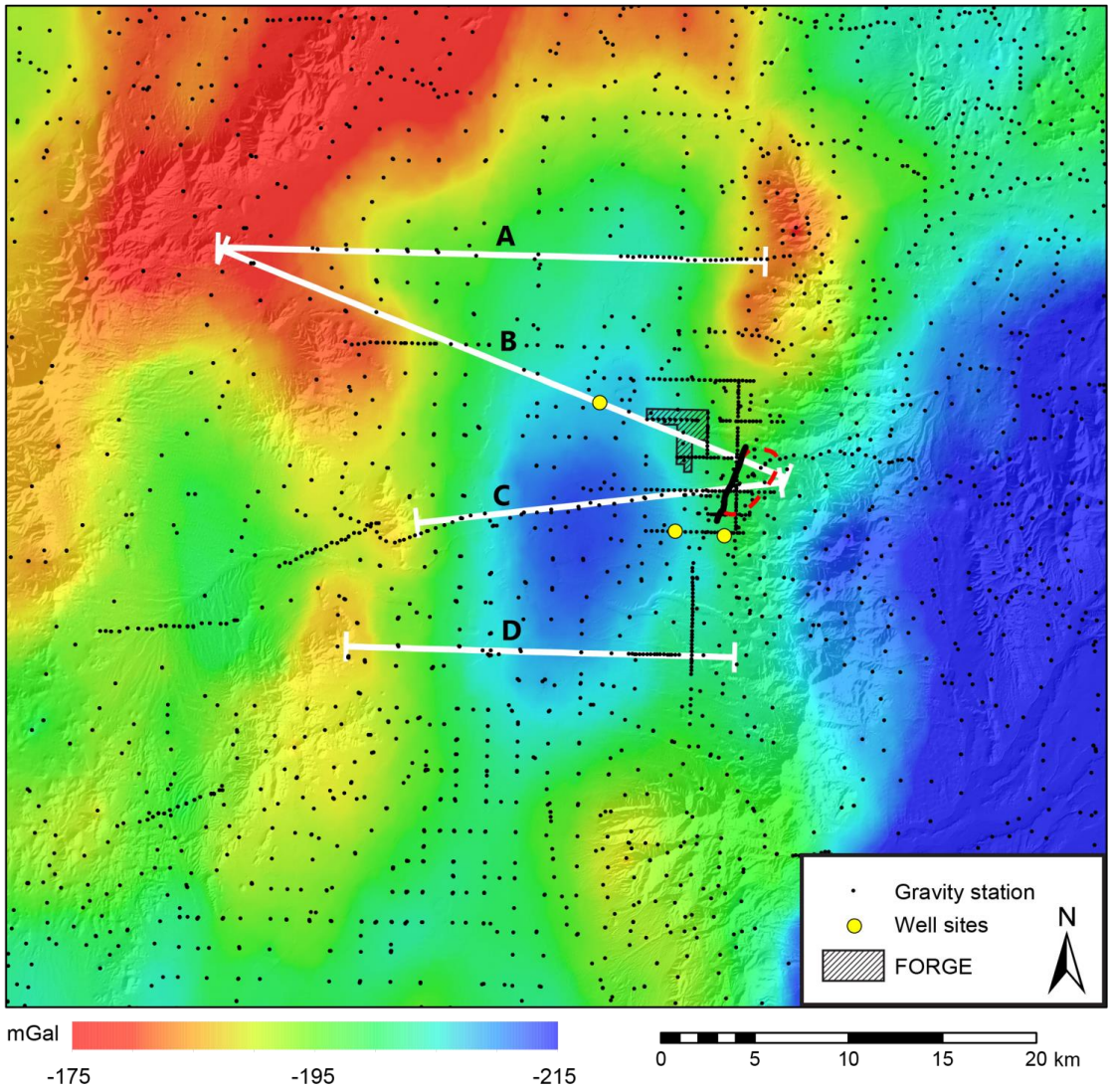

Figure E1. *Complete Bouguer gravity anomaly map for the Milford valley. Transects for 2D gravity models (A, B, C and D) are shown as white lines. The black shaded area indicates the location of the FORGE deep well site, the heavy black line is Opal Mound fault, and the red dashed line is the Roosevelt Hot Springs hydrothermal system.*

Initial models were created using a single layer of average basin fill density to establish a general shape of the basement. From the initial model, the basin fill was differentiated into a maximum of six density layers (increasing density with increasing depth) derived primarily from the density and porosity logs of the Acord-1 well (Fig. E2). The Acord-1 well penetrates 3.1 km of basin fill before reaching the basement and has a total depth nearing 3.9 km. Well data are used on transects, where available, to constrain basin-fill thickness and to augment densities for the basin fill layers in the models (Fig. E2). Figure E3 shows transects A, B, C, and D where the basin-fill density contrasts range from -0.1 to -0.65 g/cm^3 with respect to bedrock density (2.7 g/cm^3) to model the 20 mGal gravity signal.

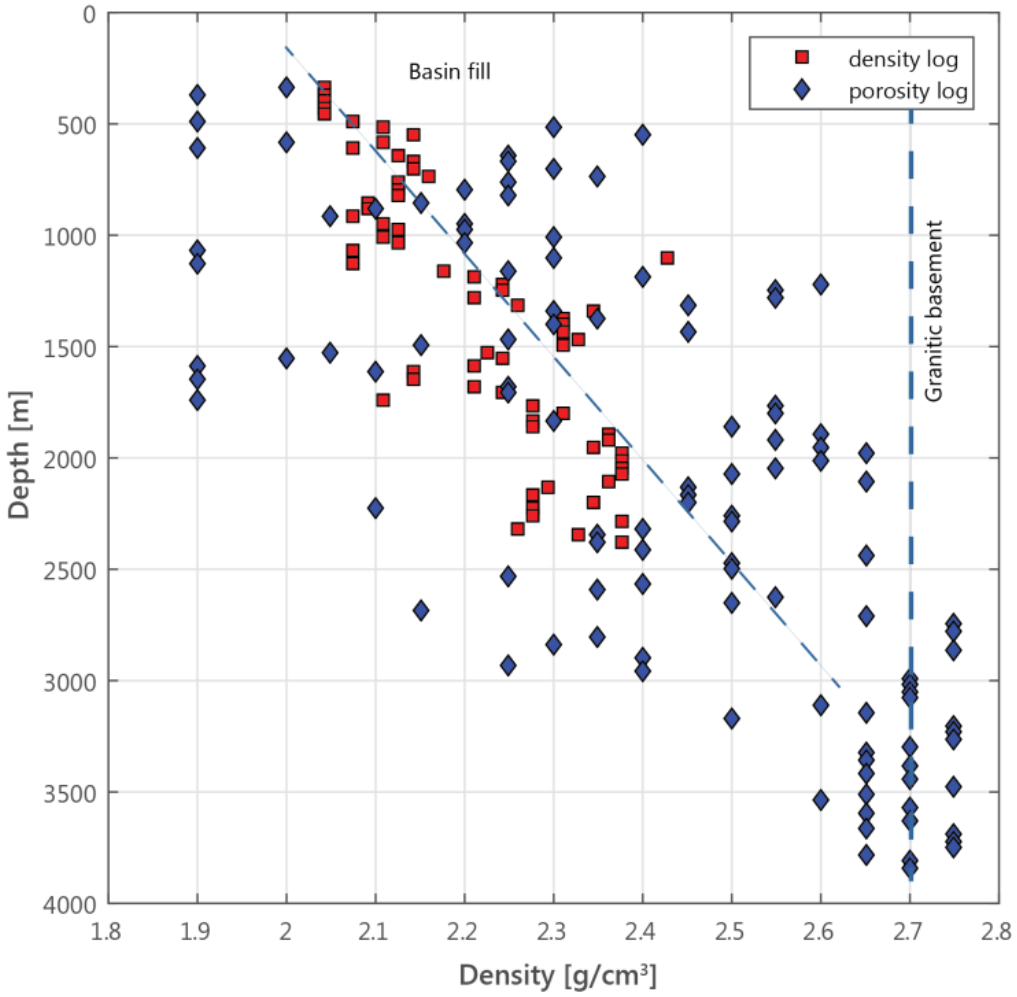

Figure E2. *Plot of density values from downhole log data of the Acord-1 well.*

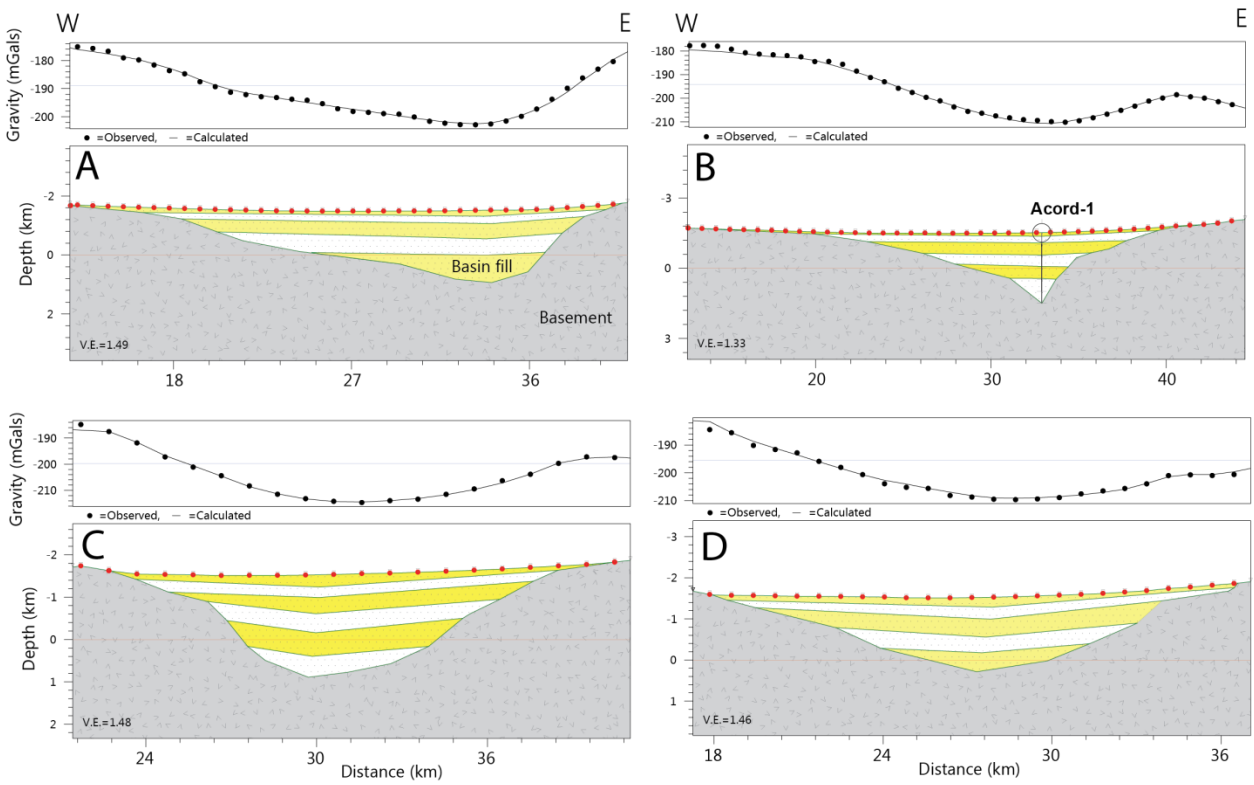

Figure E3. *Models of the gravity transects A, B, C, and D (Fig. E1). Yellow and white layers are basin fill and gray is basement.*

E.2 Magnetotelluric Data

Magnetotelluric (MT) data were acquired by the UGS in 2012 and 2014 for geothermal studies in sedimentary basins (Hardwick and Chapman, 2012, Hardwick, 2013, Hardwick et al., 2015). These data are used to estimate the characteristic electrical resistivity properties and to provide information regarding the structure and geometry of the Milford basin. Of the existing MT stations, sixteen are in, or adjacent to, the Milford basin, and the data from these are used to characterize local resistivity values and constrain the depth-to-basement. The data were analyzed using the phase tensor method of Caldwell et al. (2004). Figure E4 shows the MT response (right panel) and phase tensors (left panel) for MT stations 118, 134, 136, 138, and 3. The data were prescreened to ensure that they meet the appropriate criteria for the method. The quality of the data was checked and the dimensionality was assessed to ensure the data were suitable for 1-dimensional (1-D) modeling using the phase tensor method.

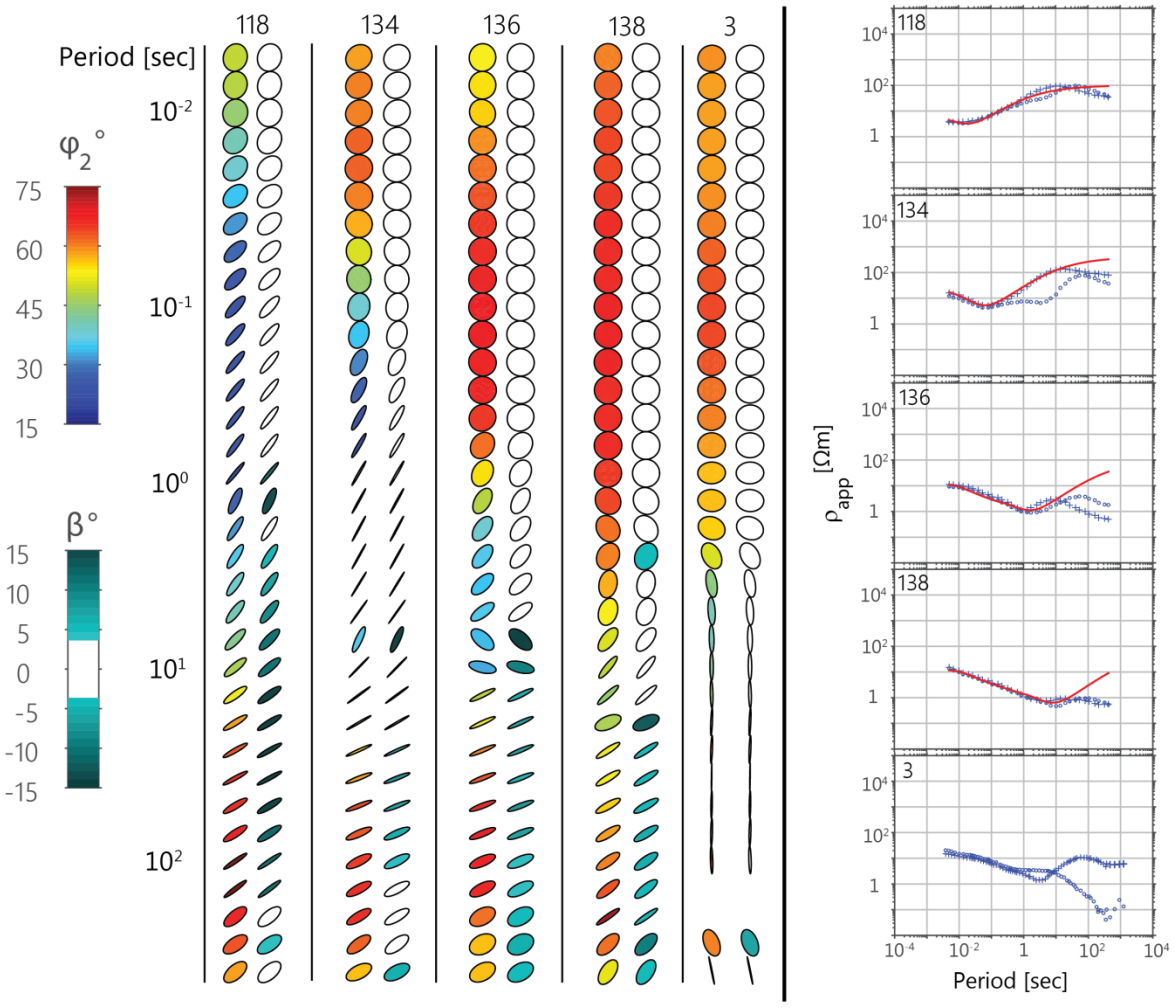

Figure E4. *MT Phase tensor profiles plotted by period for stations (locations in fig. D9) used in the 1-D models (left panel) and MT response data (right panel). Phase tensor colors in the left-hand column for each station (118, 134, 136, 138, 3) are the geometric mean of the minimum and maximum phases and the right-hand column shows the skew parameter. In the MT response plots, open circles are TE (transverse electric) mode, crosses are TM (transverse magnetic) mode, and red curves are 1-D forward models.*

For each station (Fig. E4), the small variation and smooth transitions by period indicate the data is continuous and of high quality, with the exception of station 3 beyond a period of 1 second. The phase tensors in the left-hand column for each station are colored according to the geometric mean of the minimum and maximum phases, which represents the conductivity gradient. Low phase values indicate a transition to resistive material (bedrock), whereas high phase values indicate conductive material (clays, saline pore fluids, etc.). The shape of the phase tensor indicates the dimensionality of the data. While circular tensors imply 1-D, elliptical tensors imply 2-D and 3-D conditions with the major axis of the ellipse indicating the geoelectric strike direction (90 degree ambiguity is resolved by external information such as geologic structures or gravity data). The right-hand column of each station is colored according to the skew (β) parameter. The skew value is a way to determine when dimensionality transitions from 2-D to 3-

D. Phase tensor ellipses that are uncolored ($|\beta| \leq 3°$) are generally accepted as the boundary of quasi-2-D conditions (as suggested by Booker, 2014). In this 1-D case, we are limited to using periods of the MT data where phase tensors indicate 1-D dimensionality.

The 1-D MT models of the station data (Fig. E4) permit estimates of the depth to basement of 120, 250, 710, and 1130 m for stations 118, 134, 136, and 138, respectively. Station 3 could not to be modeled as the longer period data are ambiguous. This has been observed in MT data from other deep basins in Utah and is thought to be the effect of thick accumulations of very conductive basin sediments extending to the surface. These situations require special treatment in 2-D and 3-D, and possibly more MT measurements in the vicinity will resolve the deep structure. Station 3 phase tensors do, however, have a very similar signature to station 138 for shorter periods (> 1 second). In general, the simplified best-fit 1-D models use 10–20 Ωm for the near surface sediments, 2–3 Ωm for the deeper basin fill, and 80–200 Ωm for the basement rocks.

E.3 Basin model

Geophysical data, their respective models, and well data were used to construct a pseudo 3-D basement-depth model for the Milford valley basin (Fig. E5). Depth information from four 2-D gravity cross-sections and sixteen 1-D MT models were combined with a zero-depth boundary to serve as control points for the 3-D basin model. MT station data were analyzed and then modeled in 1-D and used to verify 2-D gravity models along transect lines and to help constrain basement depth in parts of the Milford valley where no well data are available.

The data reveal a profile that reflects a basin within a basin. The center is steep walled and V-shaped, and the axis is oriented north-south, perpendicular to Basin and Range extension. Outwards and upwards, the basement contact flattens to form continuous gently dipping ramps. Beneath the area of the FORGE deep drill site, the depth to crystalline basement ranges from about 300 m on the eastern boundary to 1000 m on the western boundary. The depth to basement is about 500 m near the deep drilling site. The deepest part of the basin is close the Acord-1 well, which is the only deep control point in the middle of the basin.

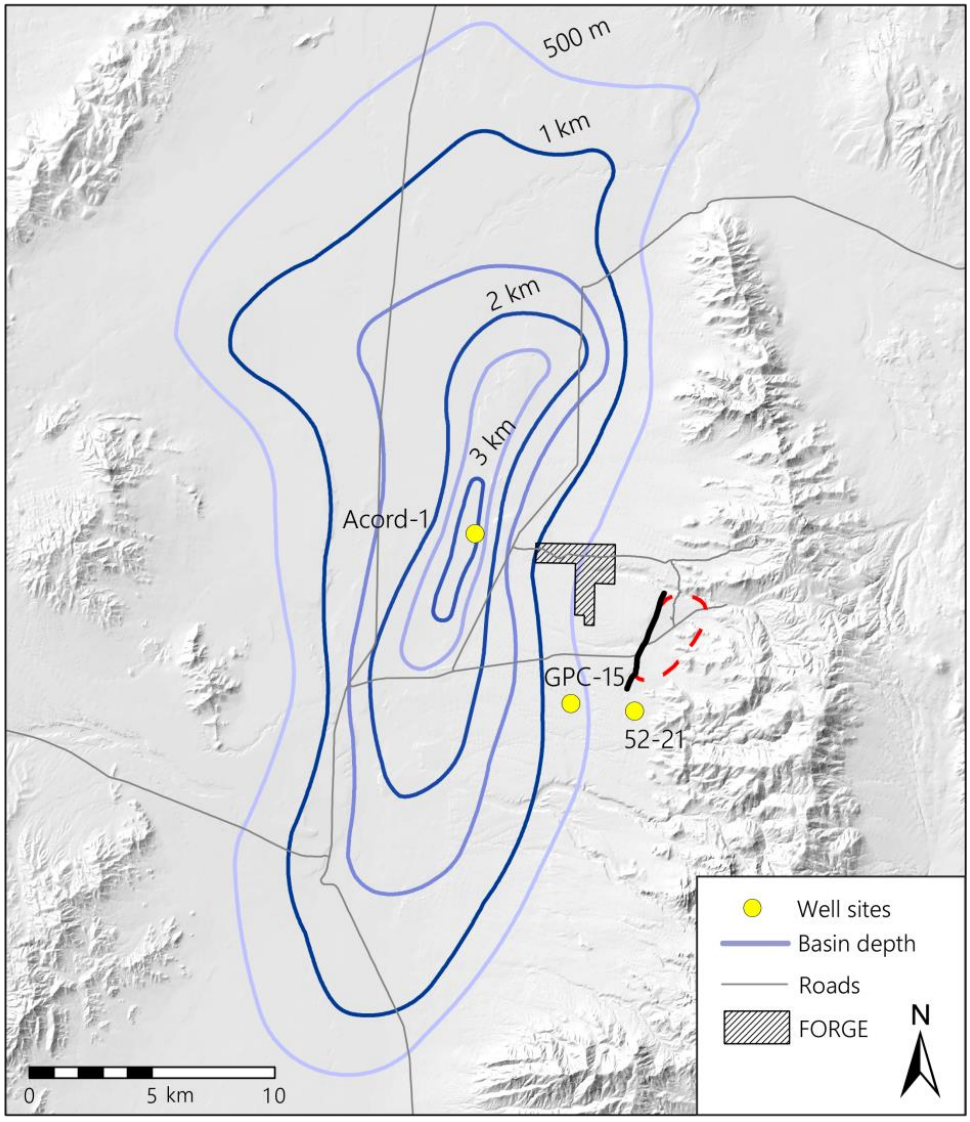

Figure E5. *Map of the basin depth model derived from geophysical data. The black shaded area indicates the location of the FORGE deep well site, the heavy black line is Opal Mound fault, the red dashed line is the Roosevelt Hot Springs hydrothermal system.*

E.4 Other Geophysical Data

Other geophysical data relevant to determining the geophysical characteristics of the Milford area include aeromagnetics, teleseismic, and downhole geophysical logs. A low-level aeromagnetic survey over the region with lines spaced one-quarter mile apart and draped at a nominal 330 m above the terrain was flown for the University of Utah in 1978 (Carter and Cook, 1978). The International Geophysical Reference Field was removed to produce residual anomalies and a reduction-to-pole technique was used to remove bipolar effects (Fig. E6; Carter and Cook, 1978). The plutonic rocks cropping out in the Mineral Mountains and the mid-Tertiary volcanic rocks are relatively magnetic compared to the Paleozoic outcrops to the north and south and the buried granite in the valley. Quaternary rhyolite flows, immediately east of Roosevelt

Hot Springs, appear reversely magnetized. The weak magnetic signature over the FORGE deep well site is due to the great depth to the relatively magnetic granite compared to the elevation of the aeromagnetic survey.

Robinson and Iyer (1981) used a teleseismic survey to assess the nature of the heat source of Roosevelt Hot Springs. A region of relatively low-velocity material (Fig. E6) appears to extend from the upper mantle to depths of about 5 km beneath the Mineral Mountains, suggesting abnormally hot temperature and a small fraction of partial melt.

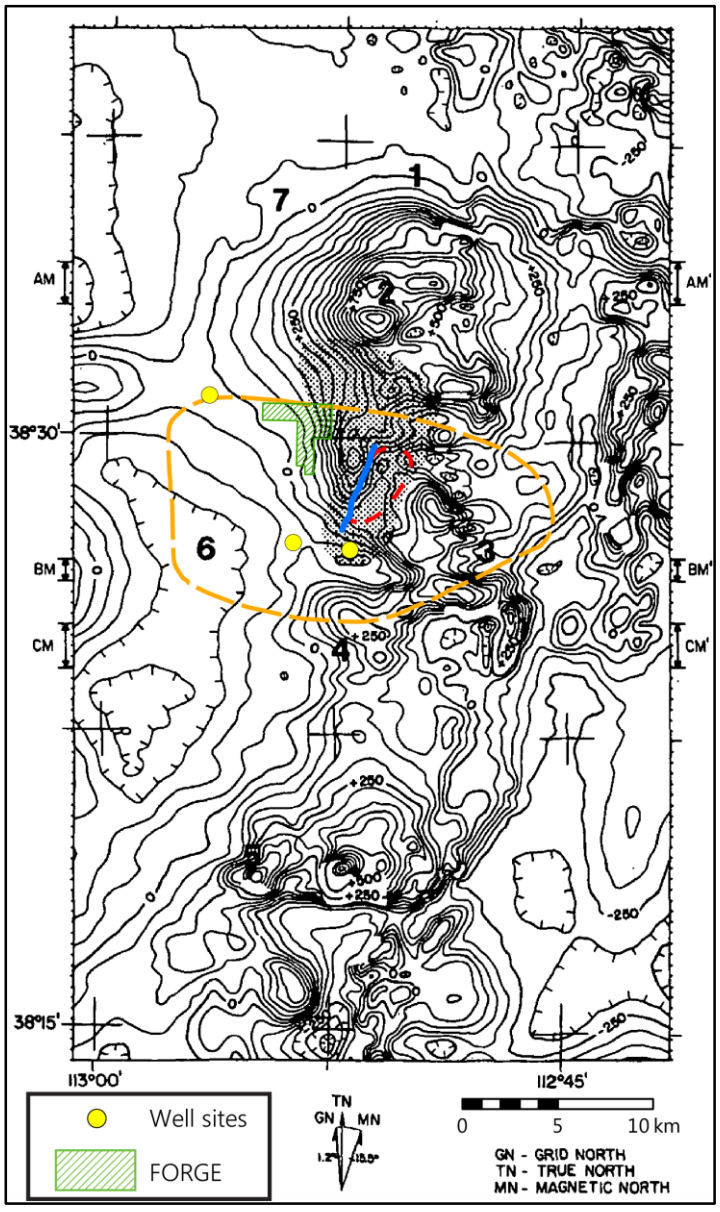

Figure E6. *Residual aeromagnetic anomaly, reduced to pole, modified from Carter and Cook (1978; gammas; 330 m draped). Orange dashed line is the -2% seismic velocity anomaly at 5–15 km depth from Robinson and Iyer (1981). The green shaded box shows the FORGE deep well site, the heavy blue line is Opal Mound fault, and the red dashed line is the Roosevelt Hot Springs hydrothermal system.*

Geophysical logs of wells in the Milford valley provide information regarding the physical properties of the basin fill and the bedrock material and show how those properties change with depth. This information is relevant for comparing layers and for creating and evaluating models based on geophysical data (density for gravity, resistivity for electromagnetics). Logs from wells GPC-15, 52-21, and Acord-1 are illustrated in Figures E7 through E9.

Figure E7 shows a set of logs from well GPC-15, which is located 3 km south of the FORGE site. GPC-15 was entirely completed in basin-fill material where interval transit times range between 75 to 125 µs/ft, the resistivity is <10 Ωm, and the bulk density is around 2 g/cm^3.

Figure E8 shows parts of a set of logs from well 52-21, 4 km southeast of the FORGE site. The interval shown for well 52-21 is entirely in basement rock where the interval transit time is 50 µs/ft and the bulk density is between 2.5 and 3.0 g/cm^3. The resistivity for the same interval of bedrock is 100 Ωm (Glenn and Hulen, 1979).

Figure E9 shows a set of logs from the Acord-1 well, which penetrates 3100 m of basin fill and terminates in bedrock at about 3900 m. The interval transit time deep in the basin fill varies from 50 to 130 µs/ft, whereas in the bedrock it is confined to approximately 50 µs/ft. The resistivity values for basin fill range from 1 to 20 Ωm, while bedrock values range from 60 to 200 Ωm. The bulk density in the basin fill is between 2.0 and 2.5 g/cm^3 and the basement values are around 2.7 g/cm^3. In the deeper section of the density log, the data are noisy, which diminishes their quality.

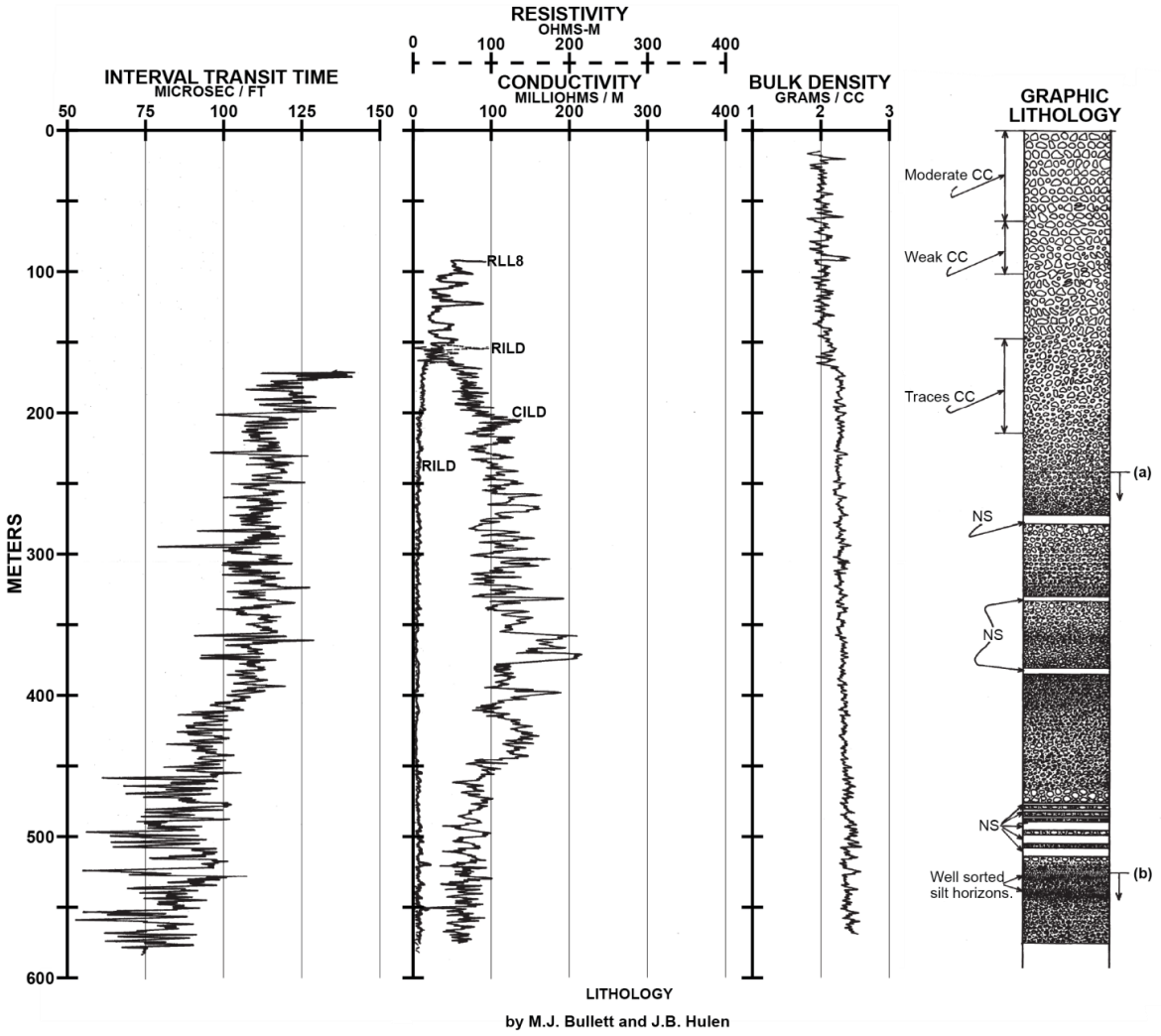

Figure E7. *Downhole geophysical logs of well GPC-15 (modified from Glen and Hulen, 1979). Logs show physical properties of basin-fill sediments in the FORGE study area. Note that the labels for the electric logs are incorrect (probably on the original logs as well). The electrical logs for other wells in Glenn and Hulen (1979) suggest that the resistivity range is 0–100 Ohms-m and conductivity units are mS/m.*

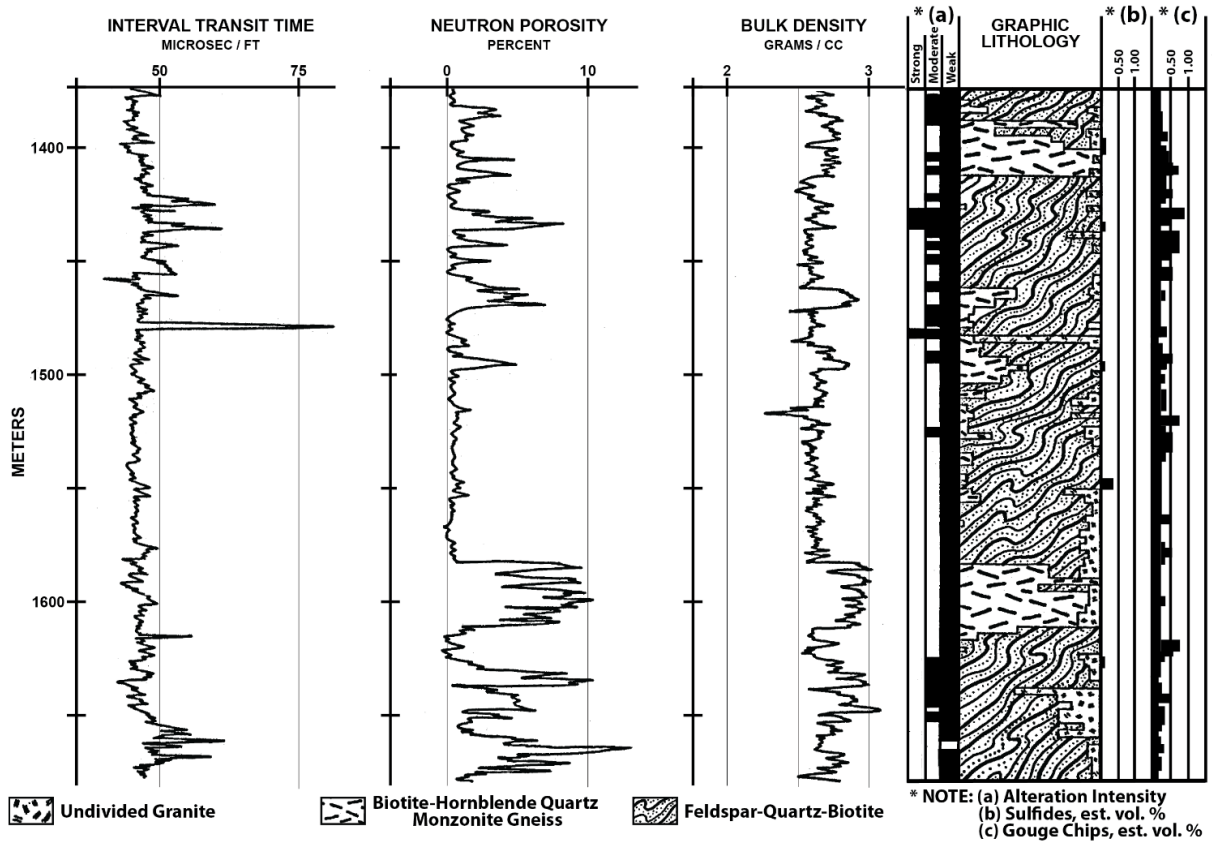

Figure E8. *Downhole geophysical logs of well 52-21 (modified from Glen and Hulen, 1979). Logs show physical properties of bedrock in the FORGE study area.*

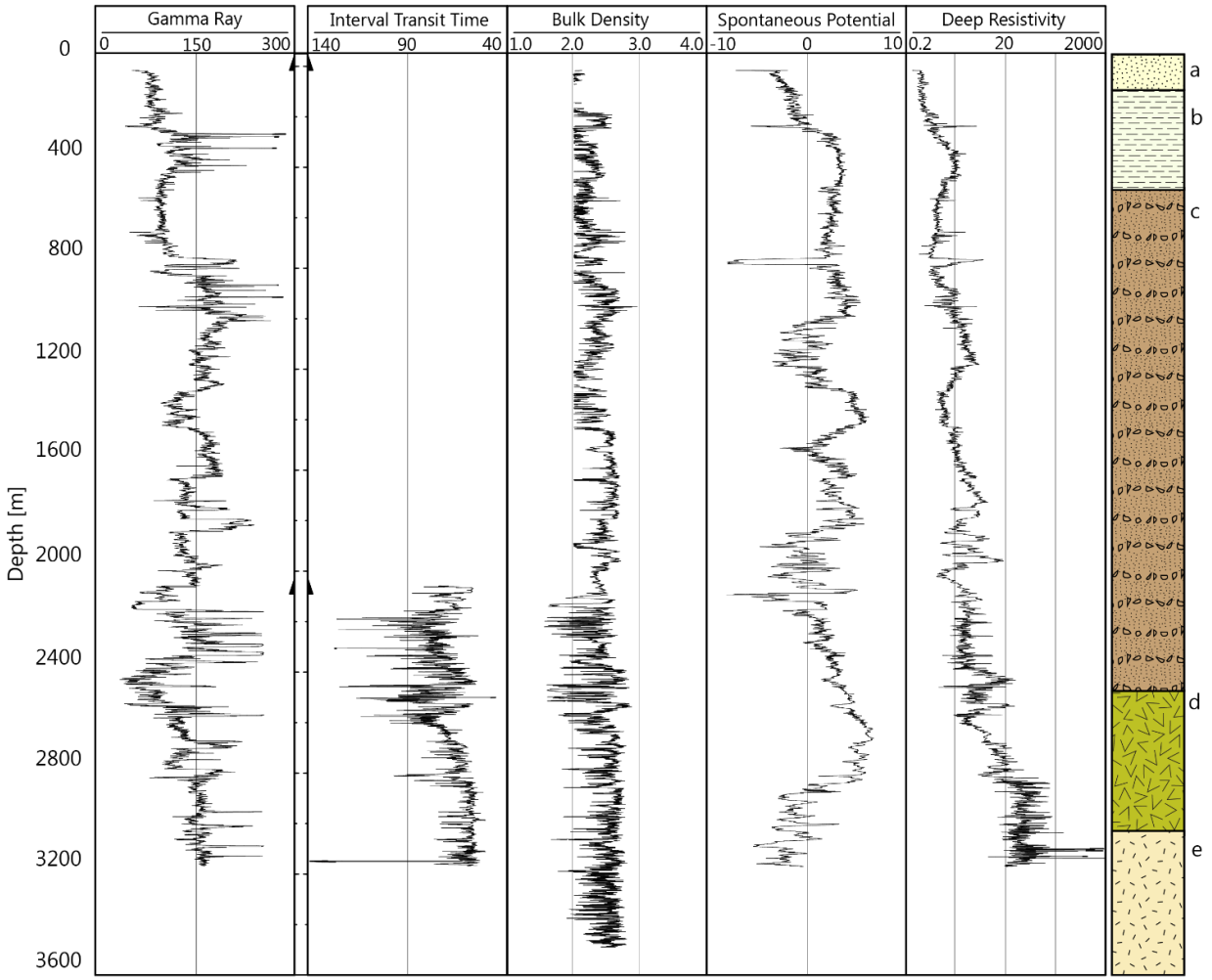

Figure E9. *Downhole geophysical logs of Acord-1 well. Logs show physical properties of basin fill and bedrock (3100 m) in the FORGE study area. The stratigraphic column is from the interpretation of Hintze and Davis (2003). Layers are as follows: a) surficial valley fill, b) claystone, c) tuffs and tuffaceous sediments, d) andesite, e) granite.*

F. SEISMICITY AND STRESS DIRECTION

The University of Utah Seismograph Stations (UUSS) installed a seismic station (NMU) 3 km (2 mi) north of the RHS in 1987. Improved resolution of the station network occurred in 2009, and in late 2015, a three-component broadband seismometer was installed 3 km south of the RHS (FORU, Fig. F1) and incorporated into the network. The estimated minimum magnitude of complete recording for the study area is M 1.5 (Pankow et al., 2004). The new station is expected to lower the detection threshold for future events in the FORGE area, and will allow for better understanding of source mechanisms. Preliminary analysis of the seismicity (occurring from 1988 - 2015) shows no events locate near the FORGE site and that seismicity rates are low in this region.

Seismic events in the UUSS catalog in the Milford region have been relocated using an improved velocity model. Two clusters of events are evident: one near Milford, and the second 10 km northwest of Milford (Fig. F1). More diffuse seismicity occurs beneath the Mineral Mountains. Waveform analysis and event timing indicates that events in the northwest cluster (outlined by the blue ellipse in Fig. F1) are the result of quarry blasts, from the quarry mines in the area, not tectonic earthquakes. Evidence for this conclusion includes the limited and small magnitudes (M 0.49 to 2.05), the shallow depths (above 2.5 km below sea level), the restricted timing (all events occur during daylight hours; Fig. F1), and the highly correlated waveforms implying a similar location and source mechanism. The second cluster outlined by the green ellipse (Fig. F1) is located near the Milford airport and not far from the M_W 4.1 1908 Milford earthquake (the largest recorded earthquake in the study area). The magnitudes in this cluster range from 0.46 to 3.87, and the events occur throughout the day without a time bias. This cluster is interpreted as being tectonic in origin.

The direction of minimum horizontal stress (T-axis, or SHmin) based on the moment tensor from an M_W 3.8 earthquake (depth 6 km) is NW-SE (Whidden and Pankow, 2012). This is close to the extension direction inferred from structural development of the Milford basin mentioned earlier. Interestingly, the focal mechanism for this event is strike-slip. A compilation of evidence from borehole breakouts from multi-arm caliper logs, the attitude of fractures, dikes and young normal faults all indicate the horizontal compressive stress (SHmax) is primarily directed N-S (170–180º) to NNE-SSW (035º) at Roosevelt Hot Springs.

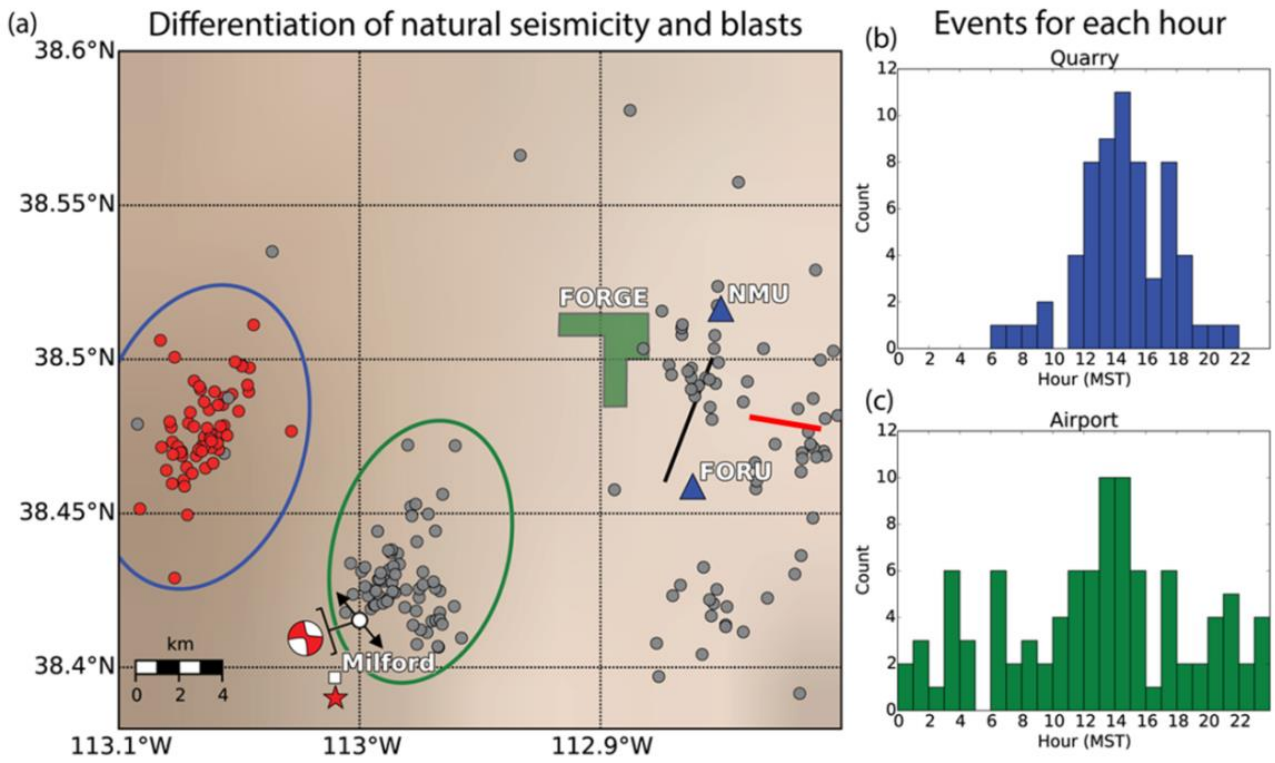

Figure F1 (a) *Compilation of seismic events in the period 1965-2012. Grey-filled circles represent natural earthquakes due to tectonic stresses, and the red-filled circles represent quarry blasts. The ellipses refer to the events within the histograms. The blue triangles are seismic stations; the green polygon represents the FORGE deep drill site. The white square represents the center of Milford, UT and the red star is the epicenter of the 1908 earthquake, magnitude 4.1. The white circle represents the April 10, 1998M_W 3.8 earthquake with T-axis and focal mechanism (displayed offset from T-axis). The red line between NMU and FORU is the earthquake swarm detected by Zandt et al. (1982). This swarm was oriented approximately west-east and shown in Figure F2. (b) shows the blasts as a function of time of day (these events occurring during daylight hours) and (c) shows that the natural seismicity occurs during all hours of the day; 62 of the 201 events displayed are blasts.*

Before production at Roosevelt Hot Springs began, a local seismic array was installed to monitor the background seismicity (Zandt et al., 1982; Nielson, 1989). From the approximate two-year period of deployment, the results indicated that there were few earthquakes M > 2. An energetic seismic swarm (1044 earthquakes M ≤ 1.5) in the period June through August, 1981 was detected. This swarm occurred east of Roosevelt Hot Springs, primarily in the Mineral Mountains, and the trend of the seismicity was mostly east-west (Fig. F1). Zandt et al. (1982) concluded that the swarm was naturally occurring and that a few of the earthquakes located on the west end of the swarm may have occurred along the Opal Mound Fault. Nielson (1989) suggested that these seismic events reflect local deviation in the regional stress field related to the hydrothermal fluid flow through Roosevelt Hot Springs system. The precise cause of the seismicity nonetheless remains poorly understood because the activity occurred outside of the seismic network and slip motions could not be determined. If this is recurring activity, the Phase 2 seismic monitoring will detect it.

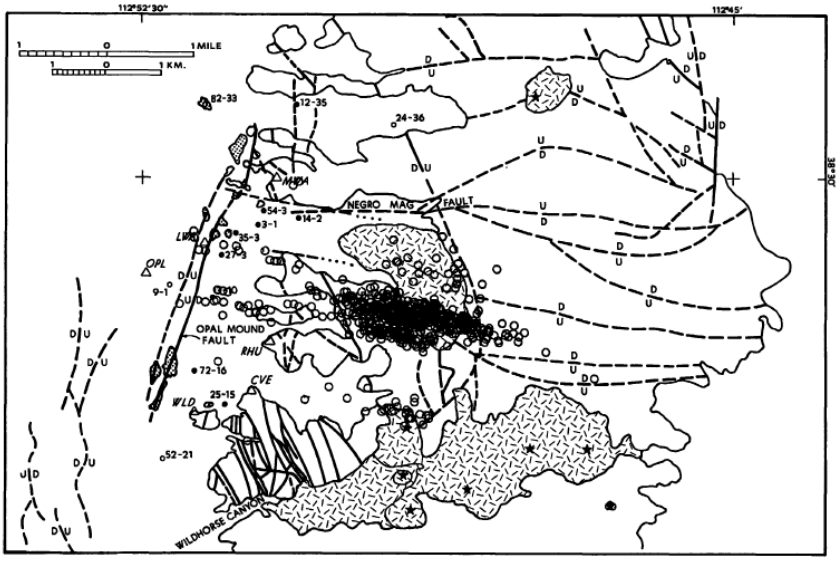

Figure F2. *Map of the faults in the Roosevelt Hot Springs and Mineral Mountains, showing the location of pre-production microseismicity along an east-west trending fault structure (Zandt el al., 1982; Nielson, 1989).*

The state of stress in the study area is constrained by analysis of: (1) Borehole breakout; (2) earthquake focal mechanisms (Whidden and Pankow, 2012); (3) geologic map data including the orientations of faults and joints (Section 9, this Task). These data indicate a largely NNE-SSW azimuth (~000-010°) of SHmax and a WNW-ESE azimuth (~090-100°) of SHmin.

Additional material is discussed under Task 1.1.3 “Update Seismicity Data”.

G FLUID GEOCHEMISTRY

Data regarding the chemical compositions of thermal and non-thermal waters across the FORGE study area are available from two datasets. Most of the data come from samples of groundwater taken mainly from shallow water wells and a few springs in the Mineral Mountains (Table G1). A second dataset comprises analyses of water and steam sampled from production wells in the Roosevelt Hot Springs steamfield (Table G2); this dataset was acquired in 2015 through DOE supported investigation of geothermal resources in southern Utah separate from the FORGE funding (e.g., Simmons et al., 2015). The compositions of groundwaters across the FORGE study area are influenced by mixing and shallow outflow of thermal water from Roosevelt Hot Springs, which flows westward through alluvium-hosted aquifer toward the center of the north Milford valley. For this reason, the chemistry and compositions of the Roosevelt Hot Springs production fluids are described first.

G.1 Roosevelt Hot Springs Production Fluids

Analysis of the compositions of pre-production reservoir waters from the Roosevelt Hot Springs (Capuano and Cole, 1982) showed that the fluid produced from well 14-2 reservoir (Table G1; Fig G1) was the hottest and most representative of the deep hydrothermal water in the system. For most of the production history, however, 14-2 has been used as an injector (Faulder 1994; Allis and Larsen, 2012). The most recent survey of production fluid chemistry (Tables G2 and G3), indicates that the reservoir fluid compositions are largely unchanged since 1984, except for effects of steam-loss and mixing with injectate (Fig. G1). These effects are the result of pressure drop in the reservoir induced by fluid production and the proximity of injection well 14-2 to reservoir (Allis and Larsen, 2012). The production-induced effects, however, are localized, and the biggest changes occur in 54-3, and to lesser extents, in 45-3 and 28-3. The enthalpy and composition of well 13-10 are unchanged over more than 30 years of fluid production.

The reservoir fluids therefore comprise near neutral pH sodium chloride waters, which contain less than 1000 mg/kg dissolved CO_2 (Table G4). The quartz-silica and H_2/Ar equilibration temperatures closely match well enthalpies, indicating a reservoir temperature close to 250° C (Table G4). Among the anions, chloride is dominant, with subordinate bicarbonate (110-285 mg/kg) and lesser sulfate (50-70 mg/kg), and among the cations, sodium is dominant (2164-2894 mg/kg), with subordinate potassium (460-563 mg/kg), and much less calcium (16-30 mg/kg), lithium (7.00 to 8.18 mg/kg) and magnesium (0.04-0.14 mg/kg).

The sources of the anions is likely to be deep seated, whereas the cations originate from water-rock interaction with country rocks and temperature controlled fluid-mineral equilibria. The Na/K and K/Mg ratios indicate relatively hot equilibration temperatures of ~300° C (Table G4), representing deep conditions (i.e. >3 km depth) in the hydrothermal system. The reservoir water compositions are saturated in aqueous silica with respect to quartz, hence the quartz-silica equilibration temperatures reflect reservoir conditions.

Preliminary geochemical modeling indicates the reservoir waters are close to saturation in calcite and anhydrite, and this result is consistent with the widespread occurrences of both minerals in hydrothermal alteration assemblages (see Fig. C4). The deep waters are also very close to

equilibrium with Na and K-bearing feldspars, quartz, chlorite, and illite (Capuano and Cole, 1982; Simmons et al., 2015).

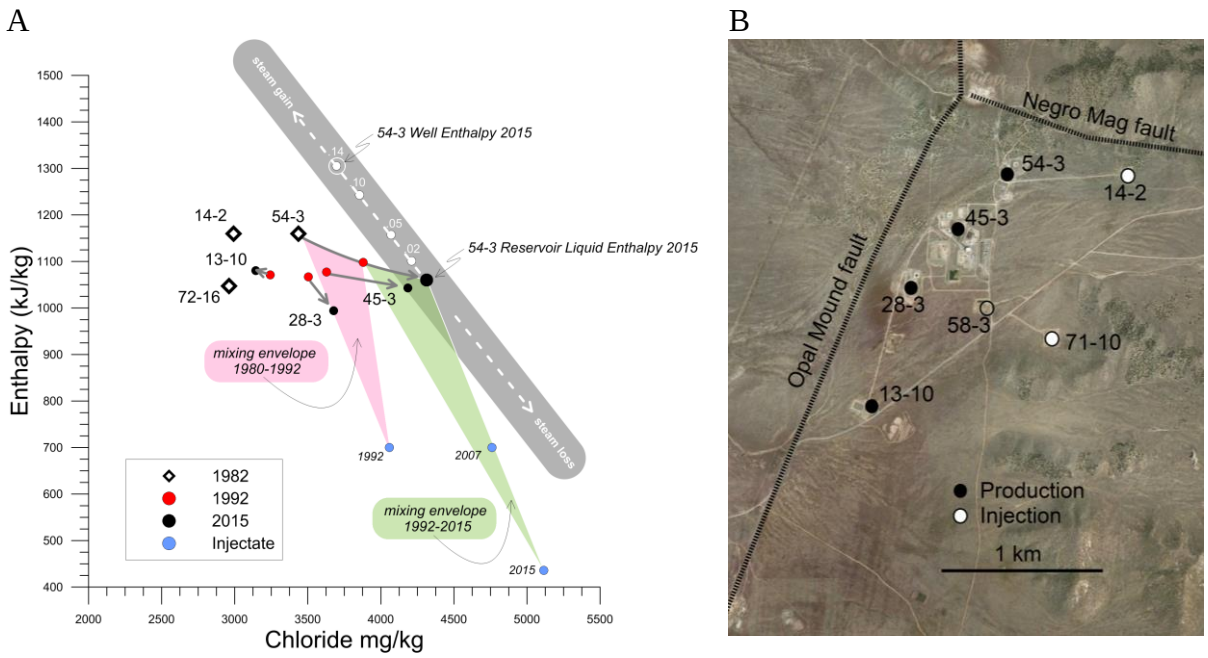

Figure G1. *A) Chloride-enthalpy plot showing the evolution of production fluids with time. B) Locations of production and injection wells at Roosevelt Hot Springs steamfield. Well 58-3 was drilled, but it was not online at the time of sampling.*

Table G1. *Compositions of shallow groundwaters across the FORGE deep well (Rohrs and Bowman, 1980; Capuano and Cole, 1982; Vuataz and Goff, 1987; Allis et al., 2015); aqueous concentrations in mg/kg (ppm) and oxygen and hydrogen isotopes in per mil.*

Site	Label	Easting[2]	Northing	date	Temp (°C)	pH	Na	K	Ca	Mg	Cl	SO4	HCO3	SiO2	B	As	δ18O	δD
14-2	14-2	339413	4262168	1/11/77	268	6.20	2200	410	7	0.08	3650	60.00	200	570	28.0	1.80	-13.90	-115.00
Roosevelt Hot Spring	RHS	338350	4262750	1/09/57	55	7.90	2500	488	22	3.30	4240	73.00	156	312	38.0	na	-12.70	-111.00
Wow 3	Wow 3	332538	4265699	19/04/83	23.5	8.28	1540	185	77	15.4	2840	3.20	90	4	21.5	na	-13.25	-112.70
South Stock Well	SSW	330036	4264716	13/08/14	19.1	7.70	919	37.5	363	70.4	2200	14.80	338	246	17.0	0.02	-13.50	-110.90
North Stock Well	NSW	333208	4269283	13/08/14	16.8	7.40	882	62.2	302	13.6	1640	22.40	828	190	12.7	0.44	-13.95	-106.90
Level # communications well	L3W	326823	4259004	13/08/14	21.4	7.90	192	11.2	93	61.6	629	2.50	63	57	1.1	<0.01	-15.08	-115.60
BLM solar panel well	SPW	329005	4256696	14/08/14	24.2	7.10	164	7.60	117	19.4	411	1.50	173	87	2.1	<0.01	-14.68	-109.90
First Wind Well	FWW	329453	4261265	14/08/14	32.4	7.90	1100	45.2	203	103	1870	172.00	580	222	11.7	0.07	-14.57	-115.90
Bailey Spring	BS	342471	4260408	19/04/83	6.1	7.20	15	2.30	32	5.60	14.2	9.30	127	56	na	na	-14.60	-106.80

Table G2. *Compositions of produced geothermal waters from Roosevelt Hot Springs, samples collected from the two-phase line near the wellhead; aqueous concentrations in mg/kg (ppm). Data collected for DOE project on Deep Sedimentary Geothermal Resources (Simmons, unpublished).*

Well	Date	*separator pressure (PSIG)*	*steam fraction (y)*	Lab pH	Li	Na	K	Ca	Mg	SiO2	B	Al	F	Cl	SO_4	HCO_3**
54-3 brine tank	Jul-15	116*	0.277	7.07	27.9	2894	544	30	0.14	538	17.1	0.3	7.5	5114	77	110
13-10 brine tank	Jul-15	111*	0.169	7.98	25	2164	460	17	0.04	585	13.9	0.27	7.7	3783	50	219
28-3 two-phase line	Jul-15	168	0.088	8.18	23.7	2297	477	16	0.06	581	13.6	0.08	7.2	4032	54	158
45-3 two phase line	Jul-15	167	0.115	7.66	26.2	2690	535	24	0.04	600	14.9	0.18	7	4728	66	143
45-3 brine tank	Jul-15	112	0.151	7.02	29.4	2836	563	25	0.05	587	15.6	0.22	7.9	4987	70	285

*brine tank is fed by stainless steel capillary tube the conductively cools brine from brine line to atmospheric pressure

**total carbonate

Table G3. *Compositions of produced geothermal gases from Roosevelt Hot Springs, samples collected from the wellhead; gas concentrations in mmol/mol and mg/kg (ppm). Data collected for DOE project on Deep Sedimentary Geothermal Resources (Simmons, unpublished).*

		separator pressure (PSIG)	*steam fraction (y)*	gas/steam	CO_2	H_2S	NH_3	Ar	N_2	CH_4	H_2	Air %	Total Gas
					mmol/mol								
28-3 two-phase line	Jul-15	168	0.088	1.49	1.42	0.00841	0.00008300	0.00006850	0.062400	0.0001580	0.000833	3.6	1.49
45-3 two phase line	Jul-15	167	0.115	3.313	3.28	0.02250	0.00008570	0.00016300	0.011400	0.0000064	0.002110	0.042	3.32
					ppm								
					CO_2	H_2S	NH_3	Ar	N_2	CH_4	H_2		
28-3 two-phase line	Jul-15	168	0.088		3460	15.9	0.0782	1.510	9.67	0.1410	0.00929		
45-3 two phase line	Jul-15	167	0.115		7940	42.2	0.0804	0.359	17.60	0.0568	0.02350		

Table G4. *Roosevelt Hot Springs well enthalpies, reservoir chloride and CO_2 concentrations, and equilibration temperatures using quartz-silica, Na-K, K-Mg, H_2-Ar, and CO_2-Ar geothermometers (Fournier, 1991; Giggenbach, 1991).*

Well	Enthalpy	Cl (mg/kg)	CO2 (mg/kg)	T-Qtz °C	T-Na/K °C	T-K/Mg °C	T H_2/Ar°C	T CO_2/Ar°C
54-3	1305	3697		230	288	302		
28-3	994	3677	304	258	298	321	251	309
13-10	1080	3144		250	301	333		
45-3	1043	4184	913	258	294	344	252	261

G.2 Groundwater Compositions across the FORGE Deep Drill Site

Most of the groundwaters are near neutral pH and dominated by sodium and chloride, similar to Roosevelt Hot Springs reservoir waters. The predominance of chloride among the three major anions is evident in Figure G2, and the linear arrangement of data points along the Cl-HCO_3 axis reflects mixing between the Cl-rich Roosevelt Hot Springs water and a HCO_3-rich basin groundwater. The most dilute water is represented by Bailey Spring, which occurs in the western Mineral Mountains, east of the Roosevelt Hot Springs, and it is a neutral pH calcium-bicarbonate water (Table G1).

The Roosevelt Hot Spring thermal waters are characterized by high concentrations of chloride and boron (Cl/B~120), and very low concentrations of magnesium. Comparisons of these three species show that most of the waters plot in a linear array at near uniform Cl/B (Fig. G3), indicating mixing with a Mg-rich groundwater.

The stable isotope data provide further evidence of the spatial variation in groundwater compositions (Fig. G4). The Roosevelt Hot Spring reservoir water is distinct from the composition of the surface seep due to steam-loss effects (Giggenbach and Stewart, 1982), but both waters have the highest $\delta^{18}O$ values of -12.7 to -13.9‰. The composition of the surface seep (-12.7‰ $\delta^{18}O$; -111‰ δD) best represents the thermal water composition affecting shallow groundwaters. The range of $\delta^{18}O$ values in the FORGE groundwaters, -13.25 to -15.08‰, thus appears to reflect mixing with basin groundwater. The range of FORGE groundwater δD values, -106.9 to -115.9‰, however, suggest that basin groundwaters have at least two separate end-member compositions, in respect to the hydrogen isotope ratios. The isotope compositions of cold springs in the Mineral Mountains (Rohrs and Bowman, 1980) are distinctly different, generally isotopically lighter, forming a coherent linear array (Fig. G4).

Another effect related to mixing is the wide range of aqueous silica (4-570 mg/kg), which decreases due to decreasing temperature and increasing proportion basin groundwater. Arsenic concentrations range also range widely (<0.01 to 1.80 mg/kg), with the highest concentration found in the Roosevelt thermal water. This and the relatively high concentration of boron make most of the shallow groundwater non-potable for human consumption.

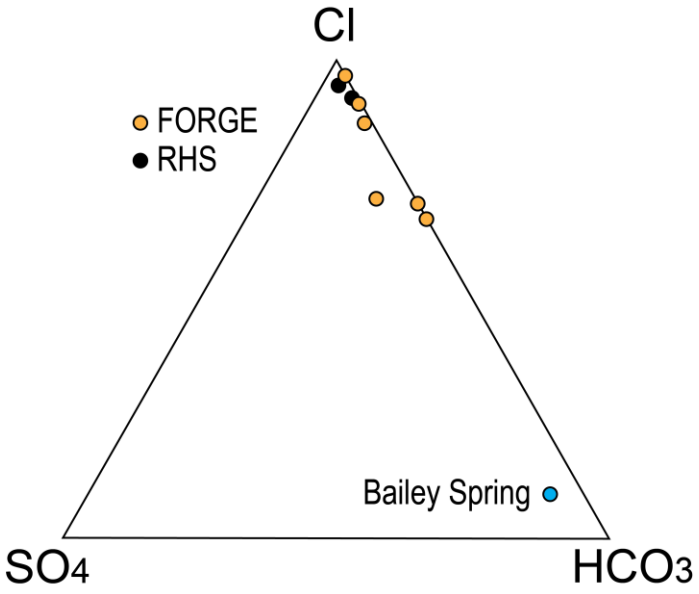

Figure 28. *Ternary Cl-HCO_3-SO_4 plot of groundwaters (Table G1) showing the distinctions between shallow aquifer waters across the FORGE deep drill site (yellow) and Roosevelt Hot Springs (RHS). Bailey Spring is located in the western Mineral Mountains*

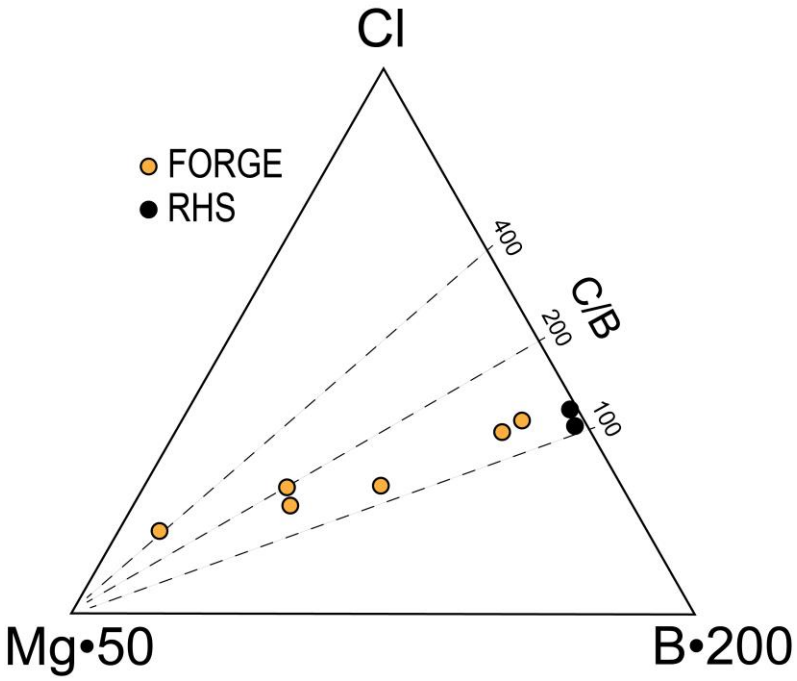

Figure 29. *Ternary Cl-B-Mg plot of groundwaters (Table G1) showing the increase in Mg at near uniform Cl/B in shallow aquifer waters across the FORGE deep drill site. Boron for Bailey Spring is lacking, hence it is not shown.*

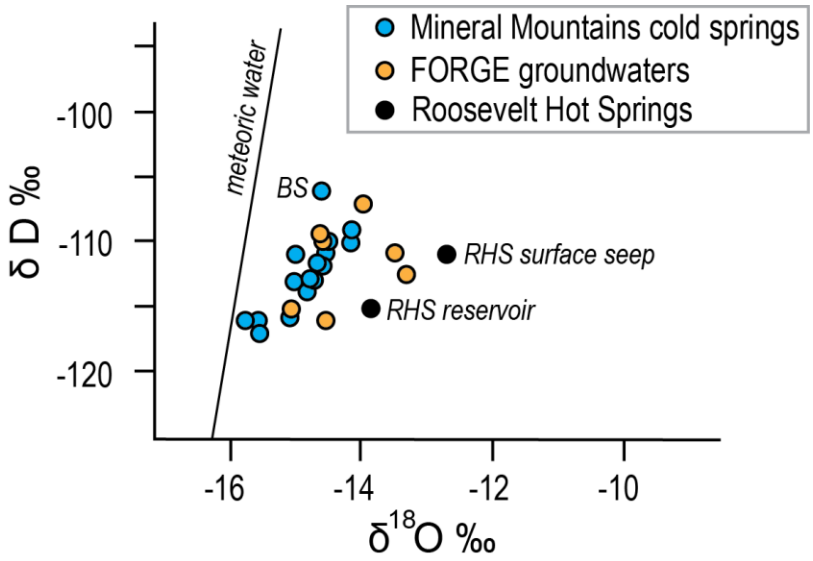

Figure G4. *Oxygen and hydrogen isotope compositions of groundwaters and cold springs in the Mineral Mountains (Table G1; Rohrs and Bowman, 1980); BS=Bailey Spring.*

H. GEOHYDROLOGY

The geohydrology is described in detail in a separate report documenting an update in the hydrologic data (see Task 1.1.1) and only the main points are summarized here. Semi-arid conditions, western sloping topography, alluvial basin fill, fractured basement rocks, steeply dipping faults, and the location of the Roosevelt Hot Springs hydrothermal system control the geohydrology of the FORGE deep well site. These are reflected in the water levels and the chemical compositions of waters from shallow and deep wells across the study area (Fig. H1; Table 1). Boiling waters associated with steaming ground and fumarolic activity north of Negro Mag wash represent the only active thermal springs, but the discharge is feeble (<0.1 kg/sec) and outflow disappears below the surface into unconsolidated gravels. At higher elevation to the east, Bailey Spring represents cold groundwater that infiltrates the Mineral Mountains.

Prior to significant production (1976-1984), deep wells east of the Opal Mound fault had a uniform pressure profile consistent with hot water, having a density of 800 kg/m^3 (Allis and Larsen, 2012; Fig. H2). The one deep well west of the Opal Mound fault, 82-33, had a pressure profile consistent with cold water with a density of 1000 kg/m^3, about 3 MPa lower than wells on the east side of the Opal Mound fault in the Roosevelt Hot Springs hydrothermal system (Faulder, 1994). Other wells west of the Opal Mound fault plot on the same pressure gradient as 82-33, including GPC-15, OH-4, and OH-5 (Fig. H2). These well data indicate the existence of a major pressure boundary, which coincides with the Opal Mound fault. Well 9-1 is located on that boundary and is unproductive, and it is used to monitor well pressure in the Roosevelt Hot Spring geothermal resource.

In summary, there are two distinct pressure regimes across the Opal Mound fault, which acts as a horizontal barrier to shallow east to west fluid flow (Allis et al., 2016), and the FORGE deep well site lies to the west of this barrier. The FORGE reservoir pressure at 2.5 km depth is expected be at 23 MPa (3300 psi). Although no pressure measurements were recorded during the drilling of Acord-1, based on its depth and temperature profile, the bottom hole pressure should be about 35 MPa (5000 psi) assuming it is successfully cleaned out.

The potentiometric surface across the study area dips west away from the Opal Mound fault and the Mineral Mountains (Fig. H1). From the Utah FORGE deep well site and to the west, the potentiometric surface forms a gentle slope that descends from 5100 to 4900 ft towards the center of the basin. Alluvial gravels host the groundwater aquifer, which is unconfined at higher elevations. Near SPW, L3W, FWW, and SSW (Fig. H1), however, the aquifer is confined beneath impermeable Quaternary claystone. East of the FORGE deep well site, the potentiometric surface slopes upward forming a sharp step between OH-4 and Roosevelt Hot Springs (Fig. H1).

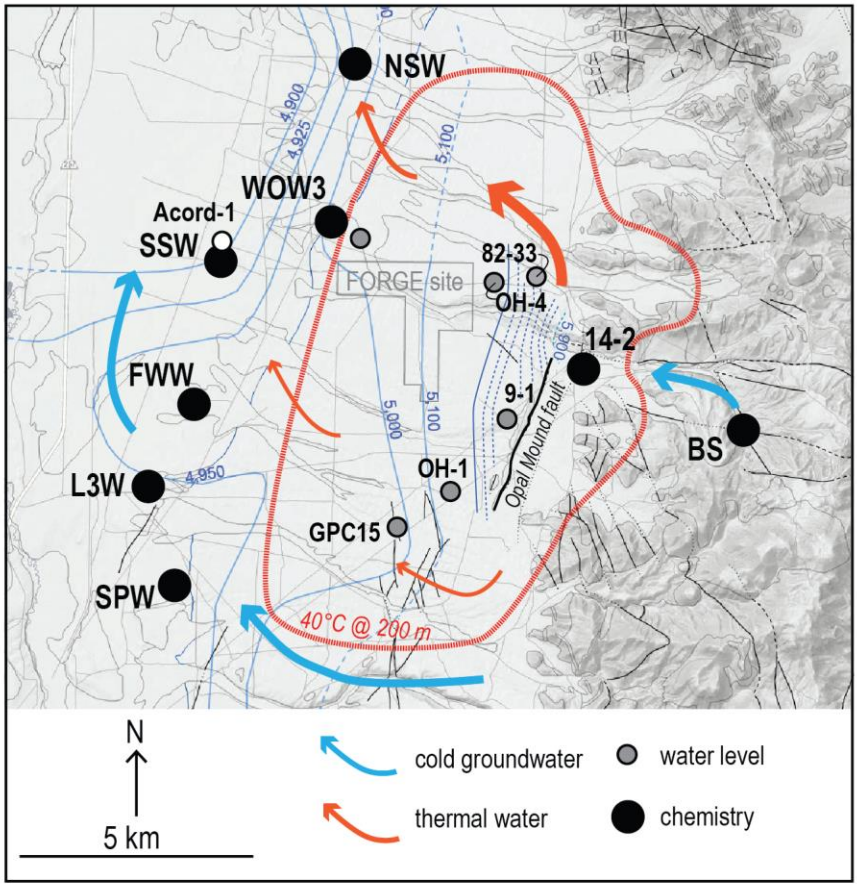

Figure H1: *Groundwater map of the Utah FORGE deep well site, Milford, Utah, showing some of the wells used to map the potentiometric surface (blue lines, elevation in feet above sea level) and water chemistry. BS is Bailey spring in the Mineral Mountains, and 14-2 is a deep well inside the Roosevelt Hot Springs system that initially produced fluid but is used for injection. Arrows indicate the approximate direction of shallow ground water (cold and thermal) flow. The red dotted line represents the 40°C isotherm at 200 m depth and the limit of the thermal anomaly in the shallow groundwater regime owing to thermal outflow from Roosevelt Hot Springs.*

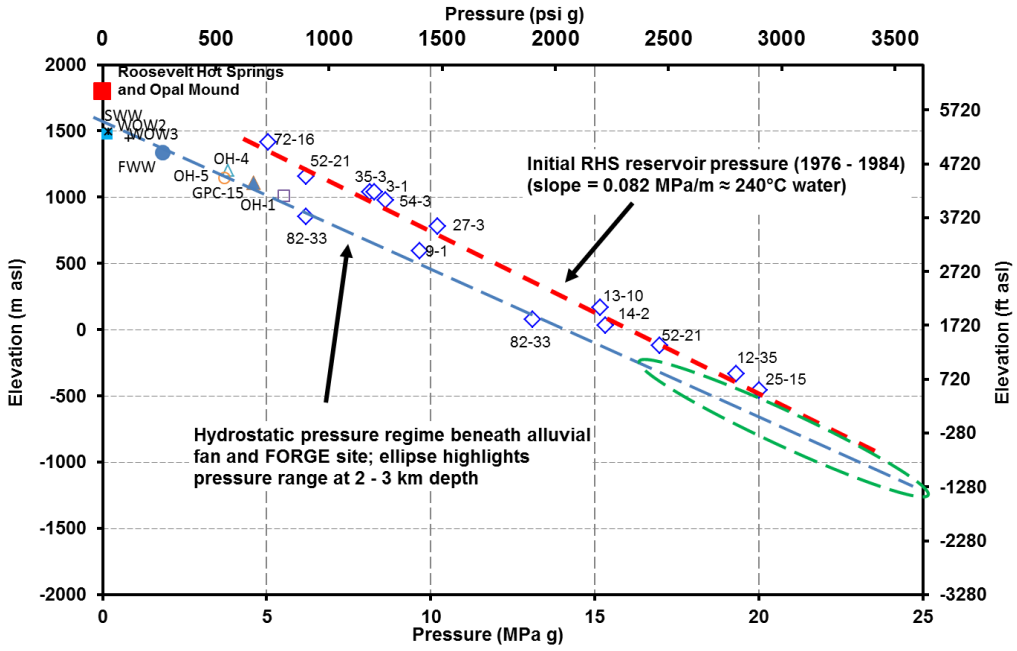

Figure H2. *Pressure trends derived from wells in the Roosevelt Hot Springs hydrothermal system and in the wells west of the Opal Mound fault. Pressures in Roosevelt Hot Springs wells represent preproduction data (Faulder, 1994). Where no other data exists, the pressure control point is assumed to be at the mid-screen depth (elevation) or at total depth.*

Geochemical data trace the outflow of thermal waters from the Roosevelt Hot Springs westward across the FORGE deep drill site, which is also supported by the trends in Figure H3. From Roosevelt Hot Springs to the groundwater wells WOW3, SSW, FWW, and NSW, the systematic decrease in chloride and boron concentrations from east to west result from mixing with relatively dilute basin groundwaters, represented by L3W and SPW; a similar linear trend is reflected in comparing chloride and oxygen isotope ratios. These results indicate that thermal water leaks into the alluvium-hosted groundwater aquifer from the intersection of the Opal Mound and Negro Mag faults, then flows downhill and to the northwest to form a large but shallow outflow that is evident in many gradient wells (Fig. H1). Another plume, probably smaller, flows west around the southern tip of the Opal Mound fault, contributing heat to the shallow thermal anomaly in the south. The groundwaters around the FORGE deep well site are chemically benign, but non-potable (Vuataz and Goff, 1987; Allis et al., 2015; 2016), and they appear to be suitable for EGS heat transfer experiments.

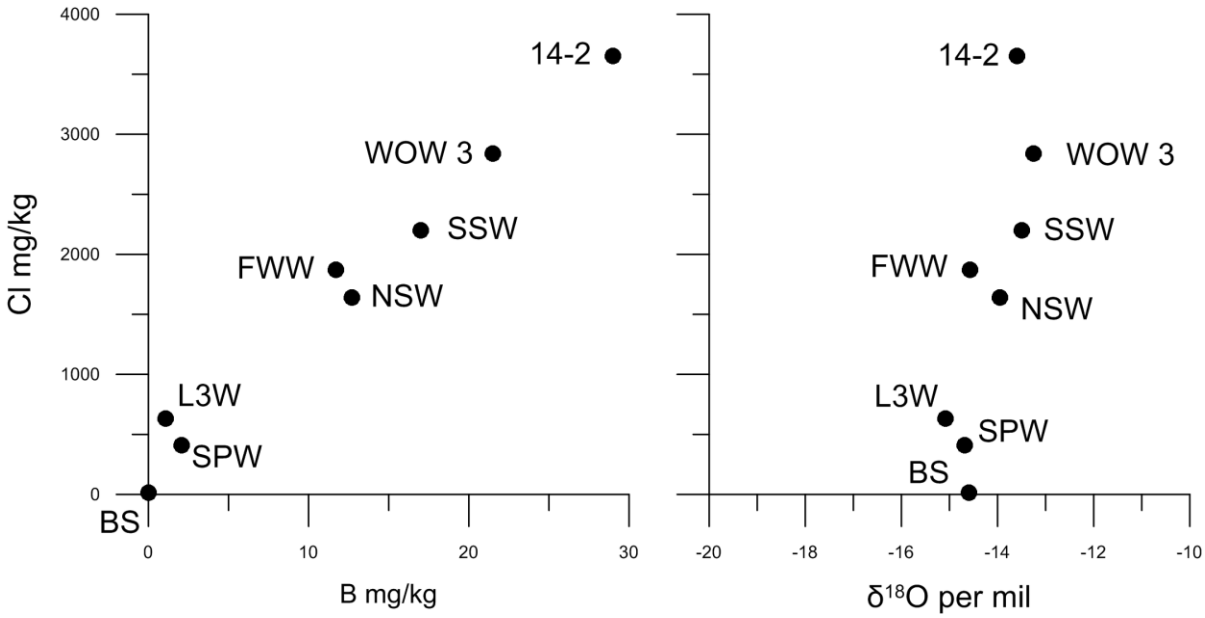

Figure H3: *Geochemical trends in Cl versus B and Cl versus $\delta^{18}O$ for groundwaters (Table G1), showing linear mixing-related trends. Sample localities are shown in Figure H1. The position of Bailey Spring as an end-member composition related to a mixing trend is purely coincidental, as the spring is located in the Mineral Mountains, upstream and to the east of Roosevelt Hot Springs.*

I. TRIAXIAL COMPRESSION AND PERMEABILITY

I.1 Triaxial Compression

Six plugs from drill core of crystalline rock comprising granodiorite (well 52-21; 3578-3591 ft depth) were subject to triaxial compression testing, and one sample was analyzed to determine porosity and permeability. The triaxial loading frame is shown in Figure I1. Figure I2 shows a sample and affiliated instrumentation for measuring axial force as well as strains (axial and in two radial orthogonal directions. Three samples were plugged along the axis of the core (presumed to be nominally vertical) and three samples were plugged perpendicular to the axis of the core. A designation of "V" indicates vertical or the long axis of the plugged sample is aligned with the axis of the core. Similarly, "H" indicates a sample that is nominally horizontal and cut orthogonal to the axis of the core.

Stress-strain curves and photographs from before and after the testing are included in Appendix 1.1B. Measurements were made under three confining pressure conditions (0, 2800 and 8000 psi). Typical data are shown in Figures I3 and for Sample GNS-1H. The confining pressure for this test was 2800 psi. A series of tests are being carried out on to define a failure envelope, to provide representative hydraulic fracture design parameters and for future geomechanical assessments. Figure I3 shows the 1.5-inch nominal diameter sample before and after triaxial testing. Figure I4 shows the stress strain data for this sample, indicating that this is an ideal and representative reservoir for effectively testing drilling, stimulation and production protocols in an environment that embodies strong, crystalline rock.

Figure I1: *Triaxial compression loading frame use to measure the mechanical properties described subsequently.*

Figure 35: *The left hand panel shows a sample encapsulated in a shrink-fit Teflon jacket to prevent penetration of confining fluid. These measurements were made at ambient temperature. Also visible are cantilever devices to determine average axial strain and radial strain in two orthogonal directions. The panel at right shows the same sample configuration mounted on a base plug and a load cell, immediately before being raised into the confining pressure vessel (at top of photograph) prior to testing.*

The triaxial compression data are summarized in Table I1. Acoustic measurements have also been made and dynamic values of Young's Modulus and Poisson's ratio are being determined. The data are being analyzed further and the values for Young's Modulus and Poisson's ratio could change slightly.

Table I1. Summary of Triaxial Compression Testing

Sample	Depth (ft)	Confining Pressure (psi)	Compressive Strength (psi)	Residual Strength (psi)	Young's Modulus (10^6 psi)	Poisson's Ratio
1-H		2800	59,400	55,400	10.49	0.21
2-H		8000	90,000	-	10.70	0.22
4-H		0	27,000	-	7.94	0.12
5-V		2800	61,200	51,500	9.49	0.24
6-V		8000	90,400	82,400	10.50	0.25
7-V		0	29,100	-	7.36	0.18

The data show no obvious directional dependency for any of the measured mechanical properties. This is further evident from the Mohr's failure envelopes shown in Figures I5 and I6.

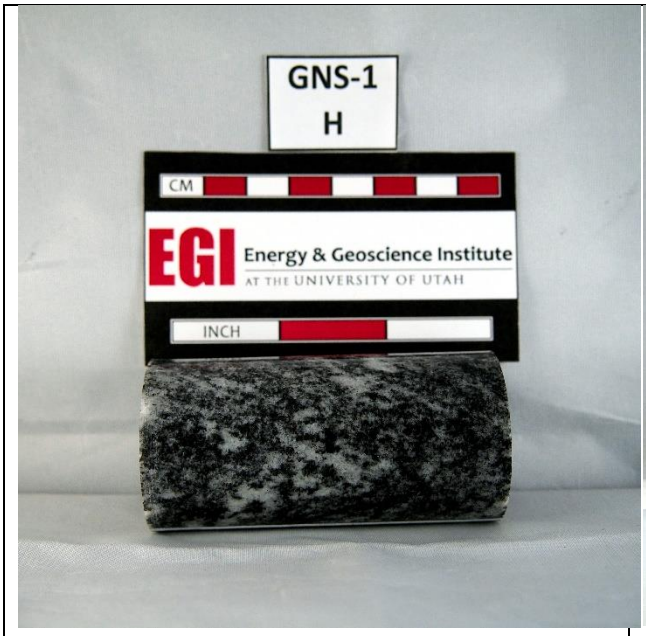

Figure I3a. *This is a pre-test view of sample GNS-1H. The H designates an orientation normal to the axis of the core (horizontal).*

Figure I3b. *This is a post-test view of sample GNS-1H. The H designates an orientation normal to the axis of the core (horizontal).*

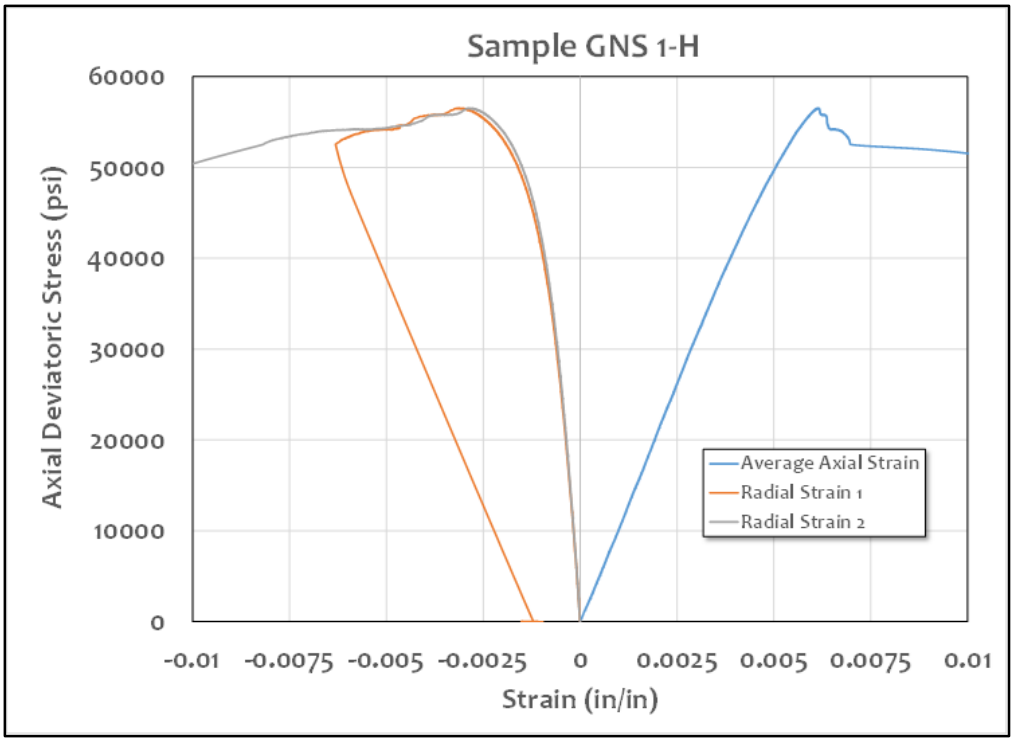

Figure I4*. Axial and radial strain recorded as a function of the axial deviatoric stress (axial stress minus confining pressure). The sample failed at an axial deviatoric stress of approximately 56,000 psig. Young's modulus, Poisson's ratio and compressive strength are among the properties that are determined.*

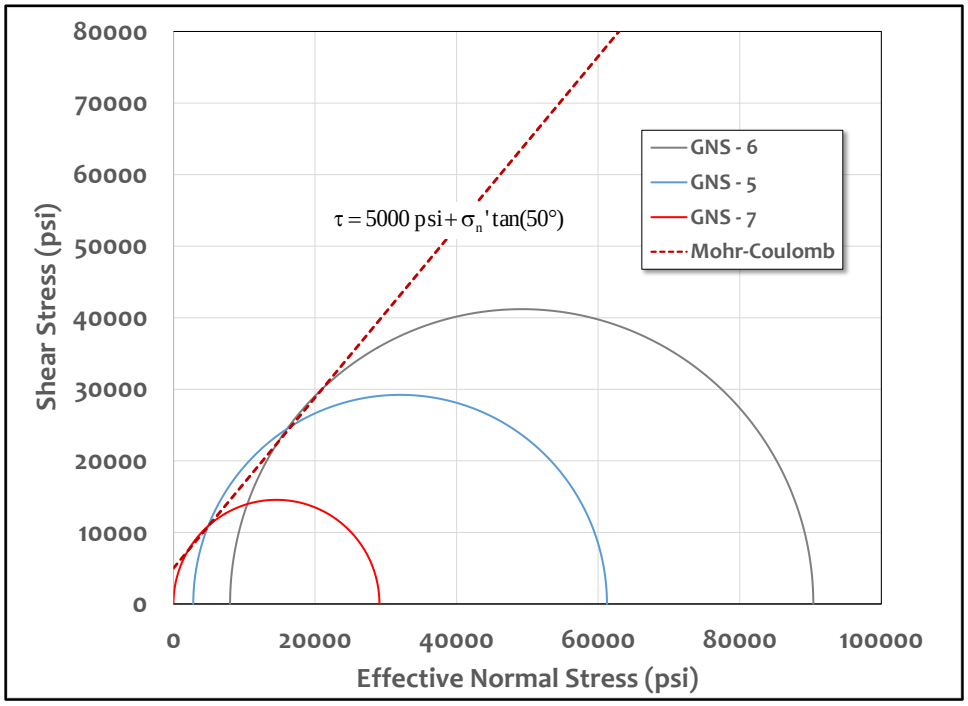

Figure I5. *Mohr-Coulomb Failure envelope for vertically oriented samples.*

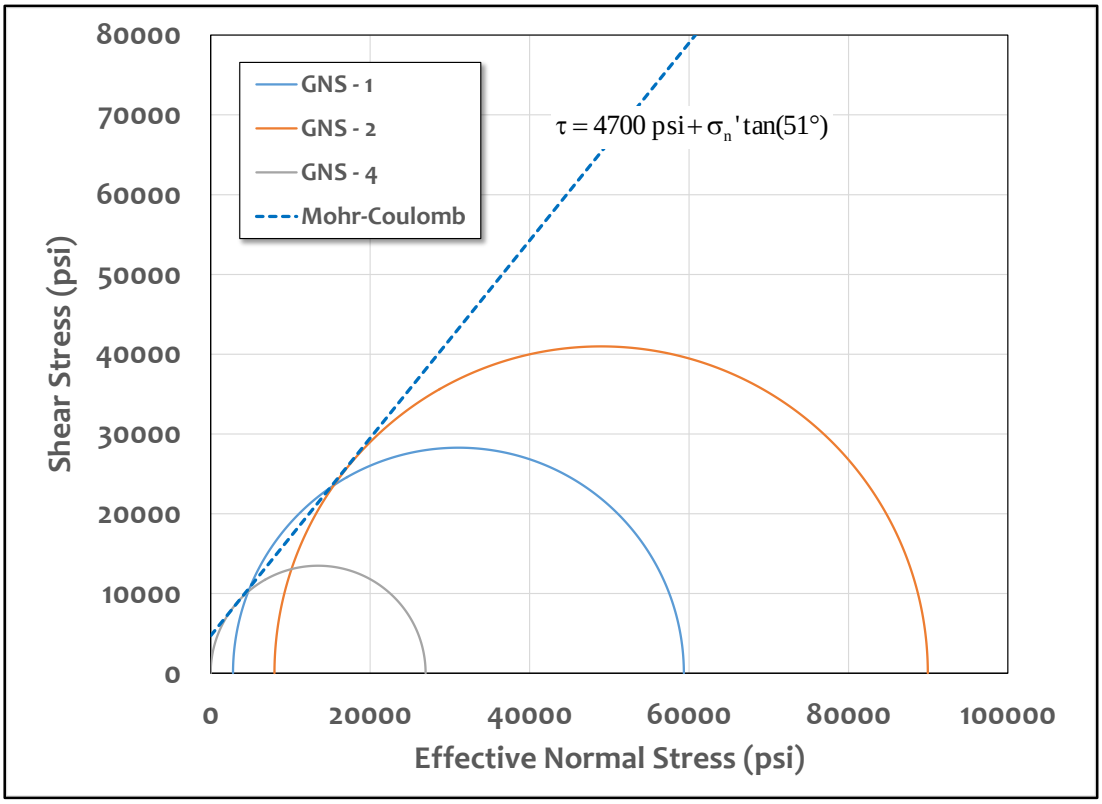

***Figure I6**. Mohr-Coulomb Failure envelope for horizontally oriented samples.*

I.2 Permeability and Porosity

Porosity was measured on Sample GNS 3-H. The porosity and bulk density measured were:

Porosity 0.13%

Bulk Density ..... 2623 kg/m^3

Absolute permeability to water was determined using the apparatus shown in Figure I7. The testing chronology is shown in Figure I8, suggesting for this sample, a relatively high permeability of 0.3± microdarcies (300 nanodarcies), at a confining pressure of 2800 psi. This permeability is attributed to partially healed micro-cracks evident visually.

Figure I7. *Permeability apparatus for steady state (one- or two-phase) liquid permeability measurements.*

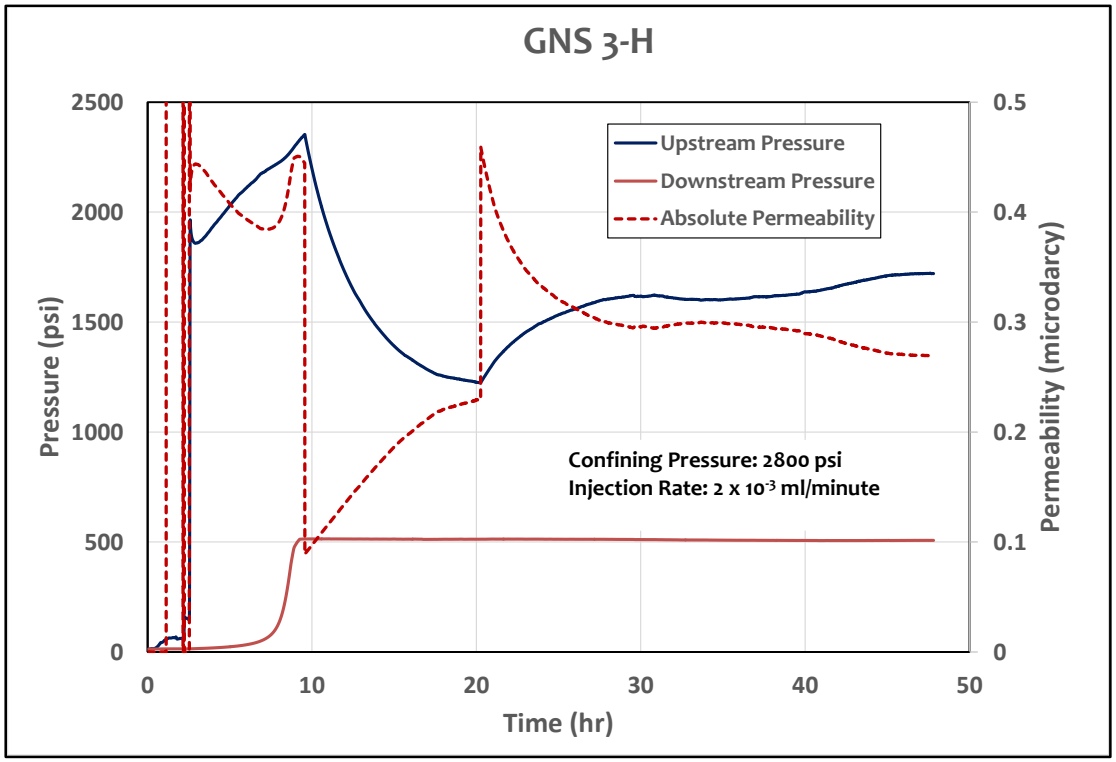

Figure 41. *Upstream and downstream pressure and absolute permeability (ambient temperature) a 500 psi backpressure and a flow rate of 0.002 ml/minute.*

J. REVIEW OF STRUCTURAL SETTING AND STRESS REGIME

J.1 Summary

Constraints on the state of stress in the FORGE area are obtained from three independent indicators: (1) Borehole breakout evident in multi-arm caliper logs provide a local direct measurement of stress direction; (2) Focal mechanisms determined in the region between 1998 and 2011 (e.g., Whidden and Pankow, 2012), with more data to come from continued seismic monitoring, provide a volume averaged measurement of the stress driving active deformation; (3) the recent integrated geologic history of stress is evident from the attitude of joints and dikes (Yusas and Bruhn, 1979), and from young normal fault scarps evident in hydrothermal opal mounds associated with modern geothermal activity. Additional work by Yusas and Bruhn (1979) provides estimates of the shallow elastic principal strains from stress relief over-coring methods. These constraints all indicate a consistent maximum horizontal compressive stress, SHmax, primarily directed N-S (170-180°) to NNE-SSW (035°) at Roosevelt Hot Springs.

J.2 Borehole Indicators of Stress

The presence of a borehole intensifies the local stress state at the borehole wall to the point where it can overcome the rock strength and break the rock (e.g., Zoback 2007) (Figure J.1). The resulting damage to the borehole wall is typically visible in image logs or caliper logs (Figure J.2). Since the amplification effect of the borehole is well-known, this damage provides a constraint on the direction in which the remote stresses act. Failure of the borehole wall is typically distributed at multiple depths along a borehole. Combining these observations provides a summary of the stress directions where the average reflects the stress state in a volume which scales with the depth extent (or length along the borehole) of the damage and the standard deviation describes the heterogeneity in the local stress state.

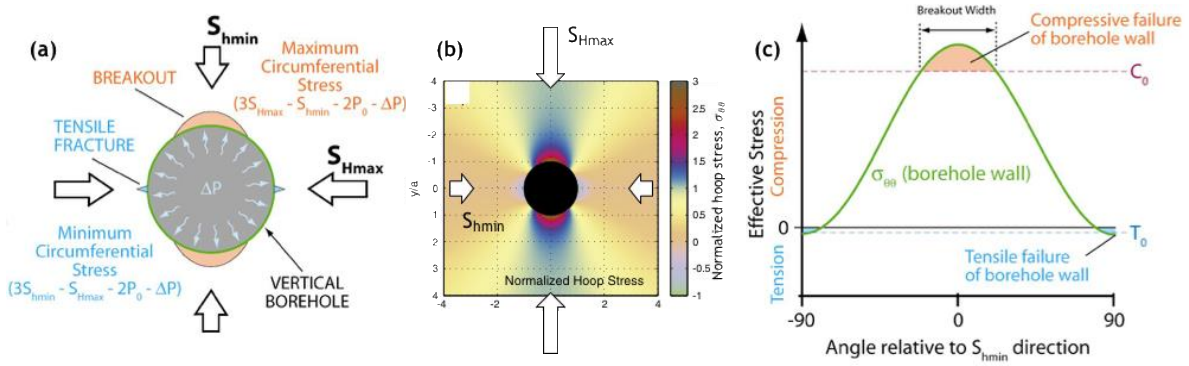

Figure J.1. *Stress state around a vertical borehole. (a) Stress at the borehole wall and in the surrounding volume results from the difference in the principal stresses, SHmax and Shmin, driving deformation, local temperature change and the balance of mud pressure to formation fluid pressure. (b) These contact stresses are amplified at near the borehole so that the local stress components parallel to the borehole wall vary in magnitude as a function of the azimuth with respect to the remote principal stresses. (c) At the borehole wall, the azimuthal extent over which the hoop stress exceeds the uniaxial compressive strength of the rock leads to borehole breakout; whereas tension can cause tensile failure. These failure sites occur in pairs 180° apart reflecting the symmetry of the borehole and stress state and uniquely define the azimuth of the remote principal stresses.*

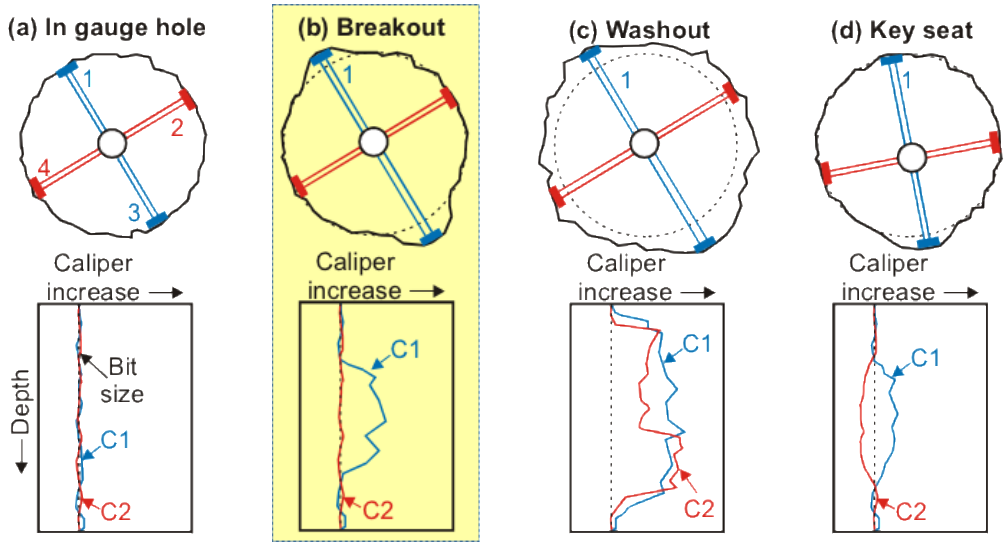

Figure J.2. *Common types of borehole enlargement due to damage and their 4-arm caliper log signatures (modified from Reinecker et al 2003; after Plumb and Hickman, 1985): (a) in gauge hole where borehole diameter corresponds to the bit size; (b) enlargement due to paired breakouts lead to a one caliper pair measuring in gauge diameter and one pair measuring diameter exceeding bit size; (c) washout represents azimuthally extensive enlargement without a strong preferred direction; (d) a key seat resulting from drag of piping against the borehole wall tends to only enlarge the borehole in one direction (usually at the high or the low side of the borehole) causing the logging tool to become decentralized so that the resulting caliper measures one diameter smaller than bit size and one diameter greater than bit size.*

J.2.1 Image logs

At Roosevelt Hot Springs geothermal system (RHS), two data sets in historical logs archived by the Utah Geological Survey have reliable indicators of borehole wall failure that can be related to the local stress state. In the late 1970's, the U.S. Geological Survey obtained an image log of a RHS well 14-2. Tensile fractures are evident in images and published in several venues (Keys, 1979a,b; Keys, 1982; Keys, 1990) and the resulting azimuth of SHmax was reported to the World Stress Map project (Figure J.3).

The image log analyzed by Keys (1979a,b) indicates S_{Hmax} Azimuth 035, NF (38.510;-112.850) based on the azimuth of observed tensile fractures, with an overall Quality rating of C, likely due to the limited depth extent of the damage. Tensile fractures are clearly evident in the published images and occur in clear pairs of good length that remain parallel to the borehole axis throughout the available images (Figure J.4).

(a)

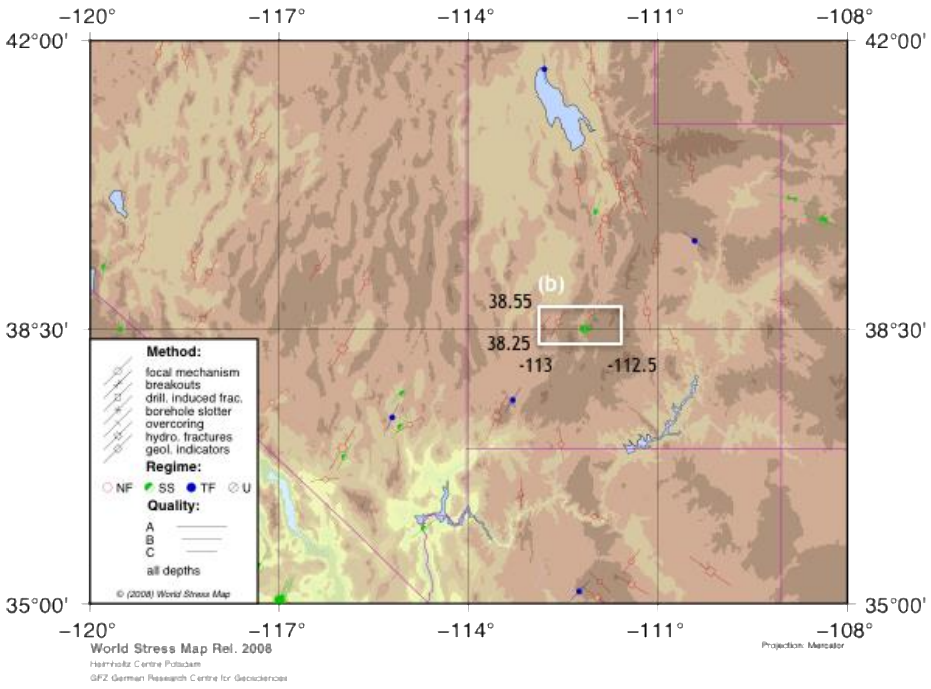

(b)

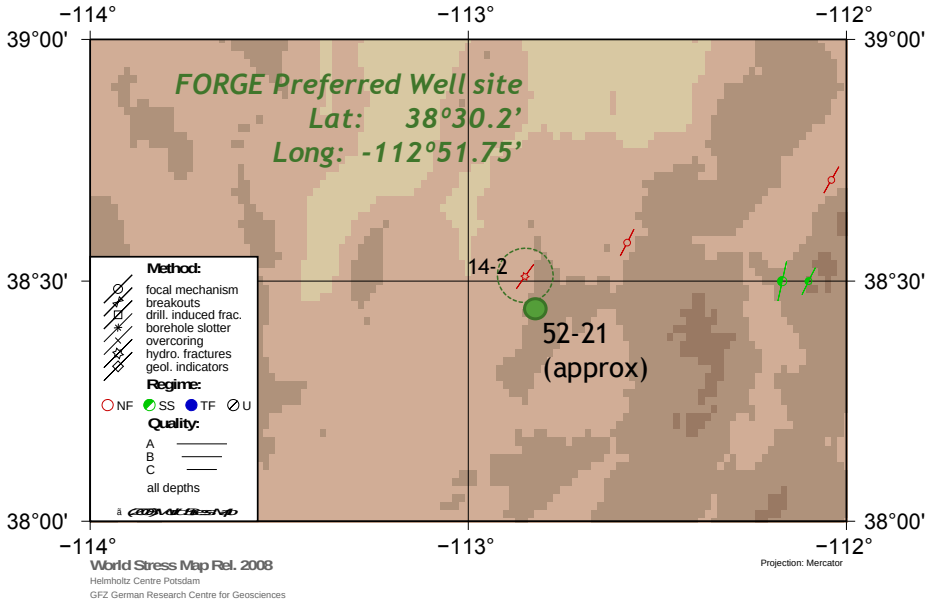

***Figure J.3**: (a) World stress map compilation of stress indicators in the region including focal mechanisms and several borehole wall breakout and tensile fracture data sets. (b) Zoom in of stress map showing local indicators, including the USGS image log of well 14-2 and location of well 52-21 in which caliper logs reveal borehole wall breakout. Note that although Keys identifies the borehole failure as a hydraulic fracture, no hydraulic fracturing test is documented, and the imaged structure should be interpreted as a borehole induced tensile fracture.*

However, the position of the tensile fractures does not precisely match the reported azimuth as they occur at an approximate azimuth of ~020. This discrepancy can be resolved if the published images are presented in a Magnetic North reference frame. Given a magnetic declination of +11º 38' and (true north) = (magnetic north) + (declination), thus 020 + 11.63º = ~032. In addition, the extensive borehole parallel geometry of the tensile fractures, in pairs 180º apart indicates the vertical stress is a principal stress (Peska and Zoback, 1995) and that minimum horizontal principal stress is the least compressive principal stress, $S_{hmin} = \boldsymbol{\sigma}_3$. This requires a normal faulting to strike slip faulting stress regime. The spot images in these papers also suggest abundant natural fractures with apparent strike directions consistent with surface breaking normal faults.

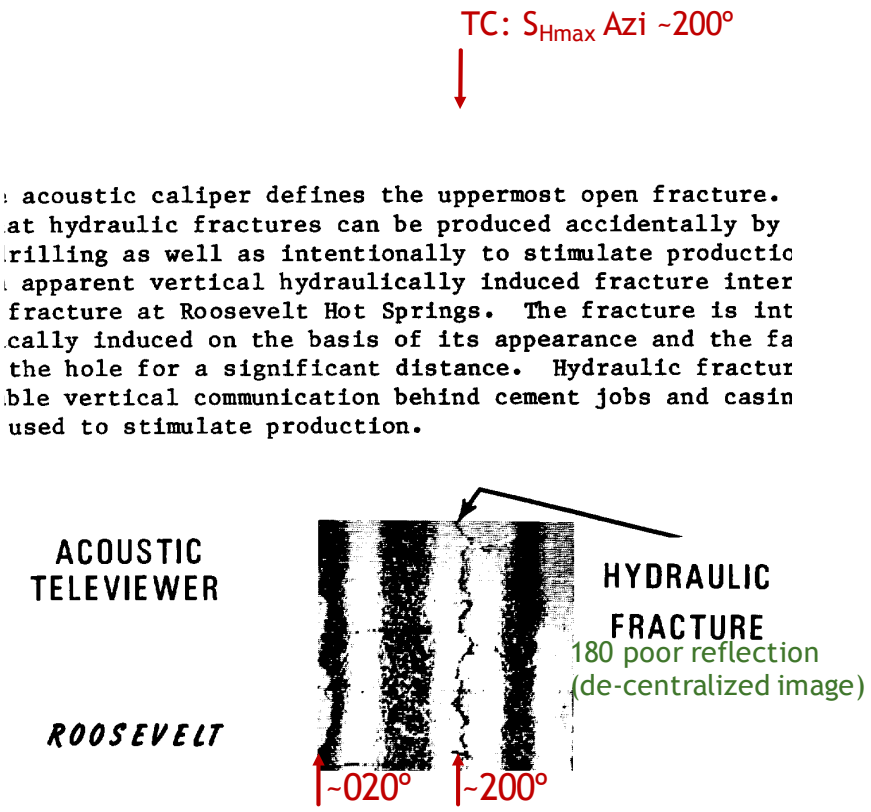

Figure J.4: *One of several acoustic image log spot images obtained from an early production well, 14-2, in Roosevelt Hot Springs in the mid to late 1970's and reported in Keys (1979a,b).*

J.2.2 Caliper logs

Several wells at RHS have been logged with oriented, multi-arm calipers. Well 52-21 shows enlargements consistent with breakout formation as illustrated in Figures J.5 and J.6. The log extends from 2043-6256 ft measured depth from a KB of 22 ft. These breakout intervals are distributed throughout the well, and maximum deviation in the well reaches only 18°, providing a strong constraint on the azimuths of the horizontal principal stresses. Overall, the azimuthal position of the breakouts indicates a representative SHmax direction of 180-190 corrected to True North. The log also provides additional information including natural gamma for correlation with available density and neutron porosity logs.

The presence of abundant breakouts evident in caliper logs and tensile fractures evident in the image log at RHS demonstrates an ability to use traditional borehole methods to characterize the detailed stress state of the proposed FORGE site. The presence of breakouts in the 52-21 well also implies strong differential stresses at the FORGE site, since breakouts require relatively large stress concentrations to overcome rock strength, although this is partly mitigated by a nitrogen lift used to reduce borehole mud pressure in the attempt to induce flow to the well. A definitive analysis of the differential stress requires mini-hydraulic fracturing experiments and an improved strength model which will be conducted in Phase 2 of this project.

***Table J.1**: 52-21 Well Parameters*

Parameter	Notes on Well 52-21
Type	4-arm caliper, Relative Bearing, Azimuth, Natural Gamma (GR)
KB (log ref depth)	22 ft
Run Date	April 11, 1978, Run 1 and Run 2
Open Hole [ft MD]	Run1: 2044-6256, Run 2: 6200-7256
Bit Size	8.5 in
Deviation	Max 18º, most common in breakout intervals 8-12º
PAZ	P1AZ = Azi + MagDec P2AZ = Azi + MagDec + 90º
Magnetic Declination	11.63º
Range of Azimuth in BO intervals	8º-10º
Measured Depth range of BO intervals [ft]	2075-2115, 2190-2460, 2520-2610, 2835-2845, 2850-2880, 2880-2890, 2902-1908, 3170-3180, 3202-3210, 3222-3234, 3516-3520, 4410-4470, 4470-4608, 4688-1692, 4752-4758, 4970-4976
Breakout Azimuthal range (corrected to TN)	090-100
Pressure History	1. Nitrogen lift to induce flow into tight well. Low borehole fluid pressure promotes breakout formation. 2. Step rate injection test to + 640 psi surface pressure
Supporting logs	Neutron porosity (NPHI) and lithodensity (RHOB) and Temperature-Fluid Pressure-Spinner

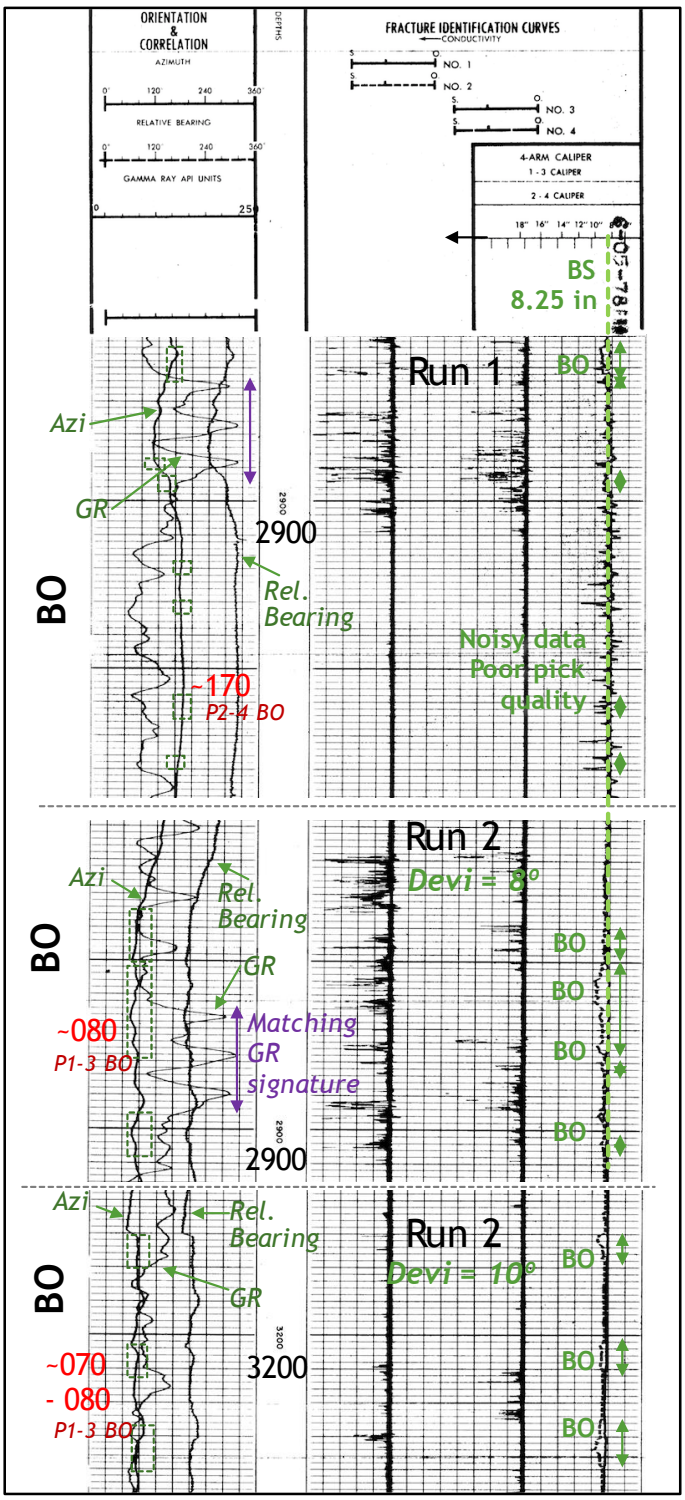

Figure J.5*. Example breakout intervals identified in the 4-arm dipmeter log in well 52-21. Note that apparent 90º offset in breakout azimuth reflects which pair of caliper pads are pressed into the breakout and is corrected as a routine analysis step, which are labeled as p1-3 or p2-4. Breakouts are revealed by the comparison of paired calipers (C1-3 and C2-4). Azimuth records the orientation of caliper 1 with respect to Magnetic North.*

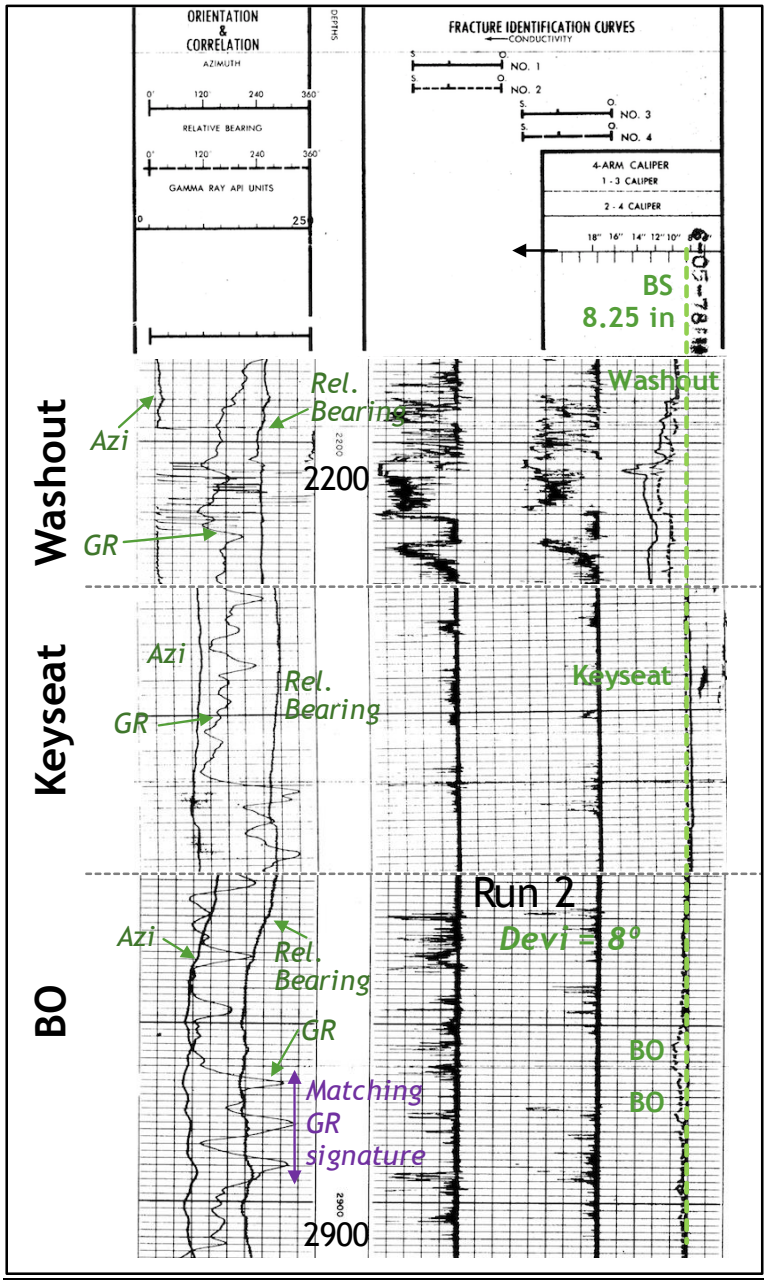

Figure J.6. *Example of 4-arm caliper signatures in the 52-21 log including washouts, keyseats, and breakouts. Refer to Figure J.2 for idealized examples.*

J.3 Seismic Indicators of Stress

The RHS and surrounding areas also host seismicity that can be used to constrain the stress state. Focal mechanisms document the attitude of active faults for comparison to the analysis of stress from the borehole data. Currently, focal mechanisms are available from prior studies including Whidden and Pankow (2012). Improved analysis of the regionally monitored seismicity as part of Phase 1 work, has also resulted in identification of several more focal mechanisms. Regional

monitoring will be augmented in Phase 2 and given results to date is likely to provide a large population of focal mechanisms in the vicinity of the FORGE site.

Individual focal mechanisms of themselves provide a consistency check for the stress state inferred from borehole observations and geologic mapping of dikes, joints and fault attitudes. Focal mechanisms (Figure J.7) indicate normal faulting (mechanisms 14, 15, 17, 1, 8, 33) to strike slip faulting (mechanism, 2) consistent with the geometry of mapped, young faults in the USGS Quaternary Fault Database (Black and Hecker, 1999; Anderson and Bucknam, 1979). The preponderance of normal faulting indicates that SHmax is the intermediate principal stress, σ_2, along planes striking approximately N-S to NNE-SSW. This is consistent with the overall stress state and direction of SHmax inferred from borehole wall failure.

In addition, focal mechanisms can be used to derive a best fitting, volume averages stress tensor including the attitude and relative magnitudes of principal stresses (Angelier 2002; Maury et al., 2013). Reliable inversion requires a large set of diverse focal mechanisms within a volume that scales with either the tectonic features in the region that cause variation in stress state or the structure to be characterized, which in this case corresponds to the FORGE volume. The current set of focal mechanisms span a volume too large for reliable inversion of a locally significant stress tensor. However, in Phase 2 the relatively high rate of local seismicity coupled with improved analysis and augmented local monitoring with improved magnitude of completeness should enable derivation of local focal mechanisms and inversion for stress.

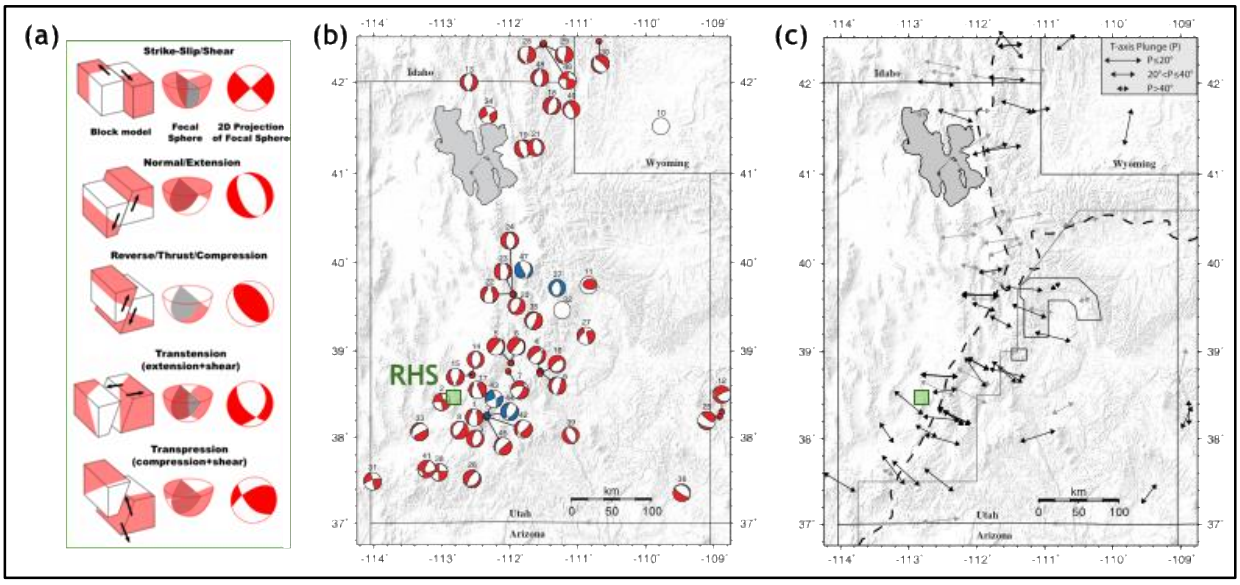

Figure J.7. *Focal mechanisms from the analysis of Whidden and Pankow with the position of RHS indicated. (Reproduced from Whidden and Pankow (2012) from earthquakes spanning 1998-2011)*

At a regional scale, Arabasz and Julander (1986) argue that the least compressive principal stress is horizontal, thus corresponding to Shmin, and is oriented along an azimuth of 102° through an analysis of active fault geometry and earthquakes. This is consistent with largely east-west regional extension and the majority of the focal mechanism solutions, corresponding to an

SHmax azimuth, and expected strike of active normal faults, of 012°. However, the Mineral Mountains to the east are dissected by a set of prominent E-W striking normal faults associated with modern seismicity (Figure 7) (Nielsen et al., 1986; Nielsen, 1989). These faults intersect the Opal Mound Fault at about the position of the hydrothermal field and are associated with thermal ground. There is also some indication of strike-slip focal mechanisms (Figure J.8). Together, this suggests potential for a locally complex stress field despite the more consistent regional stress field.

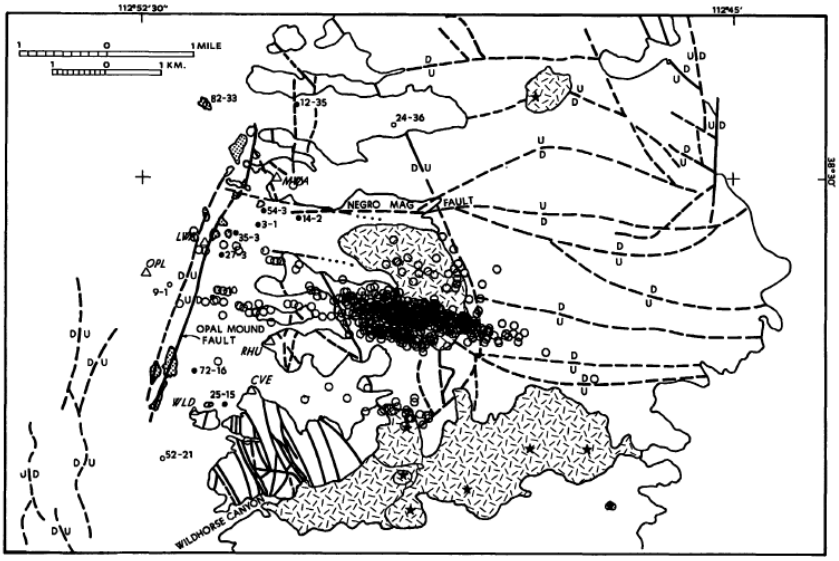

Figure J.8. *Map of the Mineral Mountains adjacent to the RHS. Notice the NNE-SSW strike the young Opal Mound Fault associated with RHS and the numbered exploration and production wells. The Mineral Mountains to the east are dissected by E-W striking faults with normal offsets and some reported, but unspecified strike slip. A band of pre-production seismicity is associated with a subset of these E-W striking faults (Modified from Nielson, 1989 which was derived from Nielson et al., 1986; Faulder; 1991).*

J.4 Geologic Indicators of Stress

Yusas and Bruhn (1979) documented geologic indicators of the strain field which can generally be correlated to stress directions including the attitude of opening mode joints and dikes and sets of fracture planes, as well as principal strains inferred from over-coring strain relief tests (Figure J.9). Joints and dikes are oriented perpendicular to the least compressive principal stress, σ_3, at the time of their formation. Poles to tensile fractures are plotted on lower hemisphere stereograms and generally reveal steeply dipping fractures which strike parallel or perpendicular to mapped faults. The two stereograms nearest RHS show some clustering indicative of steeply included planes roughly striking NNE-SSW, but generally scatter is large so this indicator should be viewed with caution.

Generally, young dikes cutting Quaternary fill or young volcanic rocks are near vertical and so are summarized as rose diagrams (Figure J.9) and reveal a strong N-S to NNE-SSW preferential alignment. Overcoring generally indicates variable strain relief directions. The greatest

extensions appear to be either parallel or perpendicular to young quaternary faults. It is important to note that both the tensile fracture and over coring measurements may be subject to scattering due to near surface whether effects, or anisotropy in the rock mechanical properties, which impact both responses and which are difficult to distinguish. Of these three data sets, the young dikes are likely the most reliable.

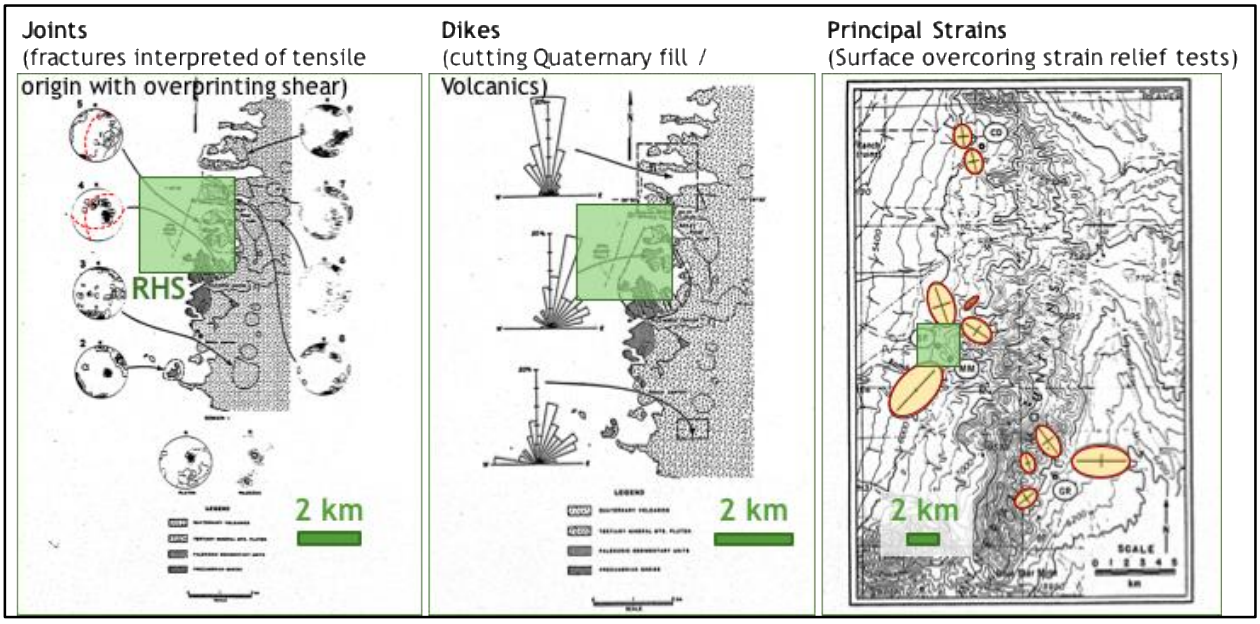

Figure J.9*. Summary of stress constraints derived from Yusas and Bruhn (1979). (Modified from Yusas and Bruhn, 1979). Green boxes represent the combined Roosevelt Hot Springs and FORGE area. (a) Opening mode fractures, joints; (b) Opening mode dikes; (c) principal strains derived from shallow over-coring.*

Figure J.10 provides a snapshot of the U.S. Geological Survey Quaternary Fault Database along with a sample of earthquake activity in the region. The map reveals young active normal faults with modern associated seismicity in the general vicinity. Some of these faults, such as the Opal Mound fault clearly cut and normally offset young silica sinter deposits. For active normal faults SHmax should roughly coincide with the fault strike revealed in the map. The coincidence of the strike of steeply dipping dikes, the strike of fault traces, and offset of hydrothermal features are consistent with a normal faulting stress regime.

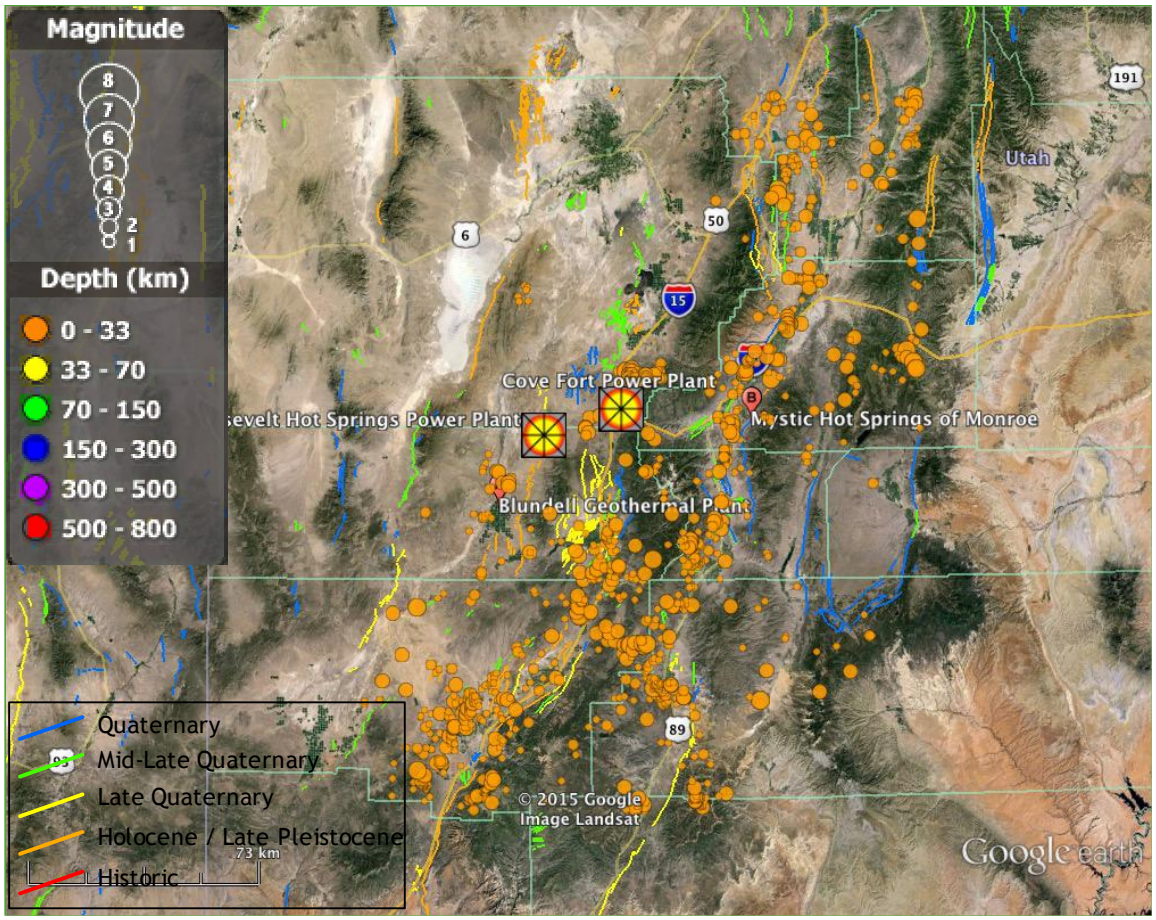

Figure J.10. *USGS Quaternary fault database and large scale earthquakes overlain in googleEarth. Faults are color-coded by relative age*

J.5 Synthesis

The modern azimuth of SHmax in the vicinity of the Milford FORGE site is currently constrained through multiple lines of evidence including (Figure J. 11): (1) borehole breakout in well 52-21 revealed by oriented, 4-arm caliper logs provide a local direct measurement of stress parameters as well as breakouts and borehole wall tensile fractures documented in image logs (Keys, 1979); (2) modern focal mechanisms where the implied strike of normal faulting mechanisms is taken as an initial indicator of the SHmax azimuth (e.g., Whidden and Pankow, 2012) which is being augmented by new local seismic monitoring, provide an, instantaneous, volume averaged measurement of the stress driving active deformation; (3) normal fault scarps in young sediments and (4) the strike of steeply dipping, opening-mode dikes cutting quaternary fill (Yusas and Bruhn; 1979). These data indicate a largely NNE-SSW azimuth of SHmax.

Additional ingredients for geomechanical characterization are already available from many wells including bulk density logs to constrain the vertical stress, neutron and sonic porosity logs to constrain porosity and rock properties including strength, cuttings which enable characterization of mineral dependent friction, and extensive fluid pressure and temperature logs. A large number of these wells have open-hole completions enabling additional logging and mini-hydraulic

fracturing measurements to obtain a more detailed characterizations of stress throughout the FORGE volume. This access provides the potential to characterize the spatial variability in the local stress conditions and fracture populations, and any association with distinct geologic units. Continued local monitoring of seismicity, including focal mechanism inversion, provides complementary insights into stress as does the potential for geologic characterization of faults mapped in the vicinity.

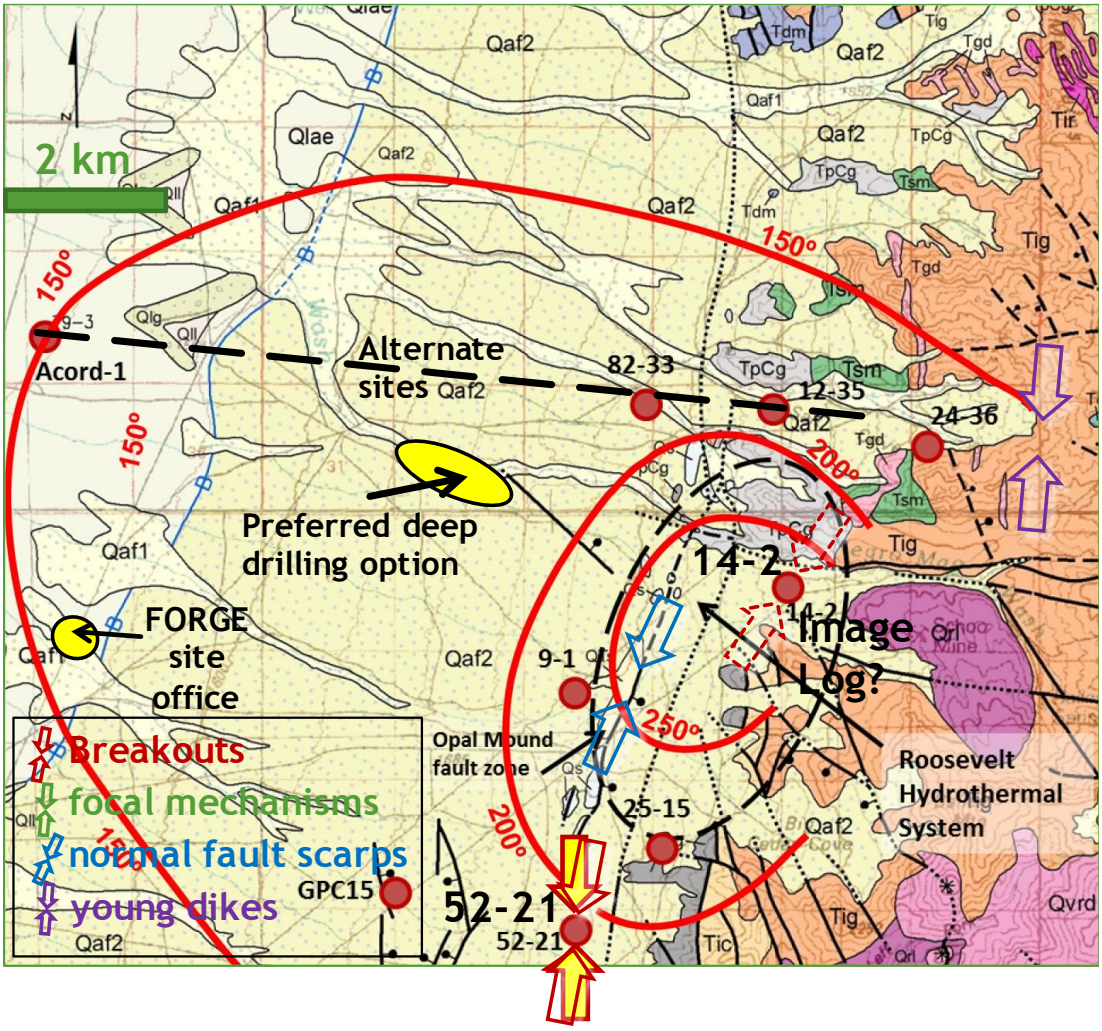

Figure J.11. *Summary map of stress indicators by type and approximate locations. This figure is overlain on an early map of the geology and temperature regime at 2 km depth. Refer to figure D. 15 for an update map of the temperature at various depths.*

K. REFERENCES

Allis R. G. and Larsen, G., 2012, Roosevelt Hot Springs Geothermal field, Utah – reservoir response after more than 25 years of power production. Proceedings. 37th Workshop on Geothermal Reservoir Engineering, Stanford University, Stanford, CA.

Allis, R.G., Gwynn, M., Hardwick, C., Kirby, S., Moore, J., and Chapman, D., 2015, Re-evaluation of the pre-development thermal regime of Roosevelt Hot Springs geothermal system, Utah. Proceedings, 40th Workshop on Geothermal Reservoir Engineering, Stanford University, Stanford, CA.

Allis, R.G., Moore, J.N., Davatzes, N., Gwynn, M., Hardwick, C., Kirby, S., Pankow, K., Potter, S., and Simmons, S.F., 2016, EGS Concept Testing and Development at the Milford, Utah FORGE Site. Proceedings, 41st Workshop on Geothermal Reservoir Engineering, Stanford University, Stanford, CA.

Alienikoff, J.N., Nielson, D.L., Hedge, C.E., and Evans, S.H., 1987, Geochronology of Precambrian and Tertiary rocks in the Mineral Mountains, south-central Utah. US Geological Survey Bulletin, 1622, p. 1-12.

Anders, M. H., Christie-Blick, N., Wills, S., and Krueger, S.W.. 2001, Rock deformation studies in the Mineral Mountains and Sevier Desert of west-central Utah: Implications for upper crustal low-angle normal faulting. Geological Society of America Bulletin, 113, p. 895-907.

Anders, M. H., Christie-Blick, N., and Malinverno, A., 2012, Cominco American well: Implications for the reconstruction of the Sevier Orogen and Basin and Range extension in west central Utah. American Journal of Science, 312, p. 508-533.

Anderson, R.E., and Bucknam, R.C. (1979) Map of fault scarps in unconsolidated sediments, Richfield 1° x 2° quadrangle, Utah: U.S. Geological Survey Open-File Report 79-1236, 15 p. pamphlet, 1 sheet, scale 1:250,000.

Angelier, J. (2002) Inversion of earthquake focal mechanisms to obtain the seismotectonic stress IV—a new method free of choice among nodal planes *Geophys. J. Int.* (2002) 150, 588–609

Arabasz, W.J. and Julander, D. R. (1986) Geometry of seismically active faults and CNStal deformation within the Basin and Range-Colorado Plateau transition in Utah: Geological Society of America Special Paper 208, p. 43-74.

Black, B.D., and Hecker, S., compilers (1999) Fault number 2489, Mineral Mountains (west side) faults, in Quaternary fault and fold database of the United States: U.S. Geological Survey website, http://earthquakes.usgs.gov/hazards/qfaults, accessed 08/06/2015 10:01 PM.

Blackett, R. E.: Review of selected geothermal areas in southwestern Utah., 2007, Geothermal Resources Council Transactions, 31, p. 111-116.

Bruhn, R.L., Yusas, M.R., and Huertas, F., 1982, Mechanics of low-angle faulting: An example from Roosevelt Hot Springs. Tectonophysics, 86, p. 343-361.

Buck, W.R., 1989, Flexural rotation of normal faults. Tectonics, 7, p. 959-973.

Capuano, R. M., and Cole, D. R., 1982 Fluid-mineral equilibria in a hydrothermal system. Geochimica Cosmochimica Acta, 46, p. 1353-1364.

Curewitz, D., and Karson, J.: Structural Settings of Hydrothermal Outflow: Fracture Permeability Maintained by Fault Propagation and Interaction, *Journal of Volcanology and Geothermal Research*, **79**, (1997), 149-168.

Coleman, D.S., and Walker, J.D, 1992, Evidence for the generation of juvenile granitic crust during continental extension, Mineral Mountains batholith, Utah. Journal of Geophysical Research, 97, 11011-11024.

Dickinson, W. R., 2006, Geotectonic evolutions of the Great Basin. Geosphere, 2, 353-368.

East, J., 1981, Hot dry rock geothermal potential Roosevelt Hot Springs Area: Review of data and recommendations. Los Alamos National Laboratory Report, LA-8751-HDR (1981), pp. 45.

Faulder, D.D. (1991) Conceptual geologic model and native state model of the Roosevelt Hot Springs Hydrothermal System, Proceedings, Sixteenth Workshop on Geothermal Reservoir Engineering, Stanford University, Stanford, California, January 23-25, p.131-142.

Faulder, D.D., 1994, Long-term flow test #1, Roosevelt Hot Springs, Utah. Transactions, Geothermal Resources Council Transactions, 18, 583-590.

Faulds, J.E. and Hinz, N.H. (2015)Favorable Tectonic and Structural Settings of Geothermal Systems in the Great Basin Region, Western USA: Proxies for Discovering Blind Geothermal Systems , Proceedings World Geothermal Congress 2015 Melbourne, Australia, 19-25 April 2015, 6 p.

Giggenbach, W.F., and Stewart, M.K., 1982, Processes controlling the isotopic compositions of steam and water discharges from steam vents and steam-heated pools in geothermal areas. Geothermics 11, 71-80.

Glenn, W.E., and Hulen, J. B., 1979, Interpretation of well log data from four drill holes at Roosevelt Hot Springs KGRA. DOE Earth Science Laboratory Report, University of Utah, pp. 74.

Glenn, W.E., Hulen, J. B., and Nielson, D.L., 1980, A comprehensive study of LASL well C/T-2 Roosevelt Hot Springs KGRA, Utah, and applications to geothermal well logging. Los Alamos Scientific Laboratory Report, LA-8686-MS, pp 175.

Goff, F., and Decker, E. R., 1983, Candidate sites for future hot dry rock development in the United States. Journal of Volcanology and Geothermal Research, 15, 187-221.

Hardwick C.L., Gwynn, M., Allis, R., Wannamaker, P., and Moore, J., 2016, Geophysical Signatures of the Milford, Utah FORGE Site. Proceedings, 41st Workshop on Geothermal Reservoir Engineering, Stanford University, Stanford, CA.

Hintze, L. F., and Davis, F. D., 2003, Geology of Millard County, Utah. UGS Bulletin, 133, pp. 305.

Hintze, L.H., Davis, F.D., Rowley, P.D., Cunningham, C.G., Steven, T.A., and Willis, G.C., 2003, Geologic map of the Richfield 30' x 60' quadrangle, southeast Millard County, and parts of Beaver, Piute, and Sevier Counties, Utah. Utah Geological Survey Map 195.

Keys, W. S. (1979) Borehole geophysics in igneous and metamorphic rocks, in Society of Professional Well Log Analysts Annual Logging Symposium, 20th, Tulsa, Okla., 1979, Tulsa, Okla., Transactions: Houston, Society of Professional Well Log Analysts, p. 001-0026.

Keys, W. S. (1982) Borehole geophysics in geothermal exploration, in Fitch, A.A., ed., Developments in geophysical exploration methods: London, Elsevier Applied Science Publishers, Bk. 3, Chap. 7, p. 195-268.

Keys (1990) Techniques of Water-Resources Investigations of the United States Geological Survey: Chapter E2: Borehole geophysics applied to ground-water investigations, 150 p. http://pubs.usgs.gov/twri/twri2-e2/pdf/TWRI_2-E2.pdf

Kirby, S., 2012, Geologic and hydrologic characterization of regional nongeothermal groundwater resources in the Cove Fort area, Millard and Beaver Counties, Utah. Utah Geological Survey Special Study, 140, pp. 46.

Lipman, P.W., Rowley, P.D., Mehnert, H.H., Evans, S.H., Jr., Nash, W.P., and Brown, F.H., 1978, Pleistocene Rhyolite of the Mineral Mountains, Utah: Geothermal and Archeological Significance. US Geological Survey Journal of Research, 6, 133-147.

Lynne, B.Y., Campbell, K.A., Moore, J.N., and Browne, P.R.L., 2005, Diagenesis of 1900 year-old siliceous sinter (opal-A to quartz) at Opal Mound, Roosevelt Hot Springs, Utah. Sedimentary Geology, 179, 249-278.

Mabey, D.R., and Budding, K.E., 1987, High temperature geothermal resources of Utah. Utah Geological and Mineralogical Survey Bulletin, 123, pp. 64.

Maury, J., Cornet, F.H., Dorbath, L. (2013) A review of methods for determining stress fields from earthquakes focal mechanisms; Application to the Sierentz 1980 seismic crisis (Upper Rhine graben) , *Bull. Soc. géol. France*, 2013, t. 184, p. 319-334

Micklethwaite, S., Sheldon, H.A., and Baker, T.: Active Fault and Shear Processes and their Implications for Mineral Deposit Formation and Discovery, *Journal of Structural Geology*, **32**, (2010), 151-165.

Moore, J.N. and Nielson, D.L., 1994, An overview of the geology and geochemistry of the Roosevelt Hot Springs geothermal system, Utah. Utah Geological Association Publication, 23, 25–36.

Nielson, D.L., 1989, Stress in geothermal systems: Transactions, Geothermal Resources Council, 13, 271–276, (1989).

Nielson, D. L., Evans, S.H., and Sibbett, B.S., 1986, Magmatic, structural, and hydrothermal evolution of the Mineral Mountains intrusive complex, Utah, Geological Society of America Bulletin 97, 765-777.

Parry, W.T., Ballantyne, J.M., Bryant, N.L., and Dedolph, R.E., 1980, Geochemistry of hydrothermal alteration at the Roosevelt Hot Springs thermal area, Utah, Geochimica et Cosmochimic Acta 44, 95-102.

Pankow, K. L., Arabasz, W.J., Nava, S.J., and Pechmann, J.C., 2004, Triggered seismicity in Utah from the 3 November 2002 Denali fault earthquake, Bull. Seism. Soc. Am. 94, S332–S347.

Peška, P., and M. D. Zoback (1995), Compressive and tensile failure of inclined well bores and determination of in situ stress and rock strength, *J. Geophys. Res.*, *100*(B7), 12791, doi:10.1029/95JB00319.

Plumb, R.A. and S.H. Hickman (1985): Stress-induced borehole enlargement: a comparison between the four-arm dipmeter and the borehole televiewer in the Auburn geothermal well. - J. Geophys. Res., 90, 5513-5521.

Reinecker, J., M. Tingay and B. Müller (2003) Borehole breakout analysis from four-arm caliper logs; World Stress Map Project: Guidelines: four-arm Caliper Logs, 5 p. http://dc-app3-14.gfz-potsdam.de/pub/guidelines/WSM_analysis_guideline_breakout_caliper.pdf

Robinson, R. and Iyer. H.M., 1981, Delineation of a low-velocity body under the Roosevelt Hot Springs geothermal area, Utah, using teleseismic P-wave data, Geophysics, 46, 1456-1466.

Rohrs, D.T., and Bowman, J. R., 1980, A light stable isotope study of the Roosevelt Hot Springs Area, southwestern Utah, Topical Report DE-AC07-78ET28392, Department of Geology and Geophysics, University of Utah, pp. 89.

Ross, H.P., Nielson, D.L., Moore, J.N., 1982, Roosevelt Hot Springs geothermal system, Utah – case study. Amer. Assoc. Petroleum Geologists, 66, 879–902.

Rowley, P.D., Vice, G.E., McDonald, R.E., Anderson, J.J., Machette, M.N., Maxwell, D.J., Ekren, E.B., Cunningham, C.G., Steven, T.A., and Wardlaw, B., 2005, Interim geologic map of the Beaver 30' x 60' quadrangle, Beaver, Piute, Iron, and Garfield Counties, Utah: Utah Geological Survey Open-File Report 454, 27 p.,1 plate, scale 1:100,000.

Shannon S.S., Goff, F., Rowley, J.C., Pettitt, R.A., Vituaz, F.D., 1983, Roosevelt Hot Springs/Hot Dry Rock prospect and evaluation of the Acord 1-26 well. Transactions, Geothermal Resources Council, 7, 541–544, (1983).

Simmons, S.F., Kirby, S., Moore, J.N., Wannamaker, P., and Allis, R., 2015, Comparative analysis of fluid chemistry from Cove Fort, Roosevelt and Thermo: Implications for geothermal resources and hydrothermal systems on the east edge of the Great Basin. Proceedings Geothermal Resources Council 39**,** 55-61.

Simmons, S., Kirby, S., Jones, C., Moore, J., and Allis, R., 2016, The Geology, Geochemistry, and Hydrology of the EGS FORGE Site, Milford Utah. Proceedings, 41st Workshop on Geothermal Reservoir Engineering, Stanford University, Stanford, CA.

Sweeney, M.J., 1980, McCulloch Acord 1-26, Roosevelt Hot Springs Area, Beaver Co., Utah. Unpublished petrography.

Vuataz, F-D., and Goff, F., 1987, Water geochemistry and hydrogeology of the shallow aquifer at Roosevelt Hot Springs, southern Utah. Los Alamos National Laboratory Report, LA-11160-HDR, pp. 63

Wannamaker, P.E., Bartley, J.M., Sheehan, A.F., Jones, C.H., Lowry, A.R., Dumitru, T.A., Ehlers, T.A., Holbrook, W.S., Farmer, G.L., Unsworth, M.J., Hall, D.B., Chapman, D.S., Okaya, D.A., John, B.E., and Wolfe, J.A., 2001, Great Basin-Colorado Plateau transition in central Utah—an interface between active extension and stable interior. Utah Geological Association Publication 30, 1–38.

Wannamaker, P. E., Moore, J. N., Pankow, K. L., Simmons, S.F., Nash, G. D., Maris, V., Batchelor, C., and Hardwick, C. L., 2015, Play Fairway Analysis of the Eastern Great Basin Extensional Regime, Utah: Preliminary Indications. Proceedings Geothermal Resources Council 39, 793-804.

Ward, S.H., Parry, W.R., Nash, W.P., Sill, W.R., Cook, K.L., Smith, R.B., Chapman, D.S., Brown, F.H., Whelan, J.A., and Bowman, J.R., 1978, A summary of the geology, geochemistry, and geophysics of the Roosevelt Hot Springs thermal area, Utah. Geophysics, 43, 1515–1542.

Welsh, J. E., 1980, McCulloch Acord 1-26, Roosevelt Hot Springs Area, Beaver Co., Utah. Unpublished petrography.

Whidden K.M. and Pankow, K.R., 1994, A catalog of Regional Moment Tensors in Utah from 1998 to 2011, Seismological Research Letters 83, p. 775–783.

Whidden K.M. and K.R. Pankow (2012) A catalog of Regional Moment Tensors in Utah from 1998 to 2011, Seismological Research Lettres, v 83, p. 775-783. doi: 10.1785/0220120046

Yearsley, E., 1994, Roosevelt Hot Springs reservoir model applied to forecasting remaining field potential. Proceedings Geothermal Resources Council 18, 617-622.

Yusas, M.R. and R.L. Bruhn (1979) Structural Fabric and in-situ stress analysis of the Roosevelt Hot Springs KGRA; Topical Report 78-1701f.a.6.5.1, DE-AC07-78ET28392, Department of Geology and Geophysics, University of Utah, 62 p.

Zoback, M.D. (2007) *Reservoir Geomechanics*, Cambridge University Press, Cambridge, U.K., 449 p.

Zandt, G., McPherson, L., Schaff, S., and Olsen, S., 1982, Seismic baseline and induction studies: Roosevelt Hot Springs, Utah, and Raft River, Idaho. U.S. Dept of Energy Report DOE 01821-T1, pp. 58.

L. APPENDICES

Appendix 1.1A: 2016 Stanford Geothermal Papers

Appendix 1.1B: Triaxial Test Data

Update Groundwater Data

TASK 1.1.1

Task 1.1.1 Update Groundwater Data

The groundwater system across the FORGE project area was evaluated 30 years ago as part of an initial appraisal of hot dry rock resources (Vautaz and Goff, 1987). Kirby (2012) examined the regional groundwater system including the study area to develop a groundwater budget and to examine the possibility of flow between hydrologic basins along Cove Creek and the Beaver River Valley. Other significant work has focused on the geothermal resources at Roosevelt Hot Springs (Faulder, 1991; see summaries in Moore and Nielson, 1994; Allis et al., 2015; Allis et al., 2016 and Simmons et al., 2016) and agricultural water and groundwater conditions in areas adjoining the study area (Mower and Cordova, 1974; Mower, 1978; Mason, 1998).

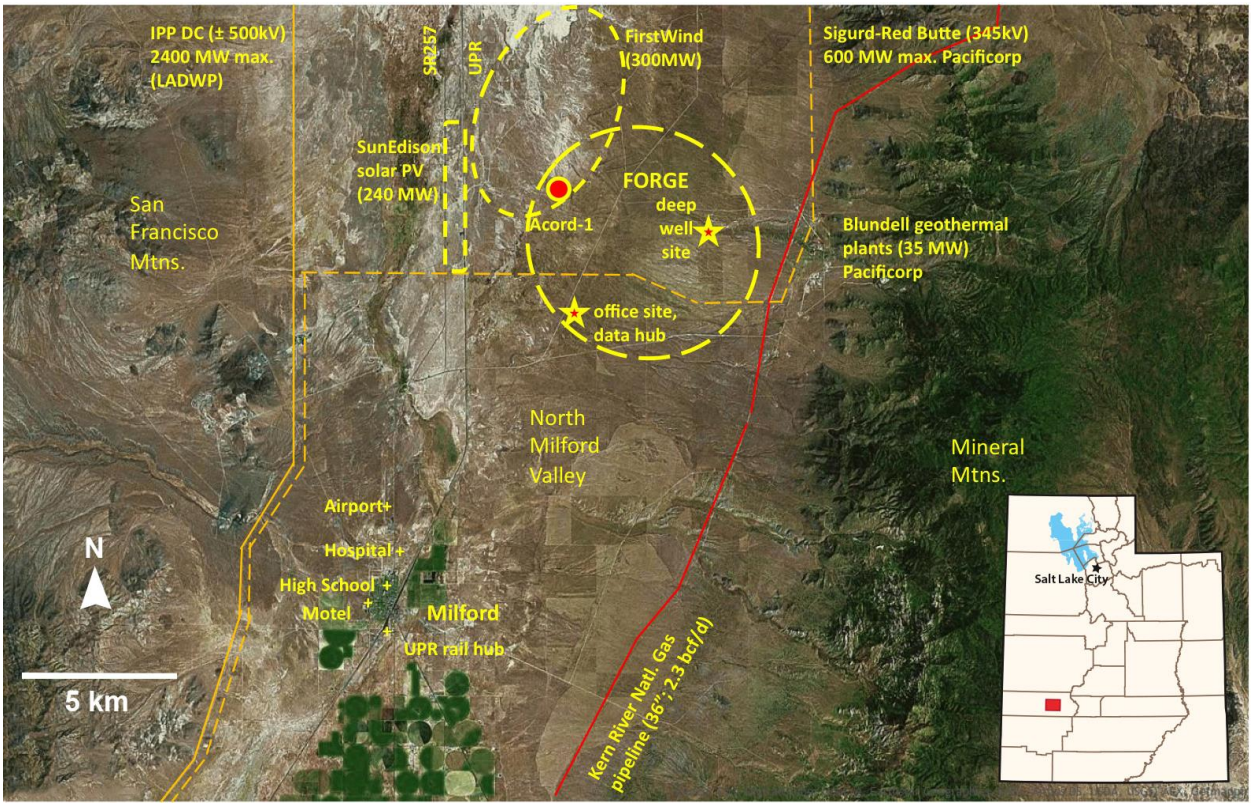

Figure 1. *Location of the FORGE deep well site near Milford, Utah, showing infrastructure and physiography (Allis et al., 2016).*

Hydrogeologic Setting

The study area lies along the eastern margin of the Basin and Range province in southwestern Utah. This area is characterized by a series of north-south trending bedrock mountain ranges separated by broad basins filled with alluvium and lake sediments. Heat flow across the area is high relative to adjoining areas (Allis et al., 2015, 2016).

The FORGE project area lies just west of the Mineral Mountains approximately 8 miles northeast of Milford, Utah. The Mineral Mountains consist primarily of Tertiary age granitic

intrusive rocks (Figure 2). Along the western margin of the range the Tertiary intrusive rocks are intrude Precambrian metamorphic rocks (Nielson et al., 1986; Coleman et al., 1997). Precambrian and lower Paleozoic carbonate and clastic sedimentary rocks crop out at the northern and southern ends of the range (Nielson et al., 1986). Quaternary volcanic rocks occur west of the crest of the Mineral Mountains as well as north of the Mineral Mountains (Rowley et al., 2005). Unconsolidated basin fill covers the remainder of the study area and consists of alluvial, lacustrine, and fluvial deposits.

Figure 3 depicts the general geologic setting of the basin fill and the bedrock across the study area. Igneous and metamorphic rocks exposed in the Minerals Mountains lie beneath basin fill across the study area (e.g., Simmons et al., 2016). The thickness of basin fill increases to the west away from the Mineral Mountains as indicated by the lithologies in the Acord-1 well. Unconsolidated basin fill along the western flank of the Mineral Mountains consists primarily of sands and gravels that lie directly on fractured Tertiary intrusives (Vautaz and Goff, 1987). Along the valley floor near the Beaver River, unconsolidated basin fill is underlain by a series of consolidated to semi-consolidated Tertiary volcanic rocks and Tertiary basin fill (Hintze and Davis, 2003). The total thickness of these deposits along the valley floor is up to 9,000 ft (Saltus and Jachens, 1995; Allis et al., 2016; Hardwick et al., 2016; Simmons et al., 2016). Based on well logs, unconsolidated basin fill exists in both unconfined and confined conditions in the study area. Confined conditions exist along the valley floor where thick clay layers occur (Kirby, 2012). Unconfined conditions generally exist across the broad alluvial fans that slope to the west from the Mineral Mountains.

Hydrostratigraphy

Unconsolidated basin fill forms the primary aquifer in the study area. It covers the entire study area west of the Mineral Mountains and includes a range of alluvial and lacustrine deposits. Along the west flank of the Mineral Mountains these deposits consist primarily of sands and gravels without significant confining layers (Vautaz and Goff, 1987).

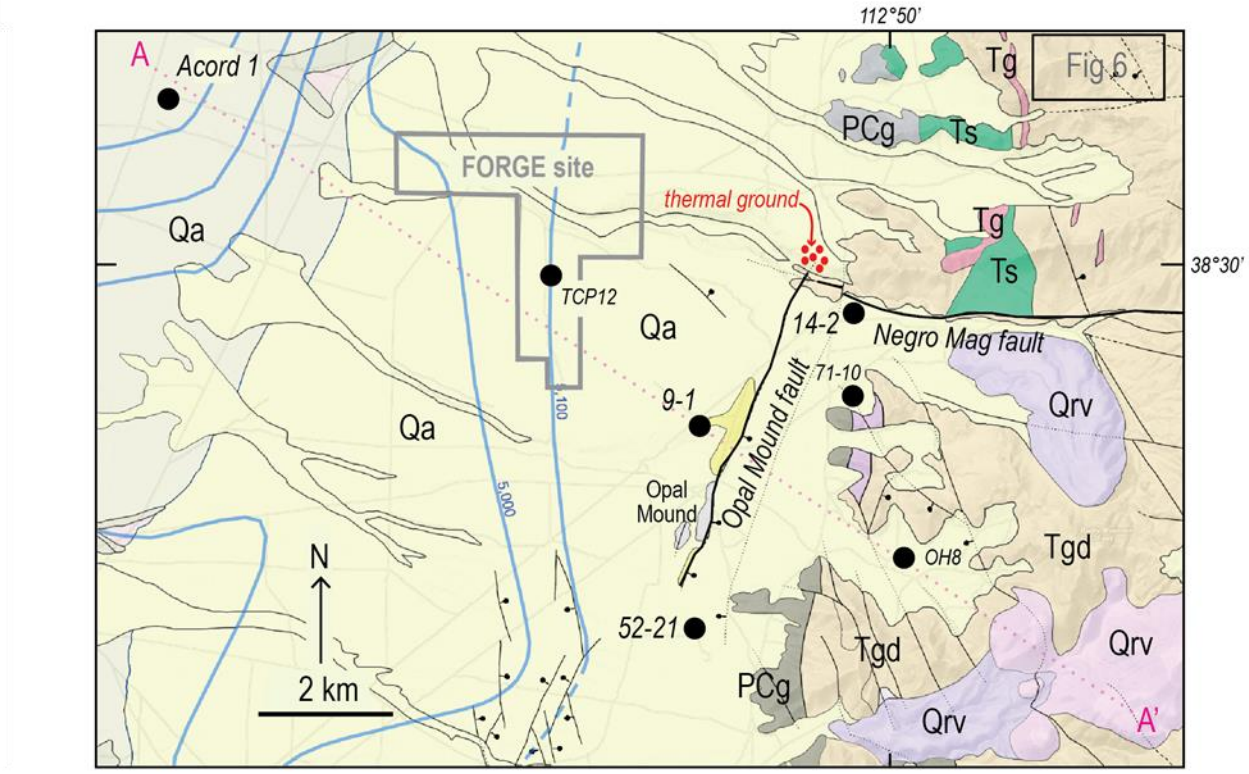

Figure 2. *Geologic map of the FORGE deep well site, Milford, Utah (Simmons et al., 2016). Geology is modified from (Hintze et al., 2003; Rowley et al., 2005; Kirby, 2012). For clarity, only a few of the many wells are shown. Blue lines represent the elevation (feet above sea level) of the groundwater potentiometric surface. Abbreviations for map units: Qa=Quaternary alluvium and claystone; Qrv=Quaternary rhyolite volcanic rock; Tgd=Tertiary granodiorite; Tg=Tertiary granite dike; Ts=Tertiary syenite; PCg=Precambrian gneiss.*

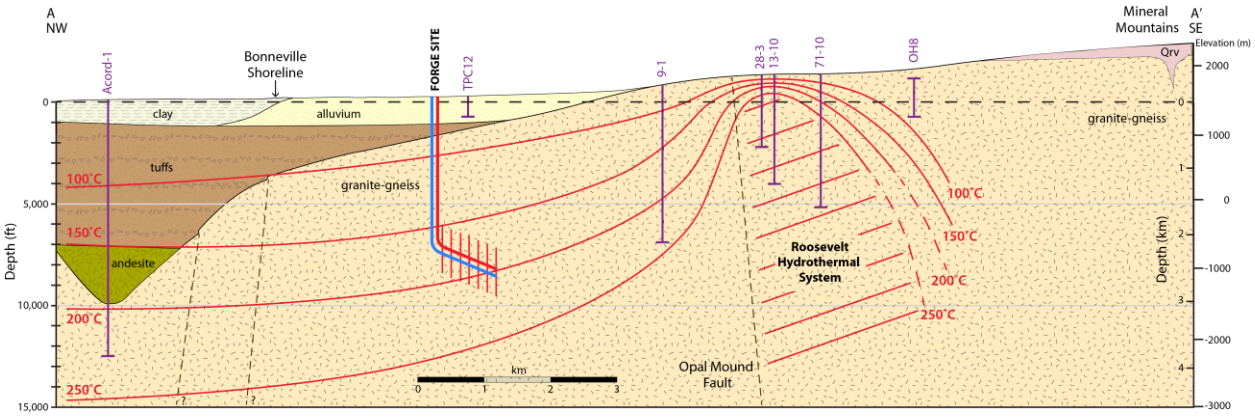

Figure 3. *Geologic cross section A-A' from Figure 2, showing the stratigraphy, structure, and the FORGE deep well site. The units labeled alluvium and clay comprise the unconsolidated basin-fill aquifer. The zero datum for the depth axes is at 1524 m asl (5000 ft asl). Precambrian gneiss and Tertiary plutonic rocks are undifferentiated. The Roosevelt Hot Springs hydrothermal system lies east of the Opal Mound fault. Isotherms are interpreted from well measurements, and the contact between granite-gneiss and overlying basin fill is interpreted from gravity measurements (Allis et al., 2016; Hardwick et al., 2016).*

Further west along the valley floor, the unconsolidated basin fill includes fine grained lacustrine deposits and thick layers of clay (Mower and Cordova, 1974). Based on well logs the clay layers may be just over 100 feet thick and laterally extensive along the valley axis (Kirby, 2012). The transition between unconfined and confined conditions in the unconsolidated basin fill is likely gradational and controlled by the extent and nature of lacustrine versus alluvial deposits (Mower and Cordova, 1974). The total thickness of the unconsolidated basin fill aquifer varies from greater than 500 feet west of the Roosevelt Hot Springs hydrothermal system to 100 to 400 feet thick along the valley floor (Mower and Cordova, 1974; Kirby, 2012)

The transmissivity of unconfined basin fill in the study area, based on a single well aquifer test with no well log information, was calculated at ~1400 ft^2 per day (Vautaz and Goff, 1987). This transmissivity is moderate and similar to transmissivities for the basin fill to the south near Milford (Mower and Cordova, 1974). Results of a recent aquifer test of the confined part of the basin fill aquifer in the study area yielded a transmissivity of 240 ft^2 per day. The recent aquifer test results are discussed in detail in subsequent sections. Current groundwater use in the study area is limited to several stock watering wells (labeled NSW, SSW, and SPW on Figure 4) and a supply well used for fire suppression at a single site (labeled FWW on Figure 4).

Groundwater Levels

Existing groundwater elevation data was compiled and used to construct a contoured potentiometric surface across the study area (Table 1, Figure 4). Most water level data are limited to the area east of the Opal Mound fault. Two upland springs in Mineral Mountains are shown to indicate the higher groundwater levels that occur in the bedrock of the Mineral Mountains.

Groundwater in the study area moves from areas of recharge along the upper reaches of the Mineral Mountains to areas of regional discharge along the valley floor to the north and south of the study area (Kirby, 2012). Groundwater elevations decrease to the west away from the Mineral Mountains (Table 1, Figure 4). Between the Opal Mound fault and OH-4, the potentiometric surface dips steeply westward and then flattens out towards the center of the valley. The Opal Mound fault represents the boundary of the active geothermal reservoir and is likely a lateral barrier to groundwater movement, with leakage into shallow aquifers occurring at the northern tip of the fault, as indicated by chemical trends (discussed below). Along the valley floor groundwater elevations are generally consistent and the potentiometric surface slopes south towards areas of significant groundwater decline near Milford or north towards areas of regional discharge (Kirby, 2012). Beneath the FORGE deep drill site groundwater elevations are near 5100 feet above sea level and between 200 and 500 feet below the land surface.

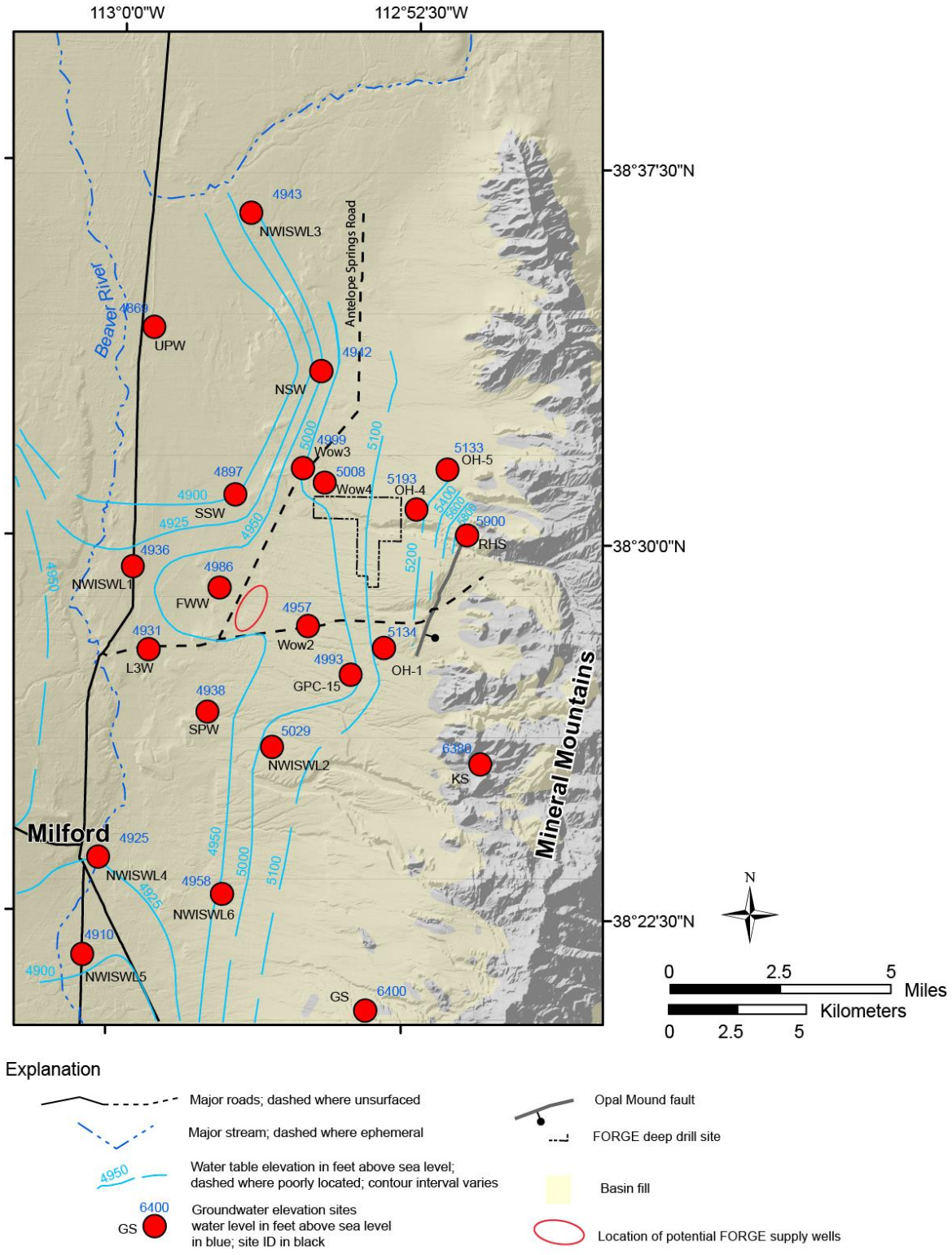

Figure 4. *Groundwater elevation map of the FORGE study area. RHS is the historic Roosevelt Hot Springs site. Site ID's correlate with Table 1.*

Depth to water is an important constraint on groundwater supply and the design of new water wells. Depth to water was calculated as the difference between the potentiometric surface (Figure 4) and the surface elevation. The depth to groundwater in the unconsolidated aquifer varies sharply across the study area, from less than 20 feet near the Beaver River to over 500 feet west of the Opal Mound fault (Figure 5), decreasing to the west away from the Opal Mound fault. Near the north end of the Opal Mound fault an area of shallow groundwater correlates with historic outflow from the geothermal system. Across the FORGE deep drill site groundwater lies within 200 feet of the ground surface along the west side and within 500 feet along the east side. Potential groundwater wells discussed in a subsequent section could be located along the Antelope Springs road east of FWW well where the depth to groundwater is approximately 150 feet.

Several wells within the study area have long-term water level data (U.S. Geological Survey, 2015). These data show changes in groundwater elevation through time for the unconsolidated aquifer across the study area (Figure 6). Long term water level change in the FORGE study area at wells WOW2 and WOW3 is less than 15 feet. Further from the FORGE project site, NWISWL1, NWISWL2, and NWISWL3 show water level changes less than 10 feet. These data indicate that over the 70 year period in which water level data have been recorded, groundwater recharge and discharge are nearly equal across the FORGE study area. In addition, there has been little fluctuation in groundwater elevation due to current groundwater use in the area. To the south near Milford, site NWISWL5 shows a decline of 50 feet, which is likely due to agricultural groundwater use.

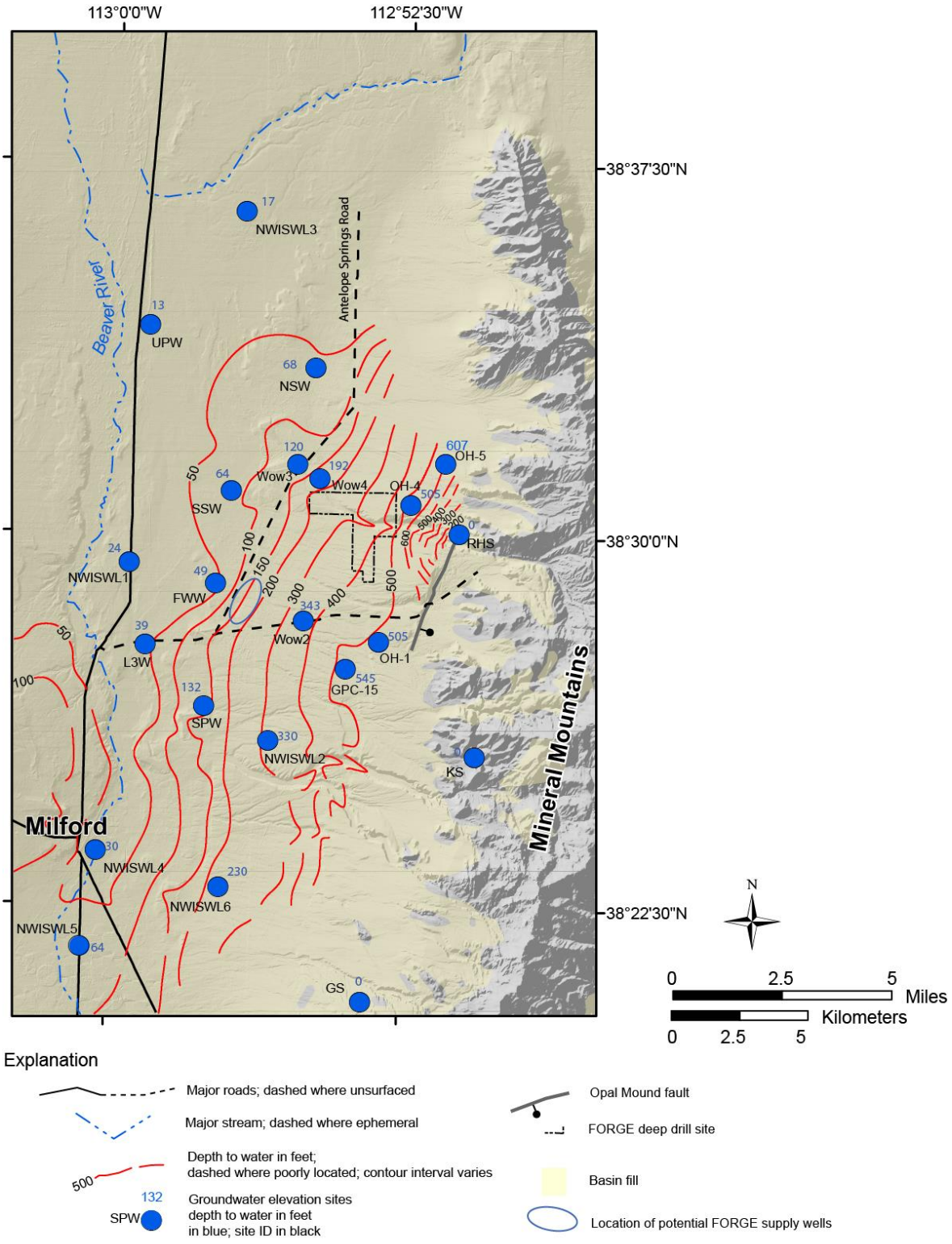

Figure 4. *Depth to water map for the FORGE study area. Depth to water calculated as the difference between the potentiometric surface in Figure 4 and a 5 meter digital elevation model.*

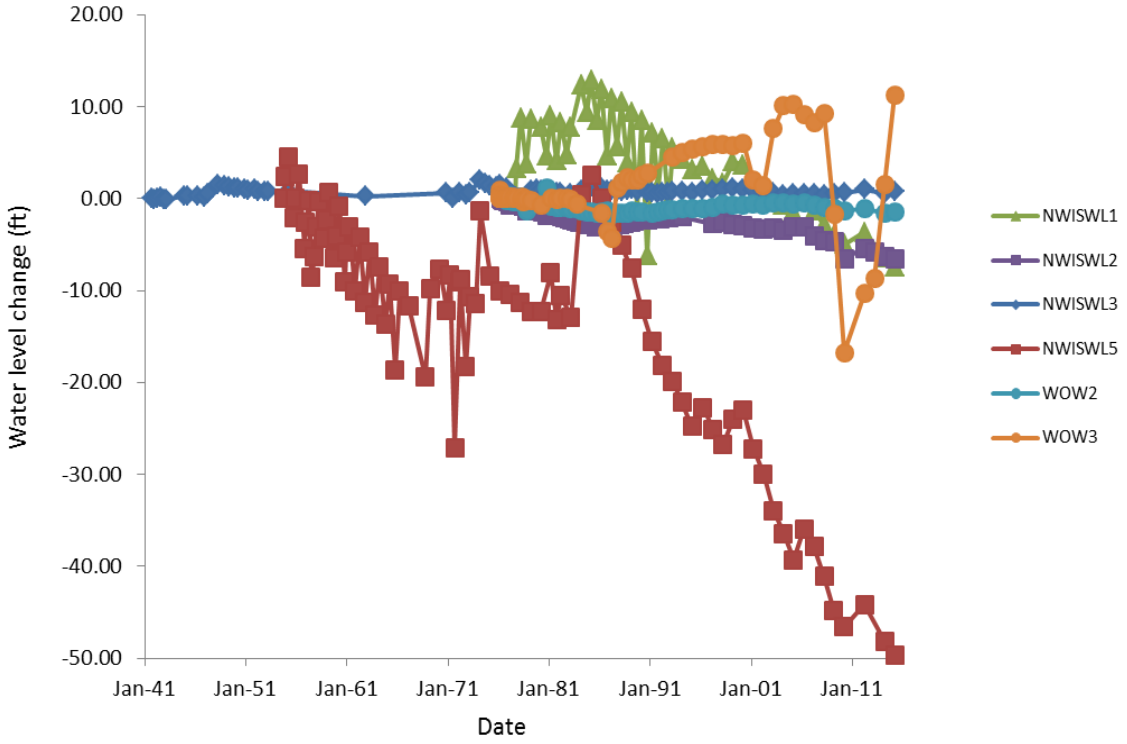

Figure 6. *Long-term water level changes in groundwater wells. Data used to construct the graph are from the USGS NWIS database (U.S. Geological Survey, 2015). Long-term water level changes near the FORGE deep drill site are less than 10 feet. To the south, near Milford site, NWISWL5 shows a decline of 50 feet, which is interpreted to be due to agricultural groundwater use.*

Groundwater Geochemistry and Isotopes

Groundwater chemistry provides basic information concerning groundwater quality and fluid flow through the shallow aquifer. Relevant chemical and isotopic data were obtained in earlier investigations (e.g. Vuataz and Goff, 1987). This section examines existing chemical and isotopic data for groundwater within the FORGE project area to constrain water quality and the potential for groundwater to supply water to the FORGE project.

The groundwater data comprises chemical analyses from: 1) two samples of the produced geothermal fluids and a sample from Roosevelt Hot Springs; 2) two samples from high elevation cool springs in the Mineral Mountains; and 3) samples of cooler groundwater from wells and springs across the study area. All water samples were analyzed for the major ions Na, K, Mg, Ca, Cl, SO_4, and HCO_3, and dissolved silica (Table 2). Some samples were analyzed for other constituents including B and the stable isotopes of deuterium and oxygen-18. Total dissolved solids (TDS) were calculated as the sum of dissolved constituents for each sample.

Major ion chemistry defines the dominant cation and anion in a sample based of meq/L concentrations (Kehew, 2000). Across the study area chemistry varies from Ca-HCO_3 to Na-Cl; a single sample is classified as Na-SO4 type (Figure 7). Samples of geothermal fluids from Roosevelt Hot Springs and geothermal production wells 14-2 and 54-3 are Na-Cl waters. Nearly all samples, down gradient and to west of these geothermal samples, share the Na-Cl chemistry. Two samples from Kirk Springs and Bailey Springs in the Mineral Mountains, up gradient of the geothermal samples, are Ca-HCO_3, representing non-thermal water. Other Ca-HCO_3 samples are located north of the project area near Antelope Springs and to the south near Milford. A single Na-SO_4 type sample occurs in an agricultural area east of Milford.

The groundwater compositions are differentiated using a Piper plot shown in Figure 8. Wells 14-2 and 54-3, and Roosevelt Hot Springs (RHS) plot in a corner of the diagram, and these waters are dominated by high Na and Cl, representing undiluted thermal water. Samples from locations west of the Opal Mound fault (sites WOW3 to L3W and SPW) show increasing relative concentrations of Ca, Mg, and SO_4 relative to Na and Cl, which results from mixing between RHS thermal water flowing down gradient and cool groundwater in the basin. Samples of upland springs BS and KS plot well to the left of the other samples with high portions of Ca and HCO_3. These waters represent cold groundwater flowing into the upper reaches of the basin fill aquifer.

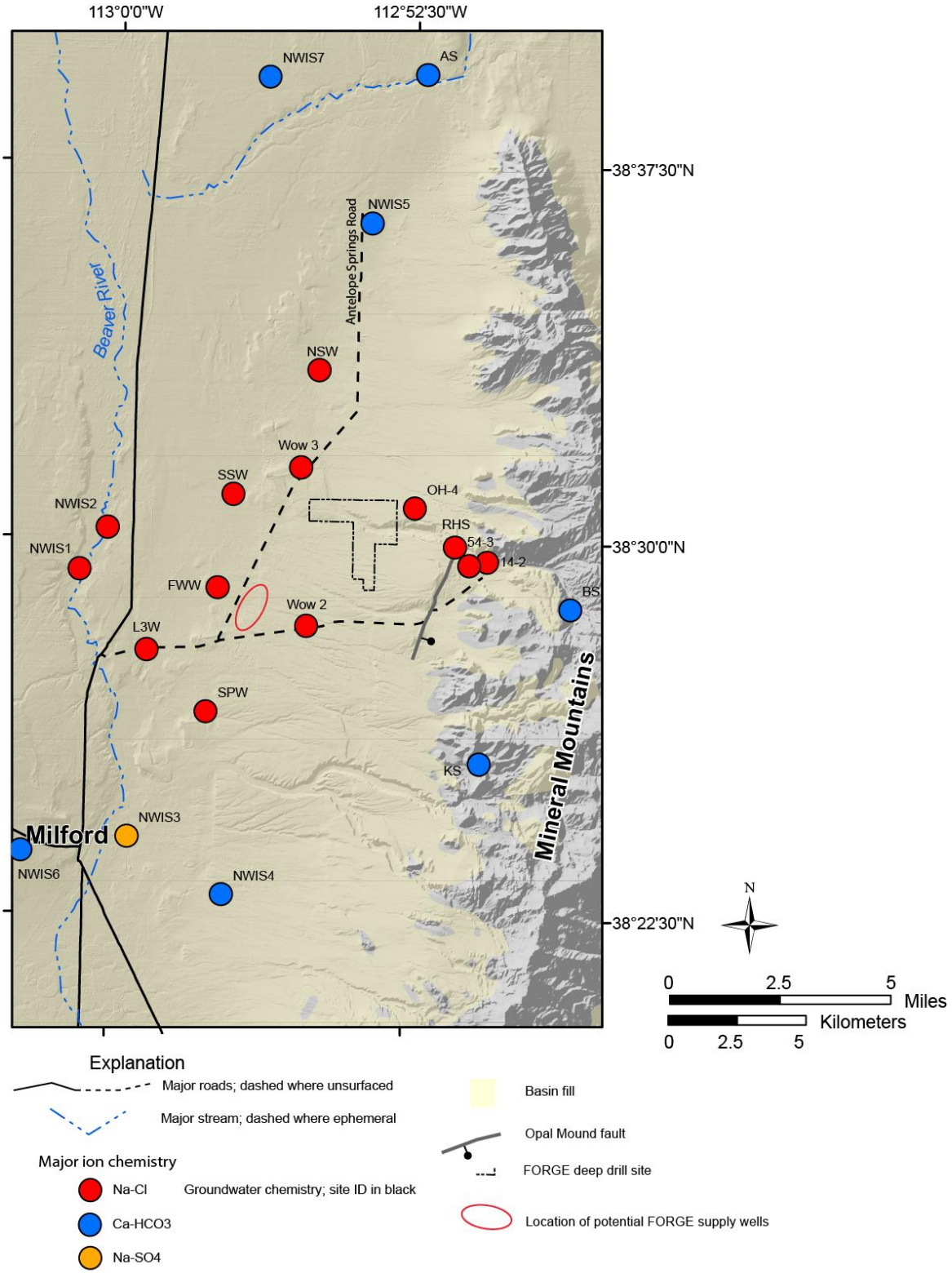

Figure 7. *Major ion chemistry for compiled groundwater samples. Site ID corresponds with those in Table 2.*

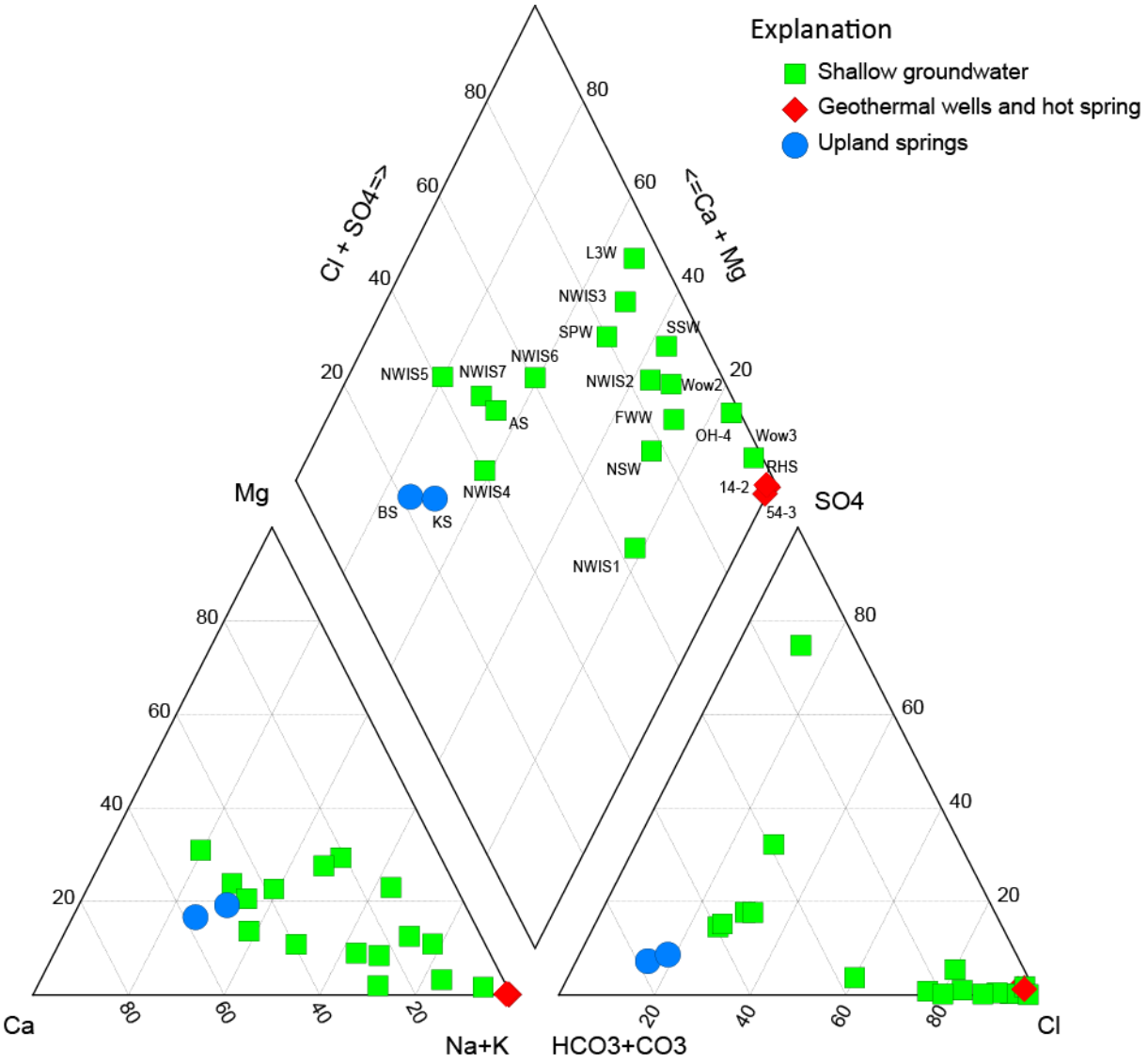

Figure 8. *Piper diagram of compiled groundwater chemistry. Site ID corresponds with those in Table 2.*

The contributions of the major anions and cations to the TDS of a given sample are shown in Figure 9. For most samples Na and Cl are the principal sources of TDS. Samples of thermal water from wells 14-2 and 54-3, and RHS are dominated by Na and Cl and have TDS values greater than 6000 mg/L. Samples from OH-4 to SPW plot along a mixing line of decreasing Na and Cl, as thermal water entrains cool groundwater with TDS less than 1000 mg/L. Samples of mixed waters (including NWIS3, FWW, NSW, and SSW) have concentrations of Ca and HCO3 that are greater than either the thermal water or cool

groundwater, suggesting some addition of solutes from water rock interaction and possibly calcite dissolution.

A map of TDS concentrations shows a plume of high TDS thermal water emanating from the north end of the Opal Mound Fault and Roosevelt Hot Springs (Figure 10). This plume broadly defines the area of thermal outflow in which TDS concentrations decrease to the west, north, and south as the plume disperses in the unconsolidated basin fill aquifer across the FORGE deep drill site. The Cl/B ratios in groundwater further reflect this process, as thermal water has a uniform Cl/B value of ~100. The groundwater Cl/B value remains consistent, as TDS decreases due to dilution from east to west (Figure 11). The Cl/B ratio rises to 200-700 on the periphery of the outflow plume where basinal groundwater is dominant.

The thresholds for primary and secondary drinking water standards are 1000 and 2000 mg/L, respectively. Groundwater beneath the FORGE deep drill site ranges from 5000, to >6000 mg/L, and it is unsuitable for use as drinking water supply. Potential supply wells located along the Antelope Springs Road east of the FWW well could encounter groundwater with TDS ranging from 2000 to just over 4000 mg/L.

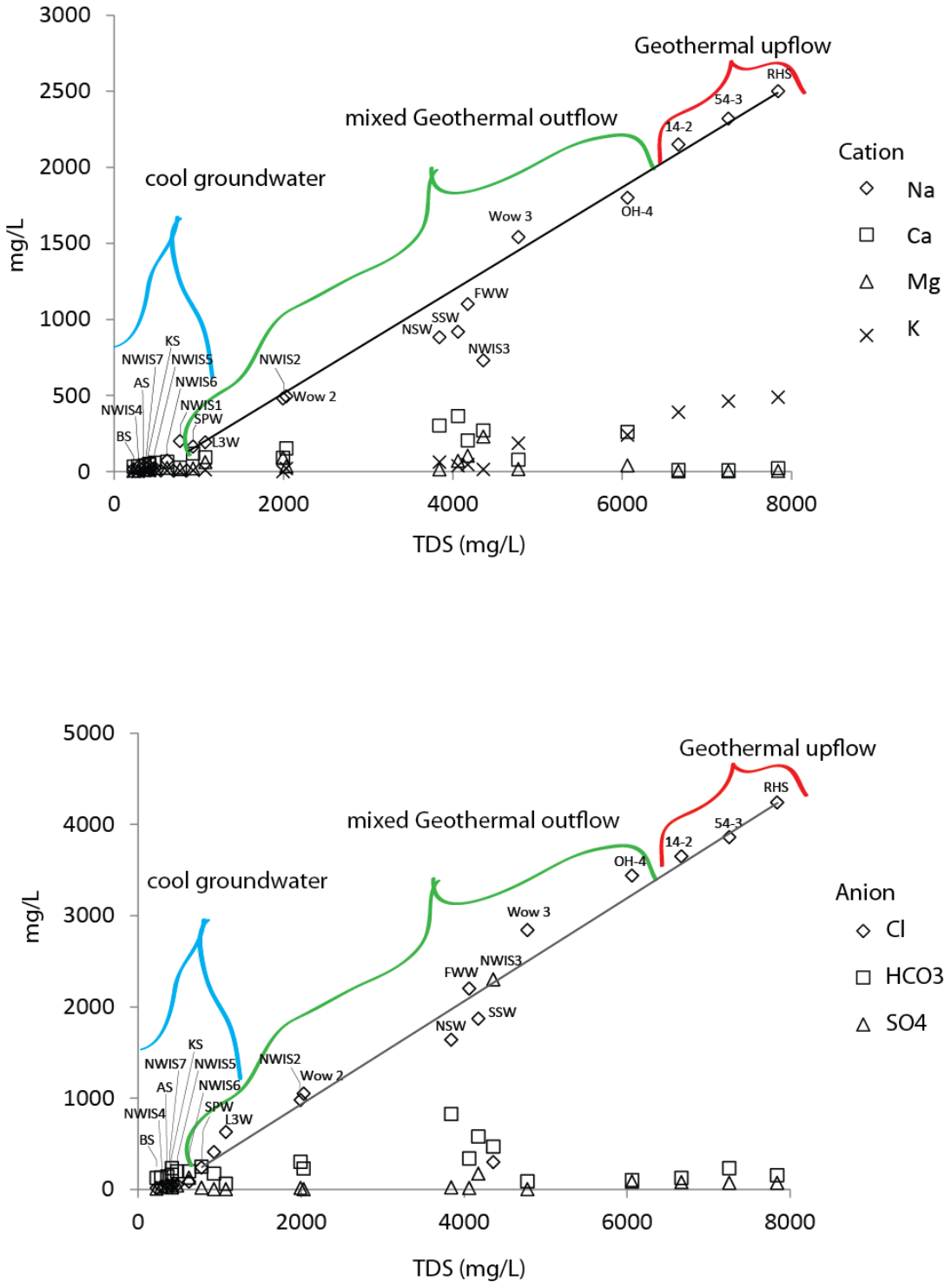

Figure 9. *Graphs of major solute concentrations versus TDS. Samples within the FORGE study area lie along Na-Cl mixing lines that extend between end-member compositions defined by thermal water from RHS and cold basinal groundwater in the center of the valley. Nearly all groundwater in the area surrounding the FORGE deep drill site has TDS values greater than 2000 mg/L.*

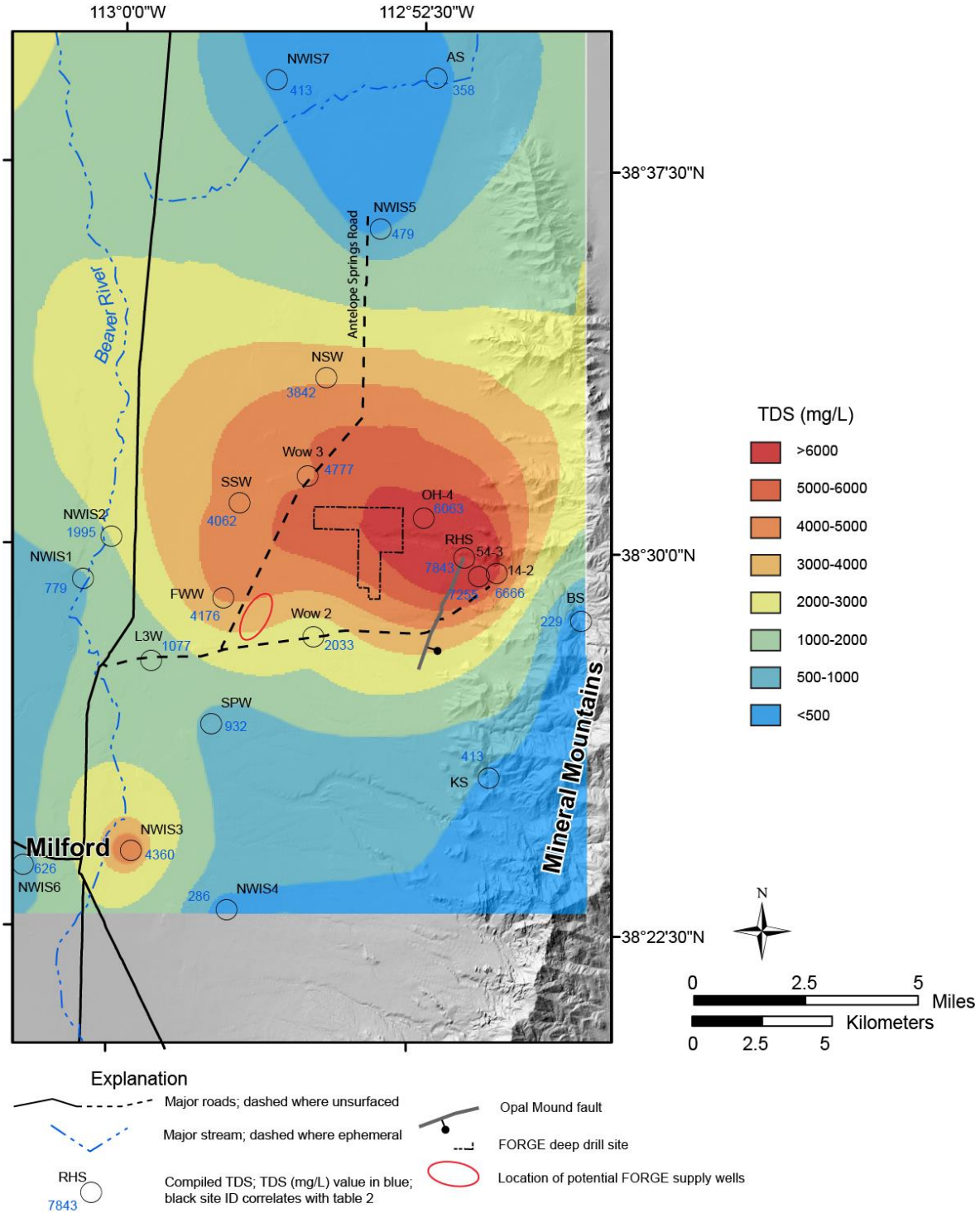

Figure 10. *Map of TDS concentrations. A high TDS plume extends to the west from Roosevelt Hot Springs (RHS) and the north end of the Opal Mound fault.*

Stable isotopes of deuterium (δ^2H) and oxygen ($\delta^{18}O$) provide information about both the source of the groundwater and the degree of high-temperature water-rock interaction (Clark and Fritz, 1997). These isotopes also provide an independent constraint on the interpretation of mixing trends. Deuterium and oxygen-18 isotope data exist for 11 samples (Table 2). Samples AS, NWIS5, SPW, BS, and NSW plot along and near the meteoric water lines and represent the compositions of local rainfall and snowmelt (Figure 12). Two samples of thermal water (14-2 and RHS) are shifted to the right from the meteoric water line by nearly 2 permil $\delta^{18}O$. These samples show evidence of isotope exchange produced by high-temperature water-rock interaction (Bowman and Rohrs, 1981). Samples L3W, FWW, SSW and WOW3 plot in between the thermal waters and the meteoric water line, reflecting mixing as the thermal (high TDS) plume disperses westward through the shallow aquifer (Figure 10).

In summary, the groundwater in the study area represents a mix of geochemically distinct waters that include: 1) thermal water; 2) meteoric water; and 3) cool basinal groundwater (Mower and Cordova, 1974; Vautaz and Goff, 1987; Kirby, 2012). The thermal water is dominated by Na and Cl, with TDS greater than 6000 mg/L, Cl/B~100, and enriched $\delta^{18}O$ values. Most groundwater in the vicinity of the FORGE deep drill site represents a mixture of thermal and basinal waters. Non thermal groundwaters have TDS less than 1000 mg/L, Cl/B>200, and stable isotope compositions that plot along the meteoric water line.

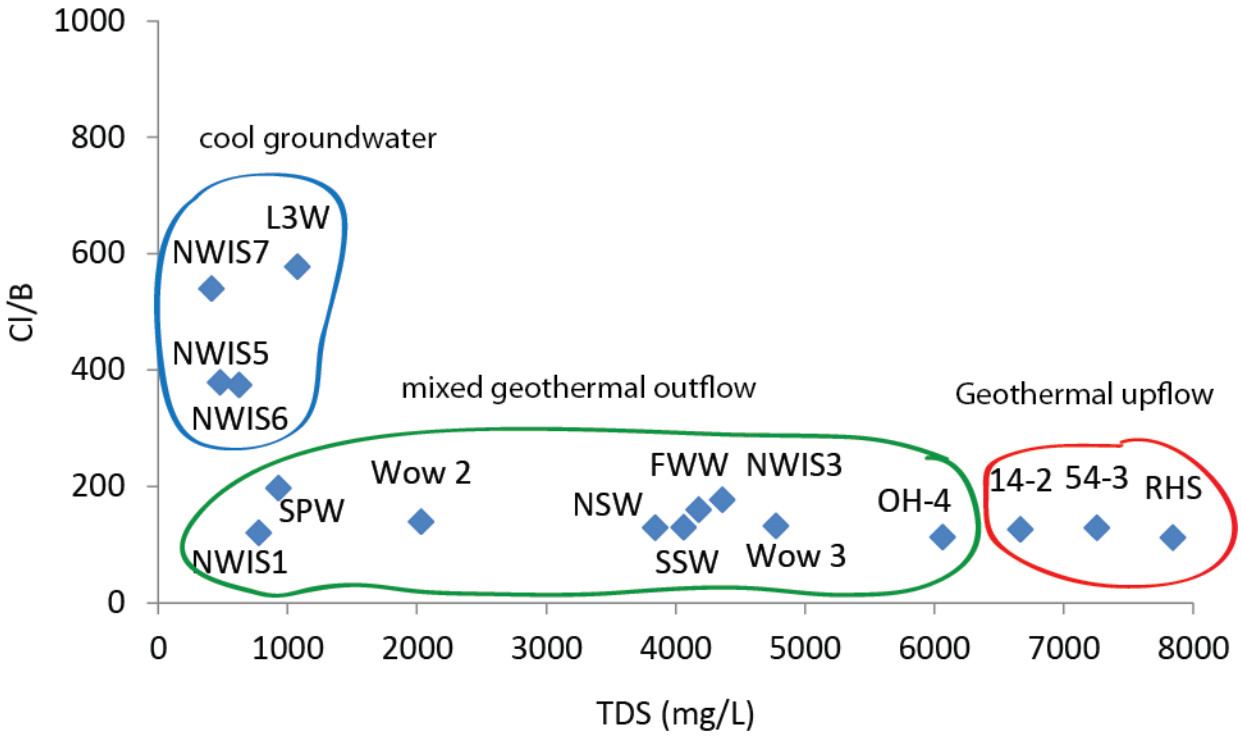

Figure 11. *Graph of Cl/B versus TDS. Most groundwater samples surrounding the FORGE deep drill site have uniform Cl/B values of ~100 with decreasing TDS resulting from mixing and dilution.*

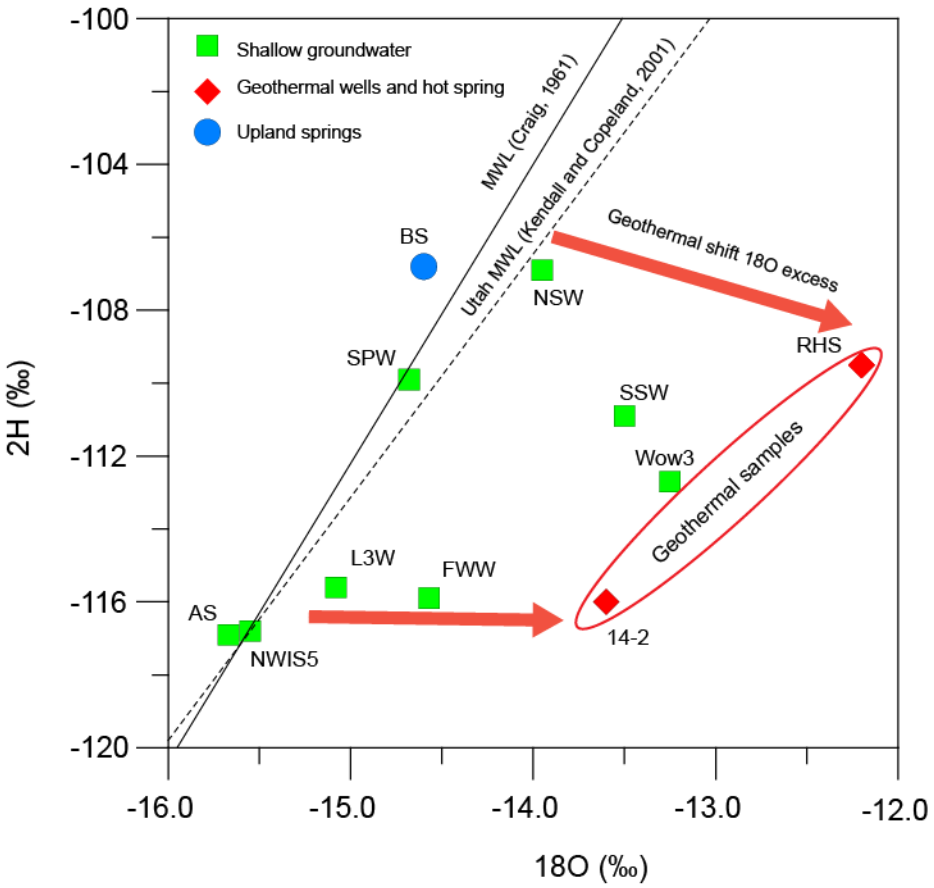

Figure 12. *Plot of stable isotope compositions (per mil) of groundwater. The meteoric water line (MWL) is defined by Craig (1961) and the Utah meteoric water line is defined by Kendall and Copeland (2001). Thermal water (14-2 and RHS) show a significant positive shift in $\delta^{18}O$ relative to local meteoric water due to isotope exchange during high-temperature water-rock interaction.*

Aquifer Test

The FORGE project will require water supply during drilling, stimulation, completion, and circulation testing. Water demands will likely be greatest during well stimulation, which could requireup to 3 million gallons during stimulation. The water will be stored in several large tanks. To fill these tanks a continuous supply of up to 200 gpm will be needed over a period of approximately 10 days. A single well aquifer test of a well near the FORGE deep drill site (completed in December, 2015) indicates sufficient availability of groundwater to meet these needs.

The drawdown test was conducted on a nine-inch diameter supply well at the First Wind maintenance facility located approximately 1 mile west of the proposed FORGE project office site. This well is labeled FWW on Figures 4 and 5, and included in Tables 1 and 2. The FWW well is completed in a confined part of the unconsolidated basin fill aquifer with a total depth of 651 feet (Figure 13). Based on driller's logs, the well is completed in sands and gravels with a

screened interval between 567 and 651 feet and a total aquifer thickness of 440 feet. Clay between 115 and 210 feet make up the confining layer.

The well was pumped at a rate of approximately 100 gpm for 24 hours, and the flow rate and total volume pumped were measured with a clamp on flow meter. Drawdown was measured in a sounding tube placed in the pumping well, by hand and with a downhole pressure transducer, during pumping and for a recovery period following pumping. Tables 3 and 4 contain the pump and drawdown data used to estimate transmissivity. Just prior to the test, the static water level was 49.1 feet below the wellhead. The water level after 24 hours of pumping was 127.1 feet and total drawdown during the test was 77.9 feet.

Transducer drawdown data and flow rate data was input into the modeling software AQTESOLVE (Duffield, 2007) and used to calculate a transmissivity of ~ 240 ft^2 per day for the FWW (Figure 14). Due to the changes in pump rate over time, the confined nature of the aquifer, and the partial well penetration, a Theis step solution was chosen for curve matching. Because there are no nearby monitoring wells, a storativity was not calculated. Instead storativity was assumed at 0.001 based on values typical of similar unconsolidated aquifers (Domenico and Schwartz, 1997). Modeled drawdown and recovery data fit well with observed data (Figure 14), and the estimated transmissivity at the FWW site appears accurate.

Two simple groundwater flow model scenarios were calculated to estimate potential drawdown from new supply wells. Each run assumes homogenous aquifer conditions with transmissivity and vertical thickness equal to that of the aquifer test well. Wells in the model runs screen the entire aquifer.

Model scenario A comprises two new supply wells, each pumping at 100 gpm, located east of the Antelope Springs Road (Figure 15). Model scenario B comprises a single supply well pumping at 200 gpm. In both models, drawdown is shown after 14 days of pumping (Figure 15). This drawdown period is greater than the 10 days required to provide the 3 million gallons of water in storage needed for drilling, completion, and testing of the FORGE project, and therefore should represent a maximum drawdown produced to supply the FORGE project.

In scenario A, the maximum drawdown in wells A and C is 87 feet. The drawdown cone rises sharply away from the model wells and in the FWW well it is only 5-10 feet. The 1 foot drawdown contour extends just over a mile radial distance from the potential supply wells. In scenario B, the maximum drawdown in well B is 138 ft. The spatial extent of drawdown scenario B is similar to scenario A and drawdown near FWW well is about 10 feet. The 1 foot drawdown contour extends radially nearly 1.5 miles from the potential supply well B. In both scenarios the amounts of drawdown are relatively small, and impacts on groundwater supply in nearby wells, and on roads and facilities should be minimal.

Model results represent a simple aquifer system based on conditions in the FWW well. Actual conditions near the potential supply wells could differ, and this could lead to different amounts of drawdown. If the transmissivity of the potential supply wells is greater than that calculated from the aquifer test well, then total drawdown could be less than the modeled values. A lower transmissivity at the potential supply wells could yield drawdown greater than the modeled values.

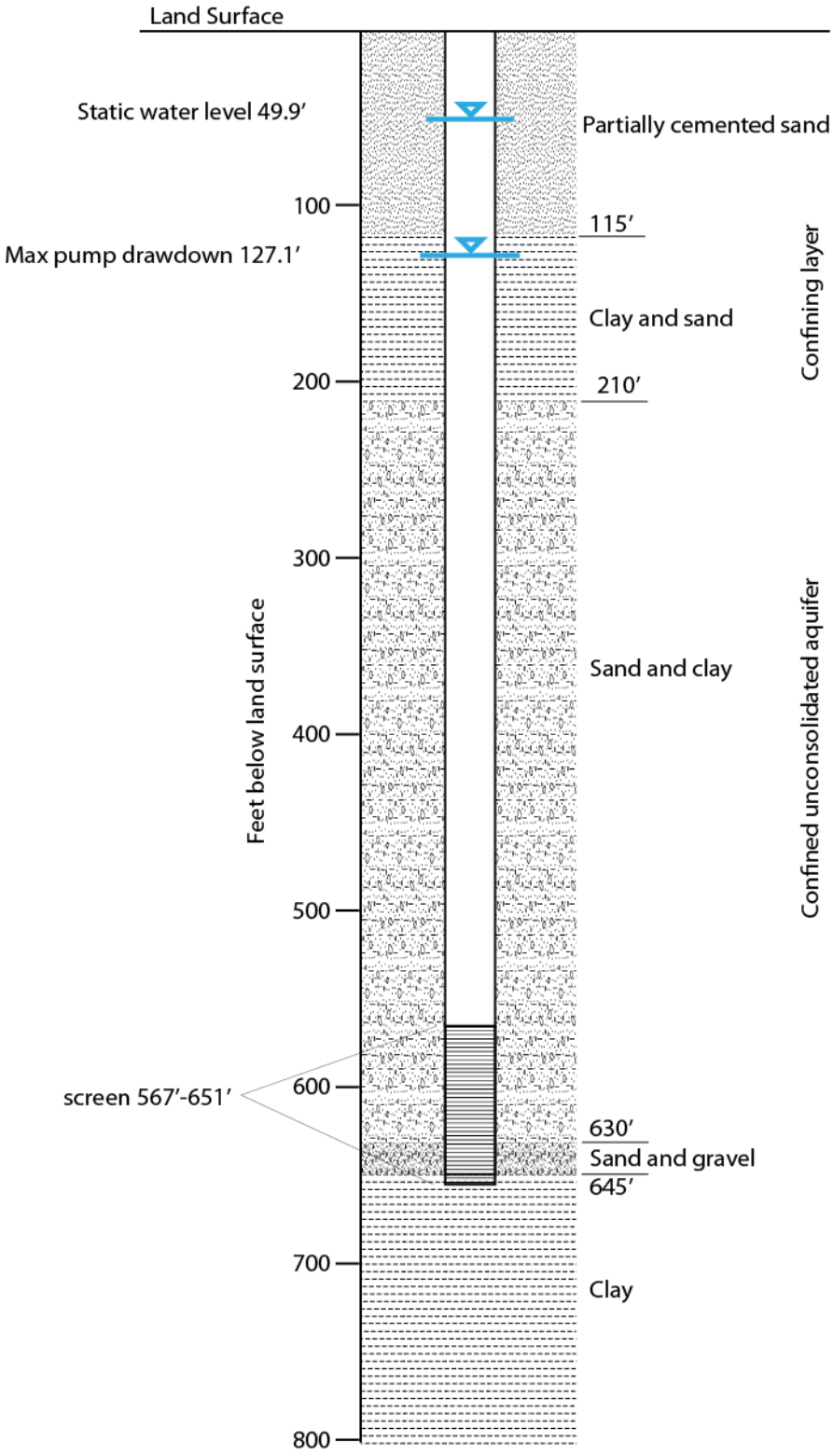

Figure 13. *Well completion schematic for the First Wind aquifer test well.*

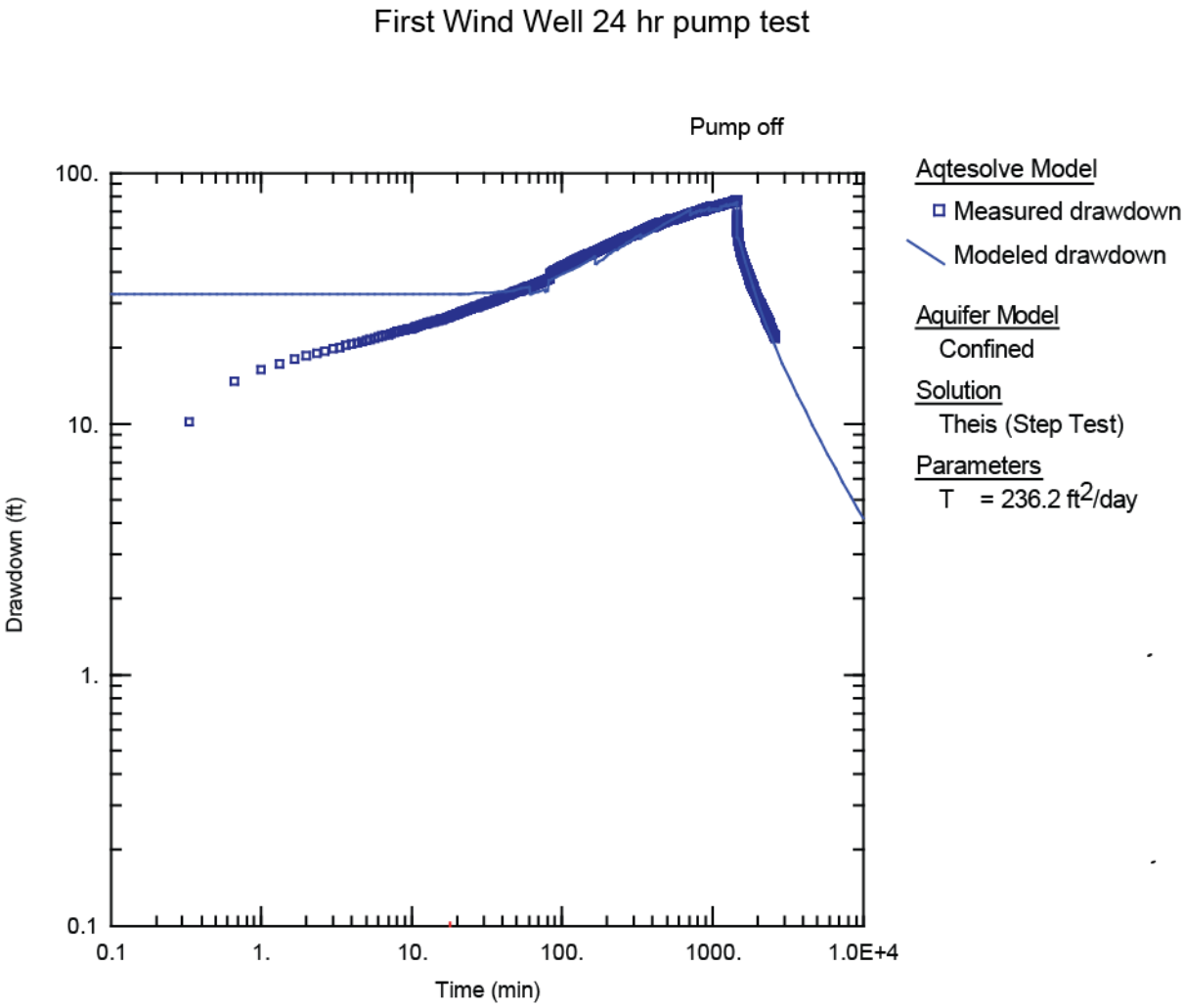

Figure 14. *Aquifer test modeled and measured drawdown.*

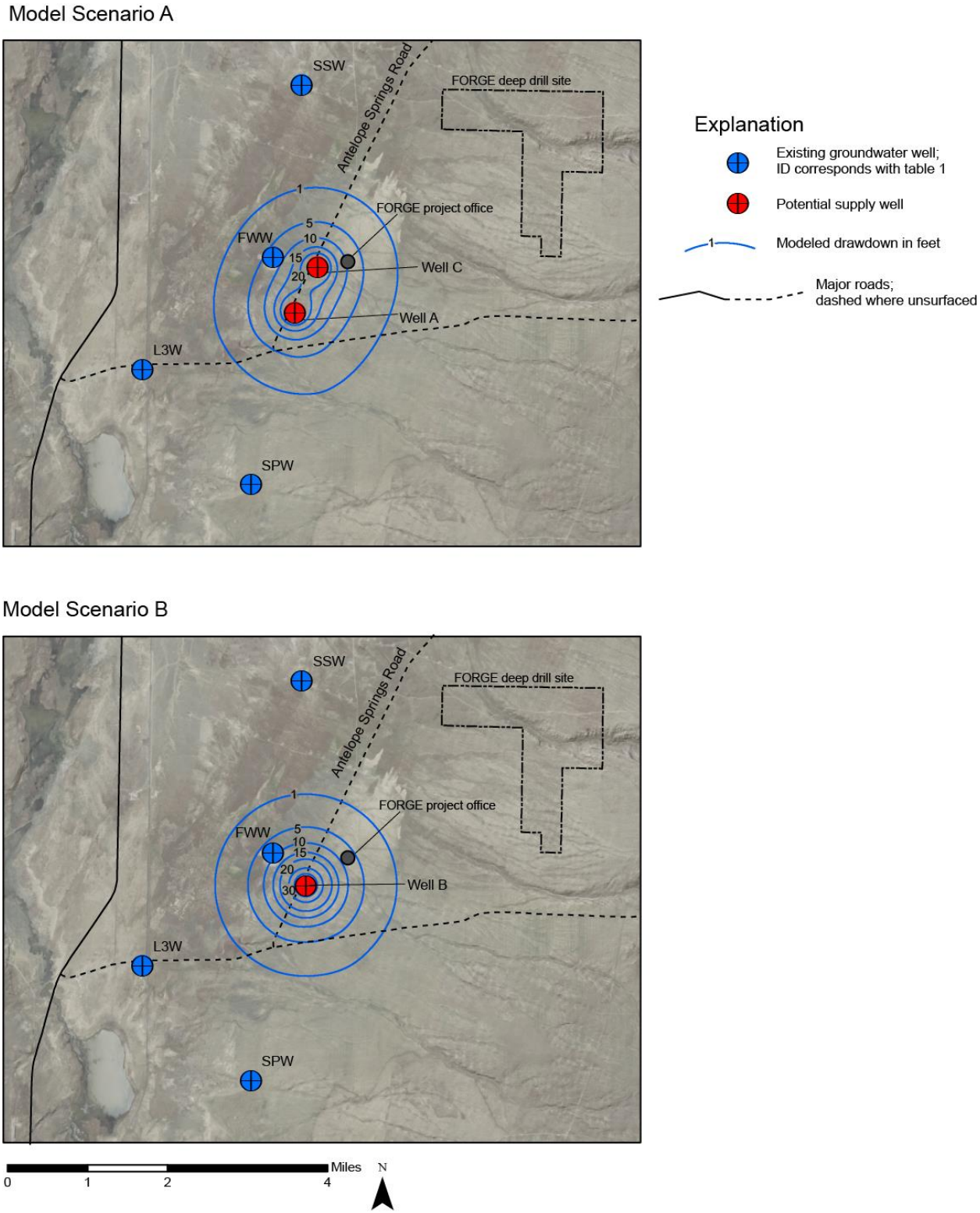

Figure 15. *Modeled drawdown for two potential supply well scenarios. See text for details.*

Error and Uncertainty

All data have a component of error and uncertainty. Error and uncertainty vary with the type of the data and its use. For the data in this report, uncertainty is discussed based on a qualitative low, medium, or high uncertainty ranking that includes a discussion of error where possible.

Hydrogeologic data presented in this report is largely based on compiled geologic mapping, previous hydrogeologic studies, and two aquifer tests. Geologic mapping in the area is well constrained and consequently the extent of the important hydrogeologic units has a low uncertainty. The permeability data for the hydrogeologic units is limited to two localized aquifer tests and permeability hydrogeologic units has a moderate uncertainty. Uncertainty in the compiled water levels is controlled by measurement error which in most cases is less than a foot. Water level data has a low uncertainty. Uncertainty in the compiled geochemical data is limited to standard laboratory error. The uncertainty for the geochemical data is low. The uncertainty related to the aquifer test data is limited to measurement error and is therefore low. Drawdown models are based on broad assumptions of aquifer properties and pumping scenarios and therefore have a moderate uncertainty.

Conclusions

The groundwater in and around the FORGE deep drill site resides in a shallow unconsolidated basin fill aquifer that overlies impermeable crystalline basement rock. This aquifer is not potable and is not used for human consumption. Groundwater that is currently used in the study area for seasonal stock watering at several wells and fire suppression.

Based on compiled water levels for groundwater in the unconsolidated basin fill aquifer, the potentiometric surface slopes to the west away from the Opal Mound fault. Groundwater depth beneath the FORGE deep drill site is between 200 and 500 feet and at about 5100 feet in elevation. Depth to water in the unconsolidated basin fill, in areas surrounding the FORGE deep drill site, ranges from tens of feet along the valley floor to greater than 500 feet west of the Opal Mound fault. Potential supply wells are located about 2.5 miles southwest from this site, where the depth to groundwater is approximately 150 feet.

Groundwater in the study area spans a wide range of chemical compositions from dilute (TDS < 500 mg/L) to saline (TDS > 6000 mg/L). The springs in the Mineral Mountains discharge dilute Ca-HCO_3 water, whereas at Roosevelt Hot Springs the groundwater is made of Na-Cl thermal water. This thermal water fills the shallow aquifer and disperses westward as it migrates downhill. Increasing dilution with cool basinal groundwater is reflected in decreasing TDS from east to west. Groundwater TDS concentrations around the FORGE deep drill site range from 2000 to >6000 mg/L TDS, exceeding both the primary and secondary drinking water standards. New water supply wells are located southwest of the FORGE deep drill site.

A new 24-hour aquifer test was completed on a supply well at the First Wind maintenance facility. Modeled results of this test yield a transmissivity 240 ft^2 per day for a confined section of the unconsolidated basin fill aquifer near the planned location of the supply wells. Forward models yield drawdowns that will produce minimal impacts on existing wells and infrastructure. Maximum drawdowns for a double supply well scenario is 87 feet and 138

feet for a single supply well scenario. Both scenarios have drawdowns of one foot at distances of just over one mile from the potential supply wells.

References

Allis, R.G., Gwynn, M., Hardwick, C., Kirby, S. Moore, J., and Chapman, D., 2015, Re-evaluation of the pre-development thermal regime of Roosevelt Hot Springs geothermal system, Utah: *Proceedings*, 40th Workshop on Geothermal Reservoir Engineering, Stanford University, CA.

Allis, R.G., Moore, J.N., Davatzes, N., Gwynn, M., Hardwick, C., Kirby, S., Pankow, K., Potter, S., and Simmons, S.F., 2016, EGS Concept Testing and Development at the Milford, Utah FORGE Site: *Proceedings*, 41st Workshop on Geothermal Reservoir Engineering, Stanford University, Stanford, CA.

Bowman, J.R., and Rohrs, D.T., 1981, Light-stable-isotope studies of spring and thermal waters from the Roosevelt Hot Springs and Cove Fort/Sulphurdale Thermal Areas and of clay minerals from the Roosevelt Hot Springs Thermal Area: Topical Report, U.S. Department of Energy/Division of Geothermal Energy, contract number DE-AC07-80ID12079, 40 p.

Capuano, R., and Cole, D.R., 1982. Fluid-mineral equilibria in a hydrothermal system, Roosevelt Hot Springs, Utah: Geochimica et Cosmochemica Acta, v. 46, p. 1353-1364.

Clark, I., and Fritz, P., 1997, Environmental isotopes in hydrogeology: New York, Lewis Publishers, 328 p.

Craig, H., 1961, Isotopic variation in meteoric waters: Science, v. 133, p. 1702-1703.

Coleman, D.S., Bartley, J.M., Walker, J.D., Price, D.E., and Friedrich, A.M., 1997, Extensional faulting, footwall deformation and plutonism in the Mineral Mountains, southern Sevier Desert, *in* Link, P.K., and Kowalis, B.J., editors, Mesozoic to recent geology of Utah: Brigham Young University Geology Studies, v. 42, part 2, p. 203-233.

Domenico, P.A., and Schwartz, F.W., 1997, Physical and chemical hydrogeology: New York, John Wiley and Sons, 506 p.

Duffield, G.M., 2007, AQTESOLVE: Hydrosolve Inc., Reston, Virginia.

Faulder, D.D., 1991, Conceptual geologic model and native state model of the Roosevelt Hot Springs hydrothermal system, *in* Ramey, H.J. Jr., Horne, R.N., Kruger, P., Miller, F.G., Brigham, W.E., Cook, J.W., editors, Proceedings of the Sixteenth Workshop on Geothermal Reservoir Engineering: Stanford, California, Stanford University, p. 131-142.

Glen, W.E., and Hulen, J.B., 1979, Interpretation of well log data from four drill holes at the Roosevelt Hot Springs KGRA: DOE Earth Science Laboratory Report, University of Utah, 74 p.

Hardwick C.L., Gwynn, M., Allis, R., Wannamaker, P., and Moore, J., 2016, Geophysical Signatures of the Milford, Utah FORGE Site. *Proceedings*, 41st Workshop on Geothermal Reservoir Engineering, Stanford University, Stanford, CA.

Hintze, L.H., and Davis, F.D., 2003, The geology of Millard County, Utah: Utah Geological Survey Bulletin 133, 305 p.

Kehew, A.E., 2000, Applied chemical hydrogeology: Upper Saddle River, New Jersey, Prentice Hall, 368 p.

Kendall, C., and Coplen, T.B., 2001, Distribution of oxygen-18 and deuterium in river waters across the United States: Hydrological Processes, v. 15, p. 1363–1393.

Kirby, S.M., 2012, Geologic and hydrologic characterization of regional nongeothermal groundwater resources in the Cove Fort area, Millard and Beaver Counties, Utah: Utah Geological Survey Special Study 140, 46 p.

Mason, J.L., 1998, Groundwater hydrology and simulated effects of development in the Milford area, an arid basin in southwestern Utah: U.S. Geological Survey Professional Paper 1409-G, 69 p.

Moore, J.N., and Nielsen, D.L., 1994, An overview of geology and geochemistry of the Roosevelt Hot Springs geothermal area, *in* Blackett, R.E., and Moore, J.N., editors, Cenozoic geology and geothermal systems of southwestern Utah: Utah Geological Association Publication 23, p. 25-36.

Mower, R.W., 1978, Hydrology of the Beaver Valley area, Beaver County, Utah, with emphasis on groundwater: State of Utah Department of Natural Resources Technical Publication No. 63, 90 p.

Mower, R.W., and Cordova, R.M., 1974, Water resources of the Milford area, Utah, with emphasis on groundwater: State of Utah Department of Natural Resources Technical Publication No. 43, 106 p.

Nielson, D.L., Evans, S.H., and Sibbett, B.S., 1986, Magmatic, structural, and hydrothermal evolution of the Mineral Mountains intrusive complex, Utah: Geological Society of America Bulletin, v. 97, p. 765-777.

Rowley, P.D., Vice, G.E., McDonald, R.E., Anderson, J.J., Machette, M.N., Maxwell, D.J., Ekren, E.B., Cunningham, C.G., Steven, T.A., and Wardlaw, B.R., 2005, Interim geologic map of the Beaver 30’ x 60’ quadrangle, Beaver, Piute, Iron, and Garfield Counties, Utah: Utah Geological Survey Open-File Report 454, 27 p., 1 plate, scale 1:100,000.

Saltus, R.W., and Jachens, R.C., 1995, Gravity and basin-depth maps of the Basin and Range Province, western United States: U.S. Geological Survey Map GP-1012, scale 1:2,500,000.

Simmons, S., Kirby, S., Jones, C., Moore, J., Allis, R., Brandt, A., and Nash, G., 2016, The Geology, Geochemistry, and Geohydrology of the FORGE Deep Well Site, Milford,

Utah: *Proceedings*, 41st Workshop on Geothermal Reservoir Engineering, Stanford University, CA.

Vuataz, F.D., and Goff, F., 1987, Water geochemistry and hydrogeology of the shallow aquifer at Roosevelt Hot Springs, southern Utah—a hot dry rock prospect: Los Alamos National Laboratory, contract report LA-11160-HDR, 63 p.

U.S. Geological Survey, 2015, National Water Information System database: Online <http://waterdata.usgs.gov/nwis>, accessed December 2015.

Review logs and cuttings from Acord 1

TASK 1.1.2

Task 1.1.2 Review logs and cuttings from Acord 1

A. Acord 1-26 Geophysical Logs

Six different geophysical logs were run on the Acord 1-26 well. Caliper, gamma ray (GR), spontaneous potential (SP), bulk density (RHOB), short laterolog (LLS), induction log medium (ILM), and deep laterolog (LLD) were collected from 1104 to 7923 feet in April, 1979. There were problems with hole conditions that impacted the RHOB curve. The operator indicates that the caliper was not working at the bottom section of the hole. There are several caliper reruns in the logs and they match the first caliper run. A second well log run was conducted in May, 1979 for DeltaT (DT), Caliper, Temperature, and GR from 7800 to 11439. The following day, SP, shallow focus, medium and deep resistivity was collect in the interval above. Gamma Ray – Neutron was collected from 7900 to 12, 148 during in late May, 1979. A second Gamma Ray – Neutron and short- and long-spaced Densilog were collected from 7900 to 12,644 in June, 1979. A final RHOB log was collected in late June, 1979 from 7900 to 12,644 feet. The caliper shows that hole conditions were not very good with large areas of slump and washout which affected the RHOB measurements and the movement of the downhole tools. Furthermore, the bottom-hole temperature (BHT) is approaching the limit where some of the downhole tools, GR, Caliper, DT, and resistivity either didn't work or the operators didn't expect them to work so they are not recorded.

Detailed normalization and modification of the curves has not been performed on the Acord 1-26 geophysical curves due to time constraints. This should be done at a later date so that petrophysical parameters of the different units can be calculated. However, other detailed information of the gneiss, granite and younger sediments are still important. There is an interesting trend in the SP and resistivity curves (LLS, ILM, and LLD) that we believe indicated the transition from volcaniclastic to sediments (9,470 ft) and then sediments to granite (9,880 ft). The SP curve between 9,400 and 10,500 increases in the positive direction suggesting that the porosity is decreasing along with formation water concentration. The resistivity logs indicate higher resistivity, possibly due to decreasing porosity and/or intergranular water. The density log also shows a similar trend of increasing values for the same interval. A review of the cuttings indicate that there is an erosional surface on top of the batholith after intrusion. From 9,740 to 10,200 feet is possibly a zone of weathered granitic clasts, granite sand, and volcaniclastic that are likely cemented with calcite or silica. We suggest that this shows the weathered sediments deposited on top of the batholith are a mixture of cannibalized, weathered granite clasts and eroded volcaniclastic sediments. From 10,200 to 10,500 is a zone of negative trending SP and higher-shifting resistivity and higher density. This is likely a zone of altered and weathered granitic rock below the top of the old erosional surface. Below 10,500, the resistivity and density curves are showing higher and nearly constant values indicating a resistive and dense granitic formation.

With limited time available to thoroughly analyze bore samples, more work is needed to create a single, high-confidence composite geologic section of the Acord 1 well. EGI composite section was inferred from the analyses of thin section samples at defined intervals. The UGS composite section was inferred from analyses of rock chip samples from drill cuttings at not only defined intervals, but also at specific depths where changes in geology were expected as taken from the work of Hintze and Davis (2003) and at depths where evidence of changes inferred from the geophysical well logs occur. Of the 3 composite sections, the Hintze and Davis (2003) work

appears to have errors in the original driller logs which propagate to the final interpretation. The EGI and UGS composite sections were created by analyzing different types of data independently. The differences observed are small and most discrepancies could be due to sampling intervals used. Regardless, the most recent analyses completed by EGI and UGS represent an updated and realistic interpretation of the geologic section of Acord 1 well.

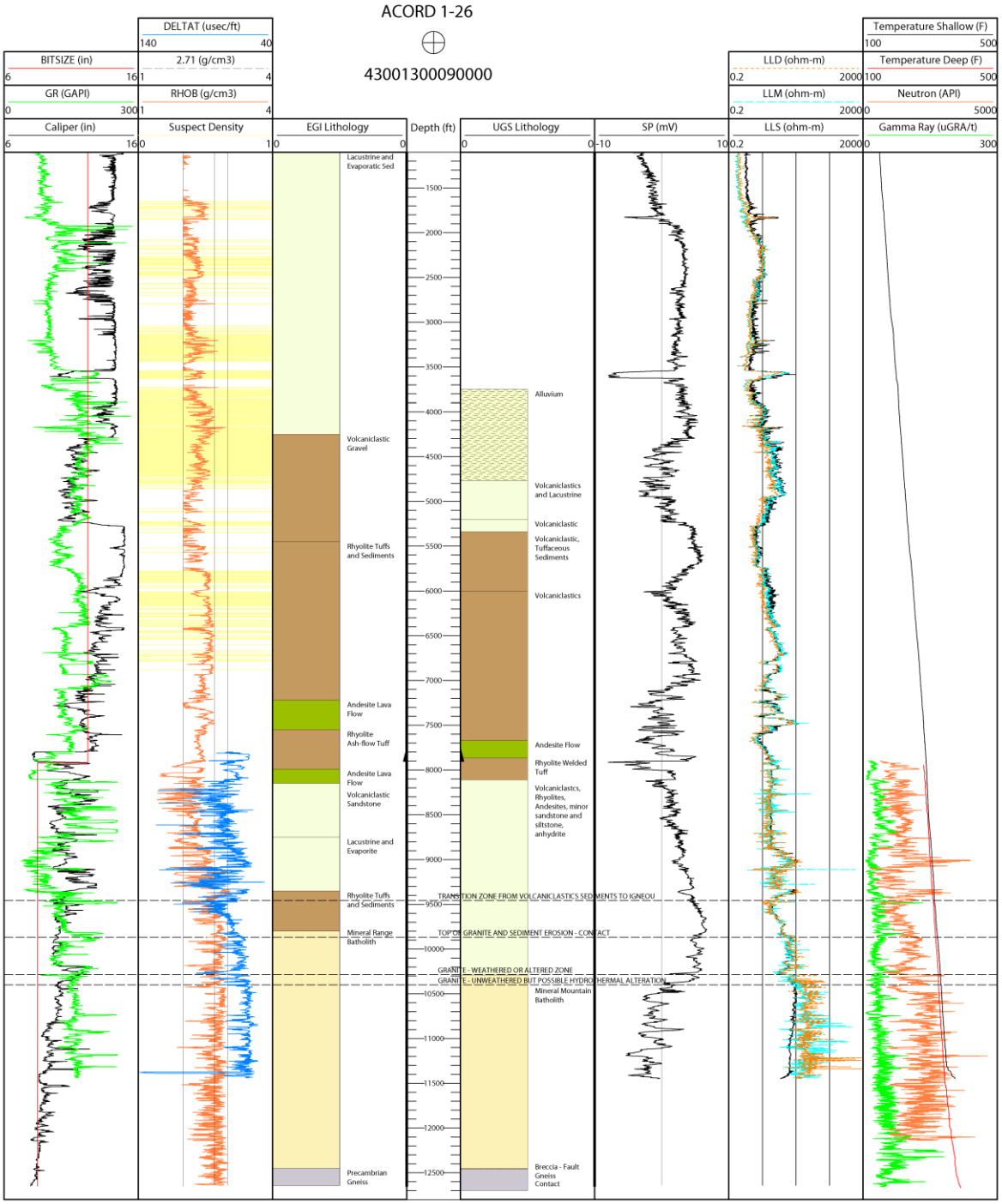

Figure A.1. *Acord 1 well geophysical log.*

B. Petrographic and X-ray Diffraction Analyses of 62 Drill Cutting Samples from Geothermal Well Acord 1-26

Sixty-two samples of well cuttings were selected from Acord 1-26 for combined petrographic and X-ray diffraction analyses.

The well penetrated a thick sequence (~10,175 ft), of basin fill consisting of lacustrine sediments, evaporite deposits, volcaniclastic deposits, ash-flow tuff and andesite lava flows before hitting crystalline basement rocks of composed of granite of the Mineral Range Batholith and Precambrian Gneiss (Figure B1.1).

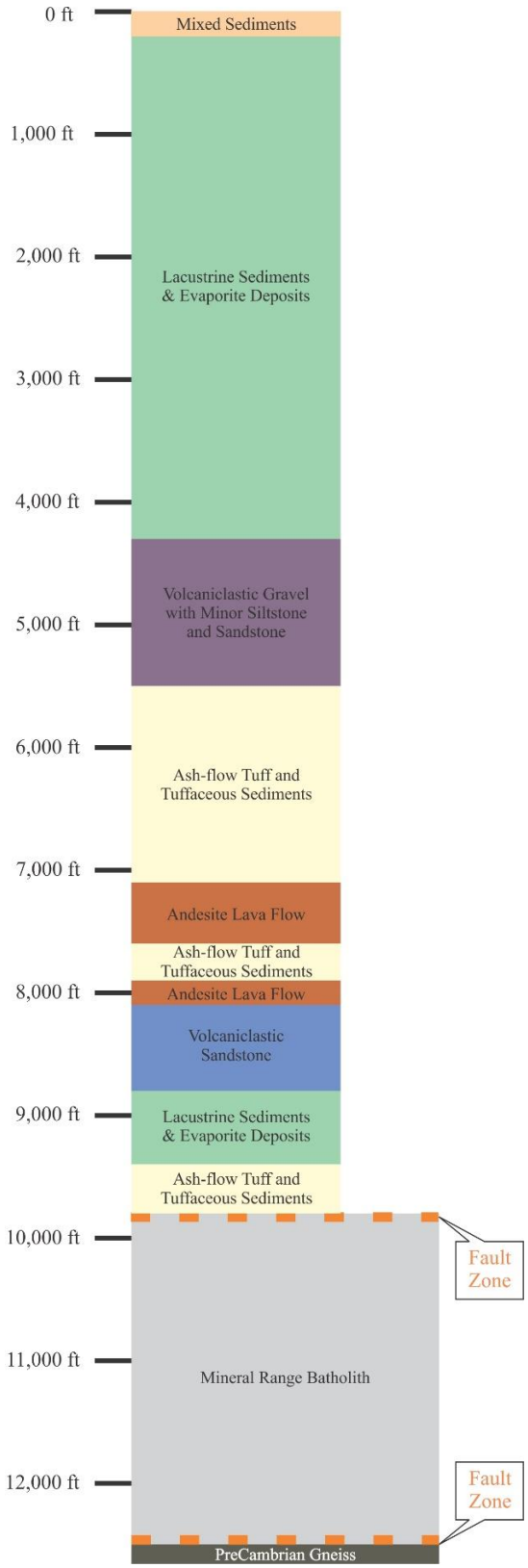

Figure B1.1: Lithologic column showing formations intercepted by Acord 1-26 as interpreted from thin section analyses of 62 samples of drill cuttings.

B2.0 X-ray diffraction methods

Whole-rock and clay-sized X-ray diffraction (XRD) analyses were performed on each sample in the XRD laboratory at the Energy & Geoscience Institute at the University of Utah, using a Bruker D8 Advance X-ray diffractometer. Phase quantification using the Rietveld method was performed using TOPAS software, developed by Bruker AXS. The Rietveld method fits the peak intensities calculated from a model of the crystalline structure to the observed X-ray powder pattern by a least squares refinement. This is done by varying the parameters of the crystal structures to minimize the difference between the observed and calculated powder patterns. Because the whole powder pattern is taken into consideration, problems of peak overlap are minimized and accurate quantitative analyses can be obtained.

The following operating parameters were used when analyzing the powdered samples: Cu-K-α radiation at 40 kV and 40 mA, 0.02°2θ step size, and 0.4 and 0.6 seconds per step, for clay and bulk samples respectively. Clay samples were examined from 2 to 45°2θ, and the bulk samples from 4 to 65°2θ. The instrument is equipped with a Lynx Eye detector, which collects data over 2.6 mm, rather than at a point, greatly increasing X-ray counts collected and decreasing acquisition time; a rotating sample stage, which increases the mineral grain orientations encountered by the incident electron beam; and an automated sample exchanger capable of holding up to 90 samples.

At a minimum, three analyses were conducted on each sample, two or more on the clay-sized fraction and one on the bulk sample.

The clay-sized fraction is prepared as follows:

- Samples are first ground in an electric mortar and pestle.
- The resulting powder is mixed with deionized water and further ground in a micronizing mill until fine enough to pass through a 325 mesh screen (particle size < 44 micrometers).
- The less than 5 micrometer size fraction is then separated using Stokes Law by placing the resulting slurry in a beaker (with a small amount of dispersant) and vigorously stirring. After allowing it to settle for 37 minutes, an aliquot (~100 ml) is pipetted out of the top ½ inch.
- The particles are removed from the water column by centrifuging for 15 min at 1500 rpm.
- The bulk of the clean water is decanted, and the sample is thoroughly mixed using an ultra-sonic homogenizer.
- The slurry is then applied to a glass slide using a pipette.
- Once the sample has dried, an ‘air dried’ XRD pattern is obtained.
- The sample is then allowed to interact with ethylene glycol vapors for at least 12 hours at 65°C to induce swelling of susceptible clays, after which a ‘glycolated’ XRD pattern is obtained.
- Additional heat treatments and scans that involve heating for 1 hour at 375 and/or 550°C may be required to confirm the presence of some clay species.

The fraction used for the bulk analysis is prepared as follows:

- Samples are first ground in an electric mortar and pestle.

- The resulting powder is mixed with deionized water and further ground in a micronizing mill until fine enough to pass through a 325 mesh screen (particle size < 44 micrometers).
- The sample is then rolled approximately 50 times to randomly orient the mineral grains.
- The powder is placed in a sample holder which has concentric ridges on the bottom to help decrease the effects of preferred orientation.
- The surface is smoothed with a razor blade to eliminate surface roughness.
- An XRD pattern of the bulk sample is obtained.

The air-dried, glycolated and heated scans of the clay-sized fraction are compared with each other to identify the clay minerals present in the sample, using methods described by Moore and Reynolds (1997). The mineralogy of the clay fraction is then used in the Rietveld refinement of the bulk sample to quantify the abundances of all crystalline phases that are present.

B3.0 X-ray diffraction results

Bulk XRD results are given in Table B3.1. Figure B3.1 shows all XRD data vs depth. Figure B3.2 shows clay mineral XRD data vs depth. Figure B3.3 shows carbonate and sulfate mineral XRD data vs depth.

Table B3.1: Results of X-ray diffraction analyses. Mineral abundances are given in weight percent of the sample, with results rounded to the nearest whole number. Fields marked with tr (trace) indicate that the mineral is present in the clay-sized fraction, but not detectable in the bulk XRD patterns; that its abundance calculated from the Rietveld refinement was less than one weight percent of the sample; and/or it was observed as a trace phase during petrographic analyses. I/S = interlayered illite/smectite. C/S = interlayered chlorite/smectite. Estimates of the extent of interlayering in I/S and C/S, made during the clay-sized fraction analyses, are given in the last column. Samples from the same lithologic units have color coded rows.

Depth (ft)	Smectite	I/S	C/S	Illite	Chlorite	Kaolinite	Plagioclase	Sanidine	K-feldspar	Quartz	Hornblende	Biotite	Apatite	Clinopyroxene	Magnetite	Titanite	Epidote	Prehnite	Rutile	Pyrite	Hematite	Aragonite	Calcite	Dolomite	Anhydrite	Bassanite	Halite	Analcime	% illite in I/S, or % chlorite in C/S
70-100	tr			7		11	17		11	28													27						
320-350	2			7		16	7		7	32													19	10	tr				
590-620	tr			12		tr	7		11	15												12	21	21			1		
830-860	tr			11			6		9	10												7	14	36	4	3			
1070-1100	tr			9			9		10	15												12	20	25					
1340-1350	tr			15			6		13	13												15	12	20	2	5			
1580-1610	tr			15			6		13	13												8	14	26	5			1	
1820-1850	tr			13	tr		4		12	9												5	10	19	13	10		4	
2090-2120	tr			14	2		16		18	27												2	10	9				2	
2330-2360	tr			4	4		22		17	35													13	3				2	
2600-2630	tr			16	3		17		20	25												1	10	4	2			2	
2840-2850	tr			10	9		11		21	35													14						
3080-3110	tr			21	3		10		19	29													12		6				
3320-3350	2			6	7		7		17	16													11	tr	35				
3590-3600	2			6	4		26		21	31											tr		4	3	2				
3840-3850	3			11	7		11		21	17											tr		14	10	6				
3990-4000	tr			17	3		14		21	23													14	5	4				

4240-4250	4			10	9		14		21	15											tr		12	6	8				
4380-4400	2			6	2		32		25	31													2		tr				
4640-4650	1			3	5		27		31	28											2		3		tr				

Table B3.1 Continued:

Depth (ft)	Smectite	I/S	C/S	illite	Chlorite	Kaolinite	Plagioclase	Sanidine	K-feldspar	Quartz	Hornblende	Biotite	Apatite	Clinopyroxene	Magnetite	Titanite	Epidote	Prehnite	Rutile	Pyrite	Hematite	Aragonite	Calcite	Dolomite	Anhydrite	Bassanite	Halite	Analcime	% illite in I/S, or % chlorite in C/S
4840-4850	1			4	5		31		28	27											2		2		tr				
5040-5050	1			3	4		28		30	30											2		2		tr				
5240-5250	2			3	4		27		34	26											1		3	tr	tr				
5440-5450	3			8	7		20		28	24											2		8		tr				
5640-5650	6			6	6		21		26	25											1		9		tr				
5840-5850	tr	tr		6	6		21	tr	30	32											2		4		tr				90%
6040-6050	tr	tr		4	6		16		39	28											2		2		2				90%
6240-6250	tr	tr		7	7		18		29	26											1		7	2	3				90%
6440-6450	tr	tr		6	6		22		26	37											1		2						90%
6640-6650	tr	tr		6	6		25		25	33											1		3		tr				90%
6840-6850	tr	tr		5	6		24		26	34											2		3		tr				90%
6990-7000	tr	tr		3	3		26	tr	31	29											1		5		1				90%
7220-7250	1		1	1			46		31	10		tr		2		tr		tr			3		4						50%
7540-7550	tr		1	1			50		27	15		tr		tr							4		tr					tr	50%
7740-7750		tr		tr	tr		30	7	28	28		2									tr		tr					3	~50 & 90%
7990-8000	10			5			41		9	12		tr		9							6		8						
8240-8250	2	2		13	6		36		10	23				tr							2		5						90%

8340-8350	7	19		tr	9		25		8	27													5	tr					90%
8540-8550		16		tr	6		22		11	41													4						~50 & 90%
8740-8750		24		tr	5		24		9	33													2	2	tr				~50 & 90%
8940-8950		22		tr	6		25		9	25													3	6	4				~50 & 90%
9140-9150		26			7		10		9	19													5	13	12				~50 & 90%
9340-9350		12			8		9		5	17													2	8	39				90%

Table B3.1 Continued:

Depth (ft)	**Smectite**	**I/S**	**C/S**	**illite**	**Chlorite**	**Kaolinite**	**Plagioclase**	**Sanidine**	**K-feldspar**	**Quartz**	**Hornblende**	**Biotite**	**Apatite**	**Clinopyroxene**	**Magnetite**	**Titanite**	**Epidote**	**Prehnite**	**Rutile**	**Pyrite**	**Hematite**	**Aragonite**	**Calcite**	**Dolomite**	**Anhydrite**	**Bassanite**	**Halite**	**Analcime**	**% illite in I/S, or % chlorite in C/S**
9540-9550		27			8		20		7	26										tr			4		7				~50 & 90%
9740-9750		4		24	9		23		8	23										tr			4		5				~50 & 90%
9940-9950		3		16	13		18		18	24										1	1		2		4				~50 & 90%
10140-10150		tr		12	12		33		11	28			tr							1			1		1				90%
10190-10200		tr		12	12		11		22	32		tr	tr	tr	tr						tr		9		2				~50 & 90%
10290-10300		tr		8	6		6		9	34		tr	tr	tr	tr						tr		35		tr				~50 & 90%
10490-10500		tr		10	13		26		18	25		tr	tr		tr	1							5		1				90%
10690-10700		tr		8	6		40		21	16	3	tr	tr		1	tr	tr						3		tr				90%
10890-10900		tr		13	11		19		12	32	tr	tr	tr		1	1	1				tr		7		tr				~50 & 90%
11090-11100		tr		4	14		36		17	20	1	2	tr	tr	1	1	tr				tr		3						~50 & 90%
11290-11300		tr		8	2		43		18	19	2	2	tr		1	1	tr				tr		3		tr				50%
11490-11500		tr		11	8		16		10	35	4	tr	tr	1	tr	tr	tr				tr		10	1	1				90%
11690-11700		tr		9	11		34		18	18	4	tr	tr		tr	tr				tr	tr		5						90%
11890-11900		tr		6	8		36		20	20		1	tr		1	1					tr		5						90%

12090-12100		tr		7	6		30		19	30		tr	tr		tr	tr			tr	tr	tr		4		1				90%
12140-12150		tr		18	6		17		15	33	tr		tr			2			tr				5	1	3				90%
12240-12250				2	9		31		20	28		1	tr		1	tr							3	1	3				
12440-12450				11	5		25		23	26		tr	tr			1							1	4	3				
12640-12650				6	4		43		19	15	6	4	tr			3							tr		tr				

Table B3.1 Continued:

Depth (ft)	**Smectite**	**I/S**	**C/S**	**illite**	**Chlorite**	**Kaolinite**	**Plagioclase**	**Sanidine**	**K-feldspar**	**Quartz**	**Hornblende**	**Biotite**	**Apatite**	**Clinopyroxene**	**Magnetite**	**Titanite**	**Epidote**	**Prehnite**	**Rutile**	**Pyrite**	**Hematite**	**Aragonite**	**Calcite**	**Dolomite**	**Anhydrite**	**Bassanite**	**Halite**	**Analcime**	**% illite in I/S, or % chlorite in C/S**
70-100	tr			7		11	17		11	28													27						
320-350	2			7		16	7		7	32													19	10	tr				
590-620	tr			12		tr	7		11	15												12	21	21			1		
830-860	tr			11			6		9	10												7	14	36	4	3			
1070-1100	tr			9			9		10	15												12	20	25					
1340-1350	tr			15			6		13	13												15	12	20	2	5			
1580-1610	tr			15			6		13	13												8	14	26	5			1	
1820-1850	tr			13	tr		4		12	9												5	10	19	13	10		4	
2090-2120	tr			14	2		16		18	27												2	10	9				2	
2330-2360	tr			4	4		22		17	35													13	3				2	
2600-2630	tr			16	3		17		20	25												1	10	4	2			2	
2840-2850	tr			10	9		11		21	35													14						
3080-3110	tr			21	3		10		19	29													12		6				
3320-3350	2			6	7		7		17	16													11	tr	35				
3590-3600	2			6	4		26		21	31											tr		4	3	2				
3840-3850	3			11	7		11		21	17											tr		14	10	6				

3990-4000	tr			17	3		14		21	23													14	5	4				
4240-4250	4			10	9		14		21	15												tr		12	6	8				
4380-4400	2			6	2		32		25	31														2		tr				
4640-4650	1			3	5		27		31	28												2		3		tr				

Table B3.1 Continued:

Depth (ft)	Smectite	I/S	C/S	illite	Chlorite	Kaolinite	Plagioclase	Sanidine	K-feldspar	Quartz	Hornblende	Biotite	Apatite	Clinopyroxene	Magnetite	Titanite	Epidote	Prehnite	Rutile	Pyrite	Hematite	Aragonite	Calcite	Dolomite	Anhydrite	Bassanite	Halite	Analcime	% illite in I/S, or % chlorite in C/S
5040-5050	1			3	4		28		30	30											2		2		tr				
5240-5250	2			3	4		27		34	26											1		3	tr	tr				
5440-5450	3			8	7		20		28	24											2		8		tr				
5640-5650	6			6	6		21		26	25											1		9		tr				
5840-5850	tr	tr		6	6		21	tr	30	32											2		4		tr				90%
6040-6050	tr	tr		4	6		16		39	28											2		2		2				90%
6240-6250	tr	tr		7	7		18		29	26											1		7	2	3				90%
6440-6450	tr	tr		6	6		22		26	37											1		2						90%
6640-6650	tr	tr		6	6		25		25	33											1		3		tr				90%
6840-6850	tr	tr		5	6		24		26	34											2		3		tr				90%
6990-7000	tr	tr		3	3		26	tr	31	29											1		5		1				90%
7220-7250	1		1	1			46		31	10		tr		2		tr		tr			3		4						50%
7540-7550	tr		1	1			50		27	15		tr		tr							4		tr					tr	50%
7740-7750		tr		tr	tr		30	7	28	28		2									tr		tr					3	~50 & 90%
7990-8000	10			5			41		9	12		tr		9							6		8						
8240-8250	2	2		13	6		36		10	23				tr							2		5						90%

8340-8350	7	19		tr	9		25		8	27													5	tr					90%
8540-8550		16		tr	6		22		11	41													4						~50 & 90%
8740-8750		24		tr	5		24		9	33													2	2	tr				~50 & 90%
8940-8950		22		tr	6		25		9	25													3	6	4				~50 & 90%
9140-9150		26			7		10		9	19													5	13	12				~50 & 90%
9340-9350		12			8		9		5	17													2	8	39				90%

Table B3.1 Continued:

Depth (ft)	**Smectite**	**I/S**	**C/S**	**illite**	**Chlorite**	**Kaolinite**	**Plagioclase**	**Sanidine**	**K-feldspar**	**Quartz**	**Hornblende**	**Biotite**	**Apatite**	**Clinopyroxene**	**Magnetite**	**Titanite**	**Epidote**	**Prehnite**	**Rutile**	**Pyrite**	**Hematite**	**Aragonite**	**Calcite**	**Dolomite**	**Anhydrite**	**Bassanite**	**Halite**	**Analcime**	**% illite in I/S, or % chlorite in C/S**
9540-9550		27			8		20		7	26										tr			4		7				~50 & 90%
9740-9750		4		24	9		23		8	23										tr			4		5				~50 & 90%
9940-9950		3		16	13		18		18	24										1	1		2		4				~50 & 90%
10140-10150		tr		12	12		33		11	28			tr							1			1		1				90%
10190-10200		tr		12	12		11		22	32		tr	tr	tr	tr						tr		9		2				~50 & 90%
10290-10300		tr		8	6		6		9	34		tr	tr	tr	tr						tr		35		tr				~50 & 90%
10490-10500		tr		10	13		26		18	25		tr	tr		tr	1							5		1				90%
10690-10700		tr		8	6		40		21	16	3	tr	tr		1	tr	tr						3		tr				90%
10890-10900		tr		13	11		19		12	32	tr	tr	tr		1	1	1				tr		7		tr				~50 & 90%
11090-11100		tr		4	14		36		17	20	1	2	tr	tr	1	1	tr				tr		3						~50 & 90%
11290-11300		tr		8	2		43		18	19	2	2	tr		1	1	tr				tr		3		tr				50%
11490-11500		tr		11	8		16		10	35	4	tr	tr	1	tr	tr	tr				tr		10	1	1				90%
11690-11700		tr		9	11		34		18	18	4	tr	tr		tr	tr				tr	tr		5						90%
11890-11900		tr		6	8		36		20	20		1	tr		1	1					tr		5						90%

12090-12100		tr		7	6		30		19	30		tr	tr		tr	tr			tr	tr	tr		4		1				90%
12140-12150		tr		18	6		17		15	33	tr		tr			2			tr				5	1	3				90%
12240-12250				2	9		31		20	28		1	tr		1	tr							3	1	3				
12440-12450				11	5		25		23	26		tr	tr			1							1	4	3				
12640-12650				6	4		43		19	15	6	4	tr			3							tr		tr				

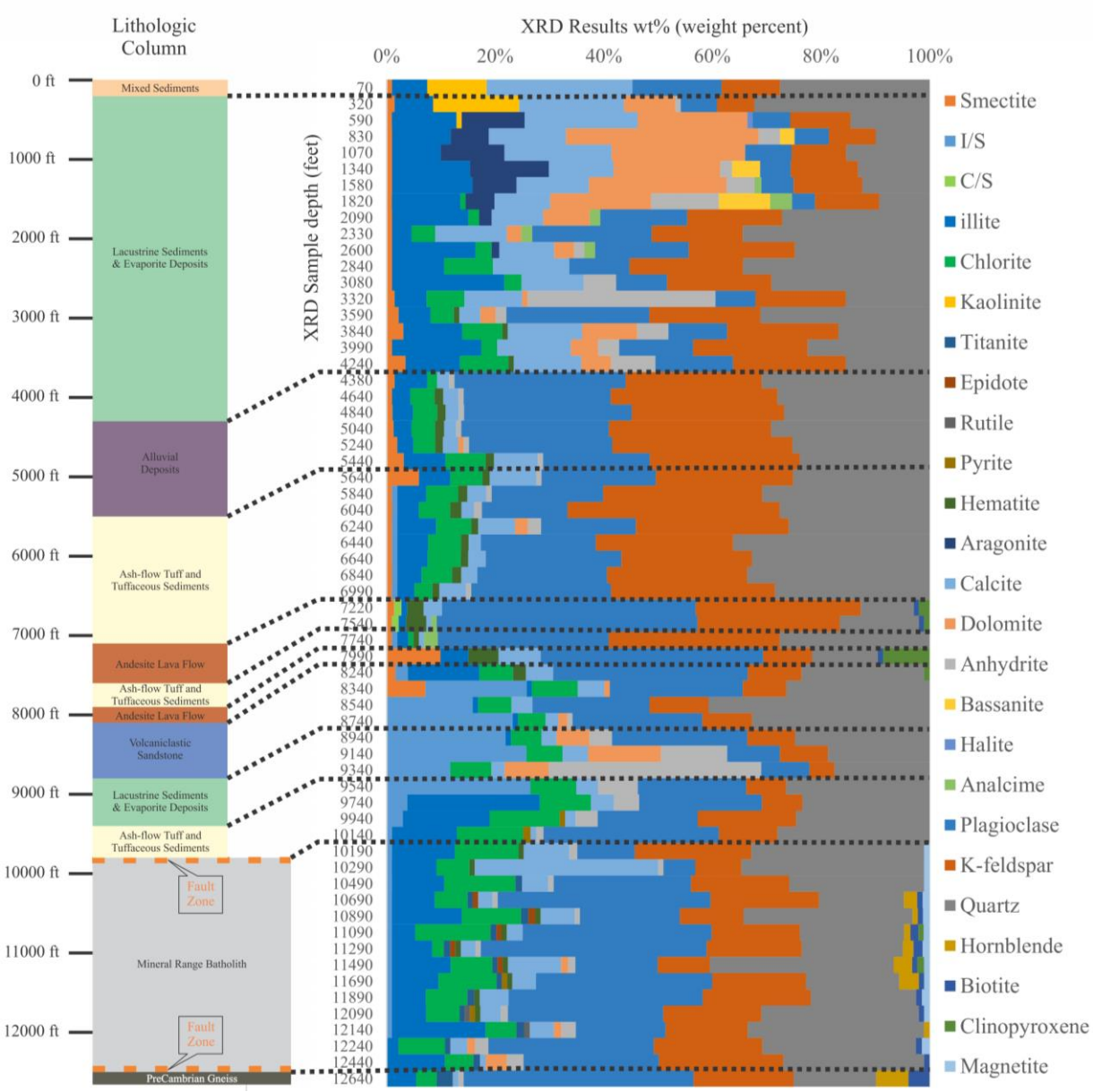

Figure B3.1: The lithologic column on the right shows lithologies vs measured depth. The right hand figure shows the complete XRD results presented in Table B3.1 with legend at far right. Lithologic contacts are shown as black dashed lines.

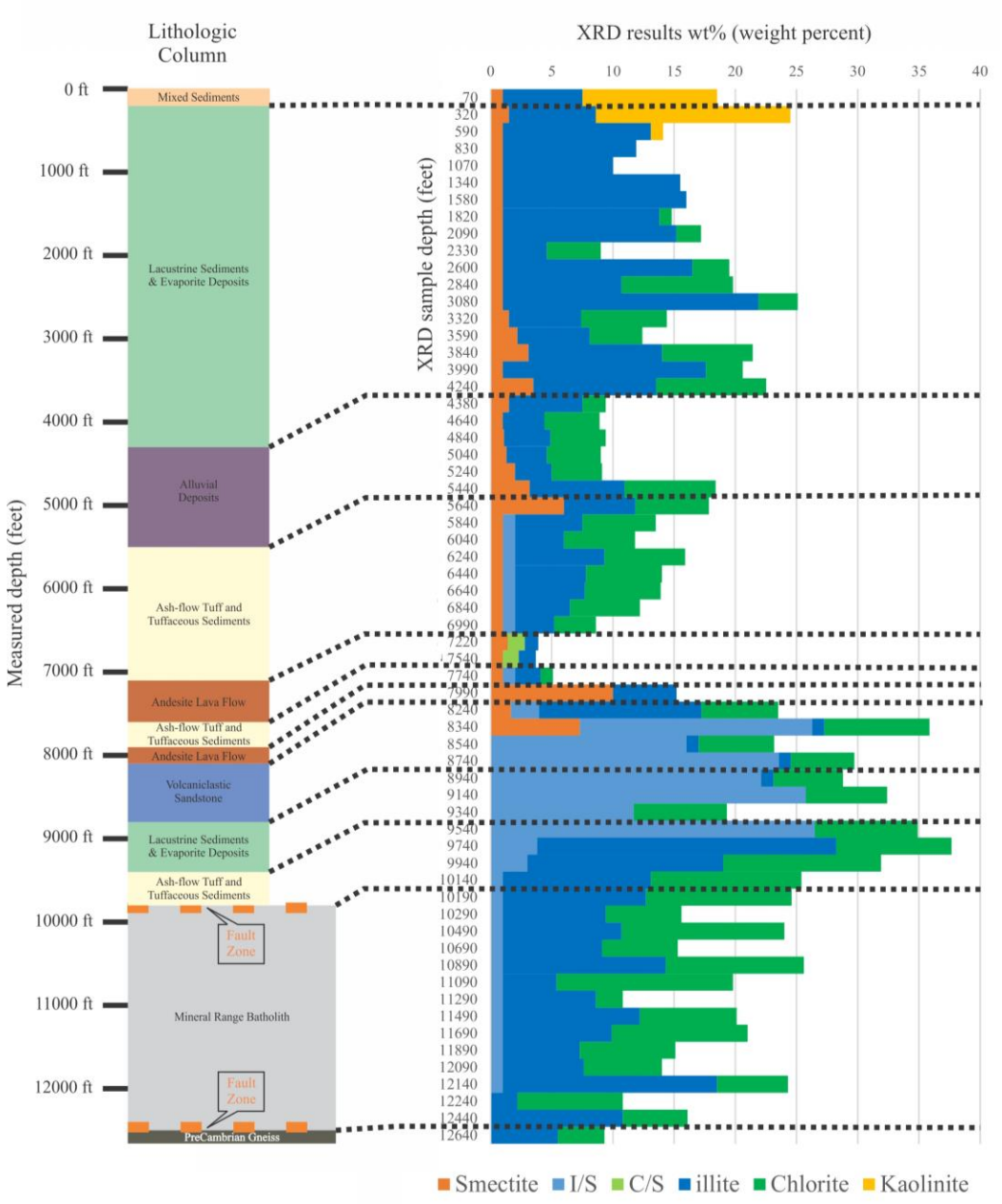

Figure B3.2: The lithologic column on the right shows lithologies vs measured depth. The right hand figure shows the clay mineral XRD results presented in Table B3.1 with legend at bottom. Lithologic contacts are shown as black dashed lines.

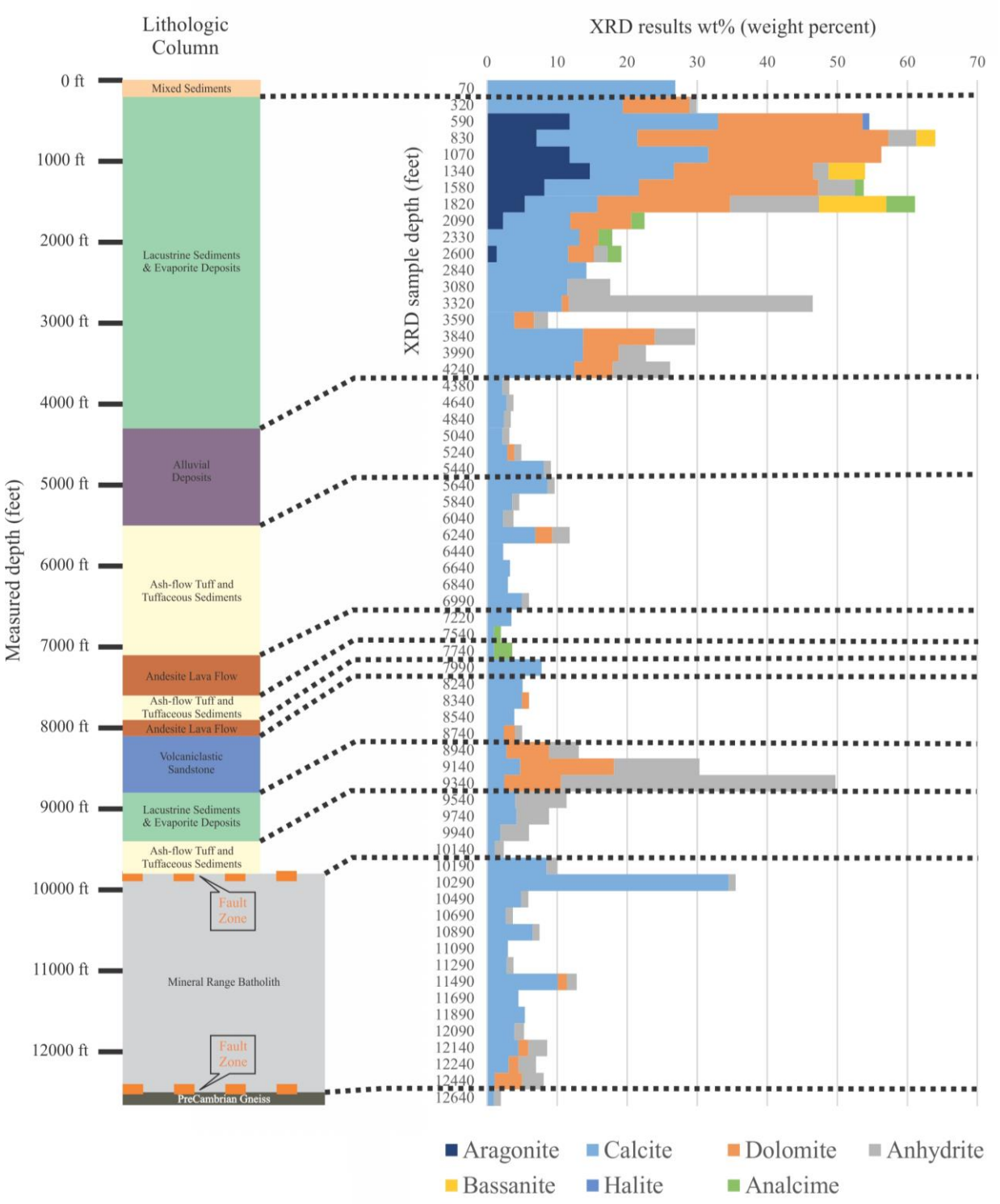

Figure B3.3: Lithologic column on the right shows lithologies vs measured depth. The right hand figure shows the carbonate and sulfate mineral XRD results presented in Table B3.1 with legend at bottom. Lithologic contacts are shown as black dashed lines.

B4.0 Petrographic methods

Sixty-two 24 by 46 mm thin sections were prepared of selected drill cuttings from Acord 1-26. Additional splits from the same depths were analyzed by XRD. The cuttings were vacuum impregnated in epoxy and one half was stained for K-feldspar. Thin sections were analyzed at the Energy & Geoscience Institute using research grade petrographic microscopes equipped with digital cameras.

Table B4.1: Summary of abbreviations used in photomicrograph annotations.

Analcime	Anl
Anhydrite	Anh
Apatite	Ap
Aragonite	Ar
Bassanite	Bas
Biotite	Bt
Calcite	Cal
Chlorite	Chl
Clinopyroxene	Cpx
Dolomite	Dol
Epidote	Ep
Hematite	Hem
Hornblende	Hbl
Illite	Ill
Interlayered chlorite/smectite	C/S
Interlayered illite/smectite	I/S
Kaolinite	Kln
K-feldspar	Ksp
Magnetite	Mag
Plagioclase	Pl
Prehnite	Prh
Pyrite	Py
Quartz	Qtz
Rutile	Rt
Sanidine	Sa
Smectite	Sme
Titanite	Tnt
Analcime	Anl
Anhydrite	Anh
Apatite	Ap
Aragonite	Ar
Bassanite	Bas
Biotite	Bt
Calcite	Cal

Chlorite	Chl
Clinopyroxene	Cpx
Dolomite	Dol
Epidote	Ep
Hematite	Hem
Hornblende	Hbl
illite	Ill
Interlayered chlorite/smectite	C/S
Interlayered illite/smectite	I/S
Kaolinite	Kln
K-feldspar	Ksp
Magnetite	Mag
Plagioclase	Pl
Prehnite	Prh
Pyrite	Py
Quartz	Qtz
Rutile	Rt
Sanidine	Sa
Smectite	Sme
Titanite	Tnt

B5.0 Petrographic results.

Based on petrographic observations twelve lithologic units have been delineated in the Acord 1-26 well (Figure B1.1). Detailed descriptions of each lithology are given in the following sections of the report. These sections include descriptions of the: lithology; secondary mineralization/hydrothermal alteration; shearing/brecciation; open space mineralization and open space mineral paragenesis. In addition, annotated photomicrographs of each lithology are presented in pairs with the same scene in both plane polarized and cross polarized light, showing representative images of the lithology and mineral relationships of interest (veining, hydrothermal alteration, shearing/brecciation, etc.). A table of the abbreviations used to annotate the images is given in Table B4.1.

Lithologies encountered have been described in order to compare with other wells in the FORGE project area, and provide information on its three dimensional structure. Lithologies encountered can be generally classified as gneiss and granite in the basement rocks and volcaniclastic deposits, pyroclastic deposits, lava flows, and various sediments in the basin fill.

During petrographic analyses qualitative assessments of the relative extent of brittle deformation and hydrothermal alteration (Figure B5.1) have been made for each sample and rated on a scale from 1 to 5 as follows: 0.5= trace; subtle=1; weak=2; moderate=3, strong=4; intense=5. The assessment of brittle deformation is based on the frequency of shearing, brecciation and veining observed in the cuttings of each sample. The assessment of hydrothermal alteration is based on

the prevalence of secondary mineralization observed as replacement textures and open space filling mineralization.

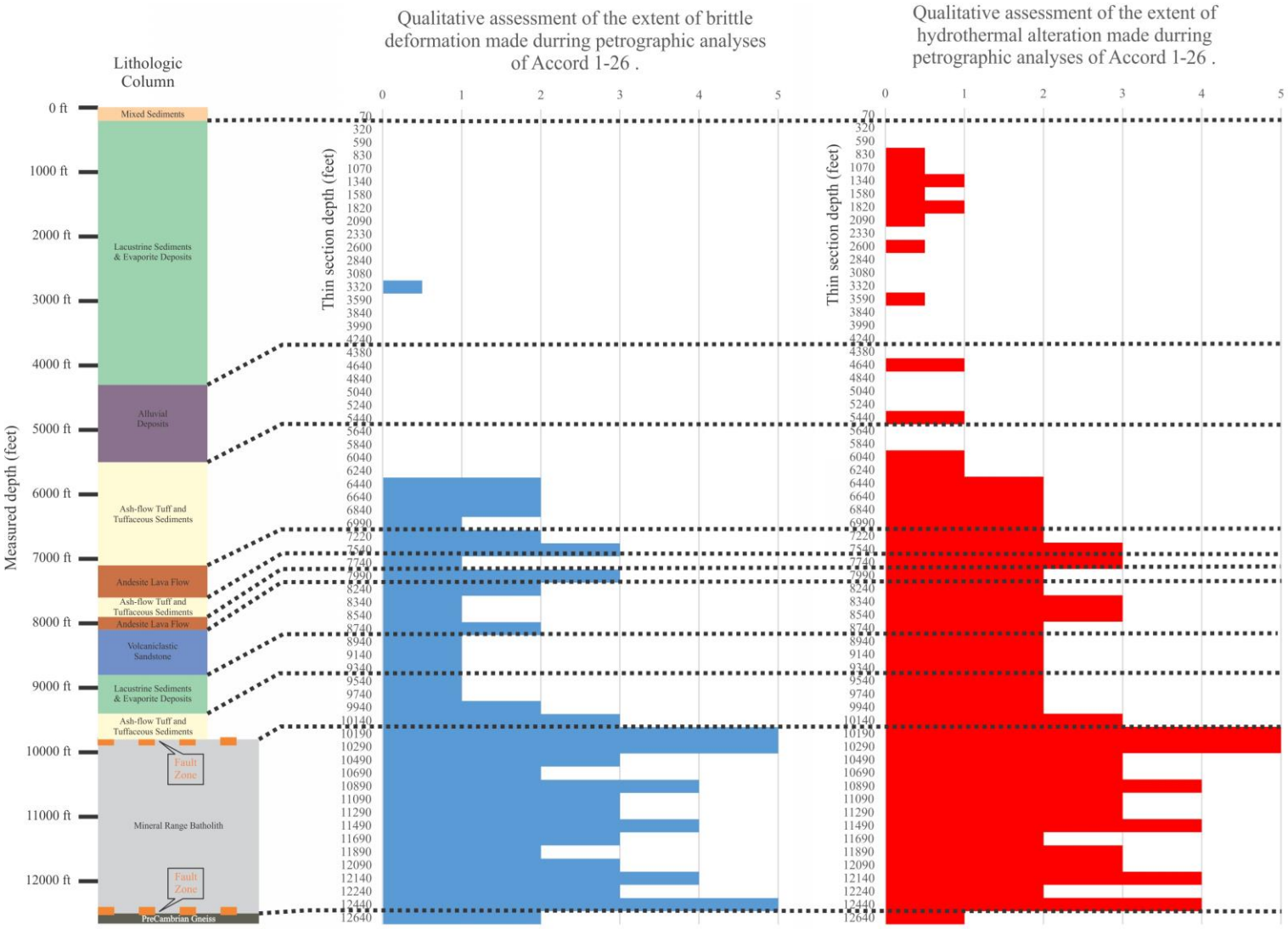

Figure B5.1: A qualitative assessments of the extent of brittle deformation and hydrothermal alteration has been made for each sample during petrographic analyses, and has been rated on a scale from 1 to 5 as follows: 0.5= trace; subtle=1; weak=2; moderate=3; strong=4; intense=5. Dashed black lines show the locations of lithologic contacts.

B5.1 Mixed sediments. Sample70-100 ft.

One sample from this unit was analyzed petrographically and by XRD from 70-100 ft

Table B5.1.1: Results of X-ray diffraction analyses in weight percent of sample. See Table B3.1 caption for more information.

Depth (ft)	Smectite	illite	Kaolinite	Plagioclase	K-feldspar	Quartz	Calcite
70-100	tr	7	11	17	11	28	27

This sample contained sediments with variable grain size ranging from large clasts of plutonic rocks and lava flows that are at least gravel-sized to fine grained silt-sized clasts that are predominantly composed of mineral grains. The siltstone has both clay-rich (illite and kaolinite) and fine-grained calcite matrix, and contains rare calcite filled burrows (trace fossils). Sedimentary rip-up clasts are also frequently incorporated into these sediments. The finer-grained fraction (siltstone and fine-grained sandstone) is generally matrix supported and the coarser-grained cuttings are cemented by calcite.

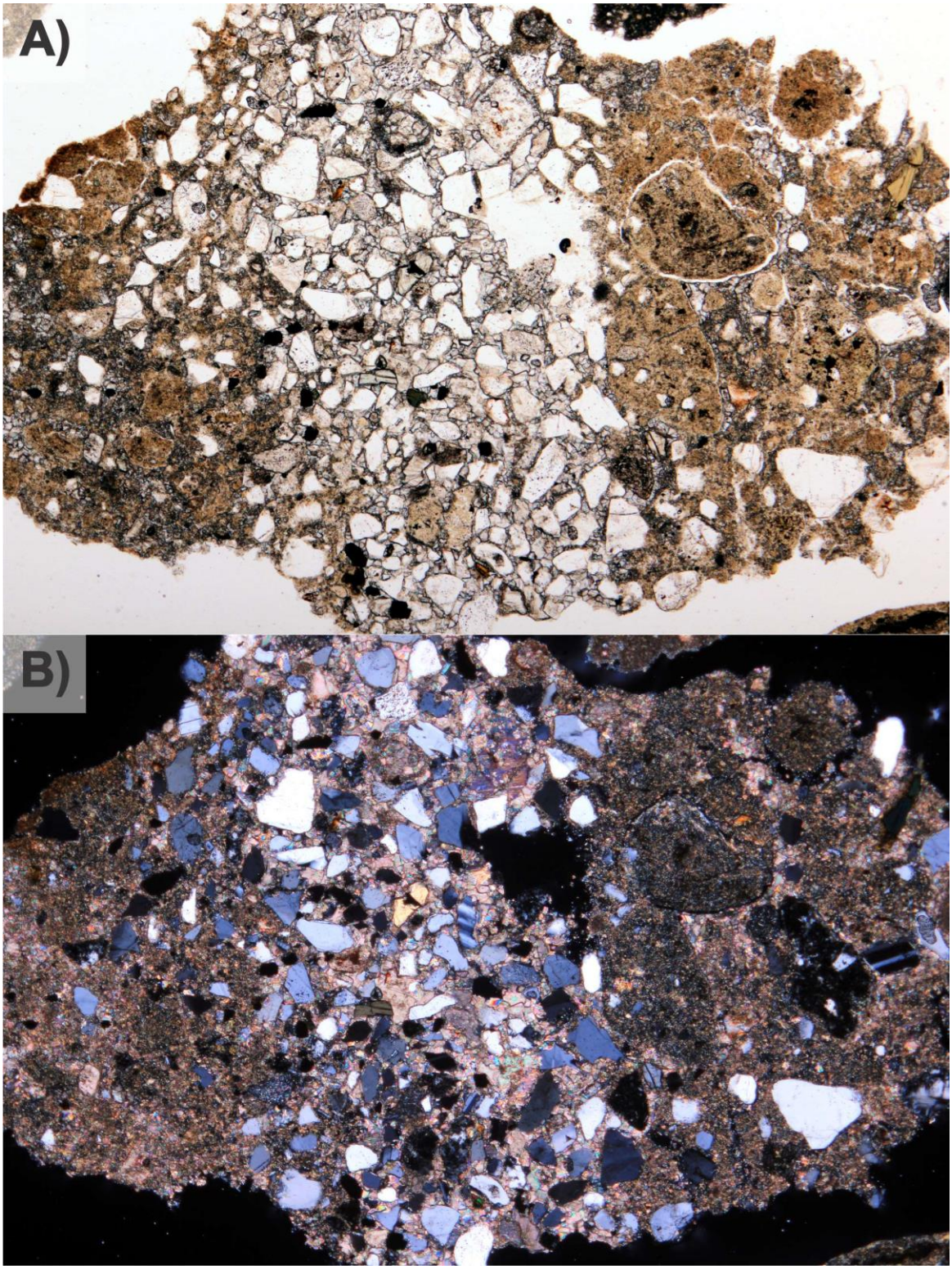

Figure B5.1.1: Interbedded siltstone and sandstone. The sandstone in the center of the image contains calcite cement in the pore spaces. The rip-up clasts of siltstone have a clay-rich matrix and are cemented by calcite. Photomicrographs were taken of the cuttings from 70-100 ft. A) Plane polarized light. B) Crossed nicols. Field of view is 3.2 mm.

B5.2 Lacustrine sediments and evaporite deposits. Samples 320-350 to 4240-4250 ft.

Seventeen samples from this unit were analyzed petrographically and by XRD from 320-350 to 4240-4250 ft

Table B5.2.1: Results of X-ray diffraction analyses in weight percent of sample. See Table 3.1 caption for more information.

Depth (ft)	Smectite	illite	Chlorite	Kaolinite	Plagioclase	K-feldspar	Quartz	Hematite	Aragonite	Calcite	Dolomite	Anhydrite	Bassanite	Halite	Analcime
320-350	2	7		16	7	7	32			19	10	tr			
590-620	tr	12		tr	7	11	15		12	21	21			1	
830-860	tr	11			6	9	10		7	14	36	4	3		
1070-1100	tr	9			9	10	15		12	20	25				
1340-1350	tr	15			6	13	13		15	12	20	2	5		
1580-1610	tr	15			6	13	13		8	14	26	5			1
1820-1850	tr	13	tr		4	12	9		5	10	19	13	10		4
2090-2120	tr	14	2		16	18	27		2	10	9				2
2330-2360	tr	4	4		22	17	35			13	3				2
2600-2630	tr	16	3		17	20	25		1	10	4	2			2
2840-2850	tr	10	9		11	21	35			14					
3080-3110	tr	21	3		10	19	29			12		6			
3320-3350	2	6	7		7	17	16			11	tr	35			
3590-3600	2	6	4		26	21	31	tr		4	3	2			
3840-3850	3	11	7		11	21	17	tr		14	10	6			
3990-4000	tr	17	3		14	21	23			14	5	4			
4240-4250	4	10	9		14	21	15	tr		12	6	8			

The dominant lithology in the cuttings from this interval is siltstone, with less abundant sandstone and lithic clasts of up to at least gravel-size. In general the sequence becomes finer-grained towards the top of the unit (fining-upward succession). The sediments have a fine-grained matrix composed of variable proportions of clay minerals (illite and smectite ± kaolinite ± chlorite,) and carbonate minerals (calcite ± dolomite). Anhydrite is intermittently observed as nodules, laths and thin bedding planes in siltstone cuttings with up to 35 wt% anhydrite in the sample from 3320-3350 ft. The siltstone contains rare carbonate fossils (can be replaced by anhydrite), but trace fossils (burrows) are consistently observed. Sedimentary rip-up clasts of siltstone are also a fairly consistent feature in this unit.

Sandstone chips are usually matrix-supported and less abundant grain-supported sandstone with calcite or anhydrite cement. The larger lithic clasts are derived from intrusions, lava flows and ash-flow tuffs, with intrusive rocks becoming the most prevalent clasts towards the top of the unit.

Little evidence of hydrothermal alteration is seen in these samples. Anhydrite is partially hydrated to bassanite in some samples. There is also rare and intermittent replacements of anhydrite by quartz and chalcedony observed as high in the well bore as 1340-1350 ft.

Minor abundances of analcime from 1580-1610 to 2600-2630 ft are most likely due to the alteration of tuffaceous material (fine-grained volcanic glass) at low temperature (ambient or higher) in what was likely an alkaline lacustrine environment.

No evidence of brittle deformation is observed in these soft sediments.

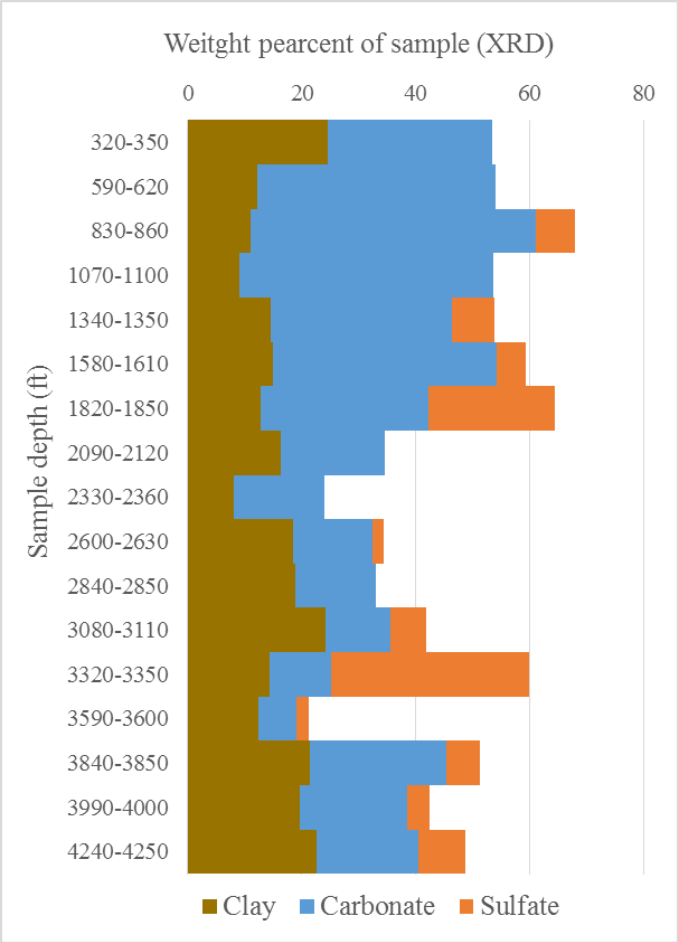

Figure B5.2.1: XRD results for the lacustrine sediments and evaporite deposits in the upper portion of well. Clay, carbonate and sulfate minerals have been grouped together to produce this figure.

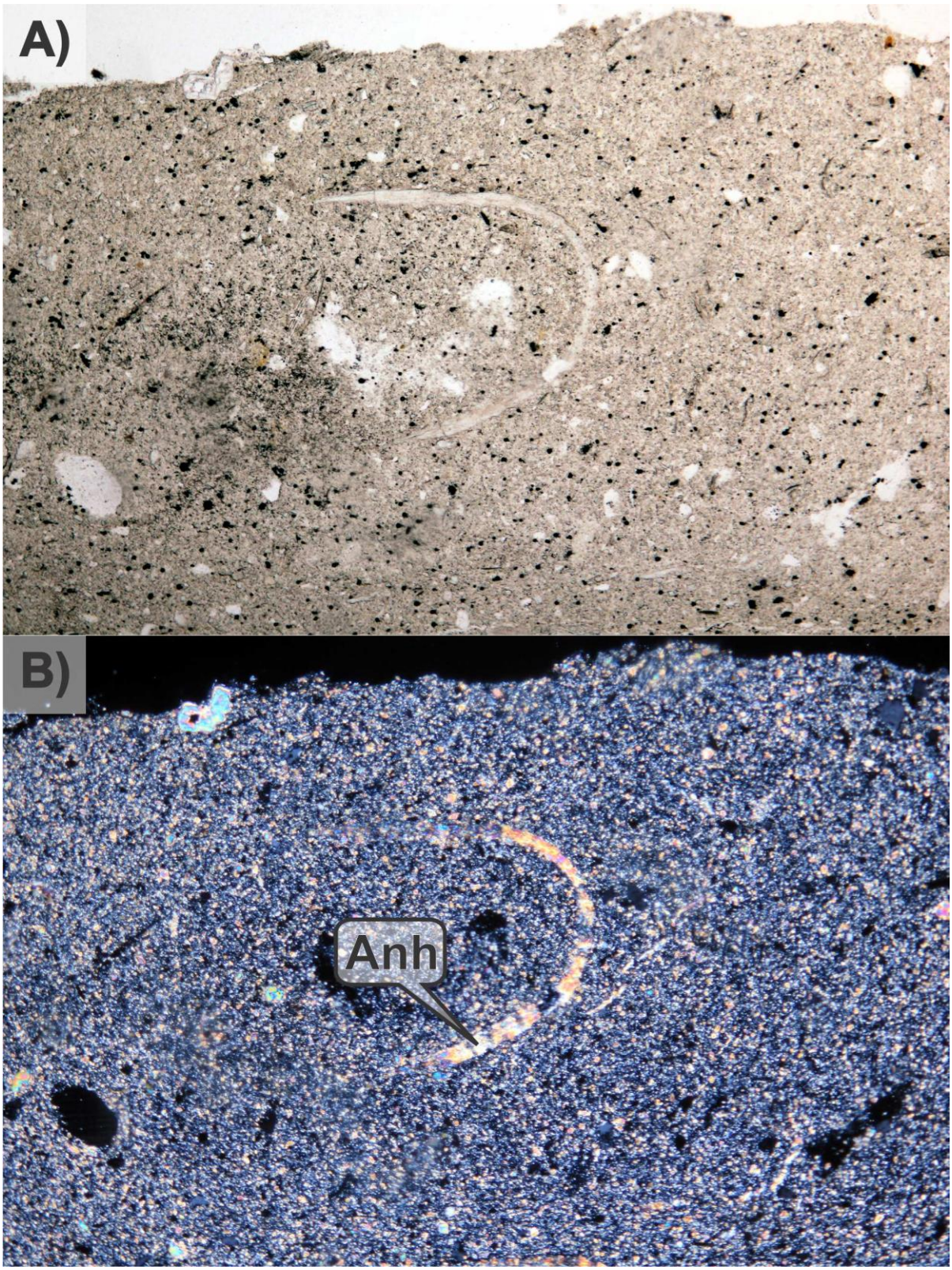

Figure B5.2.2: Anhydrite replaced fossil in siltstone. Photomicrographs were taken of the cuttings from 1070-1100 ft. A) Plane polarized light. B) Crossed nicols. Field of view is 1.6 mm.

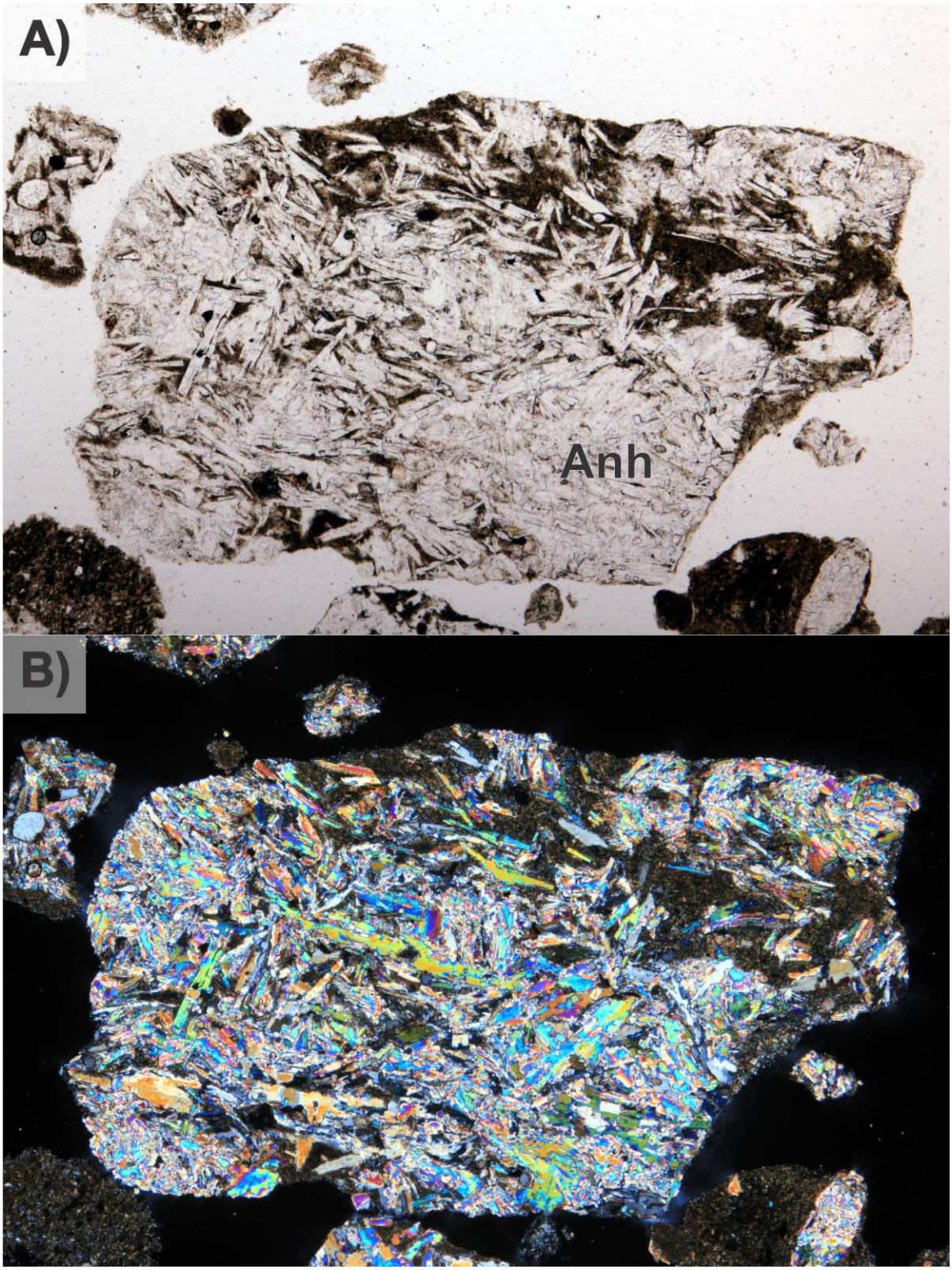

Figure B5.2.3: Anhydrite-rich bed in siltstone. Photomicrographs were taken of the cuttings from 3320-3350 ft. A) Plane polarized light. B) Crossed nicols. Field of view is 3.2 mm.

B5.3 Alluvial deposits. Samples 4380-4400 to 5440-5450 ft.

Six samples from this unit were analyzed petrographically and by XRD from 4380-4400 to 5440-5450 ft

Table B5.3.1: Results of X-ray diffraction analyses in weight percent of sample. See Table B3.1 caption for more information.

Depth (ft)	Smectite	illite	Chlorite	Plagioclase	K-feldspar	Quartz	Hematite	Calcite	Dolomite	Anhydrite
4380-4400	2	6	2	32	25	31		2		tr
4640-4650	1	3	5	27	31	28	2	3		tr
4840-4850	1	4	5	31	28	27	2	2		tr
5040-5050	1	3	4	28	30	30	2	2		tr
5240-5250	2	3	4	27	34	26	1	3	tr	tr
5440-5450	3	8	7	20	28	24	2	8		tr

The cuttings from this interval are mostly composed of large (up to at least gravel-size) angular to sub-rounded lithic clasts. Lithic clasts are dominantly intrusive rocks with variable primary textures and secondary alteration mineralogy, with less abundant lava flow and ash-flow tuff clasts, as well as rare vein fragments and metamorphic rocks. The fine-grained matrix is composed of variable proportions of clay (illite, chlorite and smectite) and carbonate (calcite ± dolomite) minerals. Less frequently calcite cement is observed at the edges of the clasts, or binding clasts together.

There are also less abundant cuttings of siltstone and fine-grained sandstone with rare fossils, hematite staining, anhydrite (as nodules and laths) with rare chalcedony replacement textures in a clay and carbonate bearing matrix,

This unit is interpreted as a poorly-sorted, incompetent alluvial deposit near the edge of a lake that was disaggregated during drilling. In addition, washing of the samples likely removed much of the clay-rich fine-grained matrix.

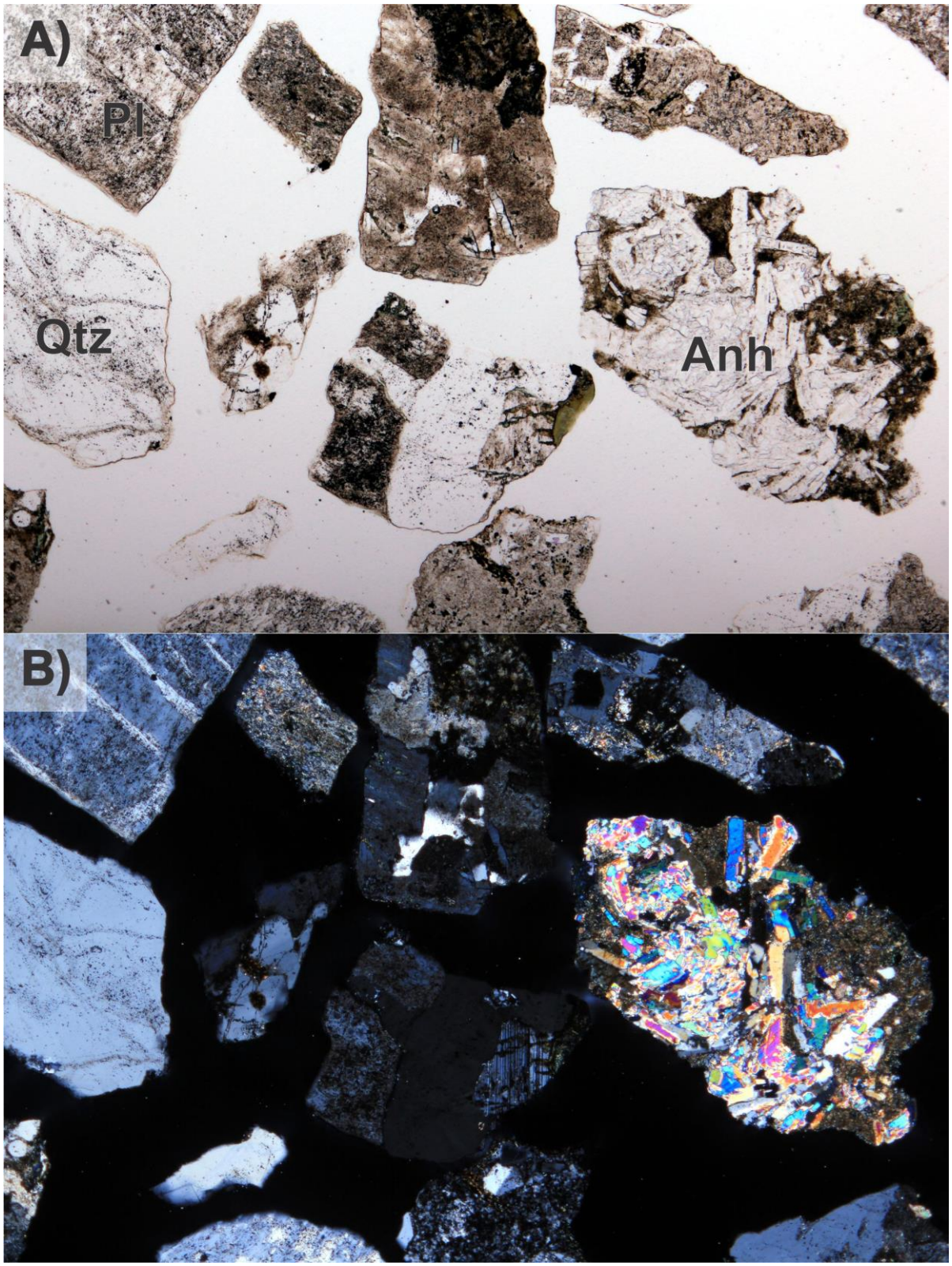

Figure B5.3.1: Coarse-grained intrusive cuttings composed of quartz and feldspar, as well as minor siltstone with anhydrite laths. Photomicrographs were taken of the cuttings from 4380-4400 ft. A) Plane polarized light. B) Crossed nicols. Field of view is 3.2 mm.

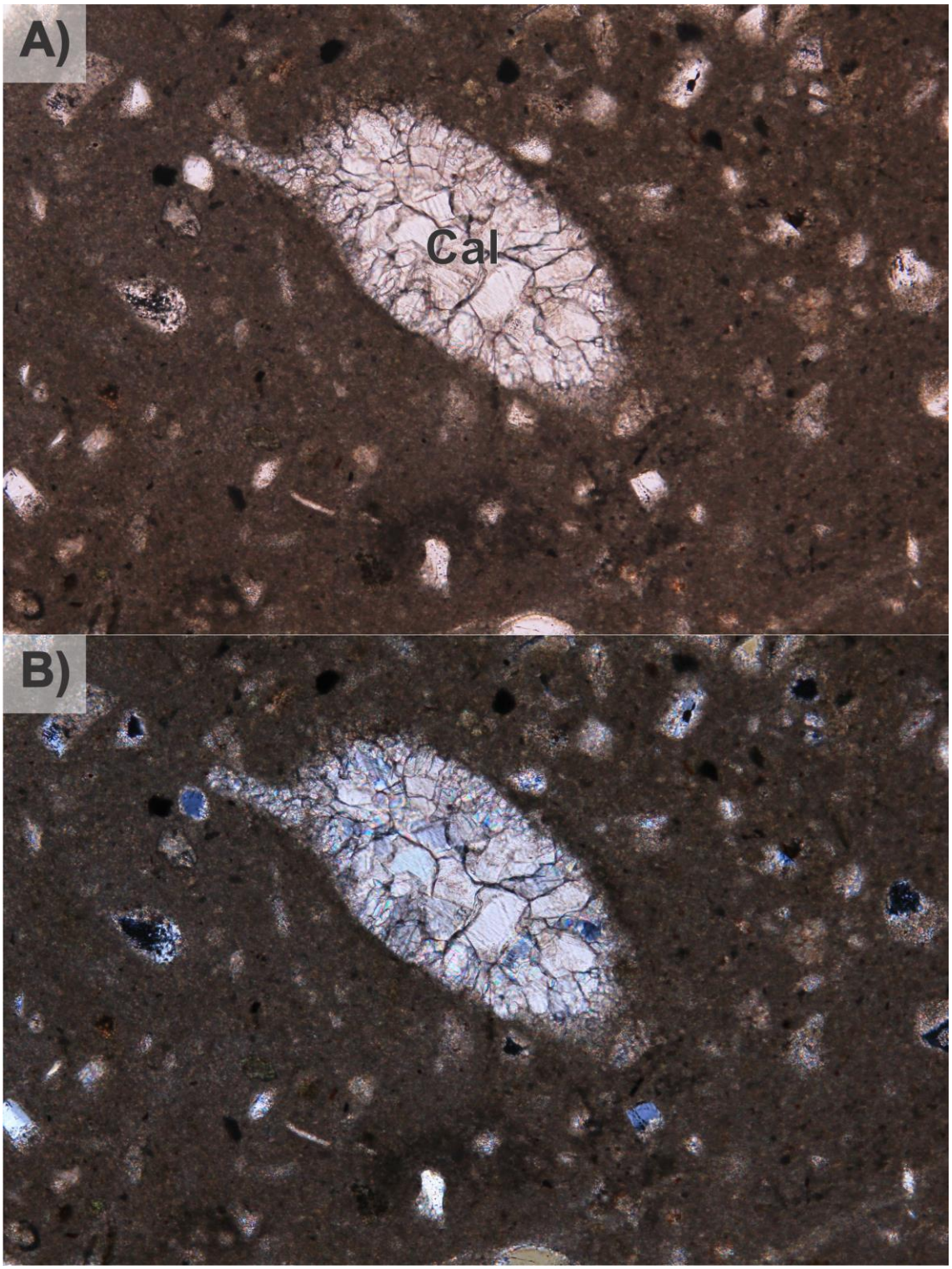

Figure B5.3.2: Calcite replaced fossil in siltstone with fine-grained calcite matrix. Photomicrographs were taken of the cuttings from 5240-5250 ft. A) Plane polarized light. B) Crossed nicols. Field of view is 3.2 mm.

B5.4 Rhyolite ash-flow tuff and tuffaceous sediments. Samples 5640-5650 to 6990-7000 ft.

Eight samples from this unit were analyzed petrographically and by XRD from 5640-5650 to 6990-7000 ft

Table B5.4.1: Results of X-ray diffraction analyses in weight percent of sample. See Table B3.1 caption for more information.

Depth (ft)	Smectite	I/S	illite	Chlorite	Plagioclase	Sanidine	K-feldspar	Quartz	Hematite	Calcite	Dolomite	Anhydrite	% illite in I/S
5640-5650	6		6	6	21		26	25	1	9		tr	
5840-5850	tr	tr	6	6	21	tr	30	32	2	4		tr	90%
6040-6050	tr	tr	4	6	16		39	28	2	2		2	90%
6240-6250	tr	tr	7	7	18		29	26	1	7	2	3	90%
6440-6450	tr	tr	6	6	22		26	37	1	2			90%
6640-6650	tr	tr	6	6	25		25	33	1	3		tr	90%
6840-6850	tr	tr	5	6	24		26	34	2	3		tr	90%
6990-7000	tr	tr	3	3	26	tr	31	29	1	5		1	90%

This unit is a mix of rhyolite ash-flow tuff and tuffaceous siltstone and sandstone (reworked ash-flow tuff deposits). The lower part of this unit 6440-6450 to 6990-7000 ft contains a higher proportion of ash-flow tuff cuttings and the upper part a higher proportion of siltstone cuttings.

The rhyolite ash-flow tuff cuttings are moderately- to densely-welded, with few shard or pumice textures observed. The ash-flow tuff chips are variable in texture and mineralogy. They may be crystal-rich to crystal poor, with quartz (often resorbed) and plagioclase, as well as rare sanadine and ferromagnesian (chlorite pseudomorphs) phenocrysts. The groundmass contains variable proportions of quartz, illite and K-feldspar most commonly as a fine-grained and equigranular groundmass, with less common spherulitic and granophyric devitrification textures.

The sediments consists dominantly of siltstone with quartz, feldspar and mica grains (mica would have been classified as illite in XRD analyses) and lithic clasts dominantly composed of texturally variable ash-flow tuff with less abundant lava flow, intrusive and metamorphic clasts in fine-grained clay (chlorite and illite ± interlayered illite smectite ± smectite) and/or carbonate (calcite ± dolomite) matrix that is commonly hematite stained. Minor anhydrite is observed as nodules in siltstone.

Silicification of tuff cuttings is commonly observed, but there was no direct evidence of in situ silicification (i.e. no silicification of fine-grained sedimentary matrix or open space fillings of quartz or chalcedony that were not contained within a clast).

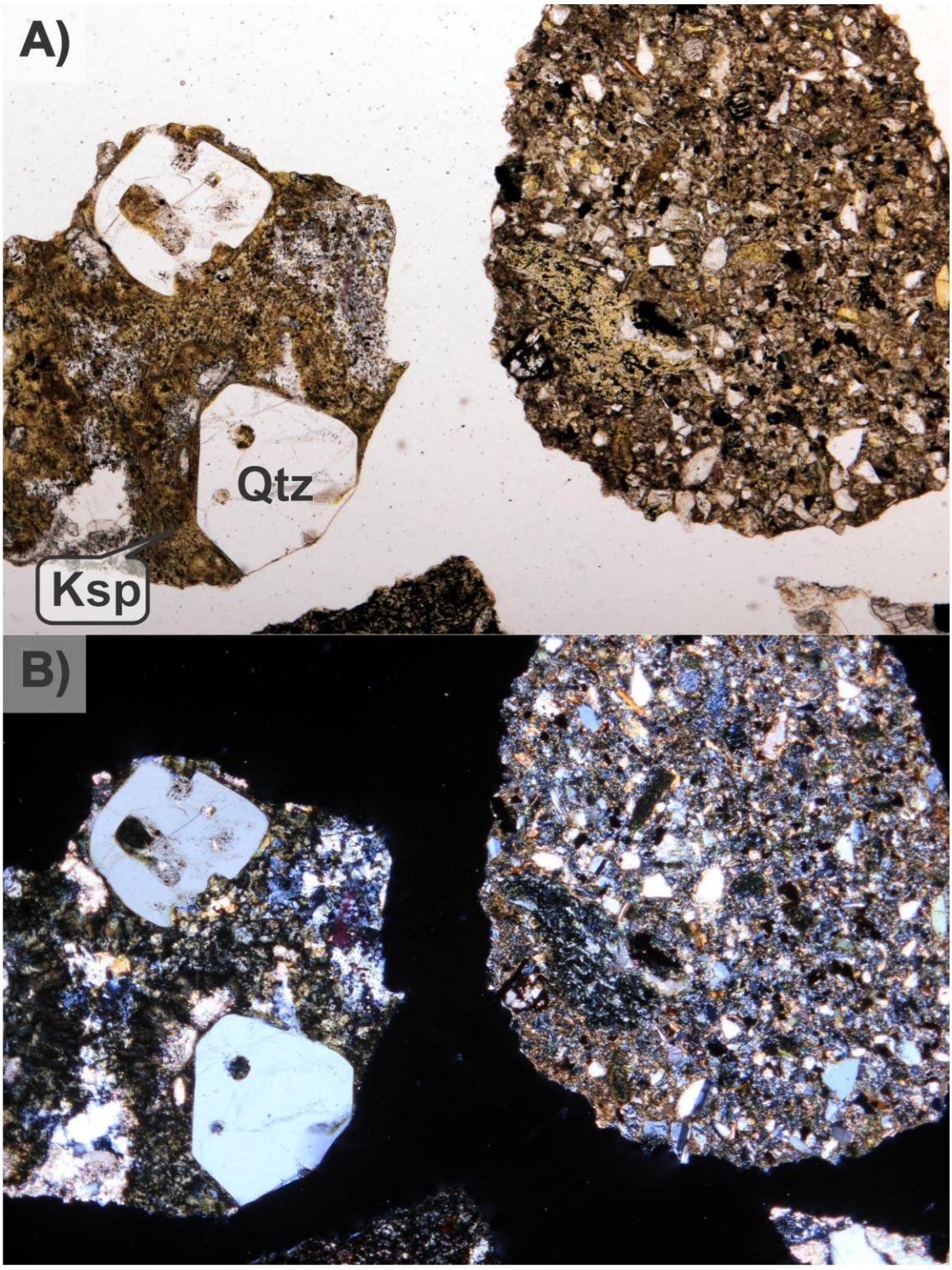

Figure B5.4.1: At left is an ash-flow tuff chip with resorbed quartz phenocrysts and a devitrified quartz and k-feldspar (stained yellow) matrix. At right is a chip of tuffaceous sandstone. Photomicrographs were taken of the cuttings from 6990-7000 ft. A) Plane polarized light. B) Crossed nicols. Field of view is 3.2 mm.

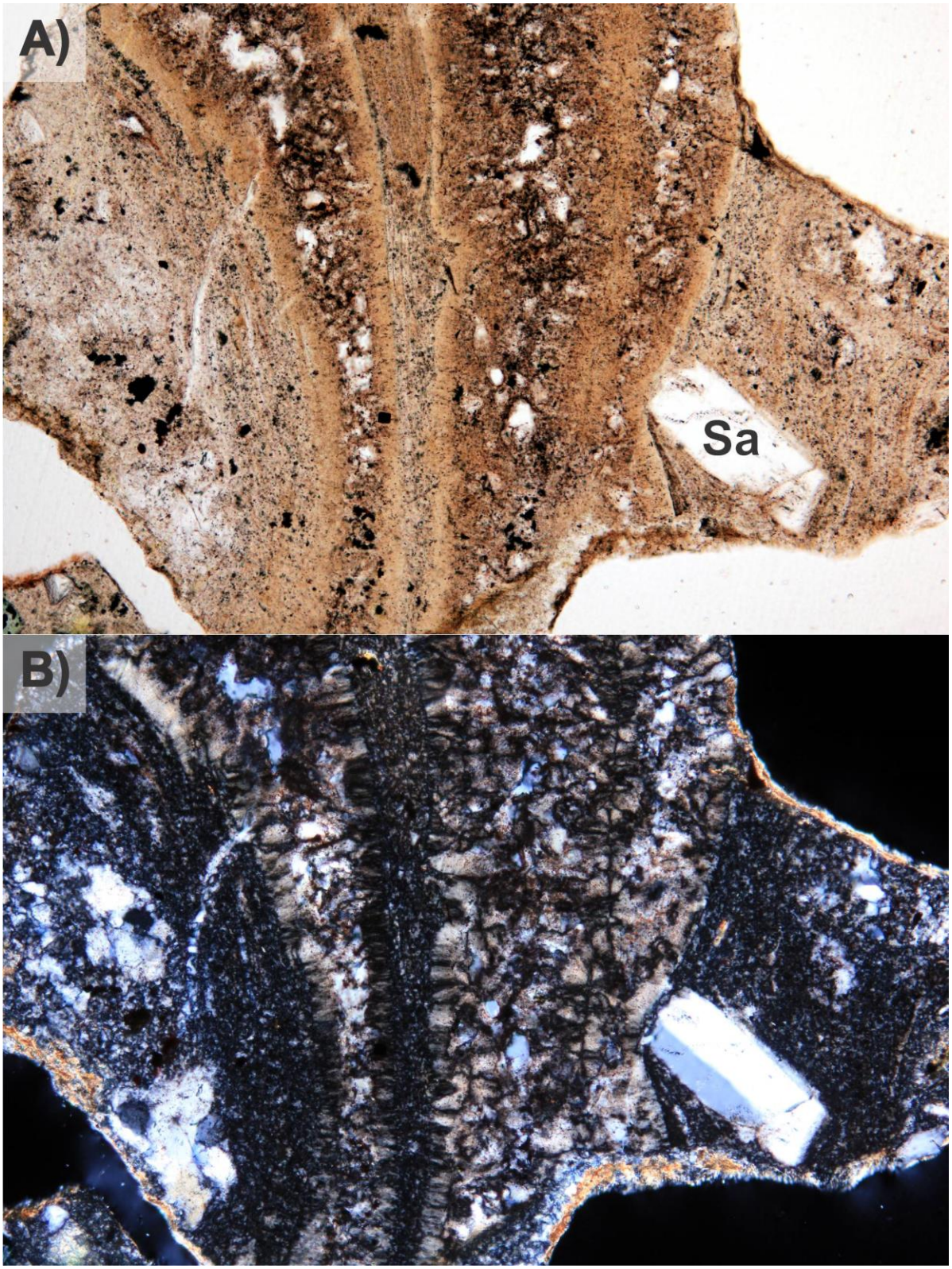

Figure B5.4.2: Devitrified ash-flow tuff with a sanadine phenocryst. The edges of the chip have a thin coating of clay-rich matrix. Photomicrographs were taken of the cuttings from 5840-5850 ft. A) Plane polarized light. B) Crossed nicols. Field of view is 1.6 mm.

B5.5 Andesite lava flow. Samples 7220-7250 to 7540-7550 ft.

Two samples from this unit were analyzed petrographically and by XRD from 7220-7250 to 7540-7550 ft

Table 5.5.1: Results of X-ray diffraction analyses in weight percent of sample. See Table B3.1 caption for more information.

Depth (ft)	Smectite	C/S	illite	Plagioclase	K-feldspar	Quartz	Biotite	Clinopyroxene	Titanite	Prehnite	Hematite	Calcite	Analcime	% chlorite in C/S
7220-7250	1	1	1	46	31	10	tr	2	Tr	Tr	3	4		50%
7540-7550	tr	1	1	50	27	15	tr	tr			4	tr	tr	50%

The samples from this unit consist of porphyritic fine- to medium-grained andesite lava flow with plagioclase, biotite and clinopyroxene phenocrysts in a fine grained groundmass composed of plagioclase laths with interstitial K-feldspar and clinopyroxene.

The rock itself is not very altered, there is not much clay in the sample (XRD) and the clinopyroxene grains are often preserved (usually the first mineral in this assemblage to alter/weather), but there is significant secondary silica precipitation in open spaces that resulted from brecciation. Open space silica is observed as chalcedony, quartz after chalcedony and anhedral to euhedral quartz. Calcite and rare prehnite are observed filling open space after earlier silica deposition. Calcite veins are also observed cutting earlier sheared/brecciated and silicified chips. Chips containing euhedral quartz growing into open space suggests remnant porosity in this lithology.

Plagioclase is partially altered to albite, K-feldspar and quartz. Biotite is partially altered to interlayered chlorite/smectite and hematite. Clinopyroxene is partially altered to interlayered chlorite/smectite, quartz, titanite, calcite and hematite.

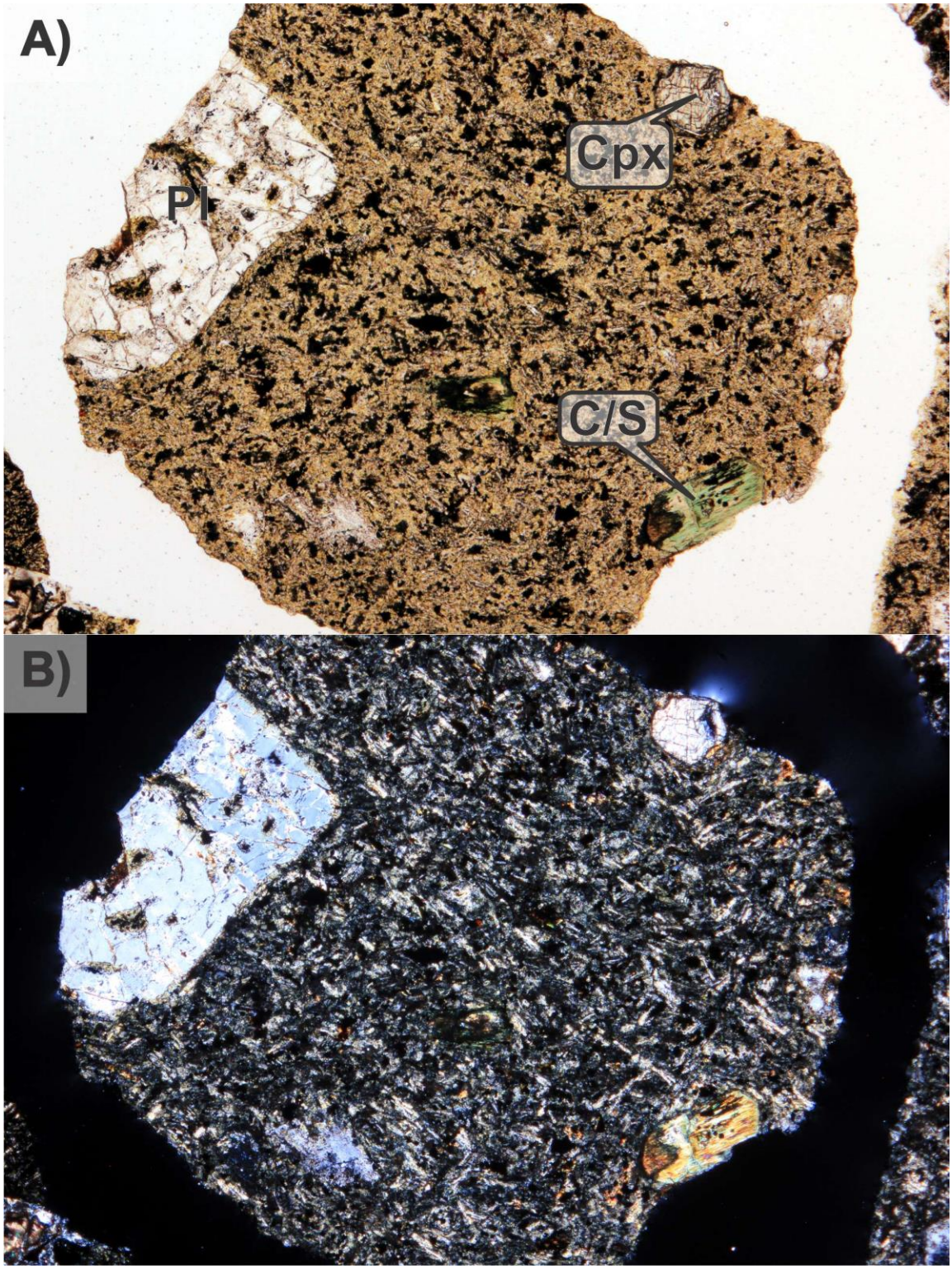

Figure B5.5.1: Porphyritic andesite flow with plagioclase and clinopyroxene phenocrysts, as well as an interlayered chlorite/smectite phenocryst pseudomorph in a groundmass of plagioclase laths with interstitial K-feldspar (stained yellow). Photomicrographs were taken of the cuttings from 7220-7250 ft. A) Plane polarized light. B) Crossed nicols. Field of view is 3.2 mm.

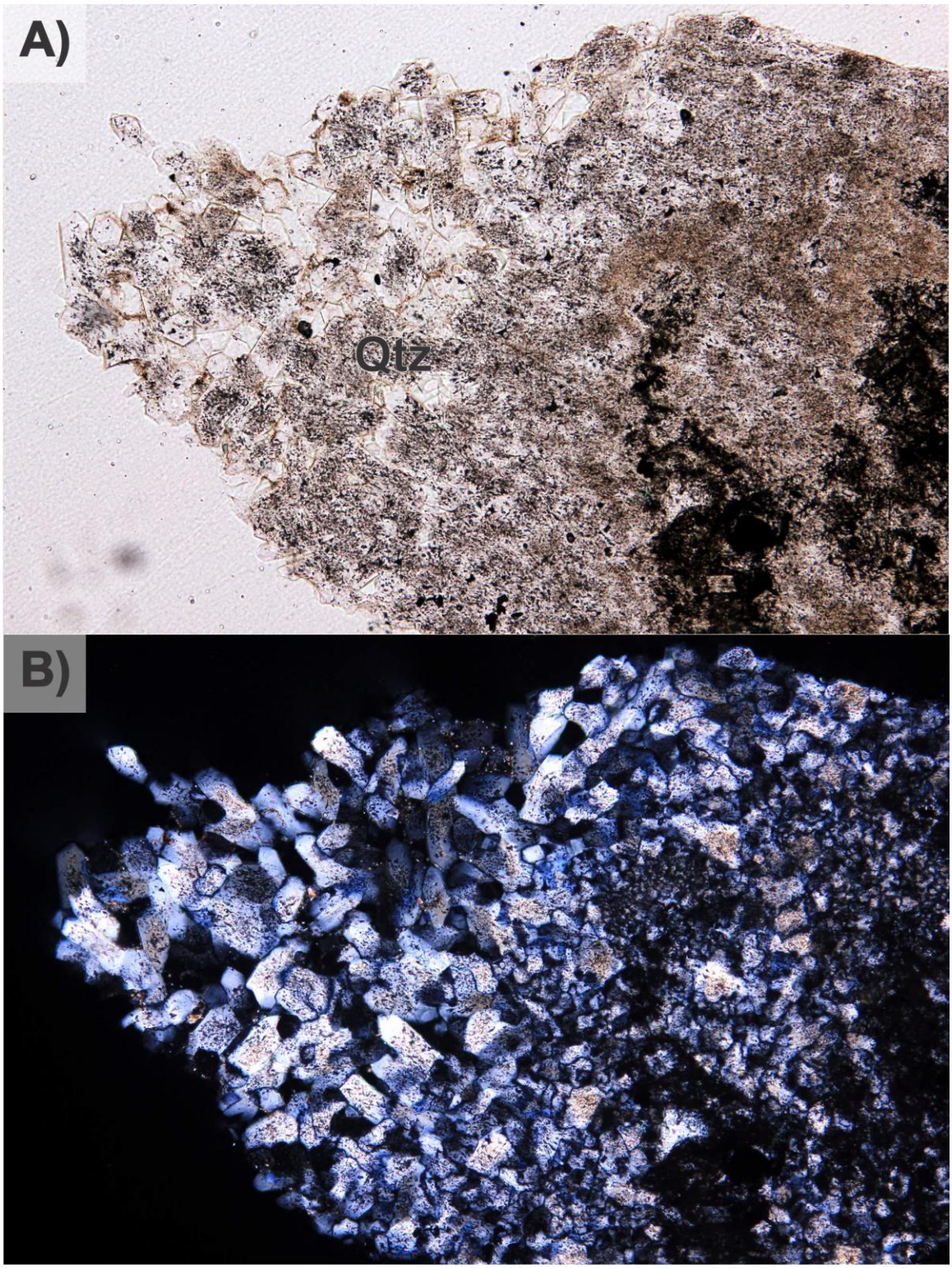

Figure B5.5.2: Euhedral quartz with abundant fluid inclusions (that give some of the crystals a dusty texture) growing into open space, suggesting remnant porosity in the brecciated andesite lava flow. Photomicrographs were taken of the cuttings from 7540-7550 ft. A) Plane polarized light. B) Crossed nicols. Field of view is 1.6 mm.

B5.6 Rhyolite ash-flow tuff. Sample 7740-7750 ft.

One sample from this unit was analyzed petrographically and by XRD from 7740-7750 ft

Table B5.6.1: Results of X-ray diffraction analyses in weight percent of sample. See Table B3.1 caption for more information.

Depth (ft)	Smectite	I/S	illite	Chlorite	Plagioclase	Sanidine	K-feldspar	Quartz	Biotite	Hematite	Calcite	Analcime	% illite in I/S
7740-7750		tr	tr	tr	30	7	28	28	2	tr	tr	3	~50 & 90% 2 species

This sample consists of moderately welded, crystal-rich, lithic-poor ash flow tuff containing plagioclase, sanidine, biotite and rare quartz phenocrysts, as well as fine-grained quartz pseudomorphs (± hematite) of an unknown ferromagnesian phenocryst (pyroxene?). Biotite is often partially altered to hematite. The groundmass contains abundant shard and pumice (fiamme) textures. The shards of volcanic glass have been altered to quartz (after chalcedony) and rare analcime. The fine-grained groundmass is K-feldspar- and quartz-rich with a mottled texture. The sparse lithic fragments that have been entrained in the ash-flow were derived from lava flows.

The sample contains abundant secondary quartz as replacements of minerals and volcanic glass, as well as open space fillings. Anhedral quartz is most commonly observed in veins and is likely after chalcedony or opal (i.e. recrystallization). Rare late (after silica) analcime is also observed in the veins.

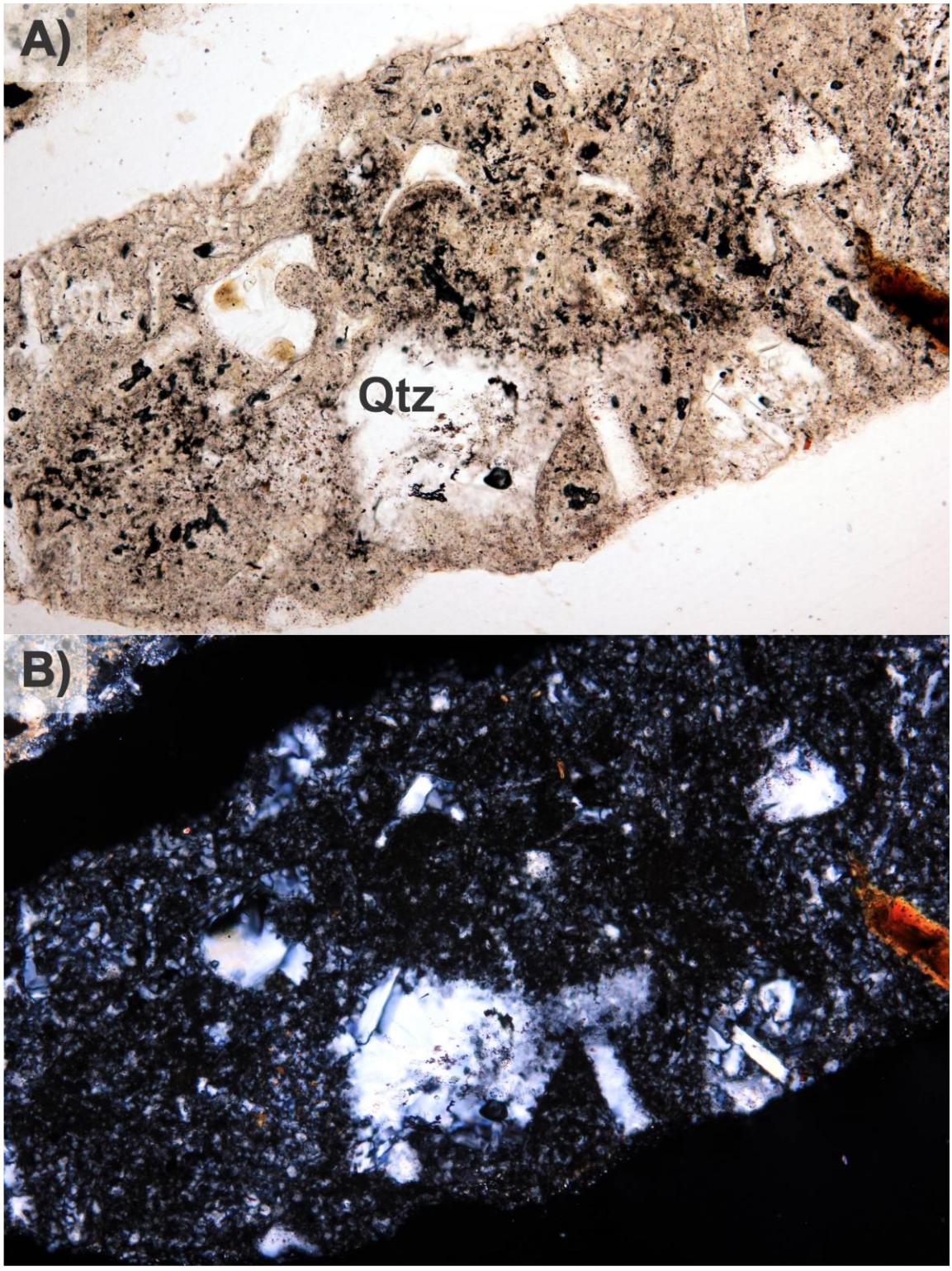

Figure B5.6.1: Shard textures in an ash-flow tuff chip that have been altered to quartz. Photomicrographs were taken of the cuttings from 7740-7750ft. A) Plane polarized light. B) Crossed nicols. Field of view is 1.6 mm.

B5.7 Andesite lava flow. Sample 7990-8000 ft.

One sample from this unit was analyzed petrographically and by XRD from 7990-8000 ft

Table 5.7.1: Results of X-ray diffraction analyses in weight percent of sample. See Table B3.1 caption for more information.

Depth (ft)	Smectite	illite	Plagioclase	K-feldspar	Quartz	Biotite	Clinopyroxene	Hematite	Calcite
7990-8000	10	5	41	9	12	tr	9	6	8

Medium- to coarse-grained andesite flow with sparse clinopyroxene phenocrysts in a crystalline groundmass consisting of interlocking equigranular plagioclase laths and clinopyroxene, with interstitial K-feldspar and quartz. Plagioclase is partially altered to illite and calcite. Clinopyroxene is partially altered to smectite, hematite and calcite.

Moderate shearing and minor veining are observed in this sample. Sheared chips are hematite stained. The majority of the open space in the sample appears to be primary (vesicles/amygdules).

The sample is cut by several generations of veins. Early calcite ± hematite (botryoidal to euhedral), calcite without hematite and finally chalcedony grading into quartz. A similar succession of mineralization is recorded in amygdules with quartz precipitating last.

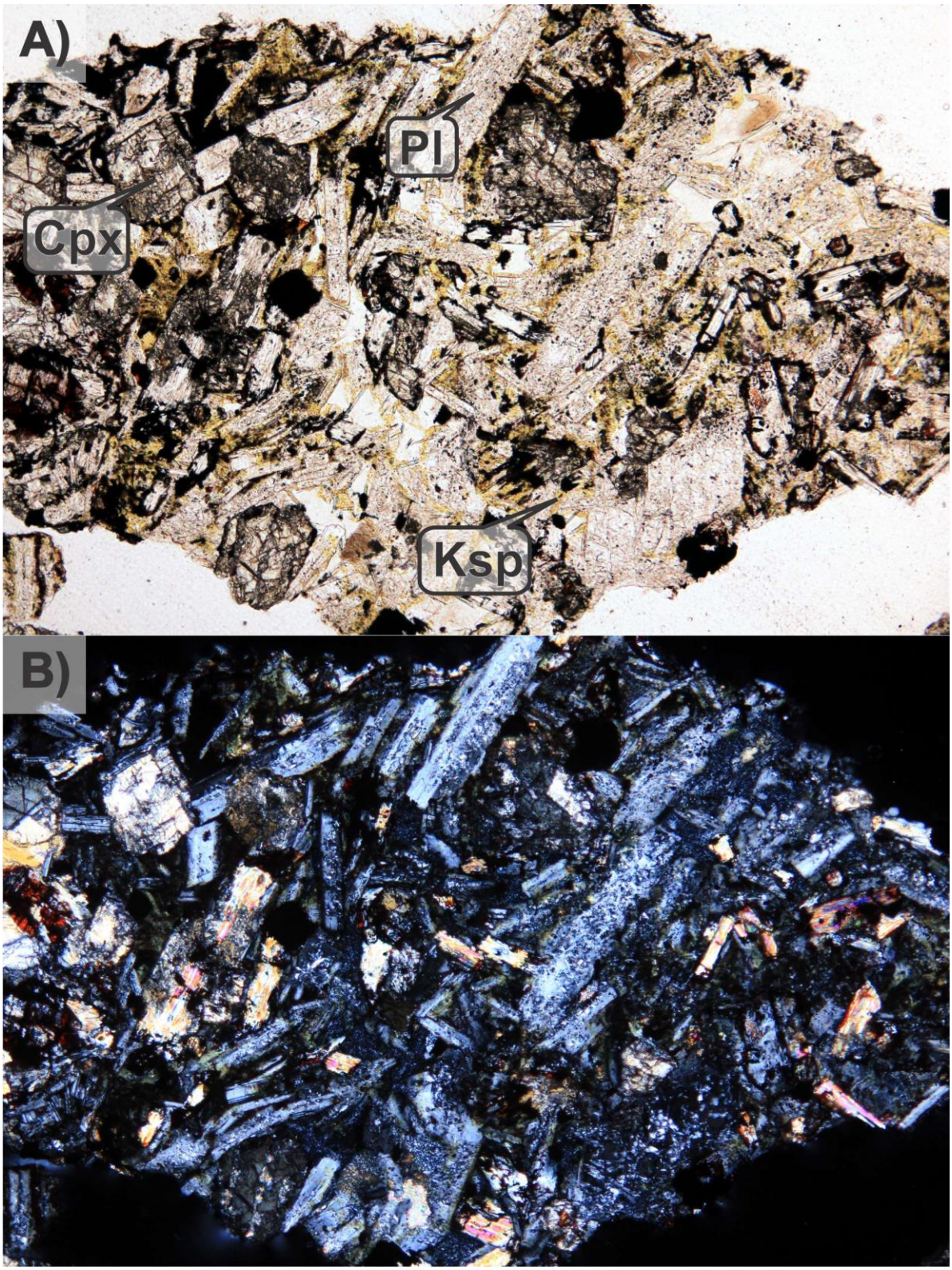

Figure B5.7.1: Equigranular groundmass of the andesite lava flow consisting of plagioclase and clinopyroxene with interstitial K-feldspar (stained yellow). Photomicrographs were taken of the cuttings from 7990-8000 ft. A) Plane polarized light. B) Crossed nicols. Field of view is 1.6 mm.

B5.8 Volcaniclastic sandstone. Samples 8240-8250 to 8740-8750 ft.

Four samples from this unit were analyzed petrographically and by XRD from 8240-8250 to 8740-8750 ft

Table B5.8.1: Results of X-ray diffraction analyses in weight percent of sample. See Table B3.1 caption for more information.

Depth (ft)	Smectite	I/S	illite	Chlorite	Plagioclase	K-feldspar	Quartz	Clinopyroxene	Hematite	Calcite	Dolomite	Anhydrite	% illite in I/S
8240-8250	2	2	13	6	36	10	23	tr	2	5			90%
8340-8350	7	19	tr	9	25	8	27			5	tr		90%
8540-8550		16	tr	6	22	11	41			4			~50 & 90% 2 species
8740-8750		24	tr	5	24	9	33			2	2	tr	~50 & 90% 2 species

This unit generally consists of volcaniclastic sandstone composed of mineral grains, texturally variable lava flow clasts and ash-flow tuff clasts in a clay-rich (ashy) matrix and less commonly calcite cement. Fine-grained quartz and less abundant chalcedony and chlorite fills open pore spaces. Silicified rock and matrix is also observed. Later calcite veins cut the earlier silica deposition and alteration.

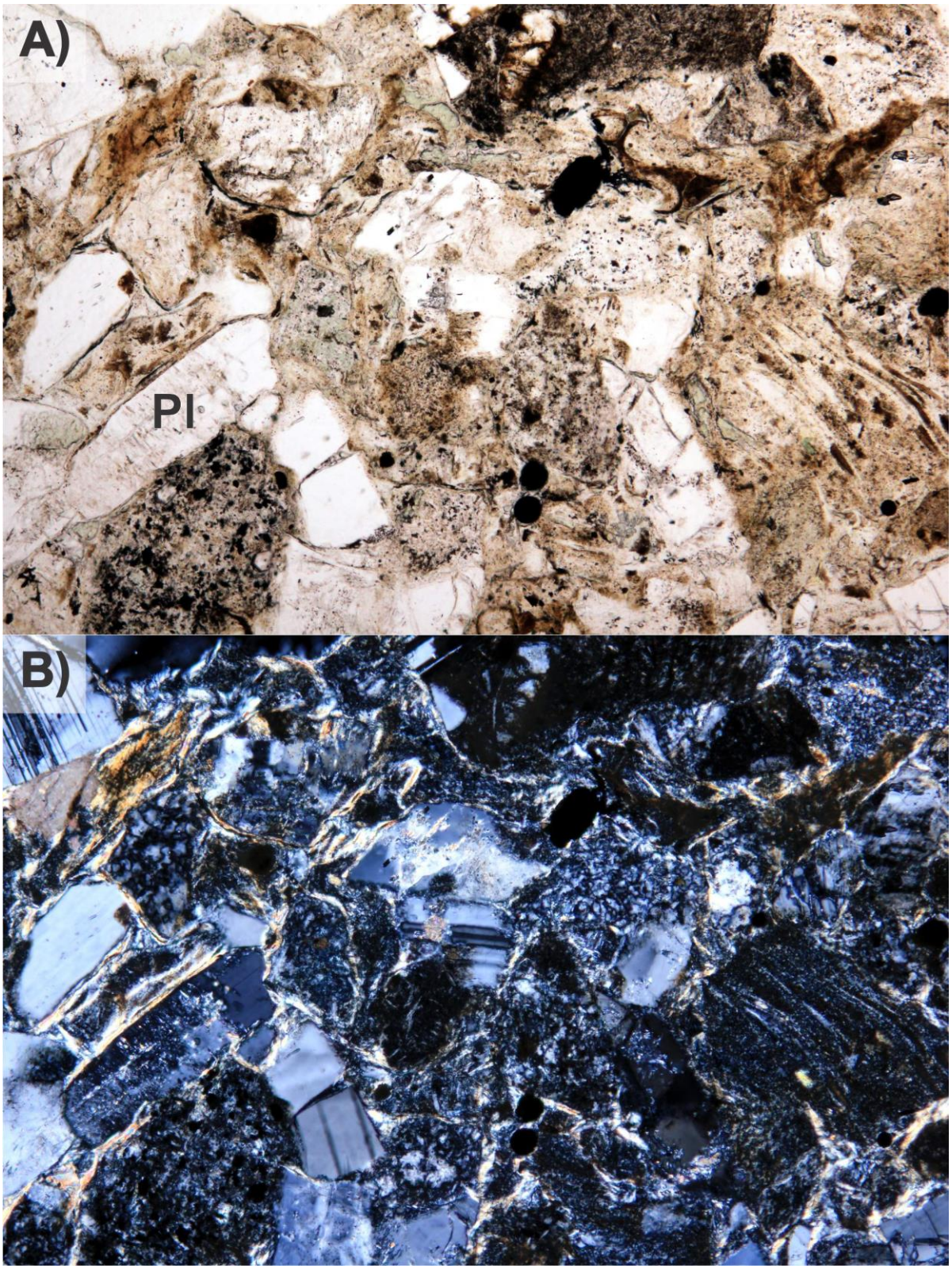

Figure B5.8.1: Volcaniclastic sandstone composed of plagioclase grains and lithic fragments of lava flows and ash-flow tuff in an ashy matrix. Photomicrographs were taken of the cuttings from 8740-8750 ft. A) Plane polarized light. B) Crossed nicols. Field of view is 1.6 mm.

B5.9 Lacustrine sediments and evaporite deposits. Samples 8940-8950 to 9340-9350 ft.

Three samples from this unit were analyzed petrographically and by XRD from 8940-8950 to 9340-9350 ft

Table B5.9.1: Results of X-ray diffraction analyses in weight percent of sample. See Table B3.1 caption for more information.

Depth (ft)	I/S	illite	Chlorite	Plagioclase	K-feldspar	Quartz	Hematite	Calcite	Dolomite	Anhydrite	% illite in I/S
8940-8950	22	tr	6	25	9	25		3	6	4	~50 & 90% 2 species
9140-9150	26		7	10	9	19		5	13	12	~50 & 90% 2 species
9340-9350	12		8	9	5	17		2	8	39	90%

This unit is dominantly composed of matrix supported siltstone consisting of mineral grains and lithics in clay-rich (interlayered illite/smectite and chlorite ± illite) and/or fine-grained carbonate (dolomite>calcite) matrix. Lithics include ash-flow tuff clasts, clay altered pumice with remnant vesicular textures, glass shards, lava flow clasts and intrusive clasts. Preserved shard textures are observed within the clay-rich matrix and as clasts in the fine-grained calcite matrix. Less common clast supported sandstone has anhydrite or calcite cement. This unit contains abundant anhydrite (up to 39 wt% at 9340-9350 ft) as nodules, laths and thin beds that are partially replaced by chalcedony and quartz. Euhedral rhombs of dolomite are associated with quartz replacements of anhydrite.

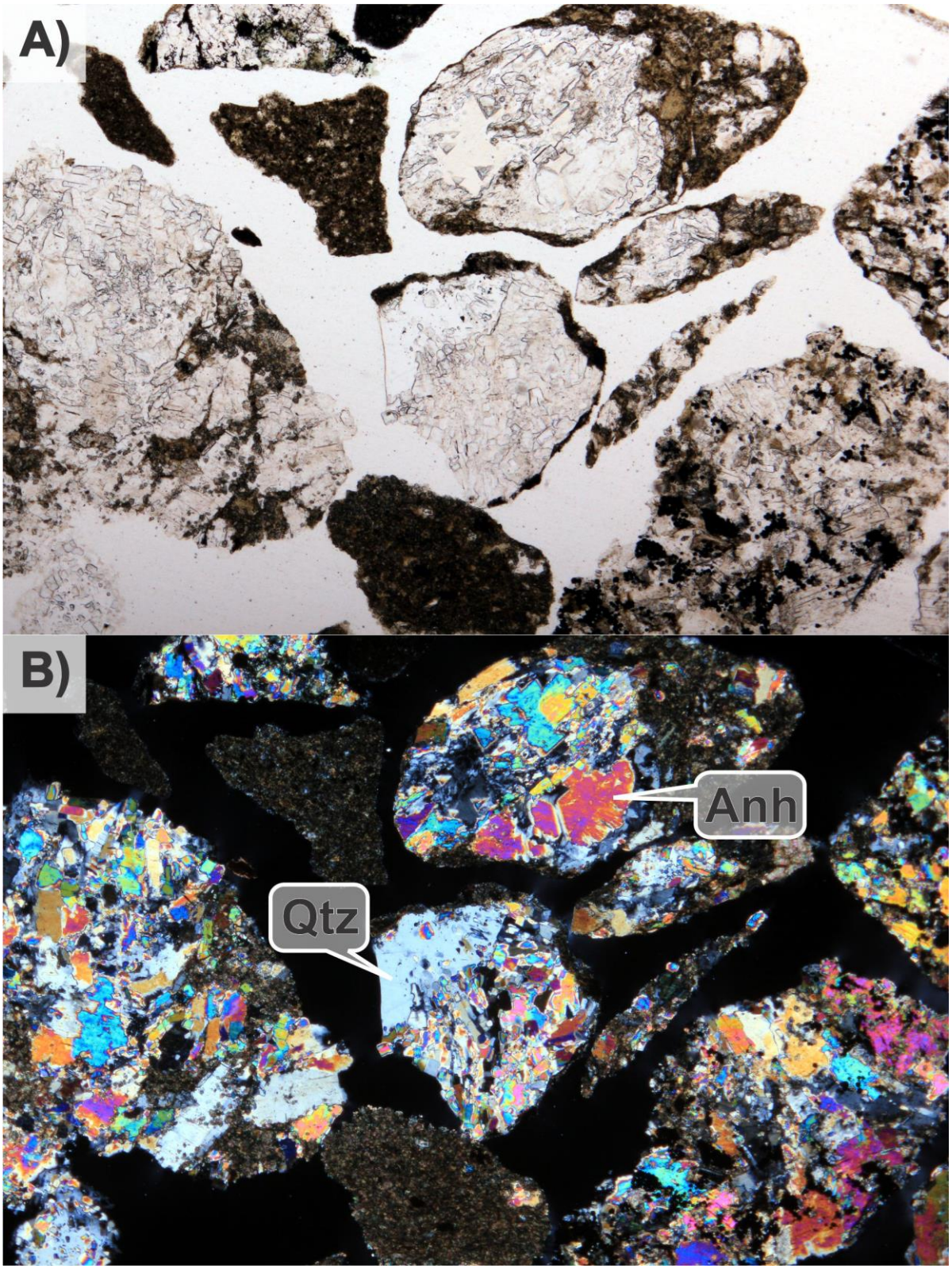

Figure B5.9.1: Anhydrite-rich siltstone. Anhydrite has been partially replaced by quartz at the center of the images. Photomicrographs were taken of the cuttings from 9340-9350 ft. A) Plane polarized light. B) Crossed nicols. Field of view is 3.2 mm.

B5.10 Rhyolite ash-flow tuff and tuffaceous sediments. Samples 9540-9550 to 10140-10150 ft.

Four samples from this unit were analyzed petrographically and by XRD from 9540-9550 to 10140-10150 ft

Table B5.10.1: Results of X-ray diffraction analyses in weight percent of sample. See Table B3.1 caption for more information.

Depth (ft)	I/S	illite	Chlorite	Plagioclase	K-feldspar	Quartz	Epidote	Tourmaline	Apatite	Pyrite	Hematite	Calcite	Anhydrite	% illite in I/S
9540-9550	27		8	20	7	26				tr		4	7	~50 & 90% 2 species
9740-9750	4	24	9	23	8	23				tr		4	5	~50 & 90% 2 species
9940-9950	3	16	13	18	18	24				1	1	2	4	~50 & 90% 2 species
10140-10150	tr	12	12	33	11	28	tr	tr	tr	1		1	1	90%

The first sample above the granite is composed of equal parts extensively sheared and altered intrusive rock and densely welded ash-flow tuff, with minor sediments. The intrusive rock is interpreted as a granite breccia (sediment). The upper three samples in this unit are composed of ash-flow tuff and tuffaceous sediments.

There are trace amounts of high to moderate temperature hydrothermal minerals in the sample just above the granite, but the tourmaline and epidote are found exclusively within the fine-grained intrusive rock chips interpreted as a sediment and no evidence of high temperature hydrothermal alteration is observed in the tuff or tuffacous sediments that lie above the thick granite body.

The ash-flow tuff cuttings are variably welded (densely to non-welded) and contain resorbed quartz and plagioclase phenocrysts. The groundmass contains abundant illite fiamme in the upper samples. In the lower samples the groundmass is often silicified with a matrix composed of fine-grained quartz with little illite or K-feldspar.

The volcaniclastic sediments range from silt to at least gravel-size and consist of minerals grains and lithics in a fine-grained clay-rich matrix (ashy) with less common fine-grained calcite matrix. Lithic clasts are dominantly ash-flow tuff with less abundant lava flow and intrusive rocks. Pumice fragments are fairly common with preserved vesicular textures that have been extensively altered to clay minerals (interlayered illite/smectite and illite). Plagioclase in tuff and flow clasts has been partially altered to calcite and anhydrite. Ferromagnesian minerals have been replaced by chlorite. Siltstone cuttings may contain anhydrite nodules, and the anhydrite nodules may be partially replaced by quartz and/or chalcedony.

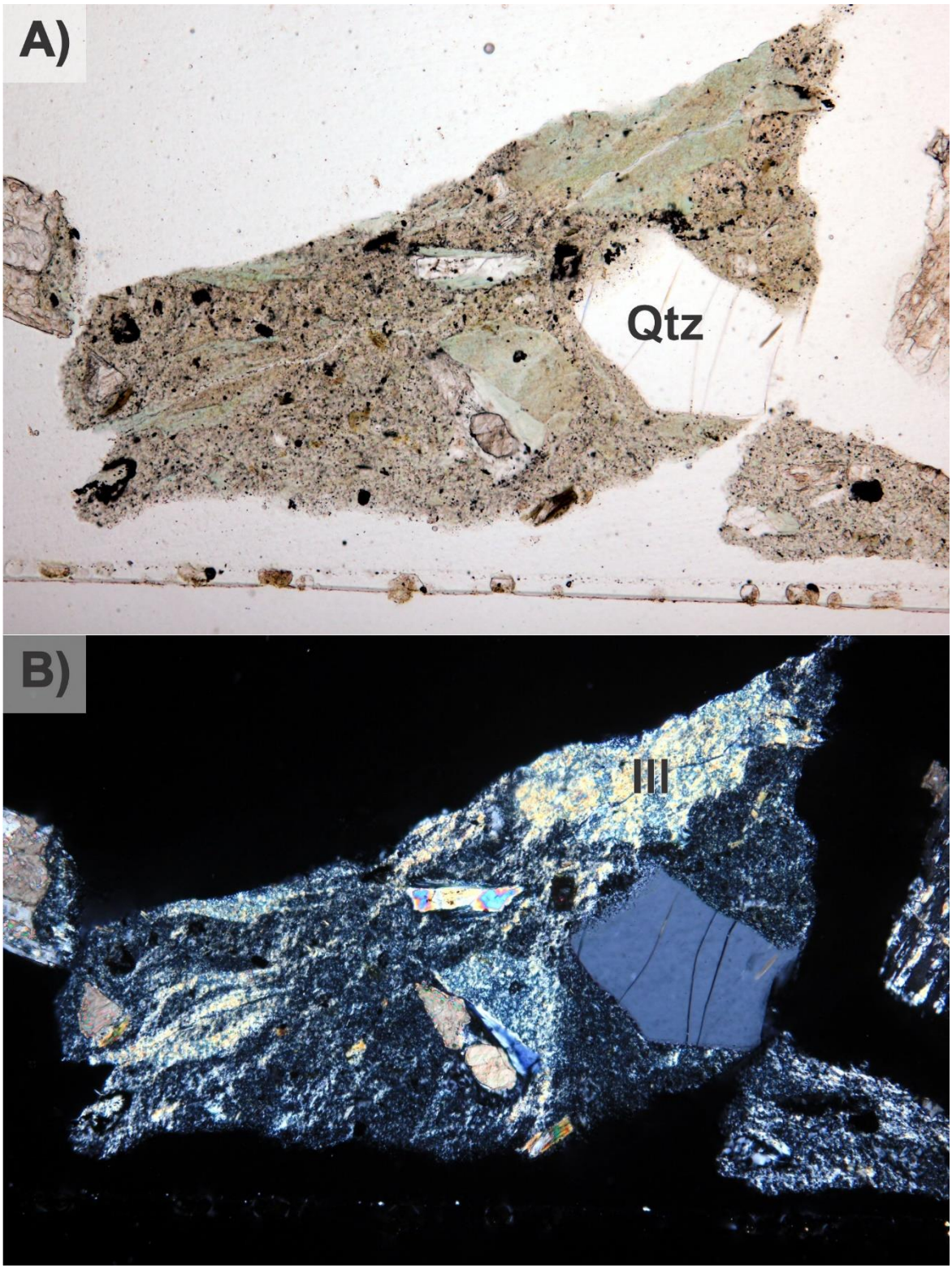

Figure B5.10.1: Ash-flow tuff with a quartz phenocryst in a groundmass containing illite fiamme. Photomicrographs were taken of the cuttings from 9740-9750 ft. A) Plane polarized light. B) Crossed nicols. Field of view is 1.6 mm.

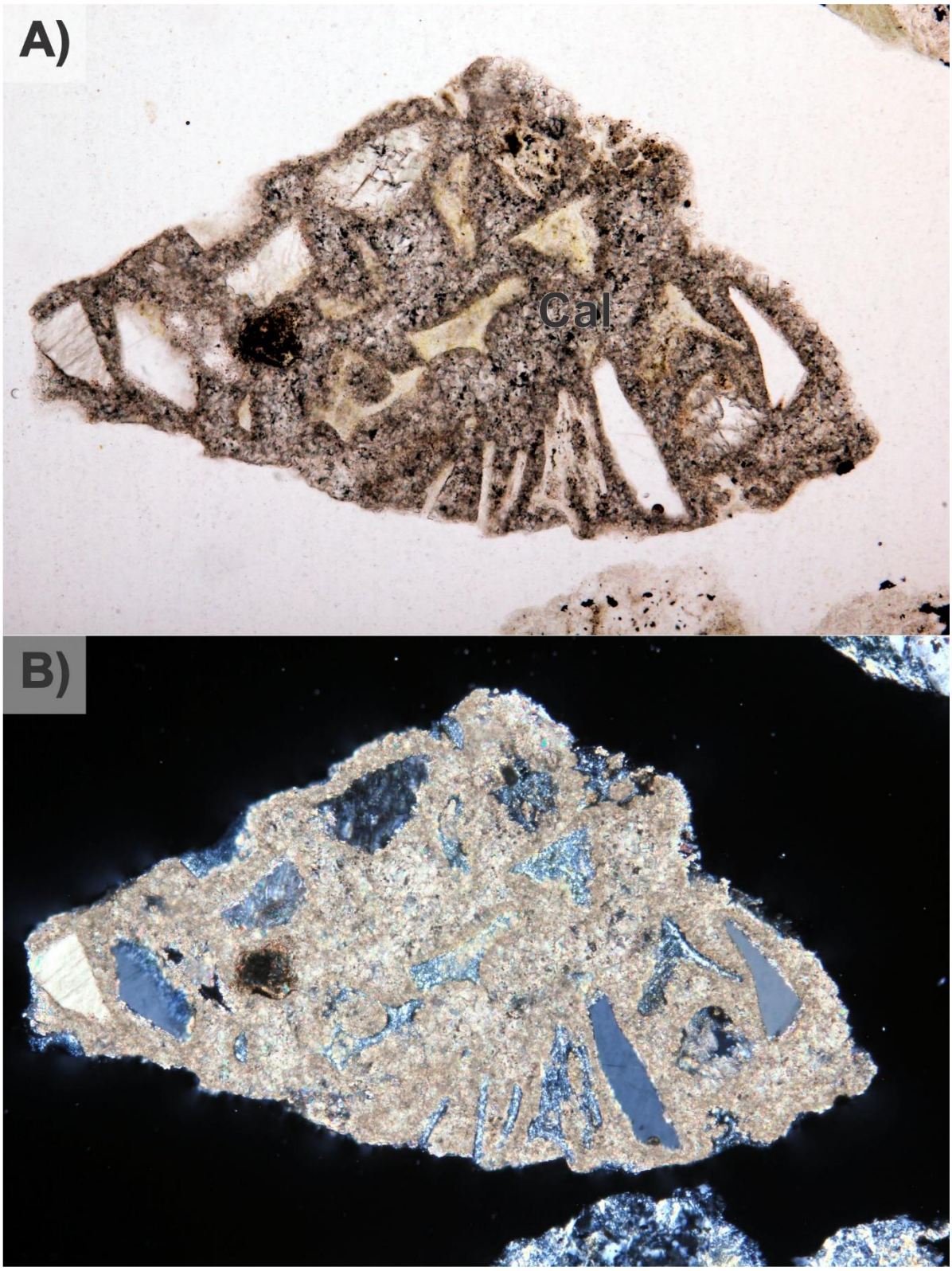

Figure B5.10.2: Glass shards and mineral grains in a fine-grained calcite matrix. The glass shards have been altered to illite. Photomicrographs were taken of the cuttings from 10140-10150 ft. A) Plane polarized light. B) Crossed nicols. Field of view is 1.6 mm.

B5.11 Granite, Samples 10190-10200 to 12440-12450 ft.

Fourteen samples of the granite were analyzed petrographically and by XRD from10190-10200 to 12440-12450 ft.

Table B5.11.1: Results of X-ray diffraction analyses in weight percent of sample. See Table B3.1 caption for more information.

Depth (ft)	I/S	illite	Chlorite	Plagioclase	K-feldspar	Quartz	Hornblende	Biotite	Apatite	Clinopyroxene	Magnetite	Titanite	Epidote	Rutile	Pyrite	Hematite	Calcite	Dolomite	Anhydrite	% illite in I/S
10190-10200	tr	12	12	11	22	32		tr	tr	tr	tr					tr	9		2	~50 & 90% 2 species
10290-10300	tr	8	6	6	9	34		tr	tr	tr	tr					tr	35		tr	~50 & 90% 2 species
10490-10500	tr	10	13	26	18	25		tr	tr		tr	1					5		1	90%
10690-10700	tr	8	6	40	21	16	3	tr	tr		1	tr	tr				3		tr	90%
10890-10900	tr	13	11	19	12	32	tr	tr	tr		1	1	1			tr	7		tr	~50 & 90% 2 species
11090-11100	tr	4	14	36	17	20	1	2	tr	tr	1	1	tr			tr	3			~50 & 90% 2 species
11290-11300	tr	8	2	43	18	19	2	2	tr		1	1	tr			tr	3		tr	50%
11490-11500	tr	11	8	16	10	35	4	tr	tr	1	tr	tr	tr			tr	10	1	1	90%
11690-11700	tr	9	11	34	18	18	4	tr	tr		tr	tr			tr	tr	5			90%
11890-11900	tr	6	8	36	20	20		1	tr		1	1				tr	5			90%
12090-12100	tr	7	6	30	19	30		tr	tr		tr	tr		tr	tr	tr	4		1	90%
12140-12150	tr	18	6	17	15	33	tr		tr			2		tr			5	1	3	90%
12240-12250		2	9	31	20	28		1	tr		1	tr					3	1	3	
12440-12450		11	5	25	23	26		tr	tr			1					1	4	3	

Cuttings from 10,140-10,150 to 12,440-12,450 ft are composed of granitic rocks of the Mineral Range Batholith. The formation is interpreted to be in fault contact with the underlying PreCambrain gneiss, and the upper contact is interpreted as an unconformity with the overlying volcaniclastic and volcanic rocks (Figure B1.1). The granite cuttings show consistent evidence of brittle deformation and hydrothermal alteration, but the extent of the deformation and alteration is variable ranging from minor to intense (Figure B5.1). Deformation and hydrothermal alteration are concomitant, with brittle deformation creating the permeability that facilitates hydrothermal alteration.

The dominant lithology (>90%) is medium-grained granite composed of equigranular, interlocking plagioclase, K-feldspar and quartz; with minor hornblende and biotite; as well as accessory magnetite, titanite, apatite, rutile and zircon.

Hydrothermal alteration is most prominent in samples that have a greater density and concentration of fractures (Figure B5.1). This can be seen in the variable plagioclase abundances (XRD) that range from 43 wt% to as low as 11 wt% in rocks with the same primary granitic mineralogy (excluding the fracture zone at 10290-10300 ft which is dominated by open space filling phases)(Figure B5.11.1). Plagioclase is altered to illite, calcite, K-feldspar, albite and quartz, as well as rare chlorite and epidote. The ferromagnesian minerals are also variably altered with some samples containing only trace amounts (<1 wt%) and others containing up to 4 wt% hornblende or 2 wt% biotite. Biotite is intensely altered to chlorite, rutile and hematite. Hornblende is intensely altered to chlorite, calcite and hematite. In contrast, K-feldspar, quartz, apatite, zircon and titanite are relatively unaltered. In the most deformed and altered samples quartz is the only major phase remaining. In deformed cuttings quartz often displays undulatory extinction and contains trains of secondary fluid inclusions.

There are minor occurrences of several texturally distinct porphyritic intrusions with fine-grained groundmass observed in the cuttings from this interval: granite at 12090-12100 and 12240-12250 ft; granodiorite at 10190-10200 ft; and diorite at 12240-12250 ft. The fine-grained porphyritic granite consists of plagioclase and quartz (can be resorbed) phenocrysts in a fine-grained groundmass composed of equigranular intergrown K-feldspar, plagioclase and quartz (with rare granophyric textures) and rare chlorite pseudomorphs of ferromagnesian minerals. The fine-grained granodiorite porphyry contains plagioclase, quartz, biotite (altered to chlorite and titanite) and hornblende (altered to chlorite) phenocrysts in a fine-grained matrix composed dominantly of interlocking plagioclase laths with less abundant K-feldspar and quartz (with accessory apatite). The fine-grained porphyritic diorite contains plagioclase, biotite and hornblende phenocrysts in a groundmass composed of interlocking plagioclase laths with interstitial K-feldspar, chlorite (most likely after clinopyroxene) and magnetite ± late stage quartz. In general the porphyritic intrusions are less altered and deformed than the more abundant medium-grained granite, and the rare spherulitic devitrification textures observed are interpreted as the chilled margins of these fine-grained intrusions. The cuttings of the fine-grained intrusive lithologies are most commonly found in the most intensely deformed samples at the top and bottom of the formation.

Evidence of brittle deformation resulting from tectonic activity is commonly observed in the cuttings from this unit. The granite is often veined, brecciated and/or sheared to varying degrees (Figure B5.1) with some samples consisting predominantly of cataclasite (fault gouge) and other samples predominantly of open space filling minerals from a fracture zone.

The cataclasite observed within the granite generally consists of sub-rounded to angular clasts supported by a fine-grained matrix of crushed rock altered to dominantly to illite. Clasts include fragments of granite (angular) and mineral grains, dominantly quartz (more likely to be rounded), with less abundant granitic minerals with cleavage (e.g. more angular fragments of feldspar) that would be more prone to disintegration during shearing. It is not uncommon to find vein fragments (usually calcite and fine-grained quartz and) as clasts in the cataclasite. Both deformed and undeformed veins are observed cutting the cataclasite showing that these structures were reactivated and sealed on multiple occasions.

Quartz and calcite are the most commonly observed open space filling minerals in veins and brecciated rock. Less abundant phases include chlorite, illite and anhydrite. Rare open space filling of K-feldspar, pyrite, rutile, fluorite, epidote and fine-grained, fibrous pseudomorphs of actinolite (?) are also observed.

Several episodes of tectonic deformation and accompanying hydrothermal alteration and open space mineralization have affected the granitic rocks as evidenced by: 1) rare early epidote (and pseudomorphs of actinolite?) deposited in open space; 2) quartz replacing calcite and anhydrite veins; 3) calcite and anhydrite veins cutting cataclasite, silica cemented breccia and silicified rock; 4) low abundances of interlayered illite/smectite (XRD) indicating retrograde argillic overprinting (<225^{o}C); 5) the incorporation of vein fragments in cataclasite; and 6) multiple dikes at different levels with distinct textures ranging in composition from granite to diorite are associated with extensively deformed rocks.

Faults are interpreted to bound the granite at top and bottom.

The bottom of the granite is interpreted to be in fault contact with the gneiss based on the marked difference in deformation and alteration between the two lithologies, with the granite hosting significantly more deformation and alteration, as well as textural evidence of intense deformation in the cuttings from 12440-12450 ft including shearing (cataclasite) veining and brecciation.

The upper contact between the granite and the volcanic/sedimentary unit above is interpreted as an unconformity with volcanic and volcaniclastic rock deposited on the exhumed footwall of a normal fault and/or a partially eroded fault zone. There is a sharp decrease in deformation fabrics in the overlying units, and the lack of contact metamorphism in the lithologies overlying the thick sequence of intrusive rock preclude this as an intrusive contact. The upper most granitic basement samples consist of a fracture zone and a shear zone. The deeper of the two samples from 10290-10300 ft is a fracture zone that is dominantly composed of open space fillings of quartz and calcite (quartz and calcite make up 69 wt% of the sample by XRD) with less abundant chlorite, illite, anhydrite and fluorite. The upper most granite sample at 10190-10200 ft is composed of intensely sheared and altered medium-grained granite with abundant cataclasite.

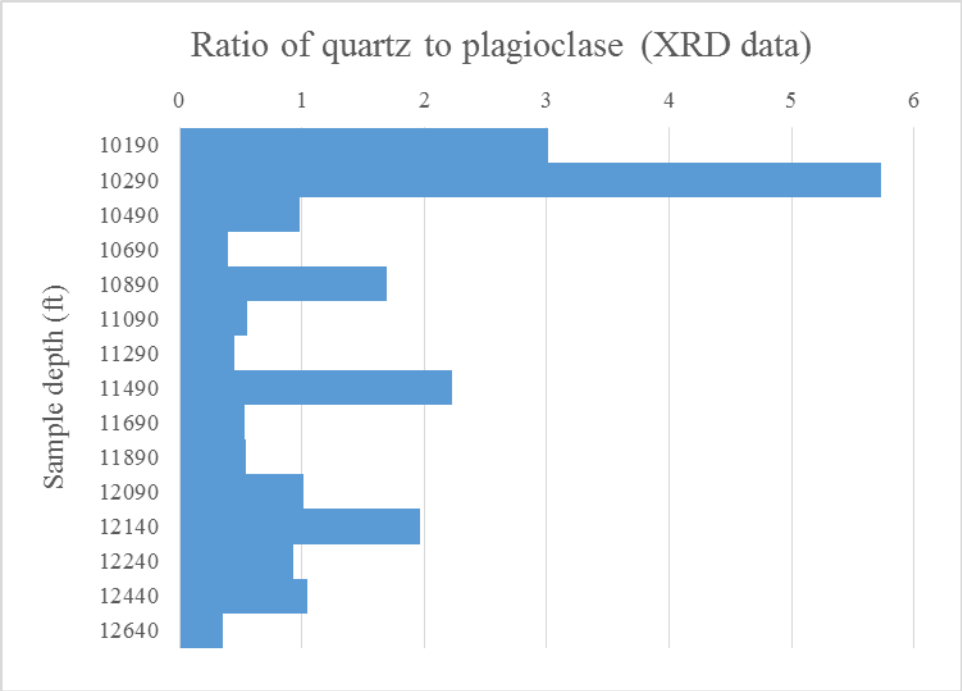

Figure B5.11.1: This figure plots the ratio of quartz to plagioclase in the granitic rocks of the mineral range batholith and the PreCambrian gneiss (12640 ft), and can be used as a proxy for extent of brittle deformation and hydrothermal alteration. Hydrothermal alteration results in the destruction of plagioclase and the formation of quartz in theses rocks with the largest ratios showing the most alteration. The results generally agree with the estimates of alteration and deformation made as part of the petrographic analyses (Figure B5.1).

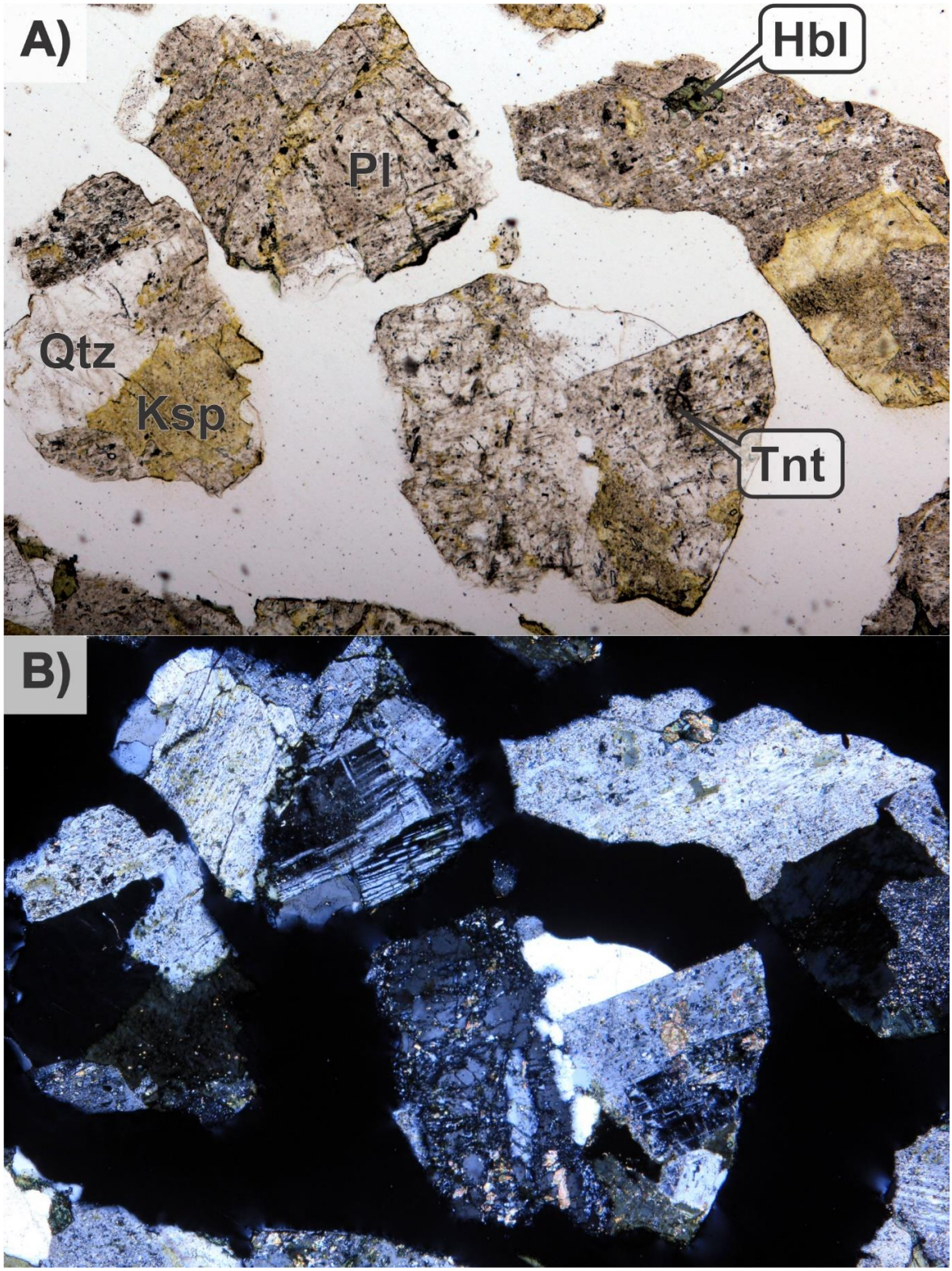

Figure B5.11.1: Representative photomicrographs of the medium-grained granite cuttings. Photomicrographs were taken of the cuttings from 11290-11300 ft. A) Plane polarized light. B) Crossed nicols. Field of view is 3.2 mm.

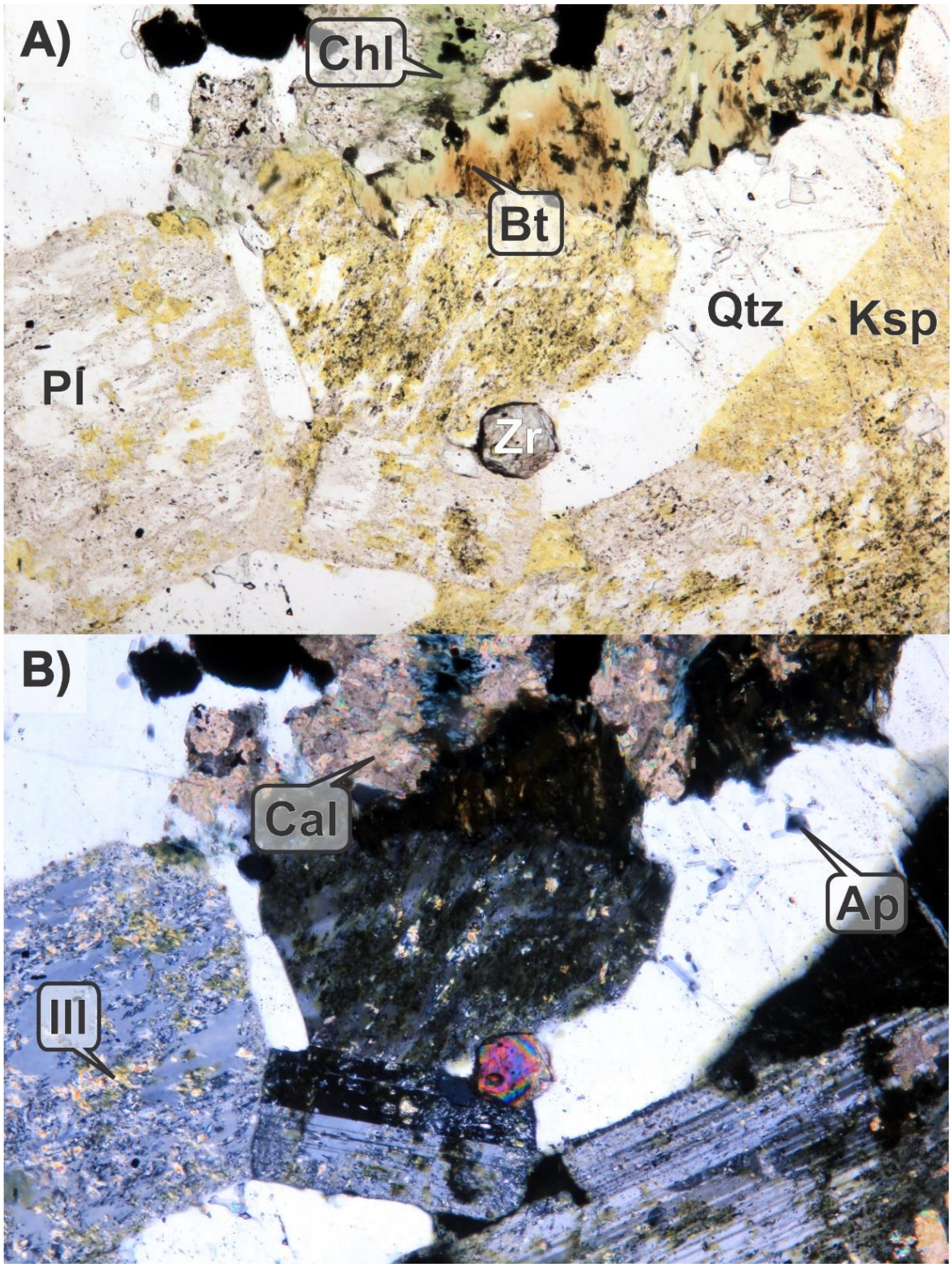

Figure B5.11.2: Representative photomicrographs of medium-grained granite. Photomicrographs were taken of the cuttings from 12140-12150 ft. A) Plane polarized light. B) Crossed nicols. Field of view is 1.6 mm.

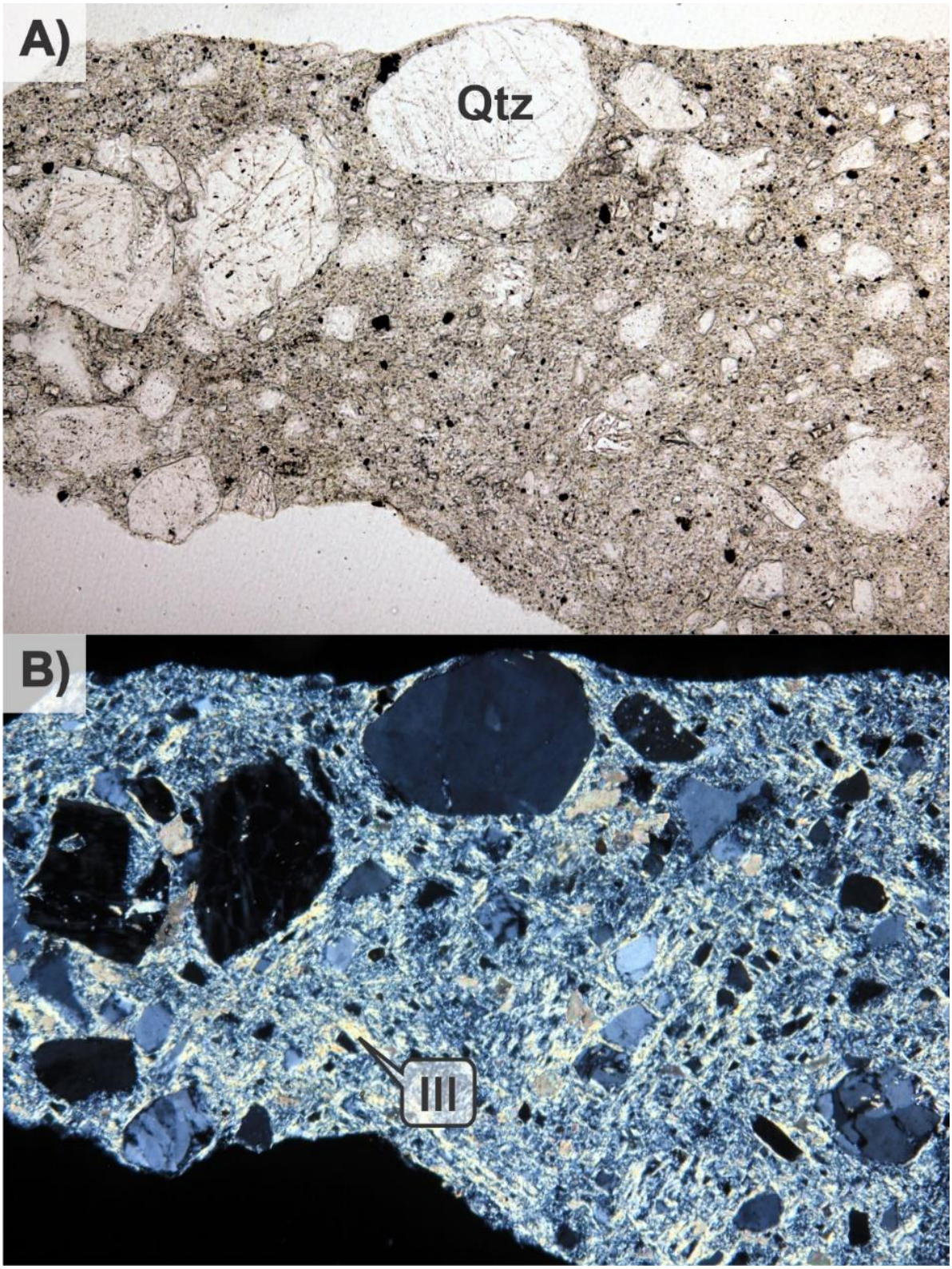

Figure B5.11.3: Cataclasite consisting of rounded quartz grains in an illite-rich, fine-grained matrix of crushed and altered rock. Photomicrographs were taken of the cuttings from 12440-12250 ft. A) Plane polarized light. B) Crossed nicols. Field of view is 1.6 mm.

B5.12 Gneiss 12640-2650 ft

One sample of the gneiss was analyzed petrographically and by XRD from 12640-2650 ft

Table B5.12.1: XRD data wt% of sample

Depth (ft)	illite	Chlorite	Plagioclase	K-feldspar	Quartz	Hornblende	Biotite	Apatite	Titanite	Calcite	Anhydrite
12640-12650	6	4	43	19	15	6	4	tr	3	tr	tr

This unit consists of a weakly foliated plagioclase, K-feldspar, quartz, hornblende, biotite, titanite, apatite gneiss. The unit is relatively unaltered with plagioclase partially altered to illite, and biotite to chlorite. Rare brittle deformation (shearing, brecciation and veining) is observed with open space filled by calcite and anhydrite.

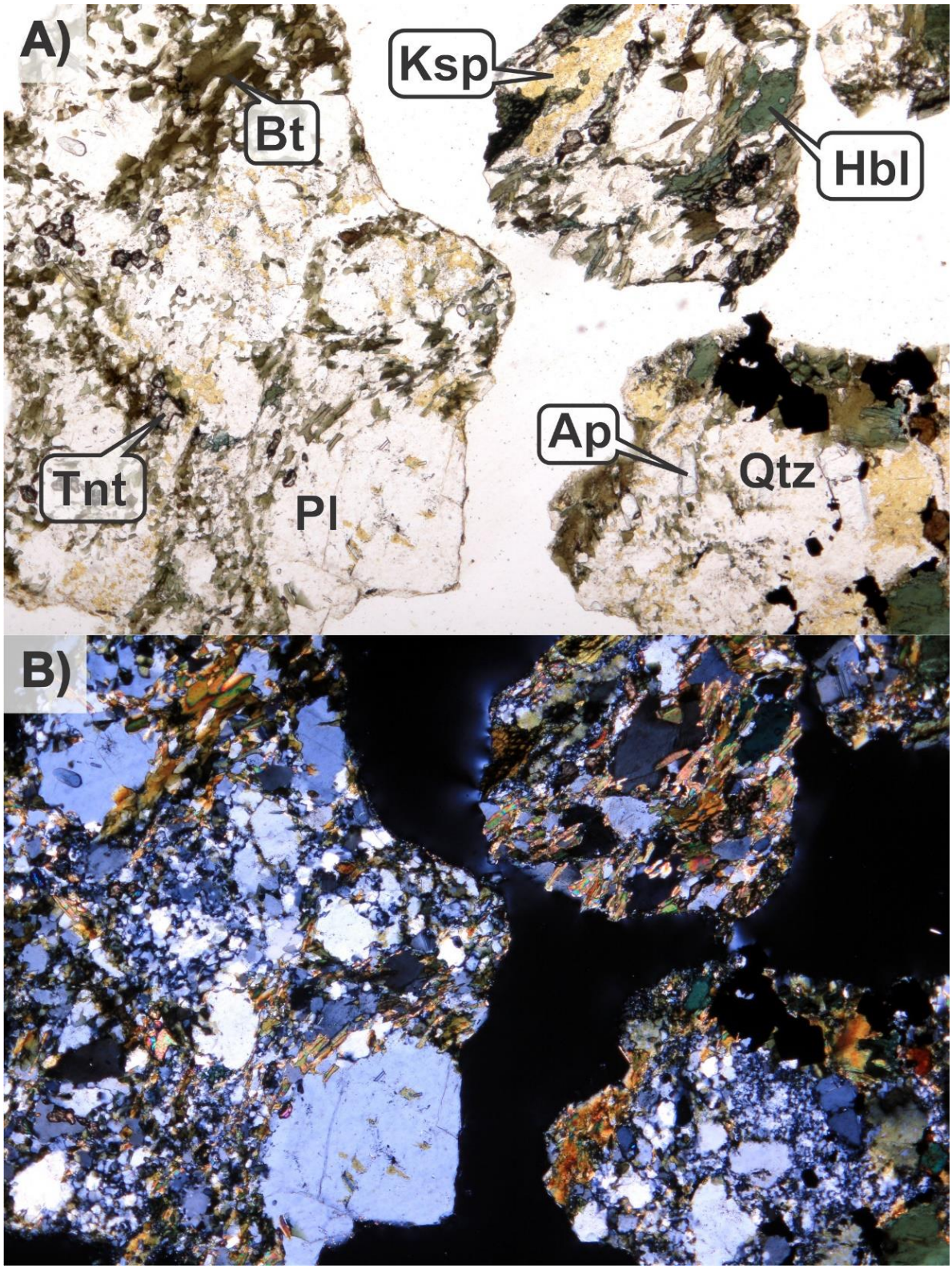

Figure B5.12.1: Weakly foliated plagioclase, K-feldspar, quartz, hornblende, biotite, titanite, apatite gneiss. Photomicrographs were taken of the cuttings from 12640-12650 ft. A) Plane polarized light. B) Crossed nicols. Field of view is 3.2 mm.

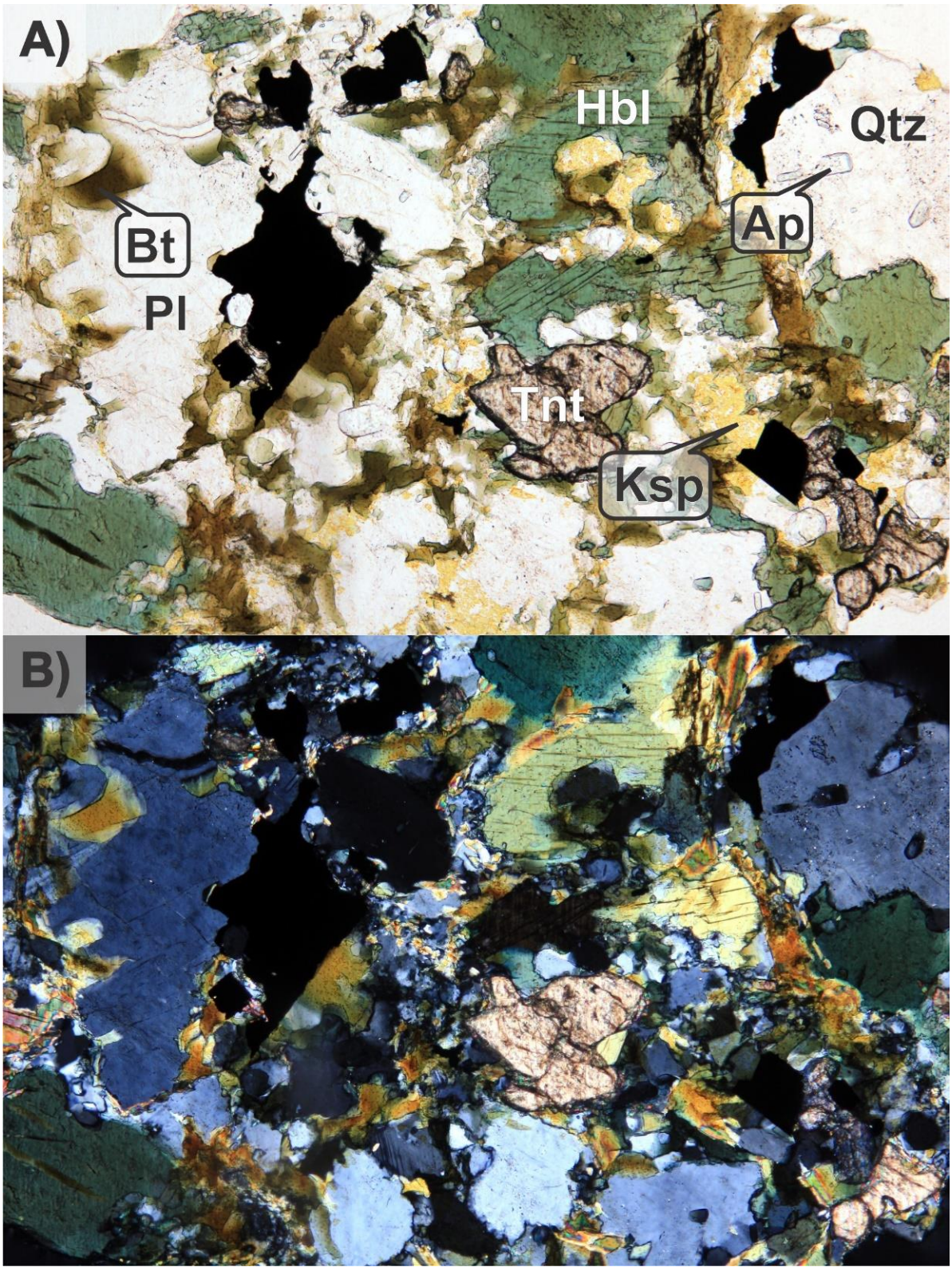

Figure B5.12.2: Weakly foliated plagioclase, K-feldspar, quartz, hornblende, biotite, titanite, apatite gneiss. Photomicrographs were taken of the cuttings from 12640-12650 ft. A) Plane polarized light. B) Crossed nicols. Field of view is 1.6 mm.

Update Seismicity Data

TASK 1.1.3

Task 1.1.3 Update Seismicity Data

Historical Seismicity of Area

To evaluate past seismic activity near to the Utah FORGE site, we review three relevant earthquake catalogs: (1) a uniform moment magnitude catalog (1850- September, 2012; Arabasz et al., 2015); (2) the microseismic catalog (August, 1979 – summer 1981) collected by Zandt et al. (1982); and (3) the University of Utah Seismograph Stations (UUSS) earthquake catalog, 1981-2015. For all three catalogs, seismicity near the Utah FORGE site is described as low-magnitude and low-frequency. Using the Arabasz et al. (2015) catalog, we see that the largest event in the study area (M_W 4.08) occurred in 1908 and was located south of Milford (Figure 1). The closest substantial earthquake (M > 6) occurred in 1901 in the Tushar Mountains north of Beaver ~75 km to the northeast of the Utah FORGE site.

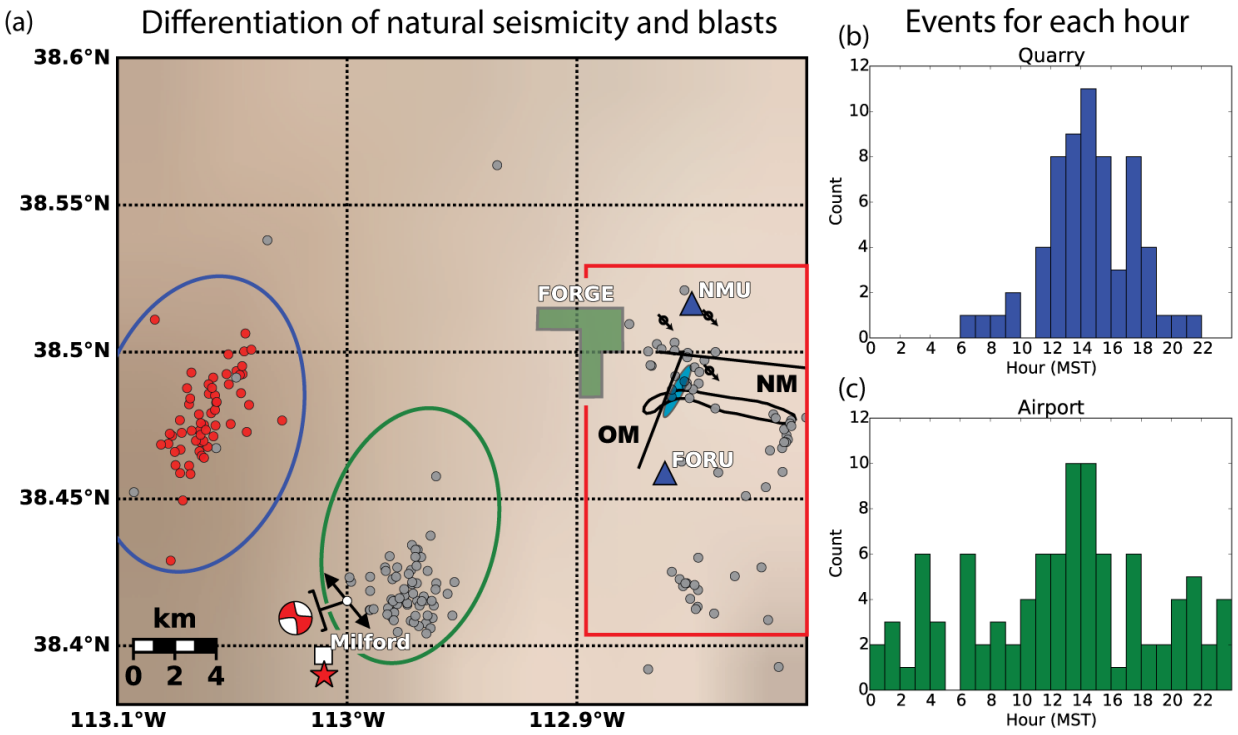

Figure 1. *The relocated earthquake catalog. (a) Differentiation between natural seismic events and quarry blasts for UUSS catalog 1981 – 2015. Red and gray circles represent blasts and natural seismicity, respectively. The blue and green ellipse outlines refer to the events within the histograms. The red outline represents the Mineral Mountains study area. The black lines in the Mineral Mountains study area represent the Opal Mound (OM) and Negro Mag (NM) fault. The NM fault continues off the study area to the east. The black outline, overlapping the OM fault, represents the area of the Zandt swarm (Zandt et al. 1982). The blue triangles are seismic stations; the green polygon represents the proposed Utah FORGE footprint. The black circles with an arrow through them, east of the FORGE drilling footprint, represent injection wells for the Blundell geothermal plant. The blue ellipse, east of the OM fault, represents the production well area for the Blundell geothermal plant. The white square represents the center of Milford, UT and the red star is the epicenter of the 1908 earthquake, M 4.08. The white circle represents the April 10, 1998 ML 3.91 earthquake with T-axis and focal mechanism (displayed offset from T-axis). (b) shows events within the blue ellipse as a function of time of day (these events occurring during daylight hours) and (c) shows seismicity located in the green ellipse (these events occur during all hours of the day). Based on the time of day and the proximity to quarries, 62 of the 201 events displayed are classified as blasts.*

Before production began at Roosevelt Hot Springs, Zandt et al. (1982) installed a local seismic array to detail the background seismicity. During the approximate 2-year deployment they concluded that there are few earthquakes M > 2. They did capture one energetic seismic swarm (1044 earthquakes M ≤ 1.5) during June through August, 1981. This swarm occurred east of the present bore field at Roosevelt Hot Springs, primarily in the Mineral Mountains (Figure 1). The trend of the seismicity was mostly east-west. They concluded that the swarm was primarily

naturally occurring and was consistent with either (or both) seismicity occurring along the projection of the east-west trending Negro Mag fault or along northwest trending faults mapped by Nielson et al. (1978). A few of the earthquakes located on the west end of the swarm may have occurred along the Opal Mound Fault, but this interpretation remains speculative.

Relocation

Events in the UUSS catalog (January 1981 – March 2015) have been relocated. The relocation incorporated updated velocity models and location algorithm. The depths of the events have all been calculated to a relative elevation datum of mean sea level. Depths are difficult to accurately constrain because of the sparseness of the seismic network.

The relocation of the events caused slight changes in location, but overall provided tighter clustering spatially. From the relocated events it is observable that no events (within the current magnitude of completeness) are located within the Utah FORGE footprint (Figure 1). Pankow et al. (2004) estimated a minimum magnitude of complete recording of M 1.5 for this region of Utah. Earthquakes occurring outside the Utah FORGE footprint during 1981-2015 range from M -0.09 to 3.91. The average horizontal and vertical 90% confidence errors for these earthquakes are 0.88 km and 4.86 km, respectively. Spatially there are two distinct clusters, to the north and northwest of Milford. In addition, there is a diffuse region of seismicity east of the Utah FORGE site in the Mineral Mountains (Figure 1).

Discrimination

For seismic hazard analysis, it is important to first analyze the catalog and remove non-earthquake events. To discriminate the catalog, we looked at spatial proximity between events and time of day. We also looked at waveform characteristics. Through waveform analyses in the region of study, we were able to group similar waveforms together. Strongly correlated waveforms indicate that the location and source mechanism are similar. Waveforms from blasts have distinct characteristics compared to an earthquake waveform, and these characteristics can be used to discriminate event types locating in close proximity.

Using the relocated catalog, work focused on discriminating quarry blasts and other non-earthquake sources from tectonic earthquakes, and in identifying clusters of seismicity that deserve further analysis to better constrain source zones. Figure 1 highlights two seismicity clusters that were analyzed to determine source type. The cluster outlined in the blue ellipse locates in an area of quarry mining (conspicuous on Google maps). The magnitudes range from 0.49 to 2.05. Seismic events from this area locate primarily at shallow depths (< 2.5 km below sea level), occur during daylight hours (Figure 1), and have very similar waveforms. Based on this evidence, we conclude that these events are not earthquakes, but quarry blasts.

The second cluster outlined by the green ellipse (Figure 1) locates in close proximity to the Milford airport and not far from the M 4.08 1908 Milford earthquake (the largest recorded earthquake in the study area). The magnitudes in this cluster range from 0.46 to 3.91, and the events occur throughout the day (without a time bias, Figure 1). This cluster is interpreted as tectonic in origin and we conclude that this is an active source zone of seismicity. The last event, to date, occurred in June 2015. It is important to note that this source zone is several kilometers to the southwest of the Utah FORGE site.

Clustering

Detailed analysis of the seismicity has been focused on the events occurring east of the Utah FORGE site, outlined in red in Figure 1. Most seismicity occurs near the Opal Mound Fault. This region includes part of the Zandt swarm recorded during 1981 (Zandt et al. 1982) (Figure 1). Spatially there is some grouping of events around the Opal Mound Fault and grouping on the eastern edge of the 1981 Zandt swarm, with a third cluster further to the south (Figure 1).

To better understand the events within the area, the Detex program (Chambers et al. 2015) suite was used to analyze and cluster the waveforms based on waveform similarity. Each individual cluster indicates a similarity in source mechanism and location of the events. Clustering results (correlation coefficient 0.76), for events in the Mineral Mountains (outlined in red, Figure 1) are shown in Figure 2.

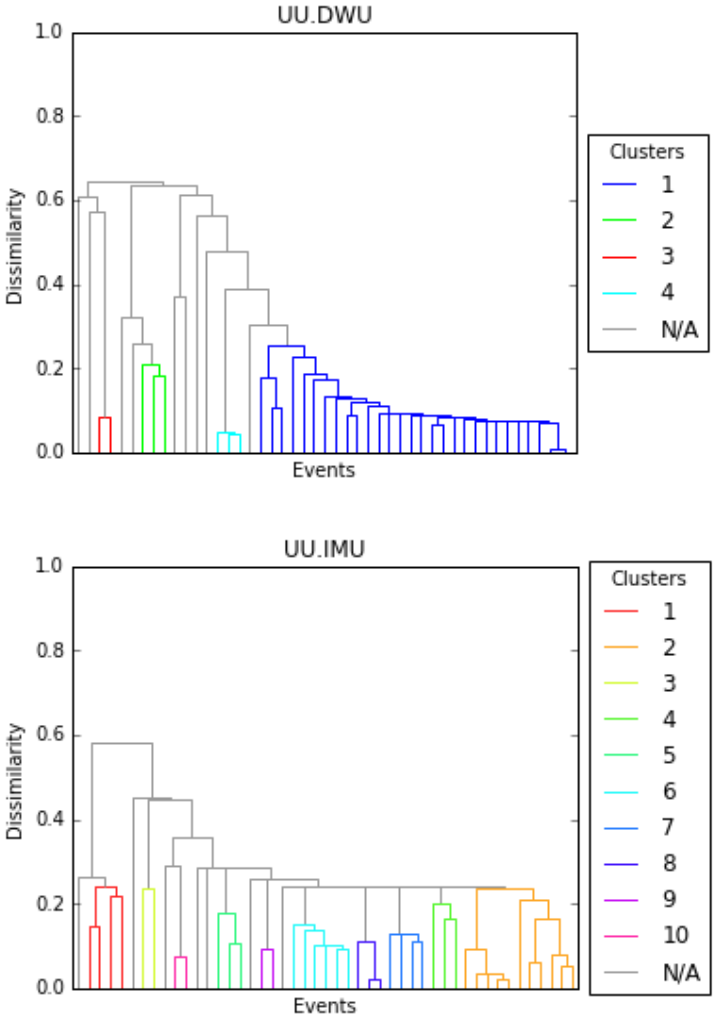

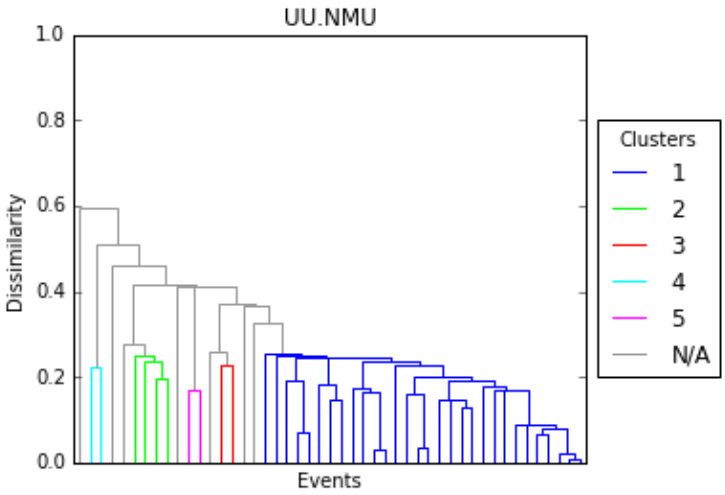

Figure 2. *Dendrograms based on waveform similarity from three separate seismic stations for events located within the red outline on Figure 1. Each event plots along the X-axis and the dissimilarity (inverse correlation) between events is on the Y-axis. Each color within the dendrogram relates to an individual cluster. The gray lines indicate that there the dissimilarity is greater than 0.24 (the input value). The location of NMU is shown on Figure 1; IMU is about 30 km northwest of Milford, and DWU is about 30 km south of Milford.*

Many different clusters, denoted by color, are apparent in this region. Most of the clusters locate on the north side of the Mineral Mountains study area, near the Blundell geothermal power plant. There are also clusters further to the east and south (Figure 3). Because of the different distances to the three stations used and different paths, the clustering at all three stations in not identical, but overall provide a similar result.

Based on the different clusters and the proximity to the Blundell Power Plant, we investigated possible correlations with pumping history and found that there is no observable connection to the events cataloged in the area to the injection/withdrawal history of the power plant (Figure 4). The plant was commissioned in 1984 and ramped up to full production and injection levels by 1986. Since then, the plant typically produces about 20 billion pounds of hot water at 250°C per year (9 million metric tons, or about 7500 acre-feet at 100°C), and it injects about 17 billion tons (7.7 million metric tons, or about 6500 acre-feet). The difference is mostly the mass of water evaporated in forced-draft cooling towers (Allis and Larsen, 2012). This deficit caused a pressure decline in the reservoir of about 4 MPa (about 600 psi) mostly in the first few years of operation.

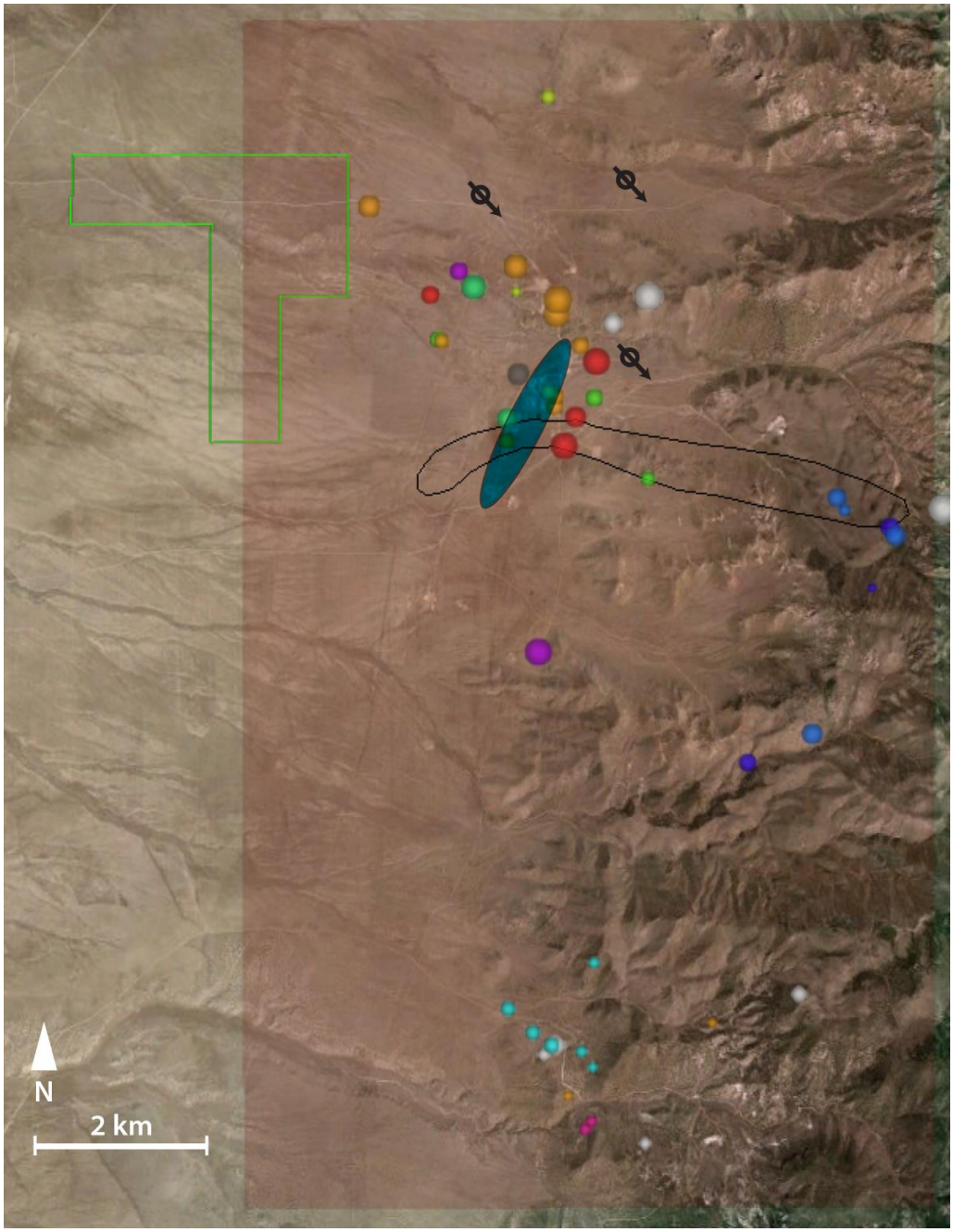

Figure 3. *Screenshot of Google Earth Pro with colors representing clustered waveforms, from original catalog data, based off of similarity from the Detex program suite. There are many various clusters of similar waveform, as seen by the different colors. The Utah FORGE deep drill site is outlined in green. The black circles with an arrow through them, east of the FORGE drilling site, represent injection wells for the Blundell geothermal plant at the Roosevelt Hot Springs geothermal system. The blue ellipse represents the production well area for the Blundell geothermal plant. The injection and production well symbols are not a part of the KML product and were added to the figure for clarity.*

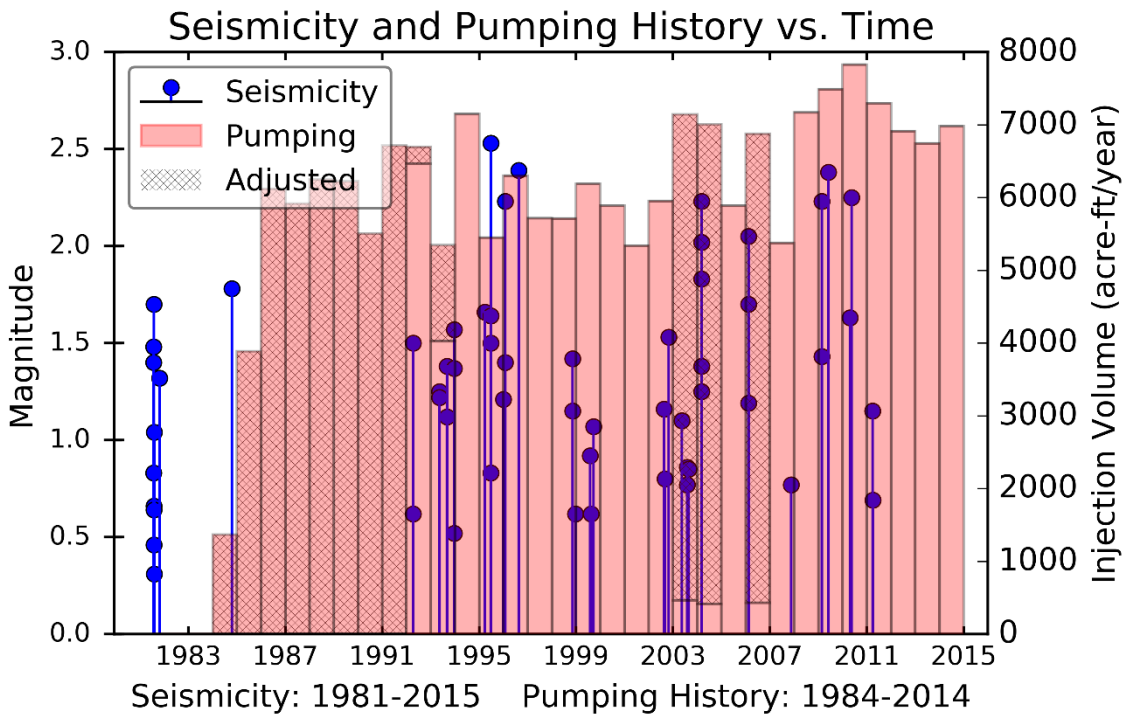

Figure 4. *Magnitude vs. time plot of events in the red outline in Figure 1, with Blundell power plant injection history compiled from Utah Division of Water Rights website. The injection data was incomplete and in places incorrect, so a correction has been applied based on the gross MW-hours produced each year and an assumption of constant production enthalpy ("adjusted" numbers). Note the seismically quiet time periods from October 1984 through April 1992 and April 2011 through 2015. The seismicity occurring in 1981 is part of the swarm described by Zandt et al. (1982). See text for volume conversions. For simplicity, 6500 acre-ft is 2.1 million gallons.*

The seismicity shows only one event cataloged from completion of the plant to 1992. The plant opened a binary power plant in 2007 (allowing more heat to be pulled from the recovered fluids) and no change is visible in the seismic activity. No events were located from April 2011 through January 2016 in the Mineral Mountains study area.

Google Earth KML Product

To better understand the spatial and temporal variations of the events with respect to the geology and geography of the area, a product was created for the Utah FORGE project that allows a visual summary of the analysis. While the dendrograms were useful in understanding the waveform similarities, the best tool for this was determined to be Google Earth for creating a visual summary of the investigation. Not only does this allow easy viewing of the dataset, it allows anyone with access to Google Earth easy access. The KML, available at http://www.forgeutah.com/site/, can be downloaded and opened in Google Earth. Snapshots are shown in figures 3 and 5.

The analysis of the clustering was used as the base of the product. We wrote a program that takes the waveform analysis from Detex and creates a KML. This was accomplished in the Python scripting language and takes all available information of the clusters and events. The waveform date, time, location, depth, magnitude and which cluster the event belongs to in the analysis is placed into a pop-up balloon that can be accessed by clicking on an event in the KML file (Figure 5). This pop-up also allows the user to view the waveform for each event directly in Google Earth by calling the information from the seismicity repository Incorporated Research Institutions for Seismology (IRIS) (Figure 5). The waveform visible in the pop-up has the same filters as applied in Detex. This allows fast and accurate viewing of all the available waveforms in their spatial and geographical context.

By using Google Earth, it is possible to also quickly look through events temporally. Google Earth has a time slider that allows the user to easily scrub through the events and visually see when each event occurs. This provides a way to straightforwardly view the events to see if there is a possible temporal pattern to the events. Each event is also colored based on the cluster (or no cluster) from the waveform analysis completed by Detex. By viewing the events in the KML, it is simple to observe the temporal and spatial relationship of various events within a cluster.

Maximum Magnitude Earthquake

To put an upper bound on the maximum induced earthquake, we use the relation developed by McGarr (2014). This relation limits the maximum seismic moment to the product of the injected volume and the modulus of rigidity. In the stimulation phase for the Utah FORGE site, we anticipate a fluid injection volume of 3500 to 20,000 m^3. The modulus of rigidity has been determined to be 2.85×10^{10} Pa based on triaxial testing of core from 52-21(see Section 1.1). Using these values and the McGarr relation, we get a maximum moment of 5.7×10^{14} N m. This is equivalent to an M_W 3.8 earthquake. This magnitude is similar to the other EGS sites analyzed in the McGarr study.

ShakeMap

Deterministic scenarios have been generated using ShakeMap (Wald et al. 1999; Worden and Wald 2016) for four possible seismic events: (1) a repeat of the 1908 M 4.08 Milford earthquake; maximum magnitude earthquakes based on fault length (Wells and Coppersmith, 1994) for (2) an M 5.4 Opal Mound fault and (3) an M 5.9 Negro Mag earthquake; and (4) an M 4 induced earthquake (conservative estimate based on the maximum magnitude calculation) located at the

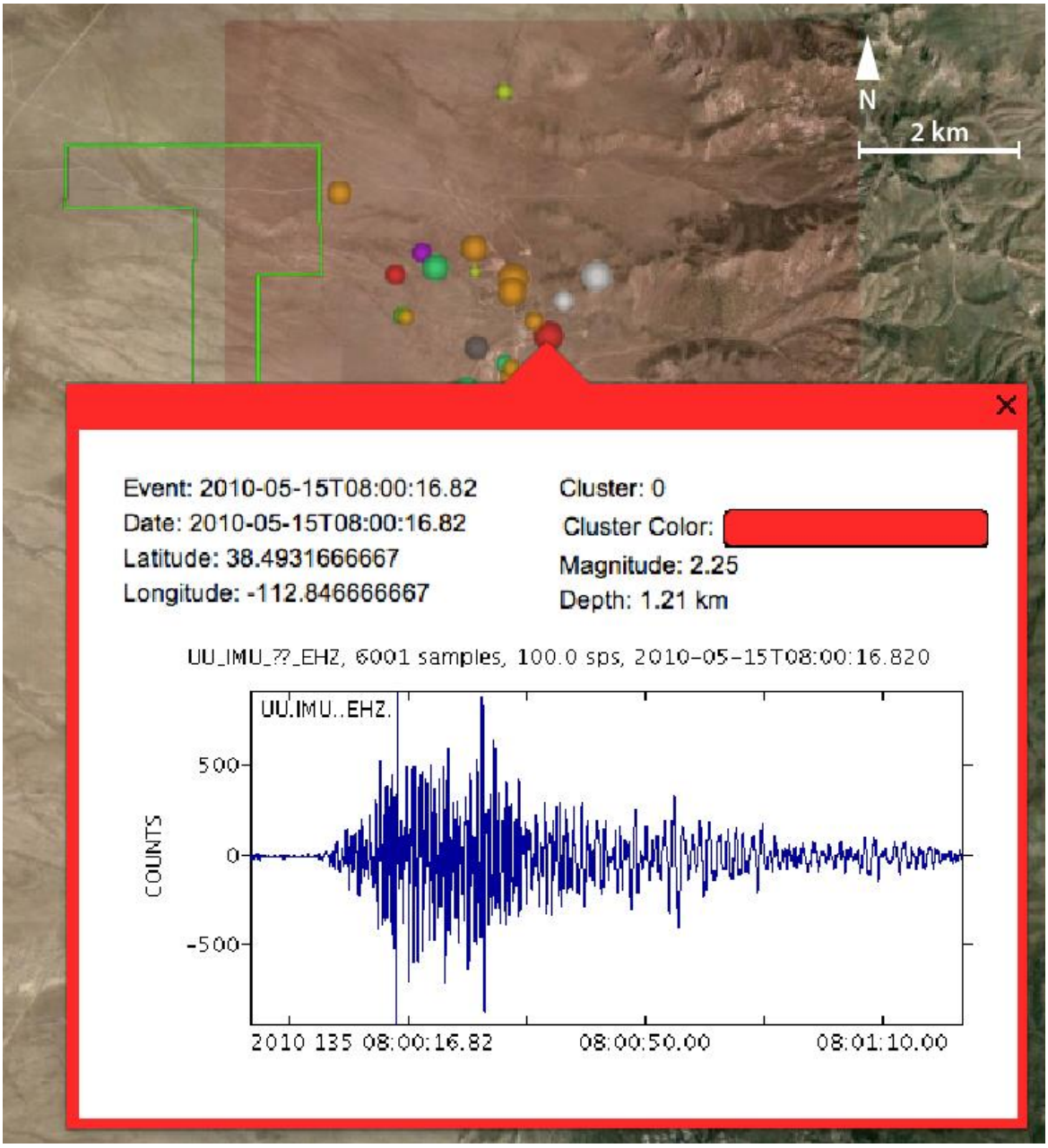

Figure 5. *Screenshot from Google Earth Pro with pop-up of available data for a single event. From relocated catalog data, based off of similarity from the Detex program suite. The outline color of the pop-up indicates which cluster the event has been associated. The waveform visible is pulled directly from IRIS. The "precise" latitude and longitude are due to a bug within the python scripting language. The actual precision is no greater than 4 decimal places.*

Utah FORGE site (Table 1 and Figure 6). Scenarios for the M > 5.0 events were generated using Chiou and Youngs (2008) ground motion prediction equation (GMPE); for the M 4.0 induced events, the Chiou et al. (2010) Southern California GMPE was used. Site amplification factors based on a statewide Vs30 (average shear velocity in the upper 30 m) database (McDonald and Ashland, 2008) were used for all scenarios. The Vs30 clearly dominates the pattern of ground

motions, as seen by the significantly larger amplitudes in the basin. The default Vs30 values used in this analysis are based on Vs30 measurements from northern Utah, which is dominated by lake sediment.

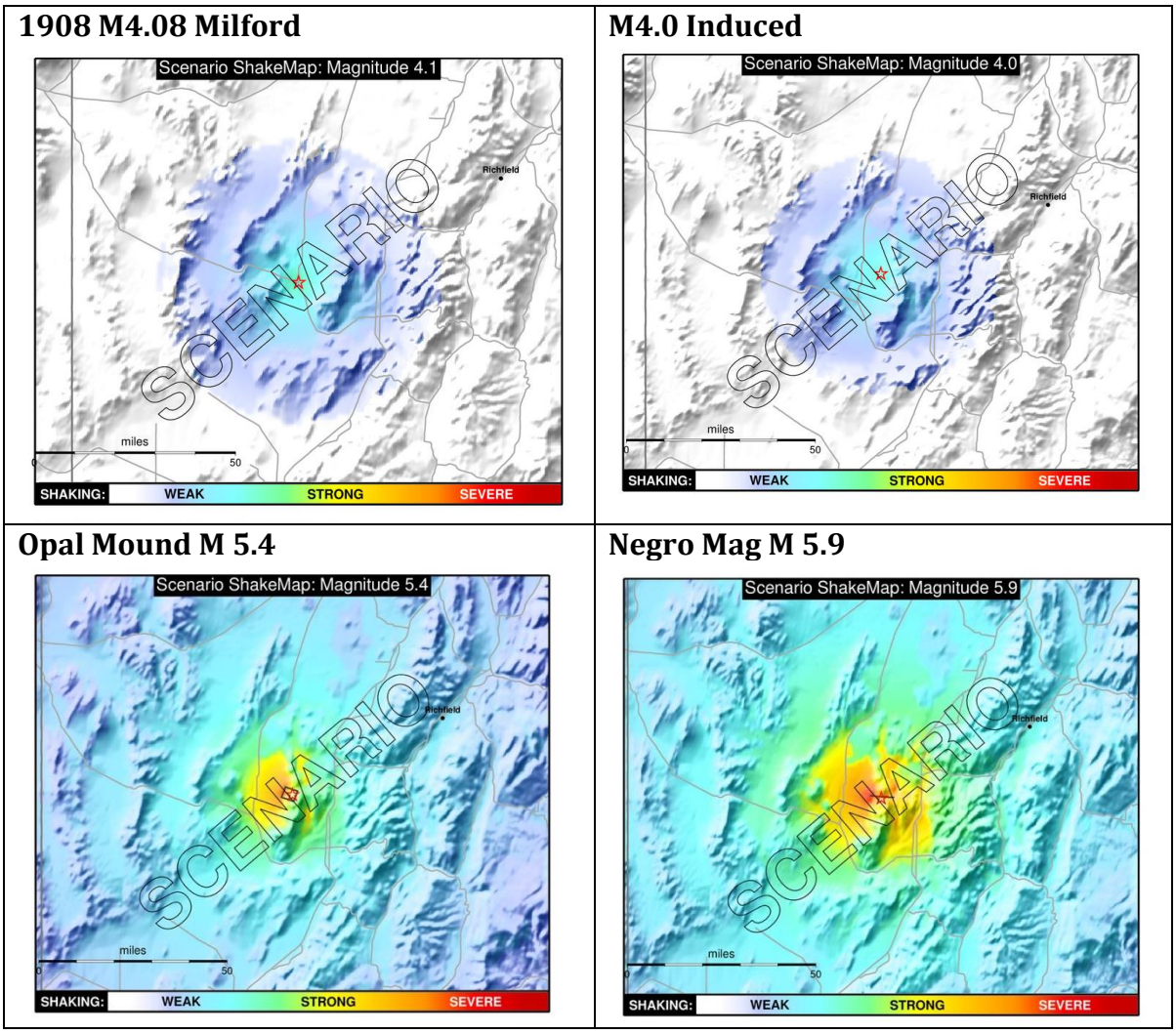

Figure 6. *Deterministic intensity maps for four potential scenario earthquakes near the Utah FORGE site. Maps were generated using ShakeMap (Wald et al., 1999; Worden and Wald, 2016). Maximum magnitude (ground motions) based on fault dimension (Table 1) for Opal Mound and Negro Mag scenarios (gray box surface projection of fault trace). Point sources assumed for Milford and potential induced earthquake.*

For the two M 4 earthquakes, Induced and Milford, the maximum PGA is ~3%g at the epicenter, which based on ShakeMap relates to light perceived shaking and no potential for structural damage. The maximum PGA for the Opal Mound earthquake scenario is ~28%g over the rupture area (close to the Utah FORGE site) and falls off to ~10%g in Milford. Again, based on ShakeMap relations, this translates to the potential for moderate damage at the epicenter, but light potential for damage in Milford. For the Negro Mag scenario PGA near the Utah FORGE site is ~35%g and for Milford and Beaver PGA is <10%g. For the area near the Utah FORGE

site, potential damage could be moderate to moderate-heavy. Based on these scenarios, potential damage to the nearby, populated centers is predicted to be light. The larger potential ground motions are located near the Utah FORGE site. Structures in the affected area include the well-site, wind mills related to the wind farm, and the Blundell Power Plant.

Table 1: ShakeMap Scenarios

Mag	Scenario	Fault Type	Rupture Length
4.08	Historic Milford	Unknown	point
4.00	Induced	Unknown	point
5.40	Opal Mound Fault	Normal	4.72 km
5.90	Negro Mag Fault	Normal	10.6 km

Hazus

We have generated a HAZUS run based on the Opal Mound deterministic scenario (Figure 6). Based on fault proximity to the proposed Utah FORGE site, we assume that this might represent the maximum earthquake for the area. Based on this initial HAZUS run, where we used the default HAZUS database, slight damage is predicted for < 5 residential structures and no damage predicted for other building types including schools and industry. There is no predicted damage to essential facilities and hospitals, schools, police and fire stations are expected to have > 50% functionality on day 1. Overall HAZUS (with the default database) shows that the damage and loss from this earthquake is predicted to be minimal. Note that the default database does not include the wind farm or power plant.

REFERENCES

Arabasz, W. J., Pechmann, J. C., and Burlacu, R., 2015. A uniform moment magnitude earthquake catalog for the Utah Region (1850–2012) and estimation of unbiased recurrence parameters for background seismicity [poster]: Proceedings Volume, Basin and Range Province Seismic Hazards Summit III, Utah Geological Survey Miscellaneous Publication 15-5 (CDROM).

Chambers, D., K. D. Koper, K.L. Pankow, and M. K. McCarter (2015). Detecting and characterizing coal mine related seismicity in the Western U.S. using subspace methods, Geophys. J. Intl., 203, 1388-1399.

Chiou, B. and Youngs, R., 2008, An NGA model for the average horizontal component of peak ground motion and response spectra: Earthquake Spectra, v. 24, p. 173–216.

Chiou, B., Youngs, R., Abrahamson, N., and Addo, K., 2010, Ground-motion attenuation model for small-to-moderate shallow crustal earthquakes in California and its implications for regionalization of ground-motion prediction models: Earthquake Spectra, v. 26, p. 907–926.

McDonald, G.N., and Ashland, F.X., 2008, Earthquake site conditions in the Wasatch Front urban corridor, Utah: Utah Geological Special Study 125, 41 p., 1 plate, scale 1:150,000, compact disk.

McGarr, A. (2014), Maximum magnitude earthquakes induced by fluid injection, J. Geophys. Res. Solid Earth, 119, 1008–1019, doi: 10.1002/ 2013JB010597.

Pankow, K. L., W. J. Arabasz , S. J. Nava, and J. C. Pechmann (2004). Triggered seismicity in Utah from the 3 November 2002 Denali fault earthquake, Bull. Seism. Soc. Am. 94, S332-S347.

Wald, David J., Vincent. Quitoriano, Tom. H. Heaton, Hiroo. Kanamori, Craig. W. Scrivner, and C. Bruce Worden, (1999). TriNet ``ShakeMaps": Rapid Generation of Instrumental Ground Motion and Intensity Maps for Earthquakes in Southern California Earthquake Spectra, 15, 537-556

Wells, D. L. and K. J. Coppersmith (1994). New empirical relationships among magnitude, rupture length, rupture width, rupture area, and surface displacement, Bull. Seism. Soc. Am. 84, 974, 1002.

Worden, C. B., and D. J. Wald (2016). ShakeMap Manual, February 01, 2016. http://dx.doi.org/10.5066/F7D21VPQ

Zandt, G., L. McPherson, S. Schaff and S. Olsen, Seismic baseline and induction studies: Roosevelt Hot Springs, Utah, and Raft River, Idaho, U.S. Dept of Energy rept. DOE/ID/01821-T1, 58 pp., 1982.

Upload Characterization Data
to the Geothermal Data Repository (GDR)
TASK 1.1.4

Task 1.1.4. Upload Characterization Data to the Geothermal Data Repository (GDR)

DOE Project Manager: Lauren Boyd
DOE Contract Number: DE-EE0007080

1. Great Basin Groundwater Geochemical Database, Nevada Bureau of Mines and Geology:

http://www.nbmg.unr.edu/Geothermal/GeochemDatabase.html

2. Utah Well and Spring Database (includes water chemistry), Utah Geological Survey:

http://geology.utah.gov/resources/energy/geothermal/geothermal-resources-in-utah/utah-well-and-spring-database/

3. Utah Temperature Gradient Database, Utah Geological Survey:

http://geology.utah.gov/resources/energy/geothermal/geothermal-resources-in-utah/#tab-id-3

4. Utah Seismograph Stations, University of Utah:

http://www.seis.utah.edu/

5. Utah earthquake information and data, USGS:

http://earthquake.usgs.gov/earthquakes/states/?region=Utah

6. Geologic maps, Utah Geological Survey

http://geology.utah.gov/map-pub/maps/geologic-maps/

7. USGS portal to aerial photography and satellite imagery.

http://glovis.usgs.gov/

8. Utah Automatic Geographic Reference Center (AGRC). Geoscience, cadastre, elevation and terrain, digital aerial photography, roads, and aquifer data.

http://gis.utah.gov/data/

9. Gravity and magnetic data – Pan American Center for Earth and Environmental Studies (PACES).

http://irpsrvgis08.utep.edu/viewers/Flex/GravityMagnetic/GravityMagnetic_CyberShare/

10. Well Acord 1-26 Logs and Data (dataset)
11. Well 82-33 Logs and Data (dataset)
12. Well 52-21 Logs and Data (dataset)
13. Well 14-2 Logs and Data (dataset)

14. Well 9-1 Logs and Data (dataset)
15. Utah FORGE Gravity Data shapefile
16. 1km_T_Contours temperature (shapefile)
17. 2km_Contours temperature (shapefile)
18. 3km_T_Contours temperature (shapefile)
19. 4km_T_Contours temperature (shapefile)
20. 200m_T_Contours temperature (shapefile)
21. Basin_Depth_Contours (shapefile)
22. MIlford_FORGE_Extent (shapefile
23. Milford_Seismometers (shapefile)
24. Milford_wells (shapefile)
25. Mineral_mtns_lineaments (shapefile)
26. MT_roosevelt (shapefile)
27. Opal_Mound_fault (shapefile)
28. Potentiometric_Contours (shapefile)
29. New_Supply_Wells (water supply wells shapefile)
30. FORGE_TDSgrid (TDS raster contour image)
31. ModelAdrwdn (ground water shapefile)
32. ModelBdrwdn (ground water shapefile)
33. FORGE_groundwater_tables
34. Great Basin 2nd invariant of strain, Nevada Bureau of Mines and Geology (raster image)

http://www.nbmg.unr.edu/Geothermal/Data.html

35. UUSS-FORGE-Seismic_Cluster-Analysis.kml (seismic activity animation)

TASK 1.2

Develop a 3D Conceptual Geologic Model

Task 1.2: Development of a 3-D Model of the FORGE Deep Well Site, Milford, Utah

Introduction

The FORGE project goal is to develop a field site where an EGS reservoir in crystalline rock can be created, which is suitable for stimulation experiments and technology development. The reservoir is required to have temperatures between 175 and 225°C at 1.5 to 4 km depth. The diverse geoscientific datasets collected over 40 years of exploration and development of the Roosevelt Hot Springs hydrothermal system are described in detail in Task 1.1, and they demonstrate that the proposed Milford site satisfies the thermal requirements (for example: temperature-depth graph in Task 1.1, Figure D.3). Three unproductive deep wells drilled west of the Opal Mound fault during the early exploration years show that the granite at depth has a conductive thermal gradient, and that there is widespread poor permeability. The proposed site lies centrally between these three wells.

The Statement of Project Objectives for Task 1.2 requires demonstration of integration of critical data with a 3-D visualization model, as well as a discussion of uncertainties, and graphical representations of geoscientific parameters for the site. In Task 1.1 and its sub-tasks there are numerous figures with graphs, maps, and tables of geoscientific data. That Task covers, temperatures, rock types and geological setting, structure, hydrothermal alteration, fluid chemistry, permeability and porosity, stress regime, seismic activity, and groundwater. The details of these parameters will therefore not be repeated in this Task, but this Task will review interactive web applications that allow the viewing of some of this data (see 2-D Interactive Imagery below). The 3-D visualization model is presented in Development of a 3-D Visualization Model and then uncertainties in critical parameters are discussed in Uncertainties in Quantifying Key Reservoir Parameters below.

1.2.1 2-D Interactive Imagery

Before discussing the 3-D model, there are several websites where natural resource information around proposed FORGE site can be interactively viewed (in 2-D formats – mainly maps and graphs), in addition to the Google Earth imagery most people are familiar with. Individual thermal and groundwater well data can be viewed interactively on the Milford FORGE website (www.forgeutah.com/site), with this data also having been deposited into the national geothermal database. The geology of the region at several scales can be viewed interactively on the UGS website (http://geology.utah.gov/apps/intgeomap/) by zooming into Milford using the "search" tab. Unfortunately there is a map join very close to the proposed FORGE deep well site, with differing unit symbolism in the two maps. A seamless geologic map is shown in Task 1.1, Figure C.2., and it is intended that the differing symbolism in those two 30 x 60 maps will be fixed within a year. One useful feature on the interactive geology site is the transparency slider on the lower left, which enables the geology to fade out so the base map shows through. If the basemap is a high resolution airphoto (the default), this allows checking of where geologists have mapped faults, and the presence or absence of cultural features. Another useful option is the tab in the upper right labelled "switch basemap". This allows the basemap to switch between, for example, imagery and topography.

Another useful site is the interactive quaternary fault and fold map for Utah (http://geology.utah.gov/resources/data-databases/qfaults/). Zooming into the Milford area shows a "poorly understood zone of middle to latest Quaternary faults on the western side of the Mineral Mountains" (quote from the metadata). The northernmost extent of this zone is the Opal Mound fault (not labeled on this website) which is the west side of the Roosevelt Hot Springs hydrothermal system. No faults are shown at the proposed Forge deep well site. Finally, on the UGS website there is also relatively high resolution (800 dpi scan) air photography from 1955 over the FORGE site at the following address: https://geodata.geology.utah.gov/imagery/ . This imagery predates all the geothermal exploration, and clearly shows the bath-house structures at the original hot spring area. It also shows the proposed FORGE site to be covered in grass with a few two-track roads, very similar to its appearance in recent imagery.

As mentioned in Task 1.1, recent earthquake activity in Utah, or more specifically near Milford, can be viewed with the interactive map at website of the University of Utah Seismic Stations (http://quake.utah.edu/earthquake-center/quake-map). The seismogram for the new broadband station of FORU (located near the southern end of the Opal Mound fault) can be viewed under the "live seismogram" tab of the "EQ Center" menu bar. The link to the interactive map of live seismograms is http://quake.utah.edu/earthquake-center/heli-map , with FORU being the yellow triangle northeast of Milford. The past 24 hours of the record for that station is displayed. As the FORGE project moves into subsequent phases additional stream feeds from seismometers around the site will be web-accessible.

1.2.2 Development of a 3-D Visualization Model

The process of deriving a 3-D thermal model which also shows the simplified geology of the site started with reviewing all the well data for quality and consistency, establishing geotherms based on temperature gradient and heat flow, deriving isotherms maps at five levels between 200 m and 4 km depth using kriging, and then fitting a 3-D isotherm surface to chosen isotherm values at each depth, in this case to 175°C, the low-temperature limit for a potential reservoir. The 3-D surface was generated using "topo-to-raster" applications in ESRI's ArcMap software.

The surface of the crystalline basement rock is also important for evaluating the site. This was derived from the gravity anomaly using a density contrast from the Acord-1 well, and four transects across the north Milford valley interpreted using a 2-dimensional, Semi-Automated Marquardt Inversion code (SAKI) (Webring, 1985; refer to Task 1.1 section E). The location of the zero-depth to bedrock around the outside of the basin, and the depth to resistive bedrock from the interpretation of magnetotelluric stations in the north, assisted with the contouring of the bedrock/granite surface. A 3-D surface to the top of basement was fitted to the contours using topo-to-raster tool in ArcMap.

Visualizing two intersecting surfaces (basement surface and 175°C surface) can be challenging. A version of the 3-D visualization model is accessible on the www.FORGEUtah.com website. This allows the viewer to move around, through, and under the two surfaces. The surfaces and other features can be turned on and off with the tabs on the right of the screen. The mode of moving around the model is controlled by the symbols on the lower left, or by the cursor using the roller and the left and right controls. Several snapshots are shown in Figures 1 – 3. Figure 1 shows two views of the crystalline basement surface emphasizing the elongate basin in the west

extending to 3 km depth, as well as the Acord-1 drilled to almost 4 km depth. There is no vertical exaggeration. The basement surface is semi-transparent so that is possible to see the proposed pair of FORGE wells with horizontal lateral extending 1 km horizontally into the basement.

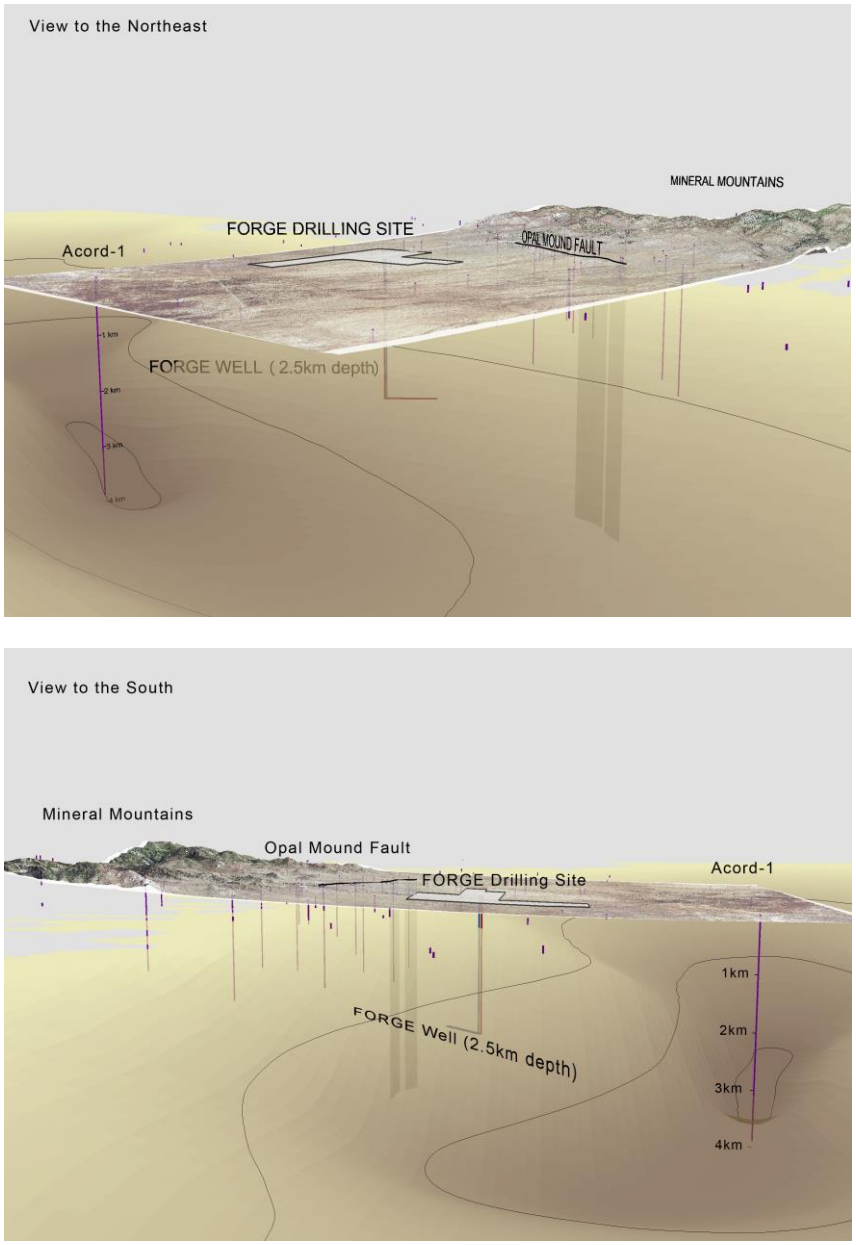

Figure 1. *Two snapshots from the 3-D visualization model showing the basement surface forming a north-south basin extending to 3 km depth beneath the Acord-1 well site. The pair of FORGE wells with horizontal laterals intersect the crystalline rock at 500 m depth, and are visible within the basement because the surface is semi-transparent. There is no vertical exaggeration. Short, vertical blue lines are thermal gradient and deep wells.*

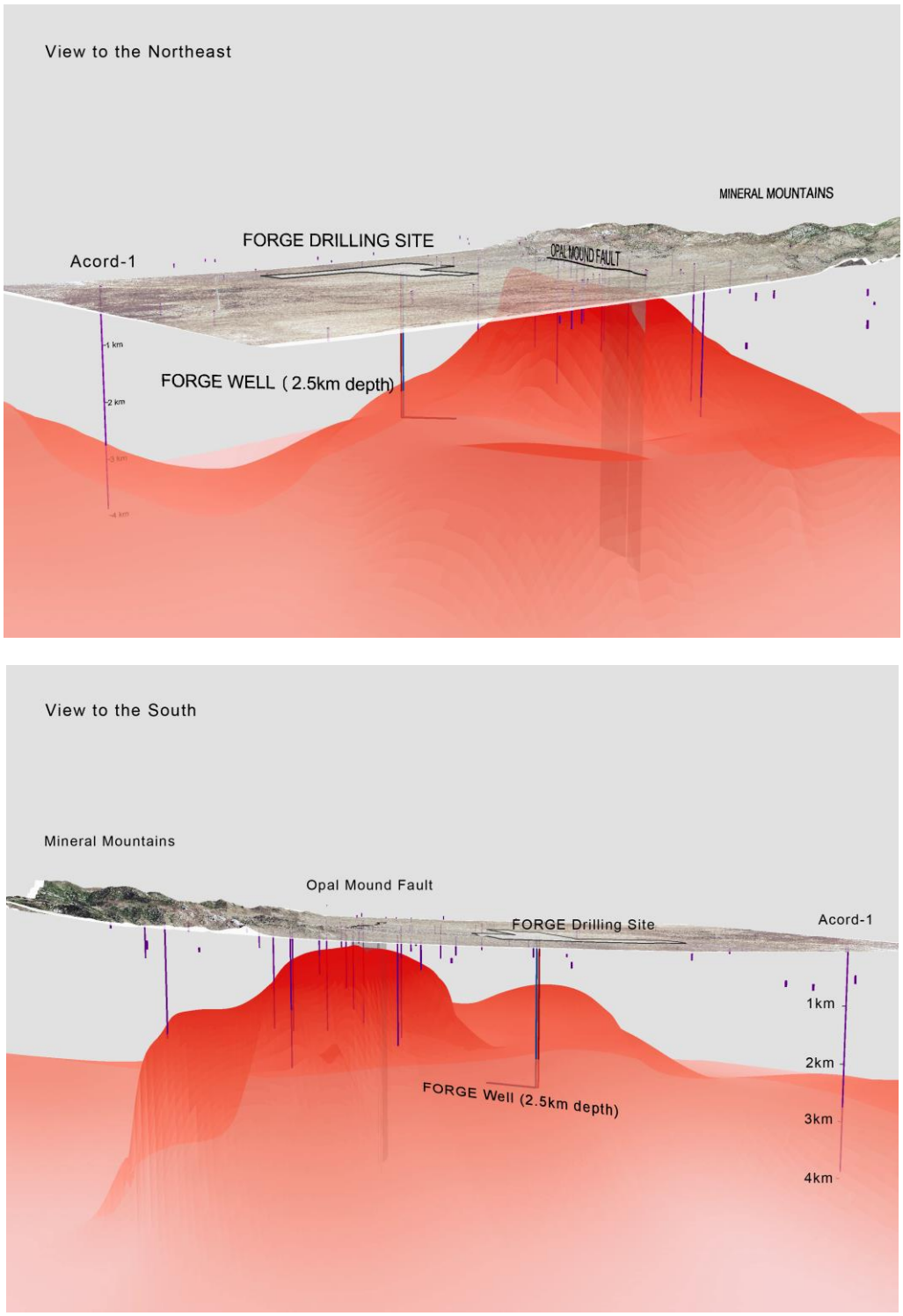

Figure 2. *Two snapshots of the 175°C isotherm surface showing the proposed pair of FORGE wells intersecting this surface at 2 km depth, and the Acord-1 well intersecting it at 2.5 km depth. The isotherm surface is semi-transparent so the full extent of the wells can be seen at greater depth.*

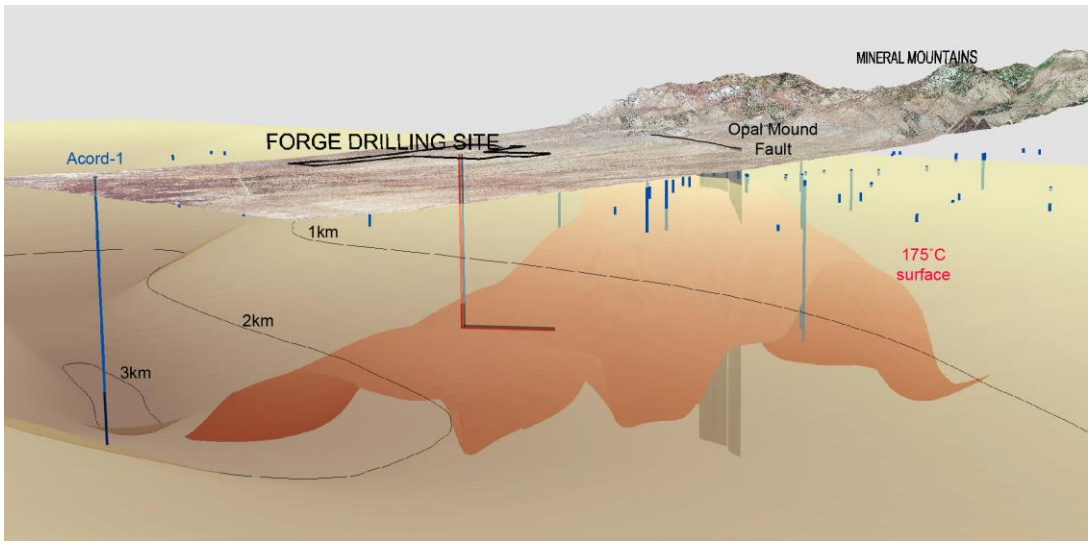

Figure 3. *Snapshot from the 3-D model showing both the basement surface and the 175°C surfaces. No vertical exaggeration.*

During Phase 2 it is hoped to extend general access to the GIS ArcMap model for the site. At the moment, access is restricted to project participants, with the model having over 20 different layers able to be switched on or off. These include the various isotherm contours at different depths, seismicity, geophysical anomalies, groundwater parameters (potentiometric head, chemistry), the geology, faults, etc., as well as a variety of base maps.

1.2.3 Uncertainties in Quantifying Key Reservoir Parameters

Before discussing the uncertainties inherent in this model, we want to emphasize that the Milford site has a very large amount of data available from the exploration activity during the late 1970s and early 1980s, with at least five companies drilling wells. At the same time, supporting research by the University of Utah, funded during the early years of the Department of Energy Geothermal Program, produced over 20 Masters and Ph.D. theses and many more publications and reports on the Roosevelt hydrothermal system, ensuring preservation of a large amount of information. With over 80 thermal gradient wells covering a broad area, and over 20 deep wells drilled before the production zone was identified on the east side of the Opal Mound Fault, this FORGE site has inherited a rich dataset of thermal and related geoscientific information. This reduces the uncertainties in the reservoir characteristics based on the Phase 1, desk-top compilation.

Thermal regime

Uncertainties associated with the geotherms depend on the degree of extrapolation, and factors unique to each well (e.g. how soon after drilling was the temperature measured; what is the appropriate thermal conductivity trend with depth). The uncertainties in heat flow measurements have been estimated at about ± 30% for most data points; however in Acord-1, the high quality of the data and the great depth of the well mean the uncertainty is at most about ± 20% (heat flow of 120 ± 20 mW/m^2; main source of uncertainty is the trend of thermal conductivity with depth). The uncertainty in deep temperature in the section at the bottom of Acord-1 containing

crystalline rock made of gneiss and granite is less than ± 10°C because of the numerous temperatures logs in that well as it came to thermal equilibrium. A similar uncertainty applies to the most of the deep exploration wells with multiple temperature logs.

The challenge has been to merge the geotherm temperature data (extrapolated based on thermal gradient well data) with observed temperature profiles in deep exploration wells, and to create both isotherm maps and then 3-D isotherm surfaces. The heat flow at the FORGE deep well site is estimated to be 180 ± 40 mW/m^2. Isotherm maps at five depths have been contoured using ESRI's ArcMap geostatistical kriging application. For each map the mean error (statistical) in the contouring is between 12 and 14°C. To then create a 3-D surface of the lower temperature limit for the FORGE reservoir (175°C), the topo-to-raster tool in ArcMap was applied. This tool used the 175°C isotherm contours on each map (that is, at each depth) to fit a 3-D surface (Figure 2). The 3-D surface has the 175°C interface at 2000 m beneath the center of the deep well FORGE site. This is in the middle of the thermal uncertainty zone identified in Figure D.3, Task 1.1, which shows the 175°C temperature at 2000 ± 200 m.

The most convincing evidence supporting the required temperatures beneath the FORGE deep well site is that this site is located centrally between deep wells 9-1 and 82-33 to the east, and Acord-1 to the west. In 9-1 and 82-33, a temperature of 175°C occurs at 1100 m and 1700 m depth respectively. In Acord-1, a temperature of 175°C occurs at 2500 m depth.

Four thermal gradient wells to 300 m depth are recommended for Phase 2B within the 5 km^2 (2 square miles) FORGE deep well area to investigate whether there is a gradient in the thermal regime across the site, and to assist in the final choice of the deep well location. With the shallow thermal outflow from the Roosevelt hydrothermal system affecting temperatures to the north of the proposed deep well site, and well 9-1 to the southeast of the site having higher temperatures at potential reservoir depths compared to 82-33, it is prudent to verify the heat flow pattern across the deep well site prior to deeper drilling in Phase 2C. These thermal gradient wells will also provide information on the groundwater level and water quality at the site.

Depth to Granitic Rock

The gravity interpretation of depth to granitic bedrock beneath the FORGE site is greatly assisted by knowing that near the center of the basin beneath north Milford Valley, the granitic surface is at 3.1 km depth in Acord-1. The gravity gradient between Mineral Mountains and Acord-1 was fitted by removing a regional gradient (attributed to lower crust gravity low in the transition zone to the Colorado Plateau farther east), and using a linear, decreasing density contrast with increasing depth based on the geophysical logs in Acord-1. This same density contrast gradient was assumed to exist across the basin, although it was recognized that the low-density lake sediments near surface around Acord-1 may not be representative of the alluvium/fan deposits adjacent to the Mineral Mountains. At the margins of the basin against the Mineral Mountains, there is no basin fill, and at most wells in the Roosevelt hydrothermal system, including injection well 82-33 the depth is typically between 100 and 200 m. However, no thermal gradient wells in the valley penetrate granite and gneiss, so the gravity modeling had no control points between 82-33 and Acord-1. At the time of the gravity modeling during Phase 1, there was information from one intermediate depth well (GPC-15, about 2 km south of Geothermal Plant Road and 4 km from the proposed FORGE site; see Figure D.1 in Task 1.1), which did not intersect the

granite at a total depth of 582 m. The model predicted the basement surface beneath GPC-15 at about 700 m depth, and across the FORGE deep well site the predicted depth ranges from 1 km depth on the west side, 500 m near the center and 300 m on the east side. Uncertainties are estimated at ± 200 m (Figure E.6, Task 1.1).

After the gravity modeling was complete, the project acquired some additional data on "Observation Holes" from old box files of exploration data held by PacifiCorp Energy at Blundell. Eight holes were drilled to between 500 and 700 m depth by Phillips during the late 1970s to better understand the groundwater regime and the shallow stratigraphy. Two of the holes were on the fan deposits west of the Opal Mound Fault zone, and intersected granite, providing new control points for interpreting the gravity. OH-1, located 1 km northeast of GPC-15, intersected the granite at 595 m depth, suggesting the modeled depth from gravity at GPC-15 is reasonable (that is, 700 m). OH-4 is located 500 m east of the east boundary of the FORGE deep drill site area, and encountered granite at 473 m depth. Based on the gradient in the granite surface between well 82-33 (where granite is at 100 m depth) about 600 m farther east, and OH4, the granite surface at the east side of the FORGE deep well area could be at 500 – 600 m depth, rather than the 300 ± 200 m estimated from the gravity model. The reason for the underestimate is the assumed density contrast in the upper 500 m of alluvium here is too high. A lower density contrast, as implied by the density log in GPC-15, would explain this difference. A layer of cemented alluvium apparently exists west of the Opal Mound fault on top of the crystalline basement, so the gravity signal may largely be originating from the uncemented alluvium thickness. More refined gravity modeling planned for Phase 2B, supported by additional measurements and a reassessment of the density variations in the alluvial basin fill, should resolve these issues. The 3-D seismic reflection survey is also expected to provide a high-resolution image of the granite survey, complementing the gravity interpretation.

Characteristics of granitic rock

All deep exploration wells in North Milford Valley have encountered crystalline basement rock at depth. These granitic and gneissic rocks are also abundant in the adjacent Mineral Mountains. There is no doubt that the FORGE deep well site has crystalline rocks at relatively shallow depths (at greater than about 500 to 1200 m depth depending on location within the site area). However, as discussed in earlier sections, the intrusive and metamorphic rock relationships are complex, with nearby well 9-1 confirming a spectrum of Tertiary plutonic rock-types, including diorite, granodiorite, quartz monzonite, syenite, and granite, as well as Precambrian gneiss. The diversity of crystalline lithologies is a positive factor when considering the challenges of creating a fracture network with hydrofracturing techniques. The strength characteristics of these rocks on a 100 m to 1 km length scale are unlikely to be uniform. Phase 2B includes a program for collecting much more data on the compressive strengths of the various crystalline lithologies so that there is database to guide hydrofracture strategies once the deep wells are drilled.

Permeability

Probably the least well-determined parameter is the permeability beneath the proposed site. All three deep wells surrounding the site (82-33, 9-1, and Acord-1) were unproductive, and 82-33 was subsequently converted into an injector for the Blundell plant. Well 9-1 has been proposed as a candidate for EGS research in the past (East, 1981; Goff and Decker, 1983). The thermal

regime west of the Opal Mound Fault has a conductive thermal gradient, consistent with the lack of fluid production from any of the wells in this region. This suggests the rocks lack permeability and fracture connectivity that could support hydrothermal convection, which is in contrast to the wells east of the Opal Mound Fault where within the Roosevelt Hot Springs, the reservoir temperature gradient is near isothermal (250-270°C), reflecting strong upflow.

Although lack of well productivity and a conductive thermal regime imply low permeability, we do not know whether this means microdarcy (or less) "matrix" permeability everywhere, as measured in laboratory measurements in Phase 1, or whether on a 1 – 1000 m scale there are zones of microfracturing in the host rock. If such zones are present they may become targets for enhancing the permeability into a larger scale fracture network and reservoir creation in Phase 3. No surface geophysical techniques are going to provide quantitative insight on this issue. However, it is possible that the high resolution 3-D seismic reflection surveying across the deep well site proposed for Phase 2B may reveal subtle reflectors within the granite indicative of a fracture fabric. Definitive evidence of the natural permeability and the ability to fracture the granite rock will have to wait for the exploratory vertical well and hydrofracture tests proposed for Phase 2C. Before then, detailed geological mapping of joint and fracture arrays in the Mineral Mountains, which is planned for Phase 2B, will provide additional data.

Stress regime and Induced Seismicity

As discussed elsewhere in this report, several sources of stress data provide a consistent indicator of the stress direction. They are the borehole breakouts, focal mechanisms from seismicity, and the integrated geologic history of stress evident from the attitude of joints and dikes, from young normal fault scarps exposed in hydrothermal opal mounds associated with modern geothermal activity, and the elongate pattern of the hydrothermal system (i.e. high permeability). These constraints all indicate a consistent maximum horizontal compressive stress, SHmax, primarily directed N-S (170-180°) to NNE-SSW (035°). That is, the most likely direction of hydrofracturing assuming isotropic strength properties of the basement rock is N-S to NNE-SSW, and wells should be deviated at right angles to this direction (E-W, 080-090°; to ESE-WNW, 125°) to optimize the hydrofracturing. Confirmation of this stress regime will hopefully come from the vertical well testing proposed for Phase 2C.

The proposed FORGE site has a 30 year history of nearby seismic monitoring sensitive to events less than M 2. Based on this historical record, there has been only one $M > 4$ earthquake in the greater Milford, FORGE study area. This was the 1908 M 4.08 Milford earthquake located south of the town of Milford, Utah. Within ~50km of the proposed FORGE site there are other earthquakes $M < 4.9$, but there is only one earthquake $M \geq 4.9$, the 1901 M 6.6 Tushar Mountain earthquake (#2, Figure 1) located ~50 km to the east. Based on both the UUSS catalog and an early study by Zandt et al. (1982), the Milford, FORGE study area is characterized by small magnitude earthquakes and a low seismic rate. The 2008 U.S. Geological Survey National Seismic Hazard Maps (Peterson et al., 2008) shows the FORGE study area to be in a region of low to moderate seismic hazard. There is a 0.2 to 0.25 probability of an $M > 5$ earthquake within 50 km in the next 20 years, and there is a 10% probability that the peak ground acceleration (PGA) will exceed 10% g in the next 50 years.

In addition to the earthquake hazard, there are other known seismic sources in the area. There is a large quarry operation northwest of Milford producing seismic events similar in magnitude (M < 2) and ground motions to the majority of cataloged earthquakes. Additionally, there is the possibility of small ground motions associated with railway traffic through the town of Milford, and noise sources related to the railroad and air traffic. Based on: (1) the rural nature (low risk) of the proposed site, (2) that expected EGS seismicity will be smaller or equal in magnitude to the background tectonic hazard, and (3) the on-going nuisance ground motion and noise related to the quarry, railway, and airport, our preliminary analysis classifies the overall risk as very low (I) to low (II).

There has now been over 30 years of production of hot water and injection of cool water in deep wells tapping the geothermal reservoir at Roosevelt Hot Springs. The circulation rates for most of the time has been in the range 250 - 300 L/s (Allis and Larsen, 2012), with no obvious induced seismicity. At the FORGE deep well site we anticipate the fluid circulation experiments to be carried out at less than about one tenth this rate, so the induced seismicity risk should be minimal.

Groundwater Availability and Suitability

Adequate groundwater supplies are crucial to a successful FORGE site, so removing uncertainty in access to groundwater has been a high priority during Phase 1. Experience at the Raft River project demonstrates that thermal conditioning of hydraulic fractures with cool water after initial stimulation may be a crucial phase of fracture network and reservoir creation. This report contains a review of groundwater chemistry and potentiometric head variations around North Milford Valley. As mentioned above, new data from Observation Holes around the Roosevelt Hot Springs hydrothermal system became available late in Phase 1 and these data are not yet fully integrated into models for the groundwater regime or the basement surface model derived from gravity trends. The new data are consistent with the groundwater beneath the proposed site being at about 150 m depth and having a temperature of about 60°C. At the proposed project office site and groundwater extraction site adjacent to Antelope Point Road, the groundwater level is at 25 m depth and is at about 30°C. A 24-hour pump test of a groundwater supply well about 1 km west of our proposed groundwater supply wells demonstrates sustainable flows of 100 gpm and suitable chemistry (dilute geothermal water). Optimizing the size and screen design of the well is expected to yield flows significantly greater than this. The project already possesses water rights for access to 50 acre-feet per year (16 million gallons per year) of groundwater at this and other sites nearby. Smithfield is granting the project another 50 acre-feet per year of their irrigation water rights at no cost, and the rights to purchase an additional 150 acre-feet per year of water from them. Our project is also requesting a new water right to increase its water right to 300 acre-feet per year, including 50 acre-feet of consumptive use. The north Milford Valley is one of the few areas of Utah which is still open to water right applications for geothermal purposes. The 50 acre-feet of consumptive use allows evaporative cooling of the production water during long-term fluid circulation experiments, if required.

Although the average water consumption for hydrofracturing tight oil and gas wells is about 5 million gallons (Induced Seismicity Potential in Energy Technologies, National Academies Press, 2013), the major use of water for the project will be during the long-term flow tests. There will likely be make-up water needs, and it could be that cool groundwater is also used to

supplement cooling of the produced hot water prior to recirculation in the injection well. The anticipated 500 acre-feet per year of water available to the project (160 million gallons per year) will cover all options regarding long-term flow testing during Phase 3.

Hydrothermal Alteration

The nature and intensity of hydrothermal alteration in the reservoir is interpreted from four deep exploration wells that penetrate into basement crystalline rocks on the east and west sides of the FORGE deep well site. In all four wells, the nature of the hydrothermal alteration is similar and weak intensity, except locally in and around zones of cataclasis. There is no evidence that such zones might be related to strong variance in rock strength, porosity, permeability, and fluid composition inferred from other well measurements. More importantly, there is no evidence of modern or recent hydrothermal activity as temperature sensitive alteration minerals lack depth level-zonation, in contrast to the distribution of clay minerals seen in wells drilled beneath Roosevelt Hot Springs. Instead, the hydrothermal alteration that is observed in Acord-1 and 9-1 are likely to be products of earlier episodes of Tertiary magmatism that have nothing to do with the modern thermal regime. At this point, only a qualitative assessment of uncertainty is possible, as constrained by data from widely spaced wells.

Fluid Content (i.e. Fluid Composition).

The compositions of fluids in the FORGE study area are constrained by data from shallow groundwater wells across the deep well site and from production wells in the Roosevelt Hot Springs geothermal reservoir. Because the groundwater comes from an outflow zone sourced from Roosevelt Hot Springs mixed with regional northward-flowing groundwater in North Milford valley, the chemical compositions of the waters are similar. Additional information can be inferred from the character and intensity of hydrothermal alteration. The regional data are consistent, indicating that fluids will resemble those found in the Roosevelt Hot Springs system. The concentrations of total dissolved salts will be in the range of 1000-7000 mg/kg, predominantly made up of sodium and chloride, and the pH will be near neutral. Because there are no wells that penetrate to reservoir depths beneath the FORGE deep drill site, only a qualitative assessment of uncertainty is possible.

As with the uncertainties in permeability of the crystalline rock, the fluid content (i.e. porosity) will depend on the intensity of microfractures. At this stage there is no information on this, and reservoir models usually assume a few percent porosity in bedrock in such circumstances. This parameter will become known once the first (vertical) well is drilled into the granite in Phase 2C.

TASK 1.1

Appendices A and B

APPENDIX 1.1A

PROCEEDINGS, 41st Workshop on Geothermal Reservoir Engineering
Stanford University, Stanford, California, February 22-24, 2016
SGP-TR-209

The Geology, Geochemistry, and Geohydrology of the FORGE Deep Well Site, Milford, Utah

Stuart Simmons[1,2], Stefan Kirby[3], Clay Jones[1], Joe Moore[1], Rick Allis[3], Adam Brandt[1] and Greg Nash[1]

[1]EGI, University of Utah, 423 Wakara Way, Salt Lake City, UT 84108
[2]Department of Chemical Engineering, University of Utah, 50 S. Central Campus Dr., Salt Lake City, UT 84112
[3]Utah Geological Survey, PO Box 146100, Salt Lake City

ssimmons@egi.utah.edu

Keywords: EGS, geology, geochemistry, mineralogy, faulting, hydrology, Basin and Range

ABSTRACT

The Milford FORGE deep well site is located 5 km west of the Roosevelt Hot Springs, on alluvial fan deposits (200-600 m thick) that overlie a large volume of hot crystalline basement rock. The site occurs within a region that is geologically complex and characterized by extensional faulting, sporadic magmatism, and zones of anomalously high heat flow, inside the southeast margin of the Great Basin.

The basement rocks at the FORGE deep well site are made up of Precambrian gneiss and Tertiary plutons. These crystalline units are exposed across the eastern part of the Milford Valley basin, from the Mineral Mountains in the east to the Acord-1 well in the west, and they are separated by intrusive and fault contacts. Gneiss contains biotite, hornblende, K-feldspar, plagioclase, quartz, and sillimanite, and isotopic dating indicates Proterozoic metamorphism ~1720 Ma. Plutonic rocks comprise diorite, granodiorite, quartz monzanite, syenite, and granite, containing variable amounts of biotite, clinopyroxene, hornblende, K-feldspar, magnetite-ilmentite, plagioclase, and quartz. The oldest intrusion was emplaced ~25 Ma followed by younger intrusion events at ~18 Ma and 11 to 8 Ma.

Hydrothermal alteration is widespread, but weak, and it is made up of quartz, illite, chlorite, mixed-layered clays, epidote, leuxcoene, hematite, calcite, anhydrite, and K-feldspar, which partly replace precursor minerals or deposited into open spaces. Temperature-sensitive phases lack well-defined depth zonation, which suggest that most of the alteration formed during earlier periods of hydrothermal activity associated with Tertiary magmatism. Modern hydrothermal activity is responsible for steam-heated acid alteration in the vicinity of fumaroles and steaming ground north of the Negro Mag fault, and silica sinter deposition along the Opal Mound fault.

High angle normal faults formed from east-west Basin and Range extension, but listric sliding and block rotation also produced low angle structures characterized by narrow zones of cataclasis in crystalline rocks. The Opal Mound fault is a prominent high-angle fault that dips east and offsets surficial deposits of alluvium and silica sinter, forming a hydrological barrier to lateral fluid flow. Additional north-south trending normal faults, which are blind to the surface, are likely to occur in basement rocks to the west beneath the alluvial cover. The Negro Mag fault is high-angle too, but it trends east-west, cutting across the Mineral Mountains. Lineament analysis and field mapping show that the crystalline rocks exposed in the Mineral Mountains host a fault-fracture mesh, characterized by relatively dense joint spacing, with fractures oriented in many different directions. Such fractures could play an important role in stimulating new permeability beneath the FORGE deep well site.

The groundwater regime across the FORGE deep well site is controlled by the west sloping potentiometric surface and an unconfined aquifer hosted in alluvial gravels. Geochemical data trace shallow hydrothermal outflow to the northwest and west, consistent with temperature profiles in gradient wells. The groundwater is chemically benign, non-potable, and suitable for EGS heat transfer experiments.

1. INTRODUCTION

The Milford FORGE deep well site (Fig. 1) is located 350 km south of Salt Lake City and 16 km north northeast of Milford, Utah, in an unpopulated area that is predominantly used for renewable energy (wind, solar, geothermal). It is situated on a west sloping alluvial fan in the North Milford valley, about halfway between the crest of the Mineral Mountains to the east and the Beaver River to the west. The deep well site covers about 1.5 km^2 and lies 5 km west-northwest of the Blundell geothermal power plant, which produces 35 MWe from flash and binary units.

This paper represents a review of geoscientific data pertaining to the geology, geochemistry, and hydrology of the FORGE site, which has been acquired over a period spanning 40 years. Much of this is the product of exploration and development of the Roosevelt Hot Springs KGRA. However, Roosevelt Hot Springs represents only a small part of a large area associated with anomalous heat flow, and the area to the west of the Opal Mound fault has long attracted interest in terms of EGS research and development (e.g. East, 1981; Goff and Decker, 1983). As a result, data are available from numerous field surveys and the drilling of many shallow and deep wells, including Acord-1, a 3.8 km deep well. These form the foundation for a 3D understanding the rock types, fault-fracture patterns, thermal structure, hydrology, and fluid types that make up the reservoir of the proposed FORGE laboratory. Companion papers by Allis et al (2016) and Hardwick et al (2016) summarize the physical attributes, including temperature and pressure regime and the basin structure based on gravity data.

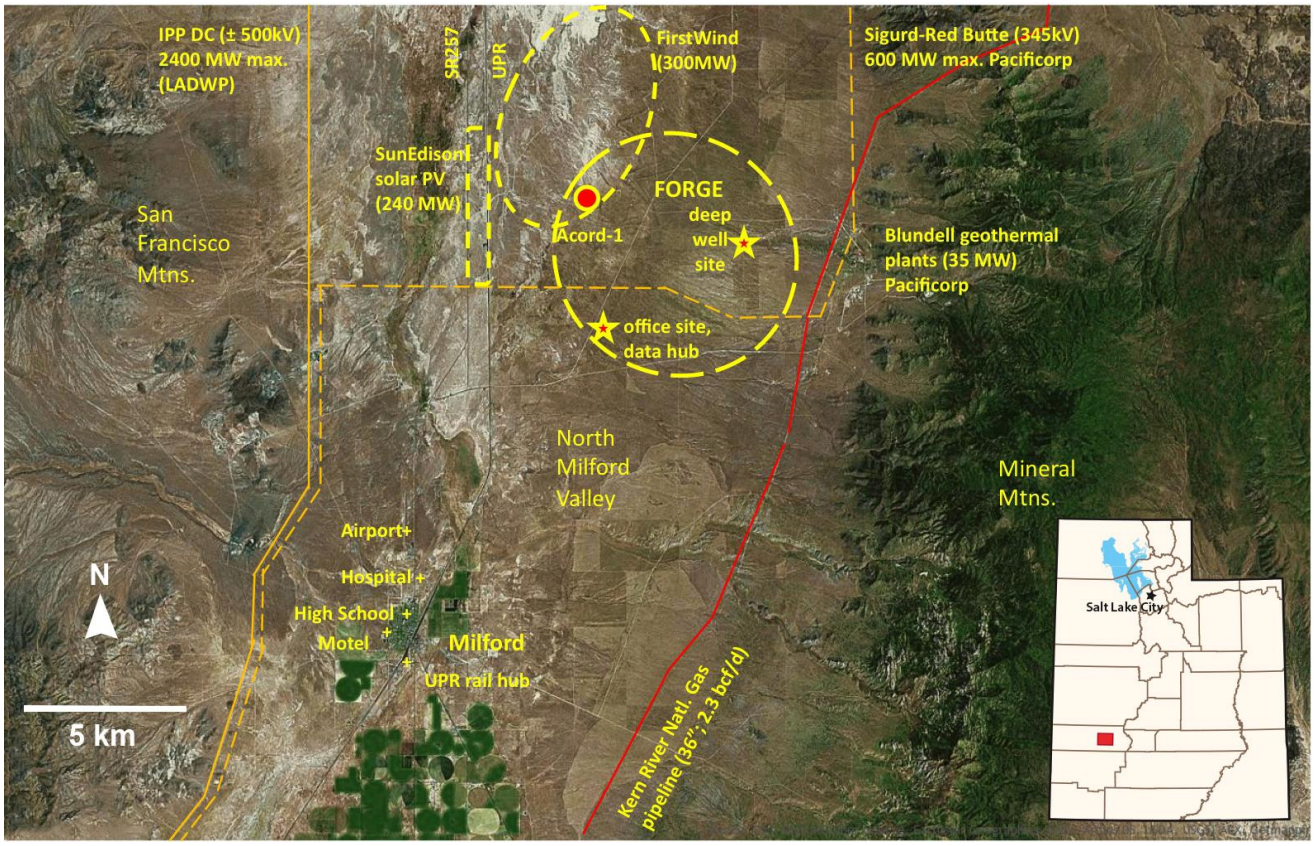

Figure 1: Location of the FORGE deep well site near Milford, Utah, showing infrastructure and physiography (Allis et al., 2016).

2. GEOLOGIC SETTING

The Milford FORGE site (Fig. 1) is located within a geologically complex zone that lies inside the southeast margin of the Great Basin and abuts the western edge of the Colorado Plateau (e.g., Wannamaker et al., 2001). Regional features include folded and imbricated Paleozoic-Mesozoic strata of the late Jurassic through Eocene Sevier orogeny, volcanic and intrusive centers resulting from Tertiary arc magmatism, detachment faulting associated with regional extension, tilting and exhumation of core complexes, and north-south trending normal faults resulting from Basin and Range extension (e.g., Dickinson, 2006; Anders et al., 2012). The zone also includes three producing geothermal fields, Cove Fort-Sulphurdale, Roosevelt Hot Springs, and Thermo Hot Springs, which are associated with young extensional faults, centers of Quaternary basalt-rhyolite magmatism, and large areas of anomalous heat flow covering >100 km^2 (e.g., Mabey and Budding, 1987; Blackett, 2007; Kirby, 2012; Simmons et al., 2015; Wannamaker et al., 2015). The FORGE deep well site lies within an area of anomalous conductive heat flow that extends west from the Opal Mound fault, outside the western boundary of the Roosevelt hydrothermal system (Allis et al., 2016).

3. LITHOLOGY AND MINERALOGY

The main rock types associated with the FORGE deep well site are crystalline basement rocks made up of Precambrian gneiss and Tertiary plutons, Tertiary basin-fill composed of volcanic strata, and Quaternary basin fill made of fluvial-lacustrine sedimentary deposits. The occurrence and distribution of these units is known from field mapping and petrographic studies of cuttings and cores mainly from four wells, 14-2, 52-2, 9-1, and Acord-1 (Figs. 2, 3 and 4; Glen and Hulen, 1978; Glenn et al., 1980; Sweeny, 1980; Welsh, 1980; Nielson et al., 1986; Coleman and Walker, 1992; Coleman et al., 1997; Hintze and Davis, 2003). Gravity data constrain the west sloping contact that separates underlying crystalline rocks, gneiss and granite, from overlying volcanic deposits and fluvial-lacustrine basin fill (Fig. 3; Hardwick et al., 2016). There is no evidence of any Paleozoic-Mesozoic strata in the vicinity of the deep well site, despite being a major component of the regional stratigraphy and exposed in the southern and northern parts of the Mineral Mountains (Nielson et al., 1986).

Precambrian gneiss is the oldest rock type, and outcrops occur sporadically at lowest elevations in the western Mineral Mountains, and it was penetrated in wells (Figs. 2 and 4). Both banded and massive varieties of gneiss exist. Segregations of quartz-K-feldspar form the light bands, whereas biotite-plagioclase-quartz-hornblende-K-feldspar form the dark bands (Glenn et al., 1980). Sillimanite occurs in outcrops. These minerals form an interlocking texture, and planes or zones of weakness, appear to be absent. U-Pb dating of accessory zircons gives an age of 1720 Ma, consistent with a model Rb/Sr whole-rock isochron of 1750 Ma, indicating early Proterozoic metamorphism (Aleinikoff et al., 1987).

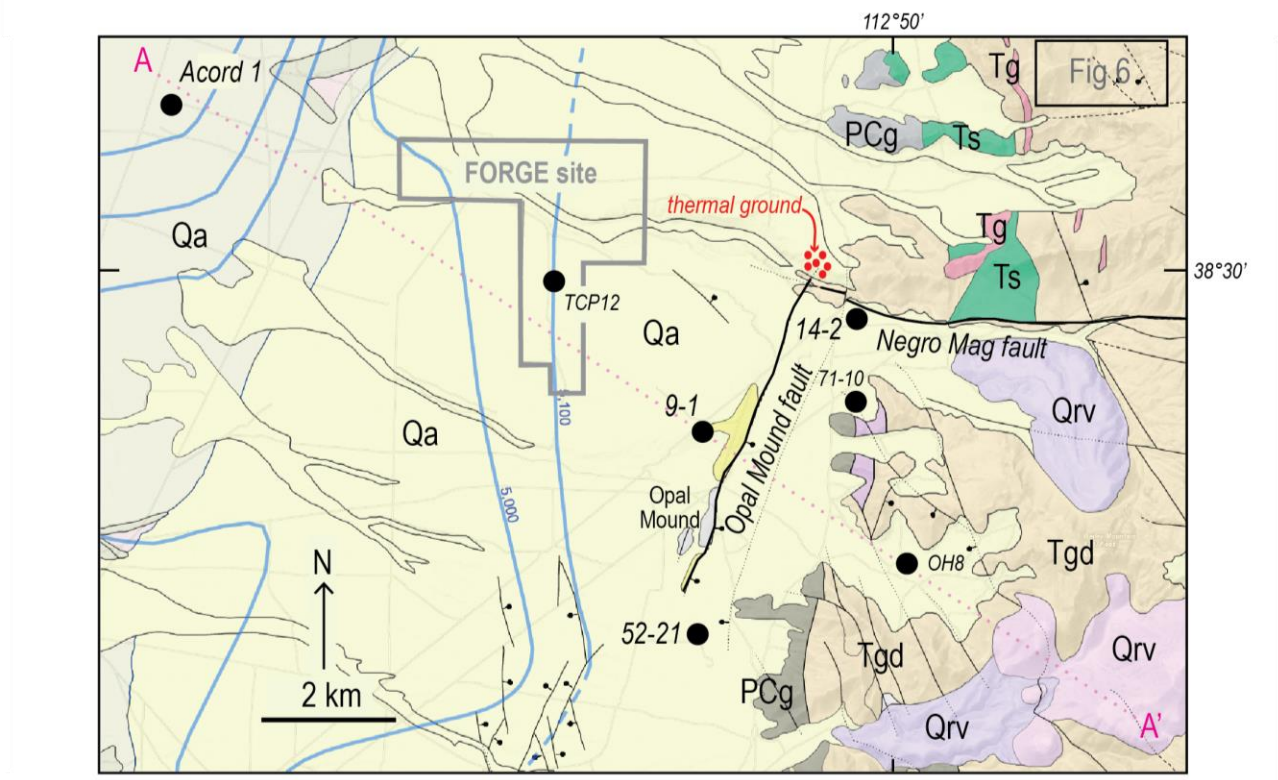

Figure 2: Geologic map of the FORGE deep well site, Milford, Utah (Hintze et al., 2003; Rowley et al., 2005; Kirby, 2012). For clarity, only a few of the many wells are shown. Blue lines represent the elevation (feet above sea level) of the groundwater potentiometric surface. Abbreviations for map units: Qa=Quaternary alluvium and claystone; Qrv=Quaternary rhyolite volcanic rock; Tgd=Tertiary granodiorite; Tg=Tertiary granite dike; Ts=Tertiary syenite; PCg=Precambrian gneiss. Inset outline in upper right corner shows the area represented in Figure 6.

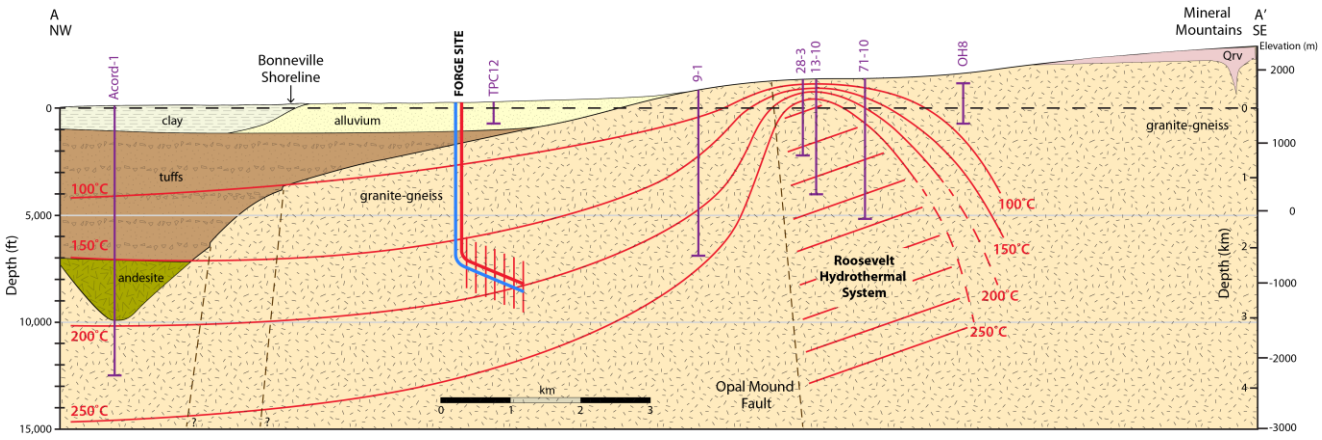

Figure 3: Geologic cross section A-A' from Figure 2, showing the stratigraphy, structure, and the FORGE deep well site. The zero datum for the depth axes is at 1524 m asl (5000 ft asl). Precambrian gneiss and Tertiary plutonic rocks are undifferentiated. The Roosevelt Hot Springs hydrothermal system lies east of the Opal Mound fault. Isotherms are interpreted from well measurements, and the contact between granite-gneiss and overlying basin fill is interpreted from gravity measurements (Allis et al., 2016; Hardwick et al., 2016).

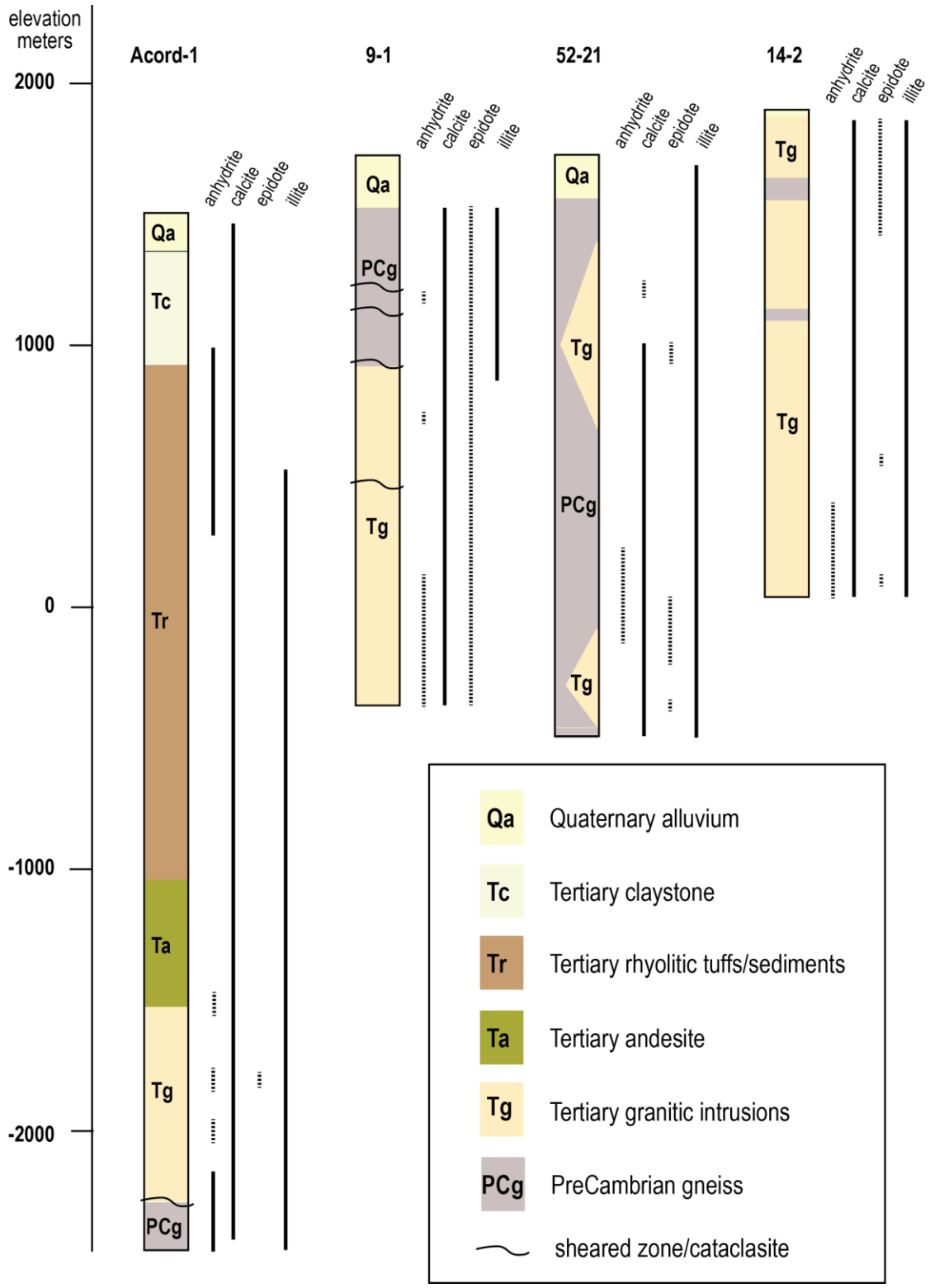

Figure 4: Stratigraphic logs for four deep wells in the study area surrounding the FORGE deep well site, Milford, Utah. Vertical intervals of hydrothermal anhydrite, calcite, epidote and illite (sericite) are based on petrography and XRD analyses. Sources of data: Acord-1 (Sweeney, 1980; Welch, 1980; Hintze and Davis, 2003); 9-1 (Glenn et al., 1980; Capuano and Cole 1982); 52-21 and 14-2 (Glenn and Hulen, 1979; Capuano and Cole 1982). Precambrian gneiss and Tertiary plutons are separated by contacts resulting from magmatic intrusion and faulting. All of the other major breaks in rock types are marked by unconformities.

Plutonic rocks of Oligocene-Miocene age form the core of the Mineral Mountains and the reservoir host rock in the Roosevelt Hot Springs system (Nielson et al., 1986), and these rocks extend to the west beneath the basin fill to the Acord-1 well (Figs. 2 and 4). The intrusions range from intermediate to felsic composition, but the outcrops east of the Roosevelt Hot Springs area mainly expose medium to coarse-grained hornblende granodiorite (Nielson et al., 1986; Coleman and Walker, 1992). Drill cuttings from well 9-1 confirm a spectrum of intrusive-types, including diorite, granodiorite, quartz monzanite, syenite, and granite; these phases are made up of variable amounts of plagioclase, hornblende, biotite, clinopyroxene, quartz, K-feldspar, magnetite-ilmentite, and accessory titanite, rutile, apatite, and zircon (Glenn et al., 1980). The oldest intrusion is associated with crystallization and emplacement of the hornblende diorite, and it has a U-Pb zircon date of 25±4 Ma (Aleinikoff et al., 1987); younger intrusion events followed at ~18 Ma and 11 to 8 Ma (Nielson et al., 1986; Coleman and Walker, 1992; Walker et al., 1997).

Tertiary volcanic rocks crop out sporadically through the Mineral Mountains, and cover large areas in the adjacent ranges, including the Tushar Mountains to the east and the Star Range to the west (e.g., Nielson et al., 1986; Coleman et al., 1997; Hintze and Davis, 2003). The thick sequence of volcanic strata (~1500 m) penetrated by the Acord-1 well (Fig. 4) is divided into a thick upper group made of felsic tuffs and flows, and a lower group made of andesite lavas (Sweeney, 1980; Welch, 1980). Quaternary volcanic rocks occur in the central part of the Mineral Mountains, representing small volume eruptions, obsidian flows and pyroclastic deposits (0.8-0.5 Ma), including the prominent Bailey Ridge flow (~6 km^2) near Roosevelt Hot Springs (Lipman et al., 1978).

Young unconsolidated basin fill covers the floor of Milford Valley. These deposits consist of alluvial and lacustrine deposits that contain interbedded sand, silt, gravel, and clay (Hintze and Davis, 2003). In Acord-1, unconsolidated basin fill has a thickness of >1000 m and spans from Recent to late Tertiary in age. Within the vicinity of the FORGE deep well site, these deposits are 200 to 600 m thick, poorly consolidated, and made up of quartzo-feldspathic alluvial fans shed off the Mineral Mountains. Point bar deposits to the west lap on to the fan deposits and mark the high-stand of Lake Bonneville 18,000 years ago .

Petrographic and XRD analysis of drill cutting indicate widespread occurrences of minor amounts of hydrothermal minerals (Fig. 4), comprising quartz, illite, chlorite, mixed-layered clays, epidote, leuxcoene, hematite, calcite, anhydrite, and K-feldspar (Glenn and Hulen, 1978; Glenn et al., 1980; Sweeney, 1980; Nielson et al., 1986,; this study). Locally, hydrothermal alteration is concentrated around narrow zones of cataclasis, characterized by comminuted rock flour, streaky foliation, and micro-veining (e.g., well 9-1; Glenn et al., 1980). Quartz, chlorite, illite, calcite, epidote and anhydrite, replace precursor phases and fill open spaces, but they lack well-defined depth zonation (Fig. 4; Capuano and Cole, 1982). A number of small prospect pits expose weakly developed hydrothermal Cu-Mo-W mineralization in granitic rocks of the central Mineral Mountains (Nielson et al., 1986). These occurrences suggest that most of the alteration formed during ancient periods of hydrothermal activity that date back to the Miocene and episodes of Tertiary magmatism.

Mineralogical products of modern hydrothermal activity occur along and east of the Opal Mound fault. In the northern part of the Roosevelt Hot Springs area, quartz, alunite, kaolinite, and hematite are products of steam-heated acid alteration in the vicinity of fumaroles and steaming ground (Parry et al., 1980). In the south, a thick deposit (>3 m) of colloform banded sinter makes up the Opal Mound. A subvertical north-south trending fissure (~0.5 m wide) filled with banded silica forms the main vent and marks the Opal Mound fault. Two radiocarbon dates indicate the sinter deposited between 1600 and 1900 years BP (Lynne et al., 2005). Although the site is no longer thermally active, a significant volume of hot near neutral pH chloride water discharged here, similar in composition to modern produced reservoir waters that feed the Blundell-Roosevelt geothermal plant. The hot water flow to the surface likely ceased due to silica deposition in combination with lowering of the water table. Today the Opal Mound Fault represents the western edge of the hydrothermal system and mineral sealing may have played a role in creating a barrier to flow.

4. FAULTS & LINEAMENTS

Three separate types of faults have been identified in the study area, and they are products of two distinct tectonic events that include late Mesozoic-early Cenozoic compression during the Sevier orogeny and middle Tertiary to Recent extension. The Sevier orogeny produced large-scale horizontal displacements and low angle thrust faults (e.g., Hintze and Davis, 2003). Examples of these are exposed in the northern and eastern part of the Mineral Mountains. The original dip of these structures may have been steepened through rotation associated with uplift and exhumation of the Miocene plutonic complex (Nielson et al., 1986).

The younger faulting episode is related to ongoing east-west Basin and Range extension, which dates back at least ~17 Ma, producing predominantly north-south trending fault zones that bound basins and range fronts (e.g., Hintze and Davis, 2003; Dickinson, 2006). In the region surrounding the FORGE deep well site and the Mineral Mountains, both older low-angle faults and younger high-angle faults exist (Nielson et al., 1986; Hintze and Davis, 2003). The Cave Creek fault in the southern part of the Mineral Mountains dips 20° west, and it is associated with a 200 m thick zone of cataclasite, which is developed mainly in the underlying 18 Ma pluton (Nielson et al., 1986; Coleman and Walker, 1994; Coleman et al., 1997; Anders et al., 2001). Evidence of early ductile deformation and foliation is crosscut by subvertical fractures and breccias that represent a transition to brittle deformation over time (Nielson et al., 1986). Another low-angle fault, dipping 15° west and named the Wildhorse Canyon fault, is identified in the western Mineral Mountains, directly east of Roosevelt Hot Springs (Nielson et al., 1986). This fault may extend to the west below the surface based on cataclasite intervals intersected in well 9-1 (Fig. 4). The presence of a continuous listric detachment surface, however, is difficult to verify since there are few drill holes with cored intervals to make stratigraphic correlations. Coleman et al (1997) suggest that rather than being the original dip of displacement, the low-angle structures started out as high angle normal faults, which were tilted as the fault zone evolved (e.g., Buck, 1988), consistent with the dip and north-south strike orientation of the youngest faults in the foothills of the Mineral Mountains (Nielson et al., 1986).

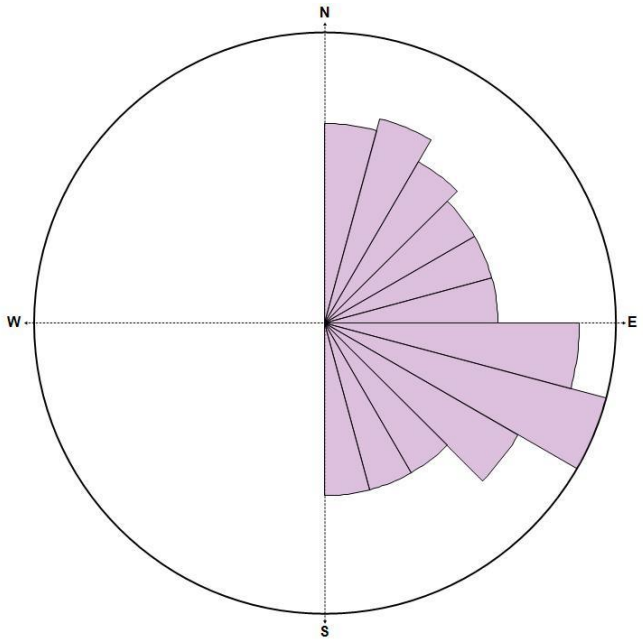

Figure 5: Summary of lineament orientations (n=4452) in granitic basement rock in the Mineral Mountains over a 9x9 km^2 area.

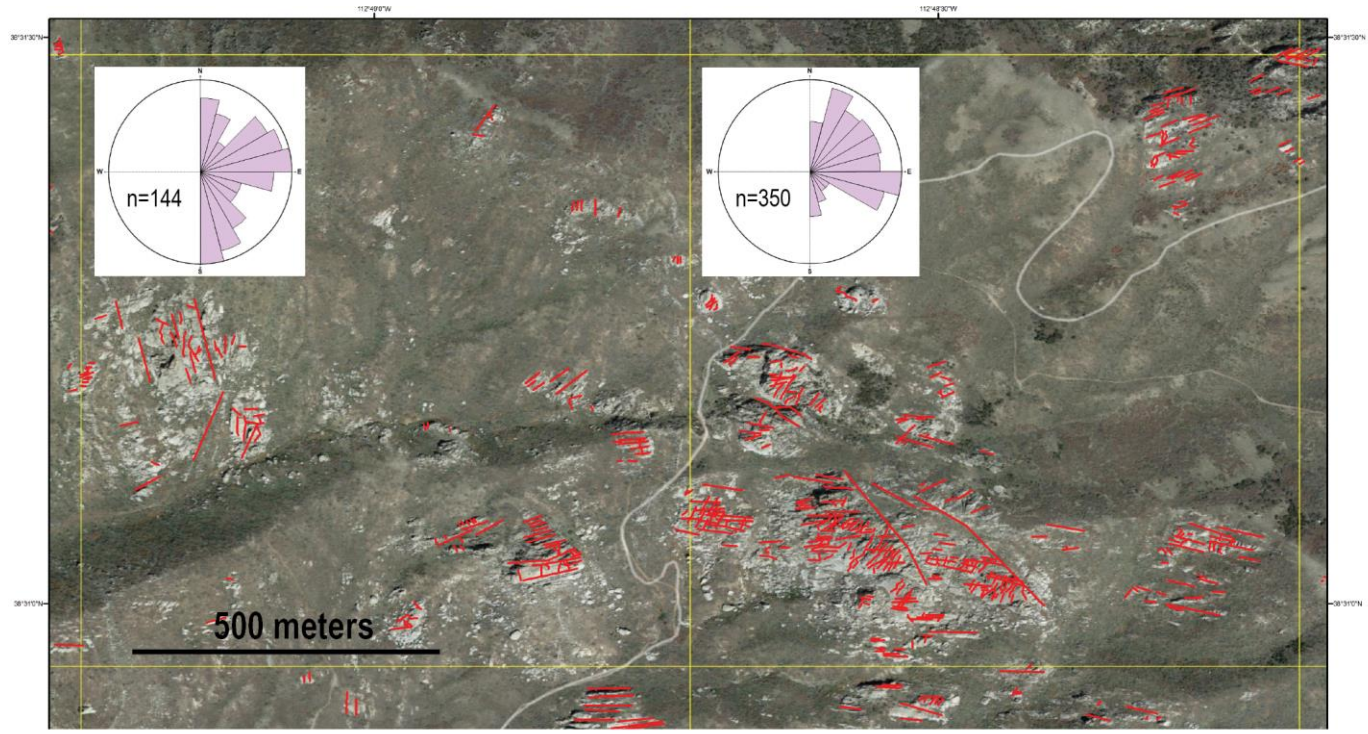

Figure 6: Illustration of lineaments in granitic basement rock in the Mineral Mountains, ~5 km northeast of Roosevelt Hot Springs. Rose diagrams show how azimuths vary within a 2 km^2 area. The location of the study area is shown in Figure 2.

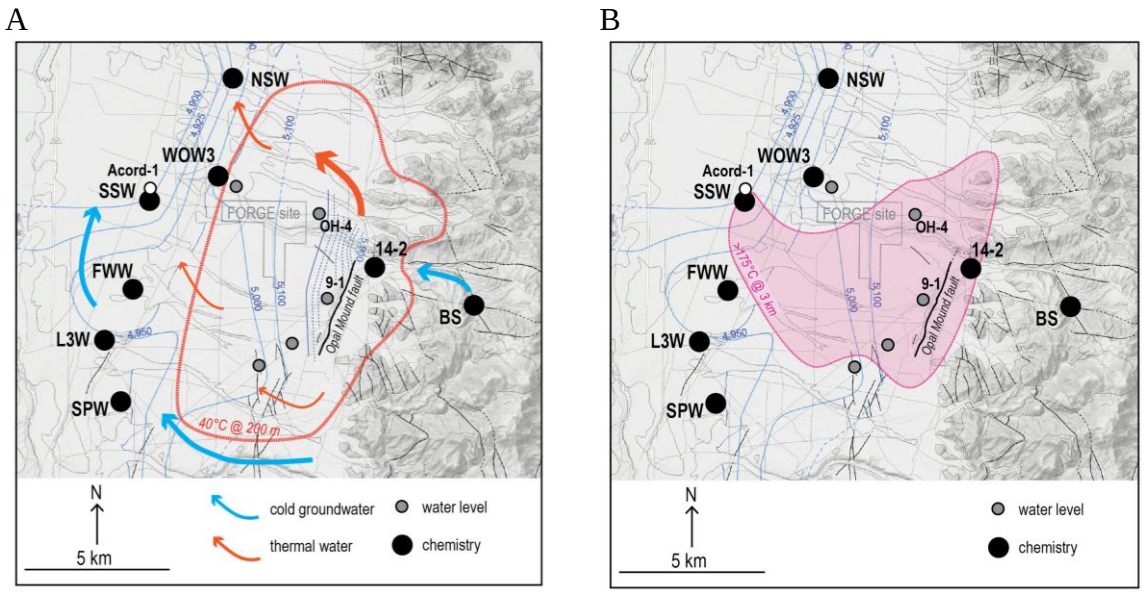

Figure 7: A) Groundwater map of the FORGE deep well site, Milford, Utah, showing some of the wells used to map the potentiometric surface (blue lines, elevation in feet above sea level) and water chemistry. BS is Bailey spring in the Mineral Mountains, and 14-2 is a deep well inside the Roosevelt Hot Springs system that initially produced fluid but is used for injection. Arrows indicate the approximate direction of shallow ground water (cold and thermal) flow. The red dotted line represents the 40°C isotherm at 200 m depth and the limit of the thermal anomaly in the shallow groundwater regime owing to thermal outflow from Roosevelt Hot Springs. B) Map showing the 175°C isotherm at 3 km depth in granite-gneiss country rock (Allis et al., 2016). Compared with A) these maps reflect two distinct thermal regimes, shallow and deep, that are disconnected across the FORGE site.

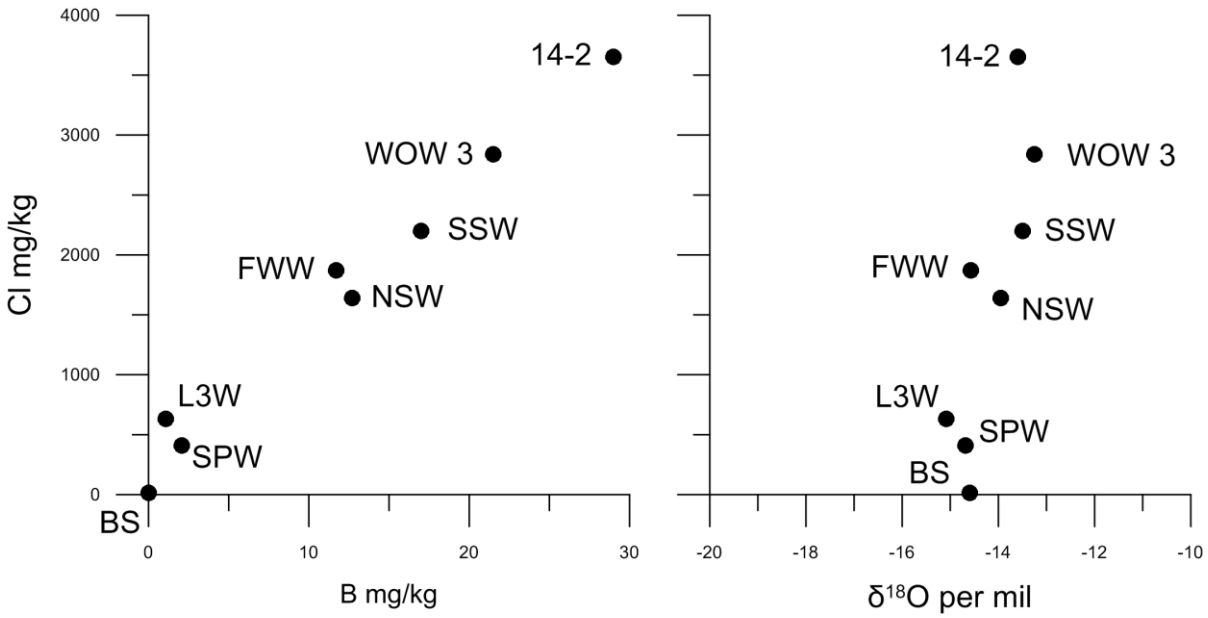

Figure 8: Geochemical trends in Cl versus B and Cl versus $\delta^{18}O$ for groundwaters, showing linear mixing-related trends. Sample localities are shown in Figure 6. Sources of data: Rohrs and Bowman (1980); Capuano and Cole (1982); Kirby (2012).

The Opal Mound fault (Fig. 2) dips steeply to the east and offsets surficial deposits of alluvium and silica sinter, with a total down-dip displacement of at least 15 m (Nielson et al., 1986). Other young north-south trending faults form a narrow graben in the fan deposits 5 km south of the FORGE deep well site (Fig. 2). The offset on these faults is small and less than 3 m. We expect that there are additional north-south trending normal faults in the crystalline basement rocks, which are blind to the surface. Similar faults are inferred from the gravity profile and westward thickening basin fill (Fig. 3; Nielson, et al., 1986; Allis et al., 2016; Hardwick et al., 2016).

The Negro Mag fault is the other major steeply dipping fault, but it trends east-west (Fig. 2). The fault cuts across the Mineral Mountains for ~6 km, however the direction and amount of displacement are unknown due to the absence of markers within the plutonic rocks (Nielson et al., 1986). An east-west trending structure 2 km to the south of Negro Mag fault was the site of micro-seismicity ~35 years ago (Zandt et al., 1982; Nielson et al., 1986; Allis et al., 2016). East-west trending faults also occur at Cove Fort-Sulphurdale and Thermo Hot Springs. These faults may reflect arc-parallel structures, which formed during southward migrating magmatism in the Eocene-Oligocene, and, or Proterozoic structures in deep-seated basement (e.g., Dickinson, 2006; Wannamaker et al., 2015).

From mineralogical investigations, the crystalline basement rocks appear to be strong, even though they vary in rock composition and mineralogy (i.e., granitic to gneissic); they are massive and banded, and they are locally sheared due to cataclasis. Nonetheless, pre-existing fractures and joints are likely to play the most important role in stimulating new permeability beneath the FORGE deep well site. The range of fracture density and orientations in crystalline rocks beneath the FORGE drill well site were therefore studied by locating lineaments in the Mineral Mountains using high-resolution aerial images. A zone covering 9x9 km^2 directly east of Roosevelt Hot Springs was studied and gridded into 1x1 km^2 sections. Overall, more than over 4450 lineaments were mapped, ranging from 10s to 100s of meters in length and having orientations in all compass directions, with a predominant west northwest-east southeast trend (Fig. 5). A finer scale representation of the distributions and orientations of lineaments in two adjacent sections is shown in Figure 6. Three major joint sets were documented in earlier field mapping (Faulder, 1991), two having subvertical dips and azimuth bearings of north-south and east-west and a third having a low-angle dip to the west. These joints are spaced <1 to ~30 m apart (Faulder, 1991).

5. GEOHYDROLOGY AND FLUID CHEMISTRY

Semi-arid conditions, western sloping topography, alluvial basin fill, fractured basement rocks, steeply dipping faults, and the location of the Roosevelt Hot Springs hydrothermal system control the geohydrology of the FORGE deep well site. These are reflected in the water levels and the chemical compositions of waters from shallow and deep wells across the study area (Figs. 7 and 8). Boiling waters associated with steaming ground and fumarolic activity north of Negro Mag wash (Fig. 2) represent the only active thermal springs, but the discharge is feeble (<0.1 kg/sec) and outflow disappears below the surface into unconsolidated gravels. At higher elevation to the east, Bailey Spring represents cold groundwater that infiltrates the Mineral Mountains. All of the rest of the data pertaining to the geohydrology come from shallow groundwater, temperature gradient, and geothermal wells (Rohrs and Bowman, 1980; Capuano and Cole, 1982; Kirby, 2012; Allis et al., 2016; this study).

The potentiometric surface dips west away from the Opal Mound fault and the Mineral Mountains (Fig. 6). From the FORGE deep well site and to the west, the potentiometric surface forms a gentle slope that descends from 5100 to 4900 ft towards the center of the basin. Alluvial gravels host the groundwater aquifer, which is unconfined at higher elevations. Near SPW, L3W, FWW, and SSW (Fig. 6), however, the aquifer is confined beneath impermeable Quaternary claystone (Figs. 3 and 4). East of the FORGE deep well site, the potentiometric surface slopes upward forming a sharp step between OH-4 and Roosevelt Hot Springs (Fig. 6). Well measurements indicate two distinct pressure regimes across the Opal Mound fault, which acts as a horizontal barrier to shallow fluid flow (Allis et al., 2016).

Geochemical data trace the direction of shallow ground water flow. The most dilute water in the area comes from Bailey Spring; westward, however, the groundwater composition changes markedly. At Roosevelt Hot Springs, the groundwater is dominated by hot mineralized waters that rise nearly vertically from a reservoir >1000 m deep. Their compositions are known from surface seeps (50-85°C) and deep wells (feed points 250-265°C), which produce near neutral pH chloride waters that contain 3000-4500 ppm Cl (Capuano and Cole, 1982, unpublished data). From production well 14-2 to the groundwater wells WOW3, SSW, FWW, and NSW, aqueous chloride, boron, and $\delta^{18}O$ show a systematic decrease in values resulting from dilution with fresh ground waters, represented by L3W and SPW. This trend suggests that thermal water leaks into the groundwater aquifer from the intersection of the Opal Mound and Negro Mag faults, then flows downhill and to the northwest to form a large but shallow outflow that is evident in many gradient wells (Fig. 6; Allis et al., 2015; 2016). Another plume, probably smaller, flows west around the southern tip of the Opal Mound fault, contributing heat to the shallow thermal anomaly in the south (Allis et al., 2016).

The geochemical data also provide clues about the states of fluid-mineral equilibria, and the tendency for fluids to dissolve or precipitate minerals. Recent sampling of production wells at Roosevelt Hot Springs indicates that reservoir fluids are similar to the native state fluid compositions, but that they have been modified by varying degrees of boiling and mixing with injectate (Capuano and Cole, 1982; Simmons et al., 2015; unpublished data). Geochemical modeling indicates the deep thermal waters are close to saturation in calcite and anhydrite, and this result is consistent with the widespread occurrences of both minerals in hydrothermal alteration assemblages (Fig. 4). The regional occurrences of sulfate and carbonate minerals in the basin stratigraphy makes them available for remobilization by any hydrothermal activity, whether they be ancient events or modern. The deep waters are also very close to equilibrium with Na and K-bearing feldspars, quartz, chlorite, and illite (Capuano and Cole, 1982; Simmons et al., 2015).

The groundwaters around the FORGE deep well site are chemically benign, but non-potable (Vuataz and Goff, 1987; Allis et al., 2015; 2016), and they appear to be suitable for EGS heat transfer experiments. A recent pump test indicates shallow wells completed in the unconsolidated alluvium should be able to supply more than 100 gallons/minute.

6. SUMMARY

The Milford FORGE deep well site is located within a geologically complex region characterized by extensional faulting, sporadic magmatism, and zones of anomalously high heat flow inside the southeast margin of the Great Basin. The geological, geochemical, and geohydrological attributes of the site are favorably suited for development of the EGS laboratory.

Crystalline basement rocks, comprising Tertiary granitic intrusions and Precambrian gneiss, crop out in the Mineral Mountains and extend westward through the center of the Milford Valley basin, as revealed by deep wells in the Roosevelt Hot Springs, well 9-1 west of the Opal Mound fault, and the Acord-1 well. They form a large volume (>100 km^3) of low porosity rock that underlies the FORGE deep well site, buried beneath a veneer of alluvial fan deposits 200 to 600 m thick.

The crystalline basement rocks comprise alumino-silicate minerals and quartz, and interlocking grain textures seen in thin section indicates the rocks are relatively strong except where fractured. Hydrothermal alteration is widespread, but weakly developed, and outside Roosevelt Hot Springs, it appears to be the product of ancient hydrothermal activity.

The analysis of lineaments in the Mineral Mountains suggests that the crystalline rocks beneath the FORGE deep well site are faulted and fractured, having a wide range of orientations, striking north-south to east-west and dipping high to low angle. Such fractures could play an important role in stimulating new permeability beneath the FORGE deep well site.

Mineralized thermal waters from the Roosevelt Hot Springs flow outward from around the Opal Mound fault to the northwest and west, through a shallow unconfined aquifer. Dilution with cold groundwater produces a linear mixing trend. Across the east side of the Milford Valley basin and around the FORGE deep well site, groundwaters are non-potable, but chemically benign and unlikely to cause significant mineral dissolution or precipitation during fluid circulation and EGS testing.

7. ACKNOWLEDGMENTS

Funding for this work was provided by DOE grants DE-EE0005128 and DE-EE0007080.

REFERENCES

Allis R. G. and Larsen, G.: Roosevelt Hot Springs Geothermal field, Utah – reservoir response after more than 25 years of power production. *Proceedings*. 37th Workshop on Geothermal Reservoir Engineering, Stanford University, Stanford, CA, (2012).

Allis, R.G., Gwynn, M., Hardwick, C., Kirby, S., Moore, J., and Chapman, D.: Re-evaluation of the pre-development thermal regime of Roosevelt Hot Springs geothermal system, Utah. *Proceedings*, 40th Workshop on Geothermal Reservoir Engineering, Stanford University, Stanford, CA, (2015).

Allis, R.G., Moore, J.N., Davatzes, N., Gwynn, M., Hardwick, C., Kirby, S., Pankow, K., Potter, S., and Simmons, S.F.: EGS Concept Testing and Development at the Milford, Utah FORGE Site. *Proceedings*, 41st Workshop on Geothermal Reservoir Engineering, Stanford University, Stanford, CA, (2016).

Alienikoff, J.N., Nielson, D.L., Hedge, C.E., and Evans, S.H.: Geochronology of Precambrian and Tertiary rocks in the Mineral Mountains, south-central Utah. *US Geological Survey Bulletin*, **1622** (1987), 1-12.

Anders, M. H., Christie-Blick, N., Wills, S., and Krueger, S.W.: Rock deformation studies in the Mineral Mountains and Sevier Desert of west-central Utah: Implications for upper crustal low-angle normal faulting. *Geological Society of America Bulletin*, **113** (2001), 895-907.

Anders, M. H., Christie-Blick, N., and Malinverno, A.: Cominco American well: Implications for the reconstruction of the Sevier Orogen and Basin and Range extension in west central Utah. *American Journal of Science*, **312** (2012), 508-533.

Blackett, R. E.: Review of selected geothermal areas in southwestern Utah. *Geothermal Resources Council Transactions*, **31** (2007), 111-116.

Bruhn, R.L., Yusas, M.R., and Huertas, F.: Mechanics of low-angle faulting: An example from Roosevelt Hot Springs. *Tectonophysics*, **86** (1982), 343-361.

Buck, W.R.: Flexural rotation of normal faults. *Tectonics*, **7** (1989), 959-973.

Capuano, R. M., and Cole, D. R.: Fluid-mineral equilibria in a hydrothermal system. *Geochimica Cosmochimica Acta*, **46** (1982), 1353-1364.

Coleman, D.S., and Walker, J.D.: Evidence for the generation of juvenile granitic crust during continental extension, Mineral Mountains batholith, Utah. *Journal of Geophysical Research*, **97** (1992), 11011-11024.

Dickinson, W. R.: Geotectonic evolutions of the Great Basin. *Geosphere*, **2** (2006), 353-368.

East, J.: Hot dry rock geothermal potential Roosevelt Hot Springs Area: Review of data and recommendations. *Los Alamos National Laboratory Report*, **LA-8751-HDR** (1981), pp. 45.

Faulder, D.D.: Long-term flow test #1, Roosevelt Hot Springs, Utah. *Transactions,* Geothermal Resources Council Transactions, **18** (1994), 583-590.

Glenn, W.E., and Hulen, J. B.: Interpretation of well log data from four drill holes at Roosevelt Hot Springs KGRA. DOE Earth Science Laboratory Report, University of Utah (1979), pp. 74.

Glenn, W.E., Hulen, J. B., and Nielson, D.L.: A comprehensive study of LASL well C/T-2 Roosevelt Hot Springs KGRA, Utah, and applications to geothermal well logging. *Los Alamos Scientific Laboratory Report*, **LA-8686-MS** (1980), pp 175.

Goff, F., and Decker, E. R.: Candidate sites for future hot dry rock development in the United States. *Journal of Volcanology and Geothermal Research*, 15 (1983), 187-221.

Hardwick C.L., Gwynn, M., Allis, R., Wannamaker, P., and Moore, J.: Geophysical Signatures of the Milford, Utah FORGE Site. *Proceedings*, 41st Workshop on Geothermal Reservoir Engineering, Stanford University, Stanford, CA, (2016).

Hintze, L. F., and Davis, F. D.: Geology of Millard County, Utah. *UGS Bulletin,* **133** (2003), pp. 305.

Hintze, L.H., Davis, F.D., Rowley, P.D., Cunningham, C.G., Steven, T.A., and Willis, G.C.: Geologic map of the Richfield 30' x 60' quadrangle, southeast Millard County, and parts of Beaver, Piute, and Sevier Counties, Utah. *Utah Geological Survey Map* **195**, (2003).

Kirby, S.: Geologic and hydrologic characterization of regional nongeothermal groundwater resources in the Cove Fort area, Millard and Beaver Counties, Utah. *Utah Geological Survey Special Study*, **140** (2012), pp. 46.

Lipman, P.W., Rowley, P.D., Mehnert, H.H., Evans, S.H., Jr., Nash, W.P., and Brown, F.H.: Pleistocene Rhyolite of the Mineral Mountains, Utah: Geothermal and Archeological Significance. *US Geological Survey Journal of Research,* **6** (1978), 133-147.

Lynne, B.Y., Campbell, K.A., Moore, J.N., and Browne, P.R.L.: Diagenesis of 1900 year-old siliceous sinter (opal-A to quartz) at Opal Mound, Roosevelt Hot Springs, Utah. *Sedimentary Geology*, **179** (2005), 249-278.

Mabey, D.R., and Budding, K.E.: High temperature geothermal resources of Utah. *Utah Geological and Mineralogical Survey Bulletin,* **123** (1987), pp. 64.

Nielson, D. L., Evans, S.H., and Sibbett, B.S.: Magmatic, structural, and hydrothermal evolution of the Mineral Mountains intrusive complex, Utah, *Geological Society of America Bulletin*, **97** (1986), 765-777.

Parry, W.T., Ballantyne, J.M., Bryant, N.L., and Dedolph, R.E.: Geochemistry of hydrothermal alteration at the Roosevelt Hot Springs thermal area, Utah, *Geochimica et Cosmochimic Acta,* **44** (1980), 95-102.

Rohrs, D.T., and Bowman, J. R.: A light stable isotope study of the Roosevelt Hot Springs Area, southwestern Utah, *Topical Report* DE-AC07-78ET28392, Department of Geology and Geophysics, University of Utah **(1980)**, pp.89.

Rowley, P.D., Vice, G.E., McDonald, R.E., Anderson, J.J., Machette, M.N., Maxwell, D.J., Ekren, E.B., Cunningham, C.G., Steven, T.A., and Wardlaw, B.: Interim geologic map of the Beaver 30' x 60' quadrangle, Beaver, Piute, Iron, and Garfield Counties, Utah: *Utah Geological Survey Open-File Report* **454**, (2005), 27 p.,1 plate, scale 1:100,000.

Simmons, S.F., Kirby, S., Moore, J.N., Wannamaker, P., and Allis, R.: Comparative analysis of fluid chemistry from Cove Fort, Roosevelt and Thermo: Implications for geothermal resources and hydrothermal systems on the east edge of the Great Basin. *Proceedings* Geothermal Resources Council, **39** (2015), 55-61.

Sweeney, M.J.: McCulloch Acord 1-26, Roosevelt Hot Springs Area, Beaver Co., Utah. *Unpublished petrography* (1980).

Vuataz, F-D., and Goff, F.: Water geochemistry and hydrogeology of the shallow aquifer at Roosevelt Hot Springs, southern Utah. *Los Alamos National Laboratory Report*, **LA-11160-HDR** (1987), pp. 63

Wannamaker, P.E., Bartley, J.M., Sheehan, A.F., Jones, C.H., Lowry, A.R., Dumitru, T.A., Ehlers, T.A., Holbrook, W.S., Farmer, G.L., Unsworth, M.J., Hall, D.B., Chapman, D.S., Okaya, D.A., John, B.E., and Wolfe, J.A.,: Great Basin-Colorado Plateau transition in central Utah—an interface between active extension and stable interior. *Utah Geological Association Publication* **30** (2001), 1–38.

Wannamaker, P. E., Moore, J. N., Pankow, K. L., Simmons, S.F., Nash, G. D., Maris, V., Batchelor, C., and Hardwick, C. L.,: Play Fairway Analysis of the Eastern Great Basin Extensional Regime, Utah: Preliminary Indications. *Proceedings* Geothermal Resources Council, **39** (2015), 793-804.

Welsh, J. E.: McCulloch Acord 1-26, Roosevelt Hot Springs Area, Beaver Co., Utah. *Unpublished petrography* (1980).

Yearsley, E.,: Roosevelt Hot Springs reservoir model applied to forecasting remaining field potential. *Proceedings* Geothermal Resources Council, **18** (1994), 617-622.

Zandt, G., McPherson, L., Schaff, S., and Olsen, S.: Seismic baseline and induction studies: Roosevelt Hot Springs, Utah, and Raft River, Idaho. U.S. Dept of Energy Report DOE **01821-T1**, (1982), pp. 58.

PROCEEDINGS, 41st Workshop on Geothermal Reservoir Engineering
Stanford University, Stanford, California, February 22-24, 2016
SGP-TR-209

Geophysical Signatures of the Milford, Utah FORGE site

Christian Hardwick[1], Mark Gwynn[1], Rick Allis[1], Phillip Wannamaker[2], and Joe Moore[2]

[1]Utah Geological Survey, PO Box 146100, Salt Lake City, UT 84114

[2]Energy & Geoscience Institute, University of Utah, 423 Wakara Way, Salt Lake City, UT 84108

christianhardwick@utah.gov, markgwynn@utah.gov, rickallis@utah.gov, pewanna@egi.utah.edu, jmoore@utah.edi.edu

Keywords: Milford, FORGE, EGS, heat flow, thermal, gravity, magnetotellurics, geophysics

ABSTRACT

Geophysical data have been utilized in a preliminary characterization of the Milford FORGE site, located in southeastern Utah. The site is situated over Tertiary-Quaternary granitic intrusions and Precambrian gneiss that crop out in the Mineral Mountains and are at 3.1 km depth in the Acord-1 well near the center of Milford Valley 10 km to the west. Modeling of the 20 mGal gravity low, caused by basin fill overlying the granite, was accomplished using a decreasing density contrast with increasing depth based on Acord-1 geophysical logs. 2D models show the granite gently dipping to the west beneath the surficial fan deposits on the western edge of the Mineral Mountains. This dip increases farther out, forming a more localized basin beneath the center of the valley. At the proposed deep drilling site, the granite is at about 400 m depth. A residual, reduced-to-pole aeromagnetic map is featureless near the proposed site due to the burial depth of the relatively magnetic granite. Long-wavelength, magnetic-high anomalies west of the site may be originating from buried Tertiary andesite which occurs in the Acord-1 well. The andesite crops out in the Beaver Lake Mountains 18 km to the west. Several magnetotelluric soundings close to the site show that the basin fill sediments have a resistivity of about 2-3 ohm-meters (Ωm) due to both their clay content and to the warm geothermal groundwater they host.

1. INTRODUCTION

A site near Milford, Utah, has been chosen by the U.S. Department of Energy (DOE) as one of five possible sites for testing and demonstrating new technologies that advance geothermal heat extraction from low permeability host rocks. The initiative, known as FORGE (Frontier Observatory for Research in Geothermal Energy), is discussed in more detail by Boyd et al. (2016). This paper reviews the geophysical characteristics of the Milford site (figure 1), including the gravity, magnetotelluric (MT), magnetic, and thermal signatures. Two additional papers accompany this paper: the geology and hydrology are reviewed by Simmons et al. (2016), and the geothermal characteristics are reviewed by Allis et al. (2016).

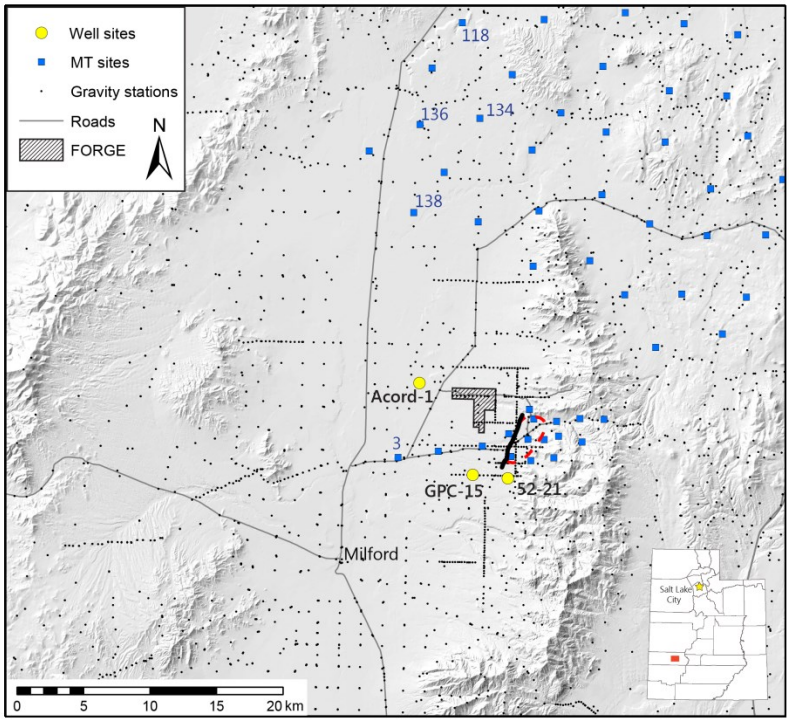

Figure 1. Map of the Milford, Utah FORGE study area. The black shaded area indicates the location of the FORGE site, the heavy black line is Opal Mound fault, and the red dashed line is Roosevelt Hot Springs hydrothermal system.

2. GRAVITY

New gravity measurements in the vicinity of the FORGE site were previously reported by Hardwick and Chapman (2012) and Hardwick (2013). The complete gravity data set for this area is comprised of data collected by the Utah Geological Survey (UGS) and legacy data from the national data repository. All data were reprocessed for terrain corrections and a Complete Bouguer gravity anomaly (CBGA) was calculated according to the methods of Hinze et al. (2005) and described in detail by Hardwick (2013). Figure 2 shows a map of the CBGA for the Milford Valley and surrounding area. A 20 mGal low in the CBGA is located in the central part of the Milford valley which indicates that there is a significant thickness of low-density material (basin fill).

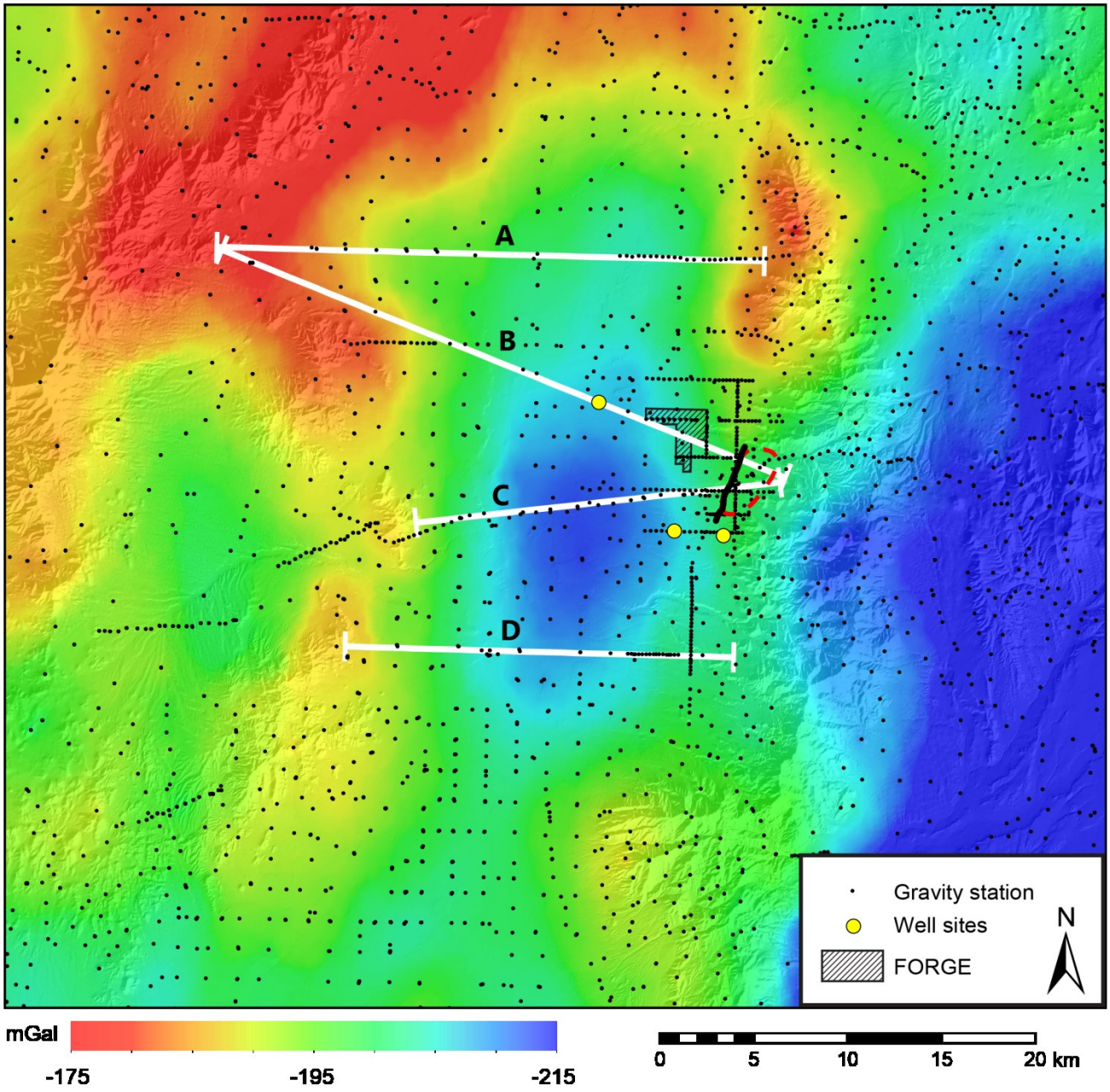

Figure 2. Complete Bouguer gravity anomaly map for the Milford valley. Transects for 2D gravity models (A, B, C and D) are shown as white lines. The black shaded area indicates the location of the FORGE site, the heavy black line is Opal Mound fault, and the red dashed line is Roosevelt Hot Springs hydrothermal system.

The large gravity low to the east has a regional effect on the local gravity field and its amplitude is enough to mask local gravity anomalies and signatures (i.e., the Mineral Mountains signature) as well as shift the inferred center/axis of the basin to the southeast. The wavelength suggests this regional anomaly is most likely associated with a large structure deep in the crust/upper mantle. This would be beneath the transition zone between the physiographic provinces of the Basin and Range and the Colorado Plateau. The work of Wannamaker et al. (2008) offers an explanation of the deep structures observed in MT resistivity modeling of the transition zone. A

complicated process of rifting/faulting, basaltic melt underplating, and possibly a piece of detached Colorado Plateau crust could be the cause of the gravity low (mass deficiency).

Figure 3 shows a map of the slope (gradient) of the CBGA for the area. A map of the slope field highlights the major gradients of the gravity field which can be useful in finding subsurface structures and/or density contrasts. By removing amplitude information of the CBGA field we are also able to get an idea of the shape of the basin, orientation and the locations of any small and large gravity related features. We observe large gravity gradients in areas north of the FORGE site and southeast of the Mineral Mountains. Milford basin is primarily trough-shaped which is narrower at the southern end and more open at the northern end. A small arm extends to the west at the northern end.

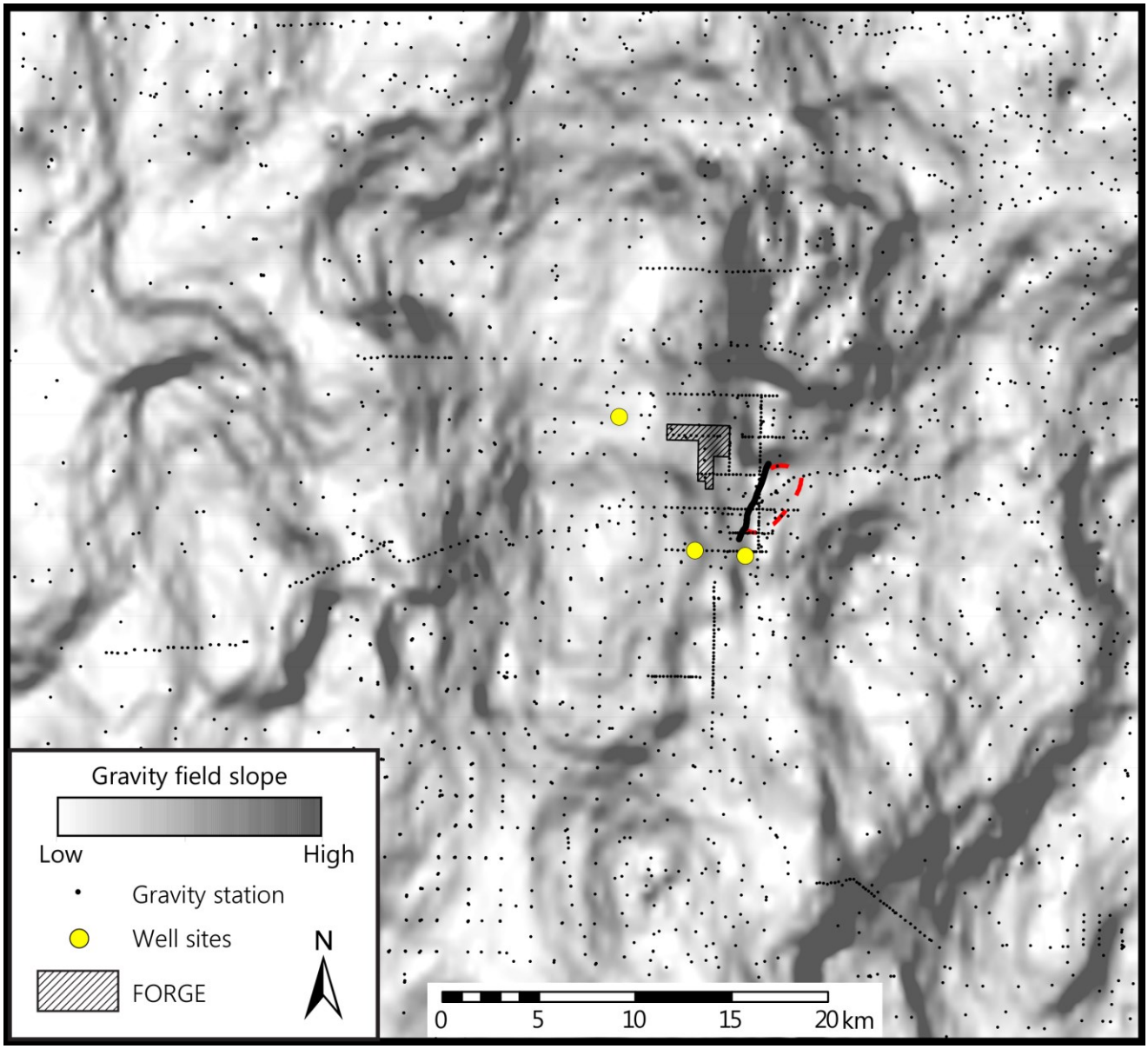

Figure 3. Map of the slope of the gravity field (gradient) for the Milford valley. The black shaded area indicates the location of the FORGE site, the heavy black line is Opal Mound fault, and the red dashed line is Roosevelt Hot Springs hydrothermal system.

After computing regional isostatic gravity corrections for the area (a function of crustal root thickness based on surface elevation), we still have to compensate for the deep anomaly. Becker and Blackwell (1993) used a low density body representating an intrusion at a depth of 5 km below the surface in their model. We believe that the structure is a regional feature of the transition zone requiring a deeper, and larger, low-density body on the eastern boundary of our study area. In order to isolate basin gravity we use transect lines (A, B, C, and D shown in figure 2) spanning from exposed bedrock on opposite sides of the valley and nearly perpendicular to the gravity field gradient. From these transects we approximated a linear correction of the gravity data and proceed to 2-dimensional (2D) modelling using the Semi-Automated Marquardt Inversion code (SAKI) (Webring, 1985).

Initial models were created using a single layer of average basin fill density to establish a general shape of the basement. From the initial model we differentiated the basin fill into a maximum of 6 density layers (decreasing density with increasing depth) derived primarily from the density and porosity logs of the Acord-1 well (figure 4).

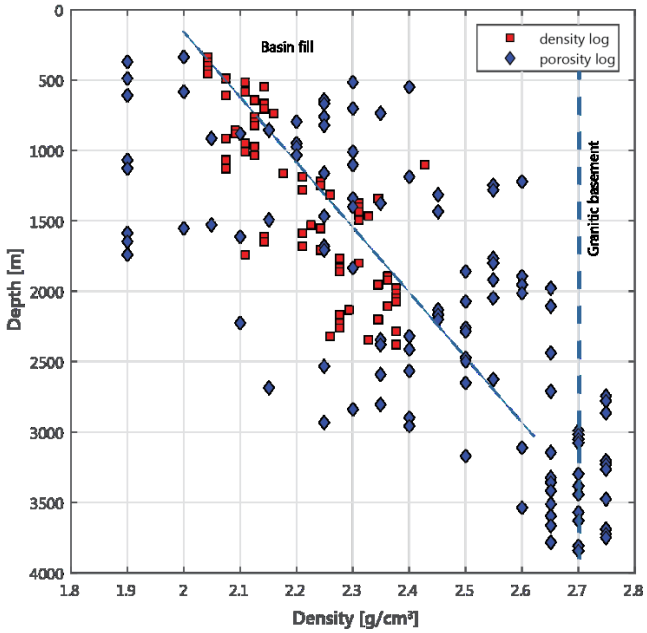

Figure 4. Plot of density values from downhole log data of the Acord-1 well.

The Acord-1 well penetrates 3.1 km of basin fill before reaching the basement and has a total depth nearing 3.9 km. Well data are utilized on transects, where available, to constrain basin-fill thickness and to augment densities for the basin fill layers in the models. Figure 5 shows transects A, B, C, and D where the basin-fill density contrasts range from -0.1 to -0.65 g/cm3 with respect to bedrock density (2.7 g/cm^3) to model the 20 mGal gravity signal.

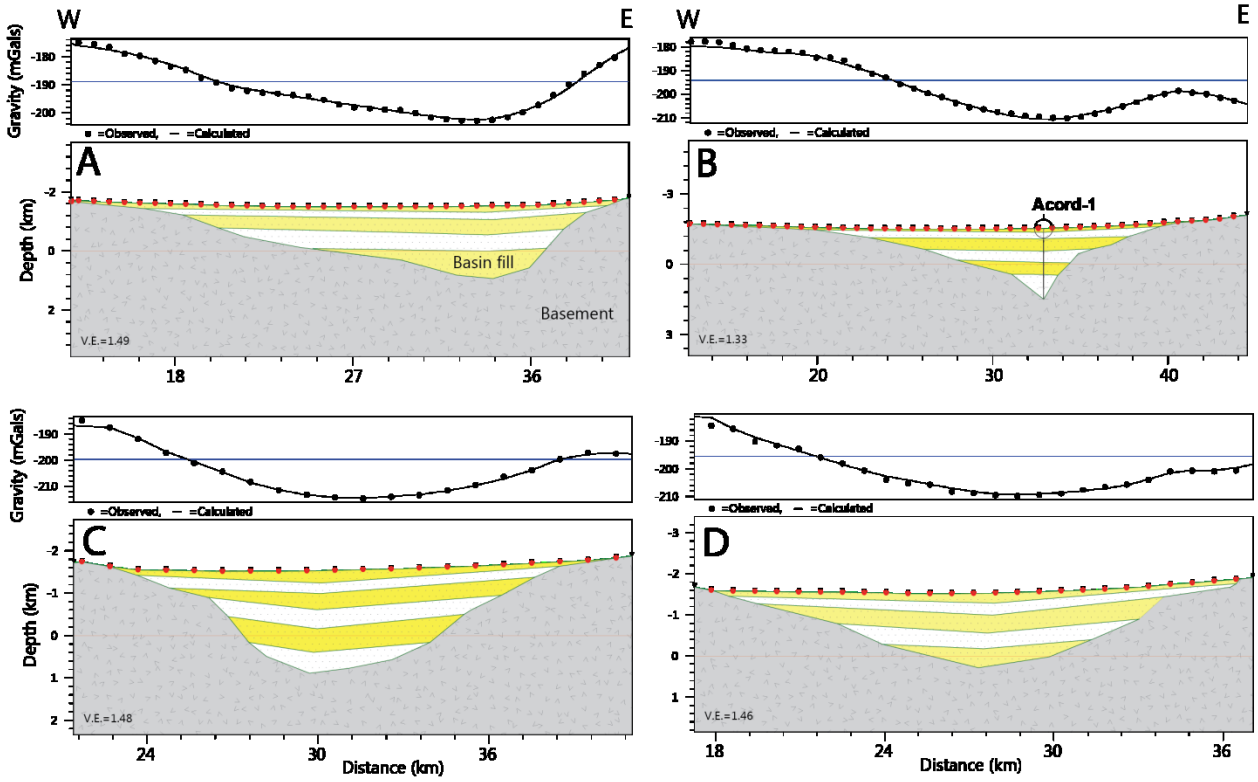

Figure 5. Models of the gravity transects A, B, C, and D from figure 2. Yellow and white layers are basin fill and gray is basement.

3. MAGNETOTELLURICS

Near the FORGE site (figure 1), existing magnetotelluric (MT) data, acquired by the UGS in 2012 and 2014 for geothermal studies in sedimentary basins (Hardwick and Chapman, 2012, Hardwick, 2013, Hardwick et al., 2015), have been incorporated into this study. Analyses of the MT data allow us to estimate the characteristic electrical resistivity properties and to provide information on the dimensionality of the study area, providing clues to the deeper structure and geometry of the Milford basin. Of the existing MT stations, 16 are in, or adjacent to the Milford basin. We use these data to help characterize local resistivity values and constrain depth-to-basement. The data were analyzed using the phase tensor method of Caldwell et al. (2004). Figure 6 shows the MT response (right panel) and phase tensors (left panel) for MT stations 118, 134, 136, 138, and 3. The data were prescreened to ensure that they meet the appropriate criteria for the method. We check the quality of the data as well as assess the dimensionality to ensure it is suitable for 1-dimensional (1D) modeling using the phase tensor method.

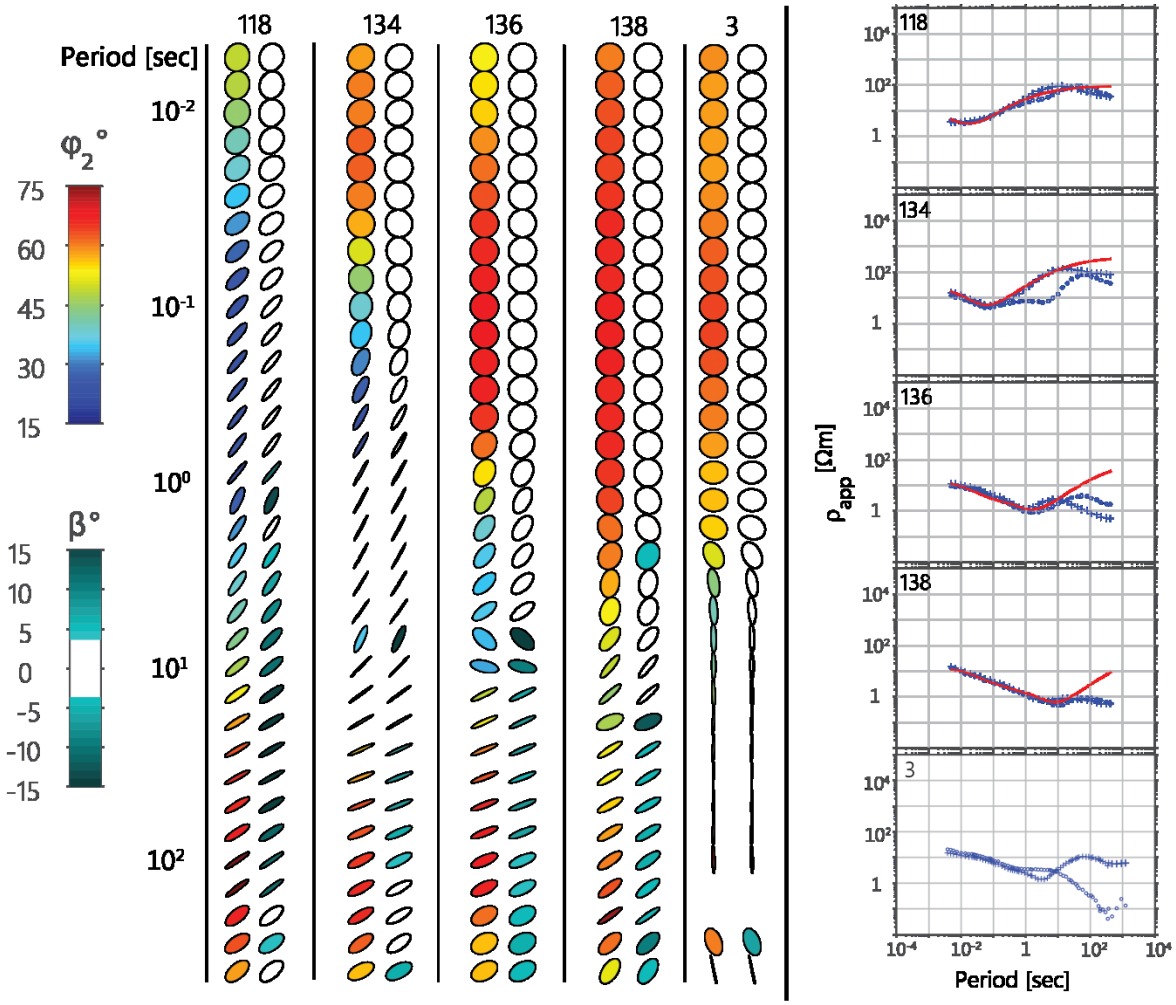

Figure 6. MT Phase tensor profiles plotted by period for sites (locations in figure 1) used in the 1D models (left panel) and MT response data (right panel). Phase tensor colors in the left-hand column for each station (118, 134, 136, 138, 3) are the geometric mean of the minimum and maximum phases and the right-hand column shows the skew parameter. In the MT response plots, open circles are TE (transverse electric) mode, crosses are TM (transverse magnetic) mode, and red curves are 1D forward models.

For each of the 5 stations shown as an example, the small variation and smooth transitions by period indicate the data is continuous and of high quality, with the exception of station 3 beyond a period of 1 second. The brightly colored phase tensors in the left-hand column for each station are colored according to the geometric mean of the minimum and maximum phases which represents the conductivity gradient. Low phase values indicate a transition to resistive material (bedrock) whereas high phase values indicate conductive material (clays, saline pore fluids, etc.). The shape of the phase tensor indicates the dimensionality of the data. While circular tensors imply 1D, elliptical tensors imply 2D and 3D conditions with the major axis of the ellipse indicating the geoelectric strike direction (90 degree ambiguity is resolved by external information such as geologic structures or gravity data). The right-hand column of each station is colored according to the skew (β) parameter. The skew value is a way to determine when dimensionality transitions from 2D to 3D. Phase tensor ellipses that are uncolored ($|\beta| \leq 3°$) are generally accepted as the boundary of quasi-2D conditions (as suggested by Booker, 2014). In this 1D case, we are limited to using periods of the MT data where phase tensors indicate 1D dimensionality.

The 1D MT models of the station data (subset shown in figures 1 and 6), generate depth-to-basement estimates of 120, 250, 710, and 1130 m for stations 118, 134, 136, and 138 respectively. Station 3 could not to be modeled in 1D for a depth-to-basement value since the longer period data doesn't seem to detect a definitive basement signal. This has been observed in MT data from other deep basins in Utah and is thought to be the effect of thick accumulations of very conductive basin sediments starting at the surface. These situations require special treatment in 2D and 3D, and possibly more MT measurements in the vicinity, to resolve deeper structure. Station 3 phase tensors do, however, have a very similar signature to station 138 for shorter periods (> 1 second). In general, the simplified best-fit 1D models use 10-20 Ωm for the near surface sediments, 2 to 3 Ωm for the deeper basin fill, and 80-200 Ωm for the basement rocks.

4. BASIN MODEL

Geophysical data, their respective models, and well data were used to construct a pseudo 3D basement-depth model for the Milford valley basin (figure 7). Depth information from 4 2D gravity cross-sections and 16 1D MT models were combined with a zero-depth boundary to serve as control points for the 3D basin model. MT station data were analyzed and then modeled in 1D (independently from gravity modeling) and used to verify 2D gravity models along transect lines and to help constrain basement depth in parts of the Milford valley where no well data is available. The modeled basin axis runs primarily north-south which is in alignment with the majority of fault strikes related to Basin and Range extension. Modeled basin geometry suggests large, gently-dipping, surfaces are present at the margins of the basin. The surfaces steepen abruptly near the center of the valleys, showing a "basin within a basin". The basement depth varies at the FORGE drilling area from about 300 m on the eastern boundary to 1 km on the western boundary. The depth to basement is about 400 m near the deep drilling site. The deepest part of this basin model is located near the Acord-1 well, which happens to be the only deep control point in the middle of the basin. It is possible that there are other deeper areas in the basin, but examination of the geophysical data do not furnish any indication of their existence outside the vicinity of Acord-1.

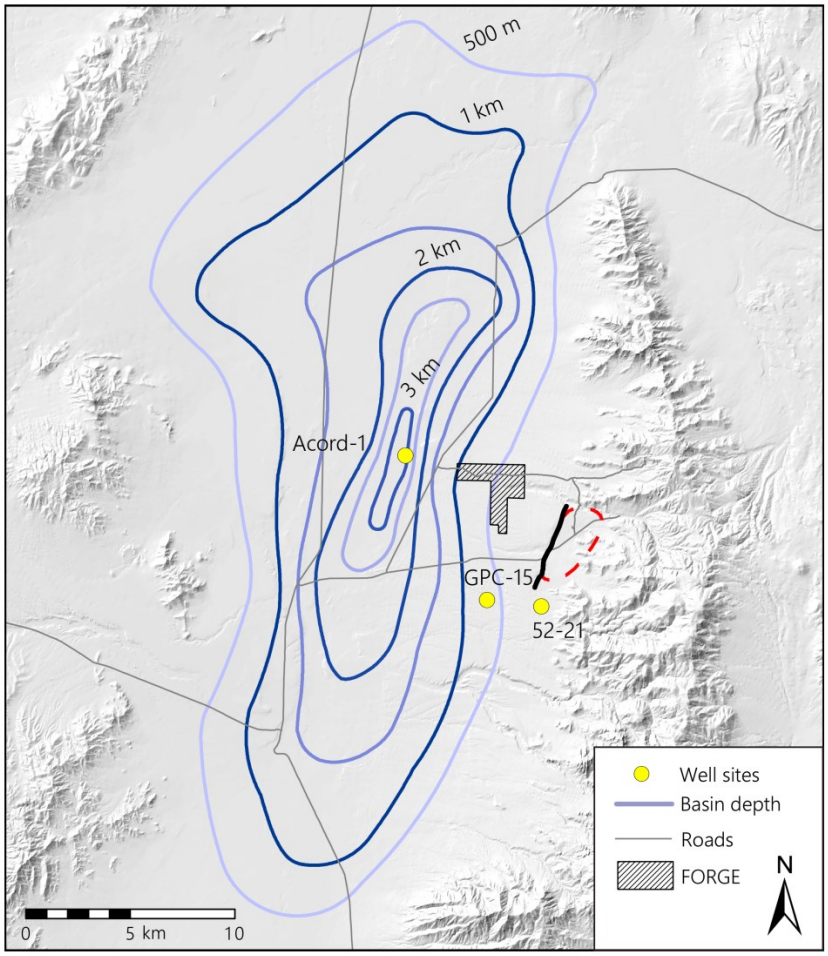

Figure 7. Map of the basin depth model derived from geophysical data. The black shaded area indicates the location of the FORGE site, the heavy black line is Opal Mound fault, the red dashed line is Roosevelt Hot Springs hydrothermal system.

5. OTHER GEOPHYSICAL DATA

Other geophysical data relevant to determining the geophysical characteristics of the Milford area include aeromagnetics, teleseismic, and downhole geophysical logs. A low-level aeromagnetic survey over the region with lines spaced one-quarter mile apart and draped at a nominal 330 m above the terrain was flown for the University of Utah in 1978 (Carter and Cook, 1978). These authors removed the International Geophysical Reference Field to produce residual anomalies and then used a reduction-to-pole technique to remove bipolar

effects. The resulting map is shown as figure 8. The intrusive rocks, cropping out in the Mineral Mountains, and mid-Tertiary volcanics are relatively magnetic compared to the Paleozoic outcrops to the north and south and the buried granite in the valley. Quaternary rhyolite flows immediately east of Roosevelt Hot Springs are thought to be reversely magnetized. The featureless magnetic signature over the FORGE site is due to the great depth to the relatively magnetic granite compared to the elevation of the survey. Long-wavelength, magnetic-high anomalies west of the site may originate from buried Tertiary andesite which occurs in the Acord-1 well (recorded by Hintze and Davis, 2003) and also outcrops in the Beaver Lake Mountains 18 km to the west.

Robinson and Iyer (1981) used a teleseismic survey to assess the nature of the heat source of Roosevelt Hot Springs. The study concluded that the low-velocity patterns observed indicate there is a region of relatively low-velocity material which extends from the upper mantle to depths of about 5 km beneath the Mineral Mountains. The preferred explanation for this anomalous region is that it is the result of "abnormally high temperature and a small fraction of partial melt." The region of -2% velocity change for the depth layer of 5-15 km is shown in figure 8.

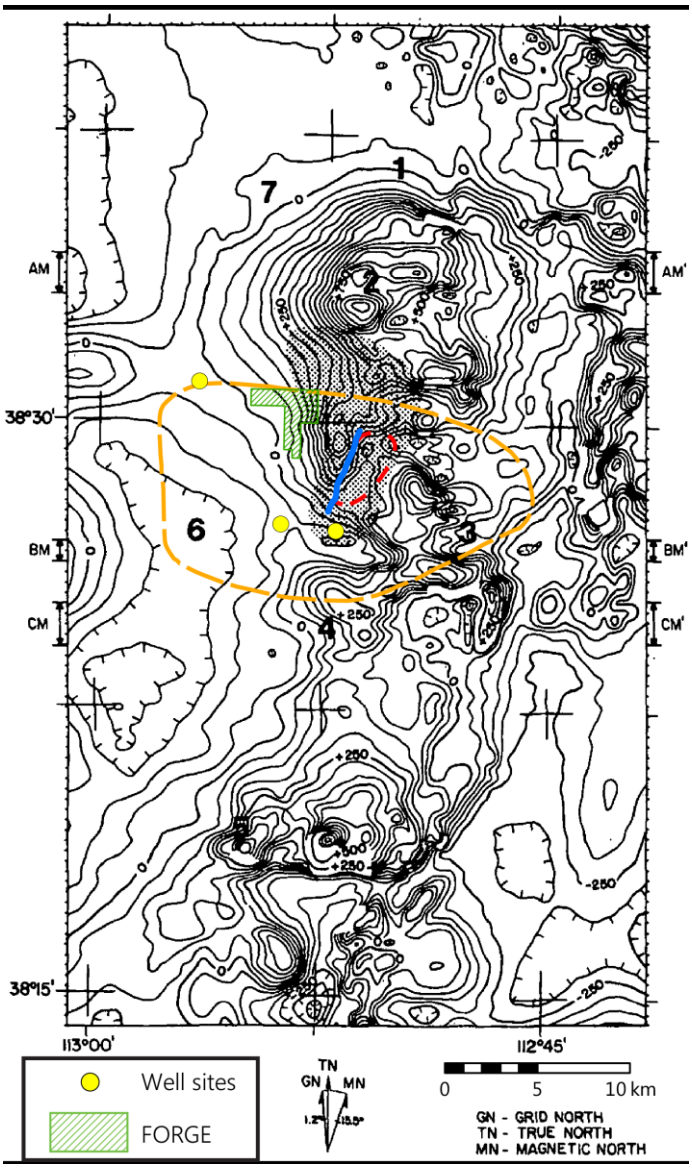

Figure 8. Residual aeromagnetic anomaly, reduced to pole, modified from Carter and Cook (1978; gammas; 330 m draped). Orange dashed line is the -2% seismic velocity anomaly at 5-15 km depth from Robinson and Iyer (1981). The green shaded box indicates the location of the FORGE site, the heavy blue line is Opal Mound fault, and the red dashed line is the Roosevelt Hot Springs hydrothermal system.

Geophysical logs of wells in the Milford valley give insight to the physical properties of basin fill and bedrock material and how those properties differ. This information is useful when qualitatively comparing layers as well as when creating and evaluating models based on geophysical data (density for gravity, resistivity for electromagnetics). Logs from wells GPC-15, 52-21, and Acord-1 (labeled on figures 1 and 7) are illustrated in Figures 9 through 11. Figure 9 shows a set of logs from well GPC-15 which is located 3 km south of the FORGE site. GPC-15 was completed entirely in basin-fill material where interval transit time ranges between 75 to 125 µs/ft,

resistivity is <10 Ωm, and bulk density is around 2 g/cm^3. Figure 10 shows parts of a set of logs from well 52-21, located next to the Mineral Mountains 4 km southeast of the FORGE site. The interval shown for well 52-21 is entirely in basement rock where interval transit time is 50 µs/ft and bulk density is between 2.5 to 3.0 g/cm^3. Resistivity for the same interval of bedrock is 100 Ωm (Glenn and Hulen, 1979). Figure 11 shows a set of logs from the Acord-1 well which penetrates 3100 m of basin fill and terminates in bedrock at about 3900 m. Interval transit time deep in the basin fill varies from 50 to 130 µs/ft, whereas the bedrock is more confined at approximately 50 µs/ft. Resistivity values in the Acord-1 well for basin fill range from 1 to 20 Ωm, while bedrock values range from 60 to 200 Ωm. Bulk density in the basin fill is between 2.0 to 2.5 g/cm^3 and basement values are around 3.0 g/cm^3.

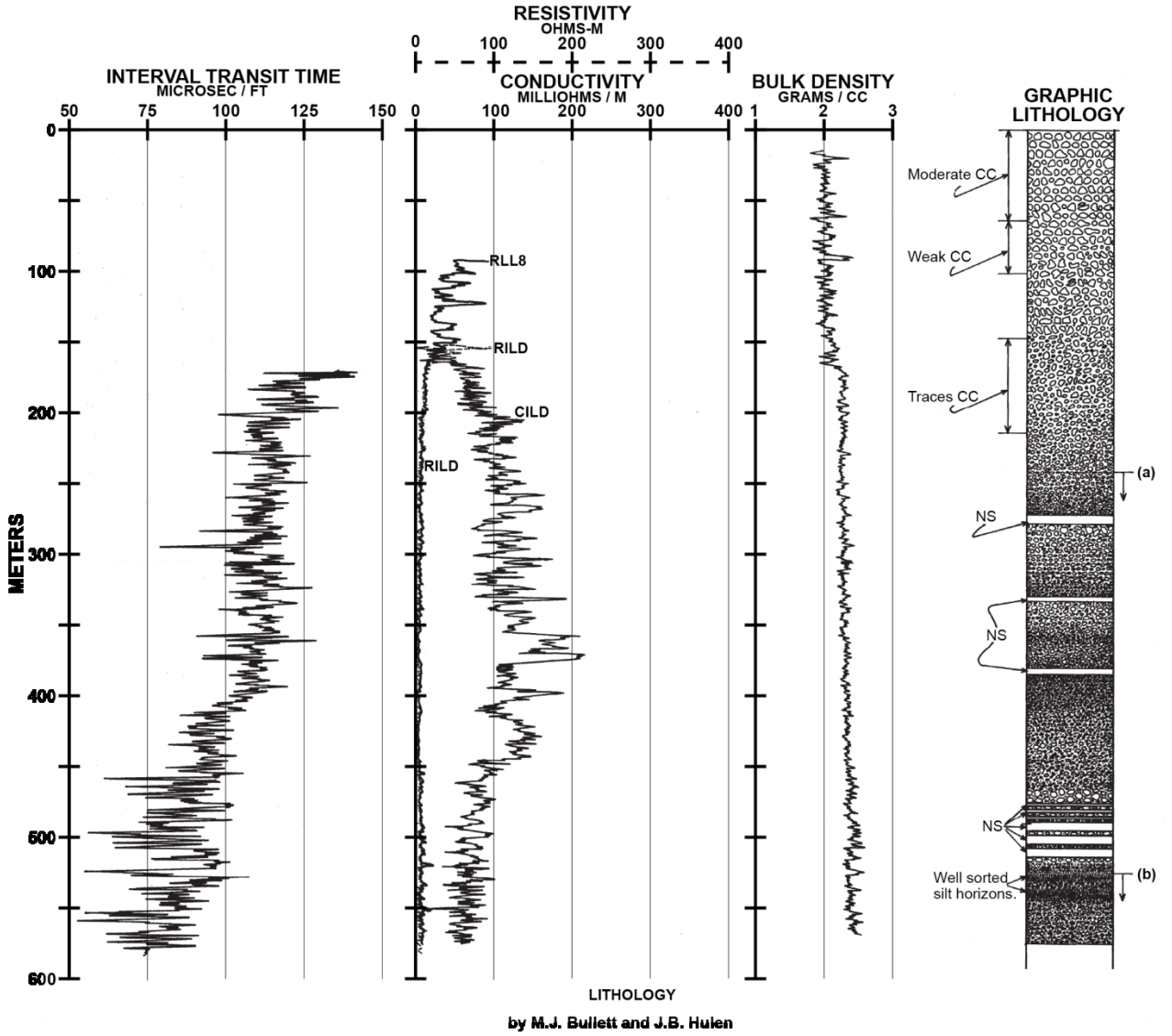

Figure 9. Downhole geophysical logs of well GPC-15 (modified from Glen and Hulen, 1979). Logs show physical properties of basin-fill sediments in the FORGE study area.

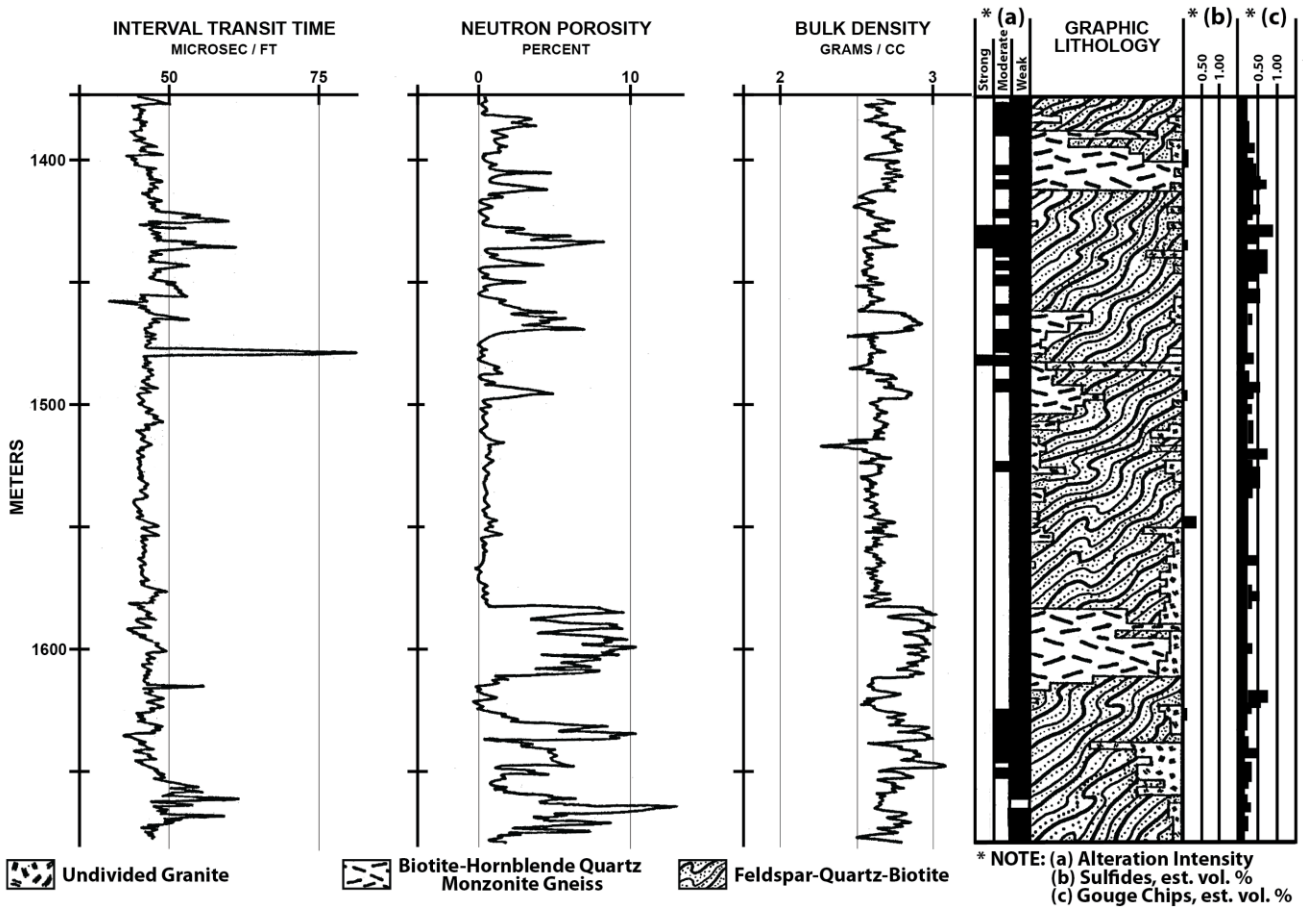

Figure 10. Downhole geophysical logs of well 52-21 (modified from Glen and Hulen, 1979). Logs show physical properties of bedrock in the FORGE study area.

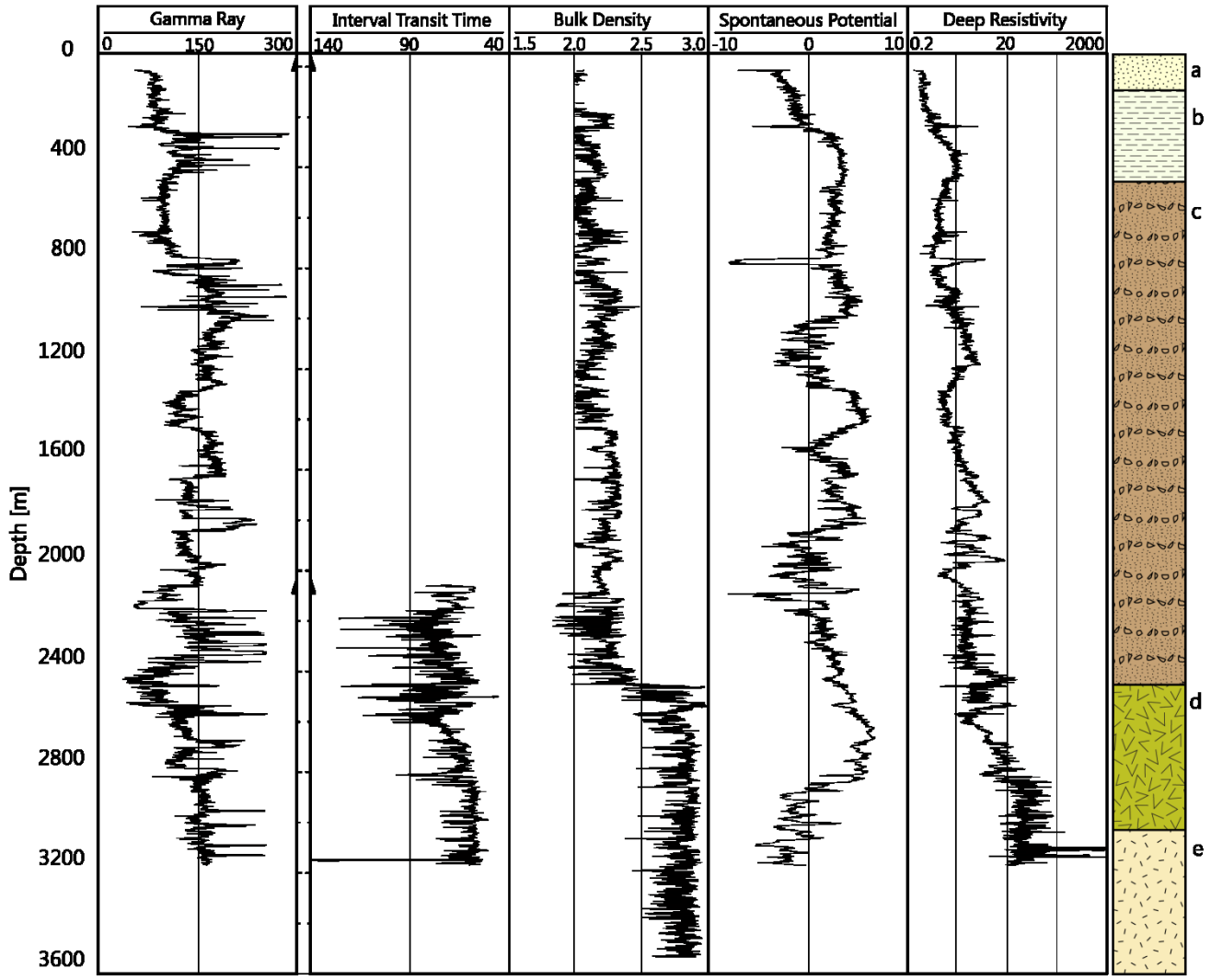

Figure 11. Downhole geophysical logs of Acord-1 well. Logs show physical properties of basin fill and bedrock (3100 m) in the FORGE study area. The stratigraphic column is from the interpretation of Hintze and Davis (2003). Layers are as follows: a) surficial valley fill, b) claystone, c) tuffs and tuffaceous sediments, d) andesite, e) granite.

6. CONCLUSIONS

An extensive suite of geophysical data exists and is available for the FORGE study area near Milford, Utah. The large quatity of available data helps to mitigate uncertainties in geophysical models and subsequent interpretations. The gravity anomaly in the Milford valley basin is a low of about 20 mGal. The local gravity field is affected by a regional anomaly related to a physiographic transition zone, which requires more care when computing and modeling the gravity as the standard methods are insufficient. MT data and models indicate that the resistivity of the basin fill is generally 2 to 3 Ωm and the basement/bedrock is 80-200 Ωm. Such values are consistent with the downhole geophysical logs of wells GPC-15, 52-21, and Acord-1. Broad, shelf-like structures are observed on the margins of the basin which abruptly change slope, steepening toward the middle of the basin. The deepest area of the Milford basin is in the vicinity of the Acord-1 well. The basement depth at the Forge drilling area varies from about 300 m on the eastern side to 1 km on the western side with the approximate center being about 400 m. Geophysical data do not indicate that there are other areas as deep as the area near the Acord-1 well, however, further evaluations using true 3D modeling routines will allow better delineation of basement geometry.

7. ACKNOWLEDGMENTS

Funding for this work was provided by U.S. Department of Energy grants DE-EE0005128 and DE-EE0007080. We thank the many stakeholders who are supporting this project, including Smithfield, Utah School and Institutional Trust Lands Administration, Beaver County, and PacifiCorp Energy. The Bureau of Land Management and the Utah State Engineer's Office have been very helpful in guiding the project through the permitting processes. Peter Nielsen and Nikki Simon (UGS) assisted with the digitizing of the Acord-1 downhole logs and stratigraphic section.

REFERENCES

Allis, R., Moore, J., Davatzes, N., Gwynn, M., Hardwick, C., Kirby, S., Pankow, K., Potter, S. and Simmons, S.: EGS Concept Testing and Development at the Milford, Utah FORGE Site, Proceedings, 41st Workshop on Geothermal Reservoir Engineering, Stanford University, Stanford, CA (2016).

Becker, D. J., and Blackwell, D.: Gravity and Hydrothermal Modeling of the Roosevelt Hot Springs Area, Southwestern Utah, Journal of Geophysical Research, 98, (1993), 17 p.

Booker, J., The Magnetotelluric Phase Tensor: A Critical Review, Surveys in Geophysics, 35, (2014), 7–40.

Boyd, L., Vagnetti, V., Metcalfe, E., Vandermeer, W., Porse, S., Henry, S., Frone, Z., and Tew, A.: The U.S. Department of Energy's Frontier Observatory for Research in Geothermal Energy (FORGE): New directions in subsurface research and development, Proceedings, 41st Workshop on Geothermal Reservoir Engineering, Stanford University, Stanford, CA (2016).

Caldwell, T.G., Bibby, H.M., and Brown, C.: The Magnetotelluric Phase Tensor, Geophysics Journal International, 158, (2004), 457–469.

Carter, J.A., and Cook, K.L.: Regional Gravity and Aeromagnetic Surveys of the Mineral Mountains and Vicinity, Millard and Beaver Counties, Utah, University of Utah, Dept. of Geology and Geophysics Topical Report for DOE/DGE, 77-11, (1978), 127 p.

Glenn, W.E., and Hulen, J.B.: Interpretation of Well Log Data from Four Drill Holes at Roosevelt Hot Springs KGRA, University of Utah Research Institute, Earth Science Lab Topical Report for DOE/DGE, (1979), 74 p.

Hardwick, C.L.: Geothermal Resources in Southwestern Utah: Gravity and Magnetotelluric Investigations, University of Utah, M.S. thesis, (2013), 67 p.

Hardwick, C.L., Allis, R., and Wannamaker, P.E.: Observations and Implications of Magnetotelluric Data for Resolving Stratigraphic Reservoirs Beneath the Black Rock Desert, Utah, USA, Transactions, Geothermal Resources Council, 39, (2015), 593–601.

Hardwick, C.L., and Chapman, D.S.: Geothermal Resources in the Black Rock Desert, Utah: MT and Gravity Surveys, Transactions, Geothermal Resources Council, 36, (2012), 903–906.

Hintze, L.F. and Davis, F.D.: Geology of Millard County, Utah, Utah Geological Survey Bulletin 133, (2003), 305 p.

Hinze, W.J., Aiken, C., Brozena, J., Coakley, B., Dater, D., Flanagan, G., Forsberg, R., Hildenbrand, T., Keller, G.R., Kellogg, J., Kucks, R., Li, X., Mainville, A., Morin, R., Pilkington, M., Plouff, D., Ravat, D., Roman, D., Urrutia-Fucugauchi, J., Veronneau, M., Webring, M., and Winester, D.: New Standards for Reducing Gravity Data: The North American Gravity Database, Geophysics, 70, (2005), J25–J32.

Robinson, R. and Iyer, H.M: Delineation of a Low-Velocity Body under the Roosevelt Hot Springs Geothermal Area, Utah, Using Teleseismic P-Wave Data, Geophysics, 46, (1981), 1456–1466.

Simmons, S., Kirby, S., Jones, C., Moore, J., and Allis, R., Brandt, A., and Nash, G.: The Geology, Geochemistry, and Hydrology of the EGS FORGE Site, Milford Utah, Proceedings, 41st Workshop on Geothermal Reservoir Engineering, Stanford University, Stanford, CA (2016).

Wannamaker, P.E., Hasterok, D.P., Johnston, J.M., Stodt, J.A., Hall, D.B., Sodergren, T.L., Pellerin, L., Maris, V., Doerner, W.M., and Unsworth, M.J.: Lithospheric Dismemberment and Magmatic Processes of the Great Basin-Colorado Plateau Transition, Utah, Implied from Magnetotellurics, Geochemistry, Geophysics, Geosystems, 9, (2008), 36 p.

Webring, M.W.: SAKI—A Fortran Program for Generalized Linear Inversion of Gravity and Magnetic Profiles, U.S. Geological Survey Open-File Report 85-122, (1985), 104 p.

PROCEEDINGS, 41st Workshop on Geothermal Reservoir Engineering
Stanford University, Stanford, California, February 22-24, 2016
SGP-TR-209

EGS Concept Testing and Development at the Milford, Utah FORGE Site

Rick Allis[1], Joe Moore[2], Nick Davatzes[3], Mark Gwynn[1], Christian Hardwick[1], Stefan Kirby[1], John McLennan[2], Kris Pankow[4], Stephen Potter[4], Stuart Simmons[2]

[1] Utah Geological Survey, PO Box, Salt Lake City, UT 84114

[2] Energy & Geoscience Institute, University of Utah, Salt Lake City, UT 84108

[3] Temple University, Dept. of Earth and Environmental Science, Philadelphia, PA 19122

[4] University of Utah Seismograph Stations, University of Utah, UT 84112

rickallis@utah.gov; jmoore@egi.utah.edu; davatzes@temple.edu; markgwynn@utah.gov; christianhardwick@utah.gov; stefankirby@utah.gov; jmclennan@egi.utah.edu ; pankow@seis.utah.edu; steppotter@gmail.com; ssimmons@egi.utah.edu.

Keywords: Milford, FORGE, EGS, heat flow, thermal regime, reservoir, granite, seismicity, stress, pressure

ABSTRACT

The Milford FORGE site, located 16 km northeast of Milford City, Beaver County, and 350 km south of Salt Lake City, is ideal as an Enhanced Geothermal System (EGS) field laboratory. The site is underlain by large volumes of granite and gneiss at temperatures in the range of 175–225°C at 2 to 4 km depth. A deep exploration well, Acord-1, drilled in 1979 to 3.8 km depth 5 km from the proposed deep drill site, encountered granite and gneiss at 3.1 km depth and a temperature at total depth of 230°C. The well did not produce fluids and its conductive temperature profile indicates the crystalline rocks at depth are impermeable. Several deep wells are situated between the eastern edge of the FORGE drill site and the Roosevelt Hot Springs geothermal system supplying the 35 MW Blundell plant located about 4 km to the east. These wells confirm the near-surface presence of granite and gneiss, high temperatures, and poor permeability at depth, demonstrating the FORGE site is outside any active hydrothermal system. All of the wells have been extensively logged, with data and cuttings available for further analysis. The existing Acord-1 well, which was plugged and suspended, will be entered and cleaned out to provide open-hole access to hot crystalline rocks prior to the drilling of the FORGE wells. Considerable infrastructure is available near the FORGE site, including power and fiber-optic cable for real-time data streaming, a major paved road, airport, graded gravel roads that are maintained year round, a rail line, and supportive private landowners. A motel and eating establishments are available in Milford and in the larger community in Beaver, Utah, located 35 km farther away. Environmental Impact Statements at neighboring wind, solar and transmission sites indicate no threatened or endangered species, and minimal risk of cultural/historic sites. The project has secured sufficient groundwater, which is not potable for human or agricultural use, but is suitable for drilling, stimulation, and heat exchange testing. The site is adjacent to a 300 MW wind farm, a 240 MW solar photovoltaic plant under construction, and several large transmission lines.

1. INTRODUCTION

A site near Milford, Utah, has been chosen by the Department of Energy (DOE) as one of five possible sites for testing and demonstrating new technologies that advance geothermal heat extraction from naturally low permeability host rocks. The initiative, known as FORGE (Frontier Observatory for Research in Geothermal Energy), is discussed in more detail by Boyd et al. (2016). This paper reviews the geothermal characteristics of the Milford site, including the surrounding infrastructure that is available to support the diverse research that will be carried out. Two additional papers accompany this paper: the geology and hydrology are reviewed by Simmons et al. (2016), and the geophysical characteristics are reviewed by Hardwick et al. (2016).

2. INFRASTRUCTURE

Milford, which is 16 km south of the proposed site, is incorporated as a city in Beaver County, and has a population of 1400 (Figure 1). It has good motel accommodation (with 24-hour diner), a supermarket, hardware store, and a hospital. A major factor in Milford's history is the Union Pacific Railroad (UPR), which passes through the town and has a siding complex and an office to facilitate freight train scheduling in this part of the state. The railroad offers the possibility of shipping drilling and stimulation equipment (e.g. pipe, pumps) by rail and then using truck transport for the final 16 km to the FORGE site. The Milford Municipal Airport, with a sealed 1525 m runway that is suitable for piston or turboprop, single- or twin-engine planes, is located two miles north of Milford. The proposed site is 350 km south of Salt Lake City, and the drive time is about 3 hours. The site is accessible year round, snow is infrequent, with Beaver County providing snow plow service on the graded gravel roads near the drill site and office.

The FORGE project will require significant power for operating pumps for both groundwater supply and the circulation of water through the stimulated reservoir during heat exchange testing. The Milford FORGE site is situated in a major energy corridor linking northern Utah and Wyoming to southern California. On the west side of this energy corridor is the high voltage direct current (HVDC) transmission line between the 1800 MW Intermountain Power Agency (IPA) coal-fired power plant near Delta (central Utah), and southern California. The power plant and transmission line is owned by the Los Angeles Department of Water and Power. The line has a capacity of 2400 MW, and also carries power from the 300 MW wind farm adjacent to the FORGE site (owned by SunEdison, originally FirstWind). On the east side of Milford valley, and crossing over the FORGE site, is a new transmission line recently

commissioned by PacifiCorp Energy. This line has a capacity of 600 MW and operates at 345 kV. A third, 138kV line designed to improve transmission capacity in the Milford region was energized in December 2015 (between Beaver and Milford; operated by Rocky Mountain Power, a subsidiary of PacifiCorp Energy; line not shown on Figure 1). A second, 3000 MW HVDC transmission line is proposed to parallel the LADWP line and is waiting for environmental clearance from BLM. This Transwest line will link new wind power generation in Wyoming with the southern California power market. The main natural gas pipeline into Southern California (Kern River) passes between the FORGE site and the Blundell geothermal plants of PacifiCorp Energy (35 MW). In addition to the geothermal and wind power generation, the FORGE site is adjacent to a 240 MW solar photovoltaic array that will be commissioned in July 2016 (operated by SunEdison). The FORGE site is positioned in a possibly unique cluster of utility-scale renewable power generation.

The site offers future private-sector power developers the opportunity to expand geothermal power generation assuming the technology demonstration is successful. Towards the end of Phase 3 of the FORGE project, when a long-duration flow test is planned, it may be possible for power generation to connect to the local grid.

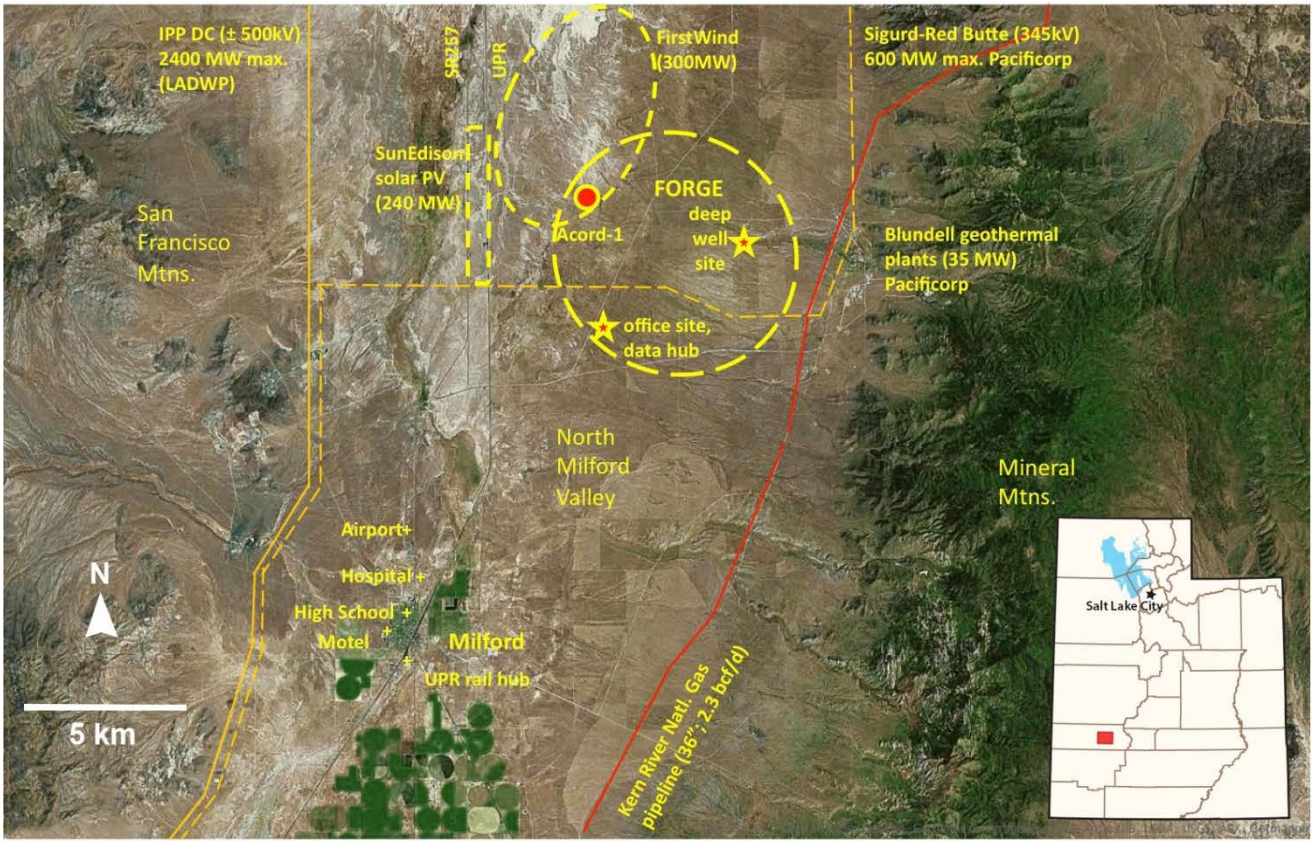

Figure 1: Large-scale infrastructure near the Milford, Utah FORGE site. The site is situated within an energy corridor and is surrounded by several transmission lines, and utility-scale wind, solar-photovoltaic, and geothermal power plants. Roosevelt Hot Springs is situated east of the FORGE drill site. Note the absence of agricultural activity in the vicinity of the drill site due to low-quality groundwater.

The Milford FORGE site is situated on gently sloping, undeveloped grass land (Figure 2). Replanting of the grass in northern Milford Valley occurred after the 2007 Milford Flat fire, the largest wildfire since pioneer settlement of Utah. Although there is heavy agricultural development in southern Milford valley (see center pivots in Figure 1), similar development north of Milford has been inhibited by poor groundwater quality. The groundwater west of the Mineral Mountains has a strong geothermal signature due to the outflow from the Roosevelt Hot Springs hydrothermal system, which is now developed by the Blundell geothermal power plants (Capuano and Cole, 1982; Ross et al., 1982; Moore and Nielsen, 1994; Allis et al., 2012, 2015). Chloride and boron are distinctive signatures of this outflow. This was recently confirmed by SunEdison, who drilled a groundwater supply well at their wind farm maintenance facility (well "Q" in Figure 3) and found warm water of poor quality (32°C, total dissolved solids greater than 4000 mg/L; Simmons et al., 2016). A 24 hour pump test of this well has shown this part of the valley is capable of yielding sufficient water for the needs of the project. A water right for as much as 60 million liters per year of groundwater has been secured from the Utah State Engineer for the duration of the project. Smithfield (a commercial hog-farm operator with undeveloped land in the FORGE area) has offered to supply a similar amount in any year when this is insufficient. Two groundwater wells near the proposed project site office are expected to provide the required supply.

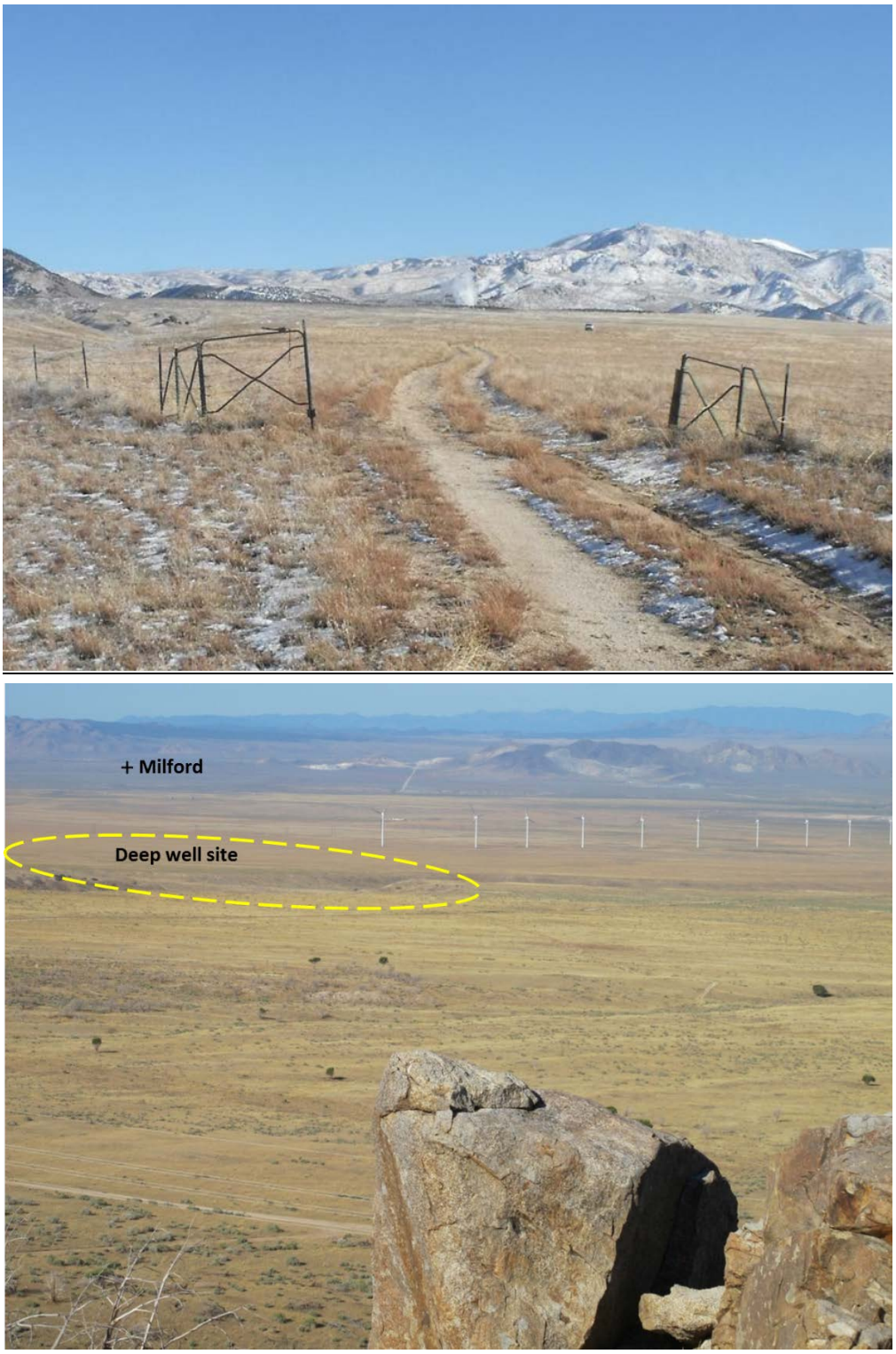

Figure 2: Two views of the Milford FORGE site. Upper photo is looking east, with the vehicle in the middle distance close to the center of the proposed deep well site. The steam plume from the cooling tower of the Blundell power plants is visible (near the center of the photograph) against the western flank of the Mineral Mountains and is 4.5 km from the fence line. The lower photo looks southwest over granite boulders to the deep well site, with Milford City in background, and an array of wind turbines to the west.

The site has a mix of private landowners, including Smithfield (with the largest holdings), Utah School and Institutional Trust Lands Administration (SITLA), and the Bureau of Land Management (BLM) being the main owner of surrounding lands. Smaller parcels are owned by other private landowners. There are three components to the FORGE site: a 5 km^2 (2 mi^2) deep-well site, the 3.8 km -deep Acord-1 well, and a project office site that will include the main groundwater supply wells, and a data collection hub connected to an

existing fiber optic line (Figure 1). Smithfield owns the land around Acord-1 and the project office site, and half of the deep well site. Both Smithfield and SITLA, the main landowners of the deep-well site, are very supportive of the project. The BLM field office in Cedar City has indicated they support approval of project activities such as geophysical surveying, drilling thermal gradient wells or wells for downhole seismometers, and a groundwater pipeline with adjacent vehicle access across their land around the FORGE site. They have indicated there are no issues related to threatened or endangered species here, and no known cultural sites where we have proposed "casual use" activities. PacifiCorp Energy is supportive, and has provided access to data collected during exploration and development phases of the power plant. Beaver County has participated in stakeholder meetings and is also supportive.

3. MILFORD BASIN CHARACTERISTICS

During the late 1970s at least five geothermal exploration companies were drilling in north Milford Valley as they assessed the extent of the Roosevelt Hot Springs hydrothermal system (RHS). The DOE at that time was supporting geothermal research, and there were many projects carried out by staff and students at the University of Utah. Much of the exploration data was preserved and published. Reassessing all the research indicates over 80 shallow thermal gradient wells and 20 deep wells were drilled, over 20 theses were written, and more than 150 reports and papers on the RHS and the surrounding geologic setting were published. Geothermal power generation ultimately focused on a 5 km^2 (1235 acres) area east of the Opal Mound Fault where the most productive, high-temperature wells were drilled. The development and effects of production and injection on the reservoir at the RHS are reviewed by Allis and Larsen (2012). The location of the FORGE site compared to the wells is shown in Figure 3.

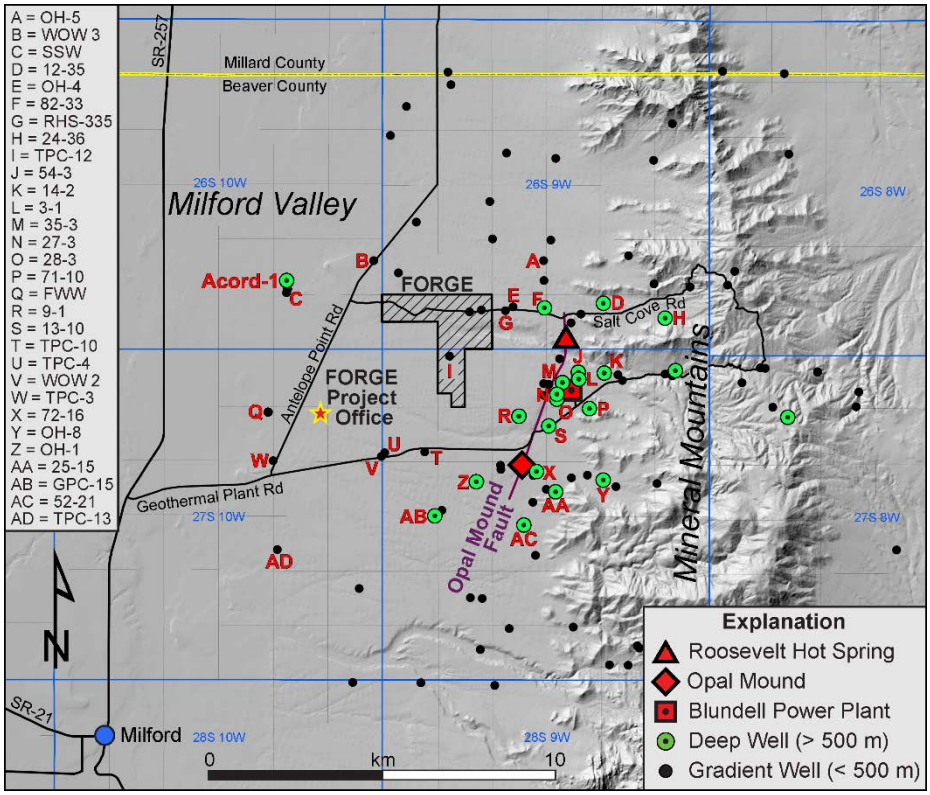

Figure 3. Location of the FORGE drill site and office area, Acord-1 well, and otherwells drilled in the area, on a shaded relief map. Wells referred to in the text are labeled alphabetically. Two additional deep wells are not shown in the cluster around the Blundell Power plant due to space constraints: 45-3 and 58-3. Production wells during the 30 years of Blundell operation have been 3-1, 54-3, 35-3, 45-3, 27-3, and 13-10; injection wells have been 14-2, 82-33, 12-35, and recently, 71-10.

Gravity surveying shows a major basin trending NNE-SSW underlies north Milford Valley (Hardwick et al., 2016). Alluvial fans derived from erosion of the Mineral Mountains gently slope towards the Beaver River over a distance of more than 10 km. Near the center of the basin are deposits from paleo Lake Bonneville, which had a high-stand 18,000 years ago. The axis of the deepest the part of the basin coincides with the location of Acord-1 at about 3 km depth. Gravity modeling shows the deepest part of basin is relatively narrow compared to the overall width of the valley between the Mineral Mountains and the San Francisco Mountains to the west (Figure 4). The steep flanks of the inner basin are suspected to be fault-controlled. The eastern edge of this inner basin is 2 km west of the FORGE deep well site, and the deep well site is situated over a west-sloping granite surface. The depth to the granite at the center of the deep well site is 400 ± 200 m.

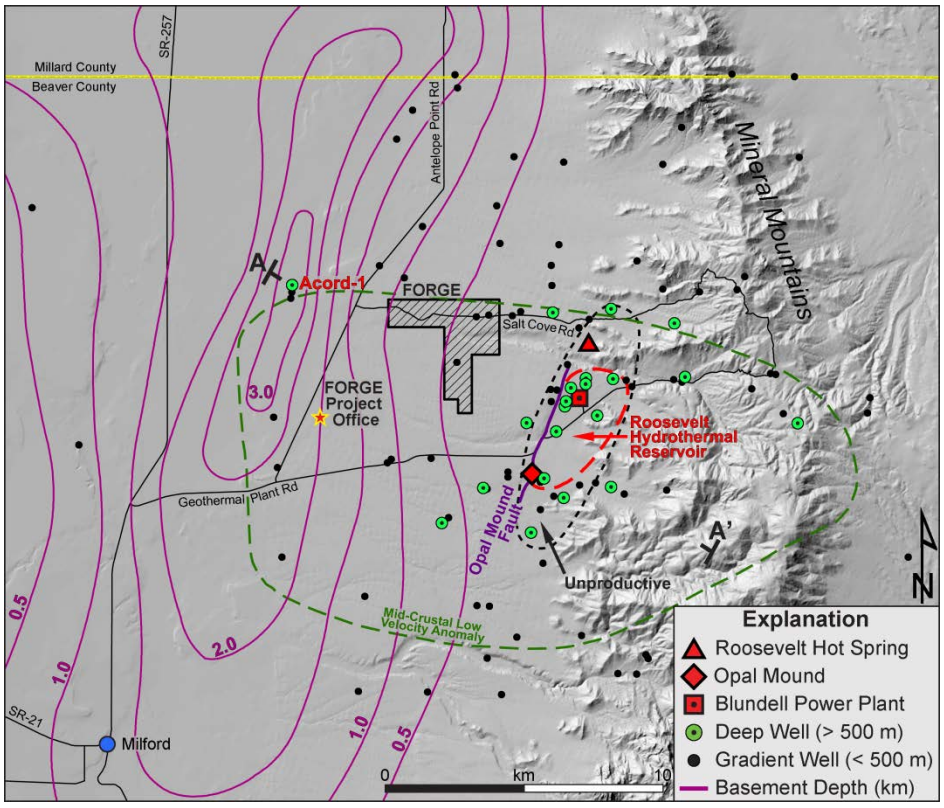

Figure 4. Contours of depth to granite bedrock beneath north Milford Valley (Hardwick et al. 2016) on shaded relief basemap. A – A' mark the line of cross section shown in Figure 10. The mid-crustal low velocity contour outlines a zone of anomalously low P-wave velocity and high attenuation below 5 km depth (Robinson and Iyer, 1981). Potentially productive wells of the Roosevelt hydrothermal system are surrounded by a zone of unproductive pressure-connected wells.

4. THERMAL CHARACTERISTICS

Analysis of the thermal gradient data shows the shallow thermal anomaly extends over most of north Milford Valley (Figure 5). Peripheral wells around north Milford Valley suggest temperatures at 200 m depth are about 20°C. In the Mineral Mountains, non-thermal temperatures range between 5 and 12°C. The area with temperatures above 40°C at 200 m depth covers about 100 km^2 and includes the FORGE deep well site. The pattern of isotherms is similar to the near-surface heat flow map first published by Ward et al. (1978). The 80°C isotherm at 200 m depth approximately coincides with the 1000 mW/m^2 contour on their near-surface heat flow map. Ward et al. (1978) interpreted the high heat flow area east of the Opal Mound fault as the main area of hydrothermal upflow, with the extension of this high heat flow to the northwest from Roosevelt Hot Springs as an outflow feature. The integrated heat output from the hydrothermal system was estimated at 60 MW$_{th}$. Reinterpretation of all the thermal data suggests subsurface outflow of fluid from the Opal Mound fault zone along at least a 10 km length, which implies it extends 4 km south of the mapped fault (Figures 3, 4). This helps explain the widespread geochemical signature of geothermal water in groundwater over much of the north Milford Valley.

4.1 Acord-1

Acord-1 was drilled to 3.8 km depth in 1979 by McCullough Oil Company. No fluid was produced and the well was plugged and suspended because of lack of production. It was permitted by the Utah State Engineer as a geothermal exploration well, and logging measurements were filed with this office. Cuttings for the entire length of this well are preserved at the Utah Core Research Center of the Utah Geological Survey. Mud temperatures while drilling indicate a steady increase with increasing depth (Figure 6). Correction of bottom-hole temperatures at logging intervals confirms a temperature of 230 ± 5°C at total depth. When combined with the temperature gradient observed in the nearby groundwater supply well for the drilling of Acord-1, a geotherm can be fitted to all the data which allows the increase in thermal conductivity with increasing depth to be calibrated (k values in Figure 6). The geotherm implies a heat flow of 120 ± 20 mW/m^2, with most of the uncertainty originating from uncertainties in thermal conductivity.

Acord-1 is lightly plugged between 300 and 365 m, and between 0 and 15 m depth (Figure 6), with the rest of the well filled with mud. A seven inch liner was cemented in the well between 2409 m and 3400 m, leaving an open hole in the granite and gneiss between 3400 and 3852 m depth. Shannon et al. (1983) identified Acord-1 as a hot dry rock prospect, recommending that it be hydraulic-fractured below 3100 m depth. The present owner of the well, Smithfield, will allow the FORGE project to clean out the well and use it for testing. Although this well is now 35 years old and the condition of the casing and cement is unknown, we hope that this well will be available for testing instruments prior to them being lowered into the relatively expensive, deviated wells in the deep well site.

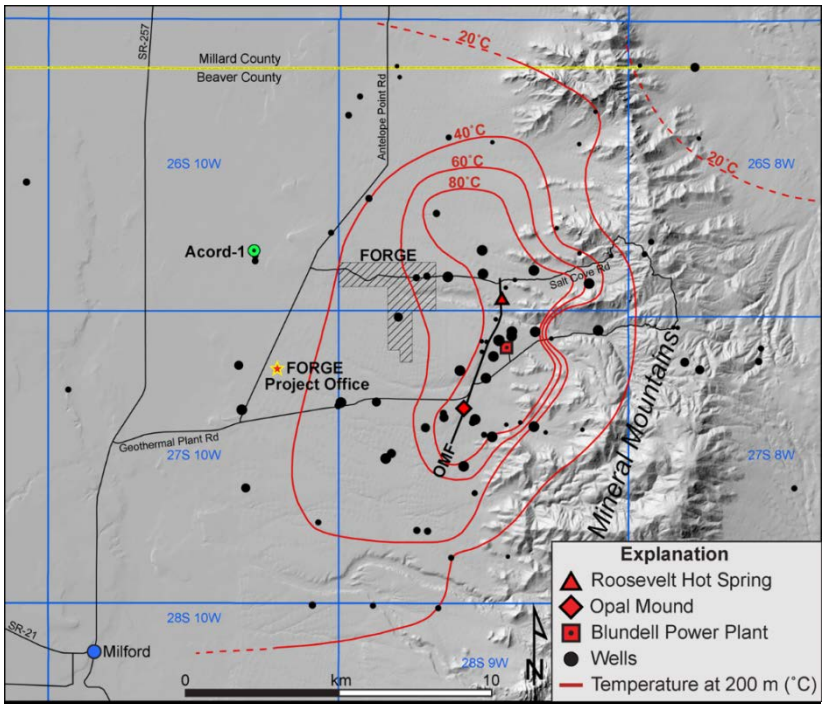

Figure 5. Temperature at 200 m depth in north Milford Valley. The degree of certainty of the thermal data is indicated by the size of the dot for the well location (all wells deeper than 50 m). The largest size is for wells greater than 200 m depth where the temperature was observed. The smallest size is for wells about 50 m deep where the temperature had to be extrapolated to a much greater depth and the temperature is considered the least certain. On the east side of the thermal anomaly, the contours represent the temperature at 200 m below the 1830 m above sea level (6000 ft asl) datum, which is the elevation of the alluvial fan near to where it laps against the Mineral Mountains. This allows the contours to be smoothed across the ridges and valleys, but requires that higher-elevation wells be extrapolated to greater depths (up to 405 m from the surface). Farther to the west, the contours are at 200 m depth from the surface, and near SR-257 in the middle of the valley this is at about 1325 m asl (4345 ft asl; ground surface about 5000 ft asl or 1525 m asl). OMF is the Opal Mound fault.

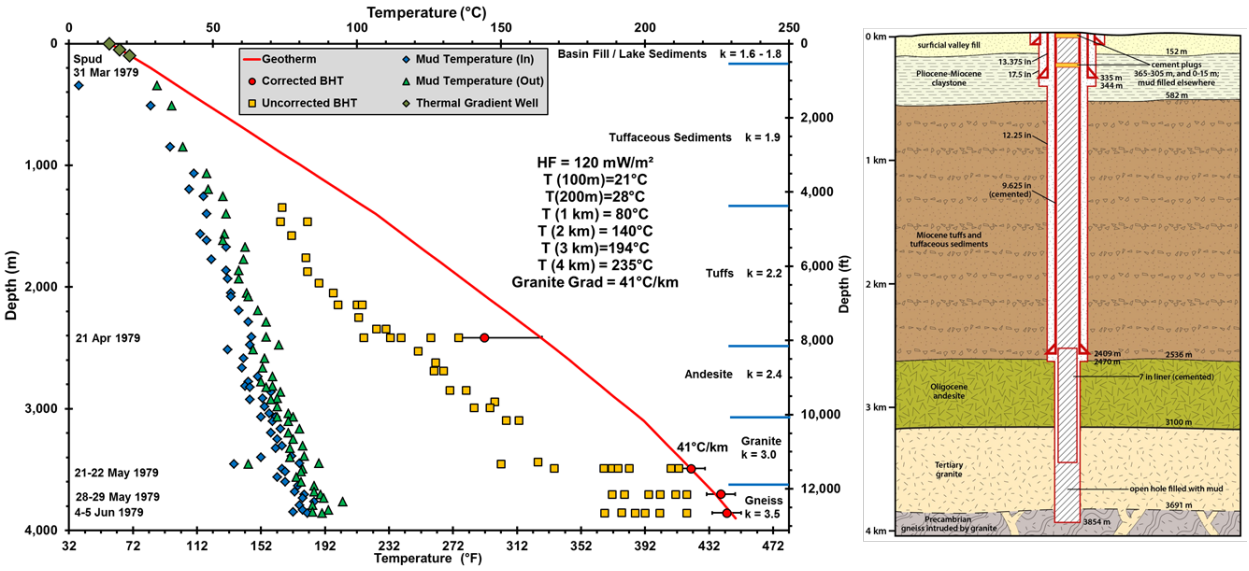

Figure 6. Temperature data from Acord-1 (graph on left) and the casing and cement status after it was plugged and suspended (right). The bottom hole temperatures (BHTs) are consistent with a conductive profile, with the best-fit geotherm having a heat flow of 120 ± 20 mW/m^2 (uncertainty due to thermal conductivity [k] assumptions; geotherm fits both the observed shallow thermal gradient at the site and the deep, corrected BHTs.) The temperature gradient in the granite is 41°C/km. Temperatures at depth increments between 200 m and 4 km are used as input to 3-D thermal modeling. The thermal conductivity variation with increasing depth is used to calculate geotherms from other thermal gradient wells in the north Milford Valley.

4.2 Shallow Temperature Gradients

A selection of shallow temperature profiles from wells between the central Milford Valley and the Opal Mound fault is shown in Figure 7 (see Figure 3 for locations). In the central valley, the heat flow increases from 90 mW/m^2 (TPC13 or AD on Figure 3; and TPC-3, W) in the south around Geothermal Plant Road, to 120 mW/m^2 further north in Acord-1. Wells farther north around the county line have heat flows of 70 ± 20 mW/m^2 (not shown on Figure 3). Midway between Acord-1 and the Opal Mound fault the heat flows are typically in the range 180 ± 20 mW/m^2 (TPC-12, I; TPC-4, U; TPC-10, T). These wells are representative of the heat flow beneath the central part of the FORGE deep well site. Farther to the east, the heat flows are significantly higher at depths less than about 500 m. However, comparison with the deep wells 9-1 (R) and 82-33 (F), which are both west of the Opal Mound fault, suggests the shallow temperatures are being affected by outflow from the hydrothermal system. The near-surface gradients exceed 150°C/km and heat flows can be in the range of 300 to more than 1000 mW/m^2 (for example, well RHS-335 (G), Figure 7). These gradients cannot be extrapolated much below 500 m depth, and when RHS-335 is compared to deep well 9-1, the gradients are clearly decreasing with increasing depth.

East of the Opal Mound fault, many of the shallow temperature profiles exhibit boiling-point-for-depth profiles, indicative of hydrothermal upflow. Although conductive heat flows can be calculated, the total heat flow is actually convective and the temperature profiles are controlled by steam-water saturation conditions, that is, pressure.

4.2 Deep Thermal Regime

Figure 8 shows temperature profiles in non-productive deep wells drilled around the Roosevelt Hot Spring system, the profile of wells drilled into the hydrothermal upflow, and two intermediate-depth wells on the adjacent alluvial fan (east of Opal Mound fault). With the exception of Acord-1, all deep wells are in granite or gneiss with less than 100 m of alluvium on top. Intermediate depth RHS-335 and GPC-15 (AB) did not reach granite basement. The trend of decreasing temperature gradients with increasing depth in the upper kilometer near the Opal Mound fault highlights the potential error in extrapolating shallow gradients to greater depth. Below about 1 km depth, the profiles trend towards gradients of 50 - 70°C/km, indicating temperatures of 150°C to more than 200°C at 2 km depth, and 200°C to more than 250°C at 3 km depth. Well 12-35 (D) is near the northern end of the Opal Mound fault and may be sensing vertical fluid movement at 190 - 200°C. Well 82-33 is northwest of the Opal Mound fault and is in the middle of the shallow outflow from the hydrothermal system shown on Figure 5, but it confirms conductive thermal gradients and higher temperatures at greater depth. Well 24-36 (H) is the easternmost deep well near the northern end of the hydrothermal system, and is distinctive with a concave-upwards temperature signature. Another intermediate-depth well that is east of the southern end of the hydrothermal upflow (OH-8, Y on Figure 3; profile not plotted here) has a similar signature of increasing temperature and gradient with depth. This pattern is repeated in other wells in the Mineral Mountains, and is indicative of cold meteoric recharge depressing the near-surface temperatures.

Deep (productive) wells inside the Roosevelt Hot Springs hydrothermal reservoir have boiling point profiles at less than 500 m depth, and trend toward the system upflow temperature of about 270°C at greater depth (Figure 8 and Faulder, 1994). Outside of the hydrothermal reservoir, the wells are unproductive and have deep temperature gradients of 50 - 70°C/km, indicating deep conductive heat flows of 150 to more than 200 mW/m^2. Despite the similarity in gradients at depth, the temperatures at 2 km depth between wells vary by up to 100°C depending on the near-surface thermal conditions related mainly to the hydrothermal outflow. It is not known how deep or how hot the temperature profiles can be extrapolated to. Thermal models for this FORGE project assume a maximum temperature of 270°C. The pattern of deep conductive temperature gradients surrounding the hydrothermal reservoir is consistent with a large volume of low permeability, hot granite, which is the target of the FORGE project.

Modeling of the deep thermal regime on the alluvial fan between Acord-1 and the Opal Mound fault is based on calculating heat flows and fitting geotherms to the thermal gradient wells with apparently reliable data. The trend of increasing thermal conductivity with depth derived from the best-fit geotherm through the basin fill for Acord-1 has been assumed to apply to all wells. This implicitly assumes the basin fill everywhere has similar lithologies and a similar compaction trend with increasing depth. Once the geotherms reach the granite surface (depth from gravity modeling, Hardwick et al., 2016; and Figure 4) a thermal conductivity of 3 W/m°C is assumed. Compilation of the geotherm trends has allowed maps of isotherms to be compiled at 1 km increments down to 4 km depth. Here we show the maps at 2 and 3 km depth (Figure 9). Because of the thermal and depth constraints for the FORGE deep well site provided by DOE, the area of each map where there is granite exceeding the lower temperature limit for the FORGE laboratory, 175°C, has been highlighted. The 2-km depth isotherms indicate that the eastern edge of the FORGE deep well site satisfies this condition. At 3 km depth, most of the site has a temperature of more than 175°C, and the eastern side of the site may exceed the high-temperature limit of 225°C. The deep well site therefore provides a range of depths for optimizing reservoir stimulation and thermal heat recovery.

A NW-SE cross-section of the thermal regime is shown in Figure 10. The figure shows the deep wells deviated towards the southeast from the western side of the deep-well site. Final decisions on the best location and deviation direction for the deep wells will await the characterization research in Phase 2 of this project. The 100 and 150°C isotherms are near-horizontal and cross from granite to tuffs without obvious deflection despite a thermal conductivity contrast (2.0 to 3.0 W/m°C) because of the compensating effects of increasing heat flow from east to west (120 mW/m^2 at Acord-1 to 180 mW/m^2 at the FORGE site).

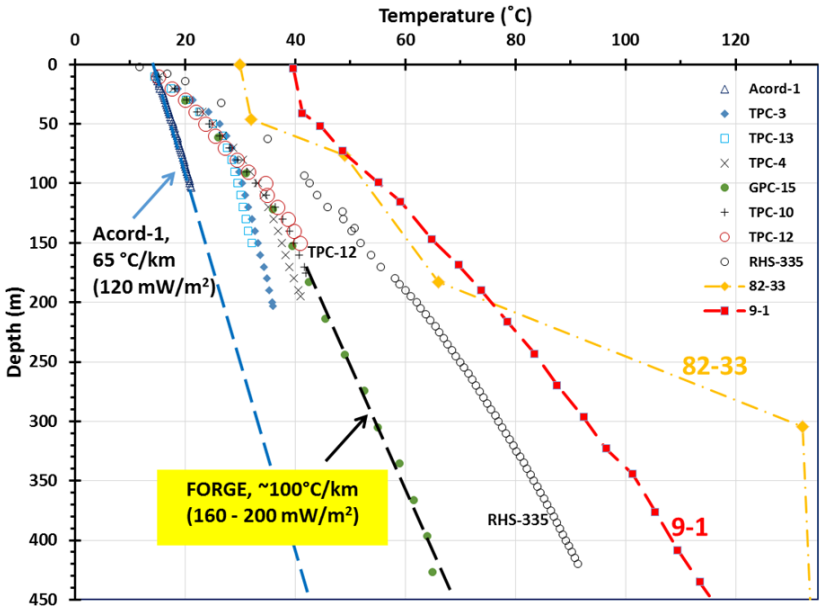

Figure 7. Details of the thermal regime in selected geothermal gradient wells, together with the upper portion of thermal profiles from the three deep wells west of the Opal Mound fault zone. The thermal gradients vary from 50–65 °C/km in the central valley and increase east towards the Opal Mound fault zone. TPC-12 is within the FORGE deep drilling zone and indicates a deeper gradient of close to 100°C/km. Well RHS-335 indicates higher temperatures and is located 300 m east of the western boundary of the FORGE deep drilling zone. All wells are located on Figure 3. The profiles for 82-33 and 9-1 are from Faulder (1994).

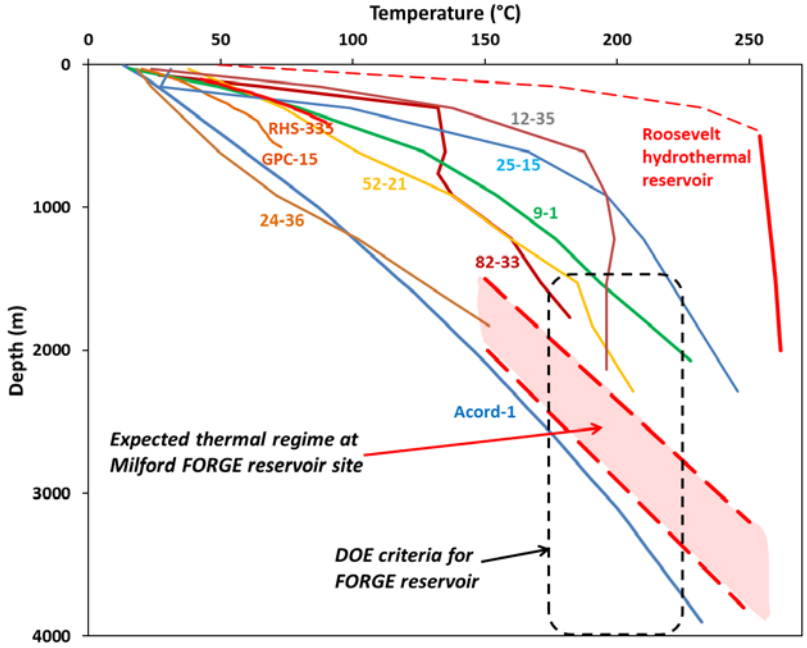

Figure 8. Likely thermal regime at the FORGE deep drilling site based on profiles in surrounding deep wells, and the thermal gradients in shallow wells shown in Figure 7. The expected thermal regime beneath the site lies centrally within the bounding constraints specified by DOE. The two dashed lines bound the likely uncertainties. The nearest wells to the site are 9-1 and 82-33, and are mostly in granite; the only wells mostly in basin fill are Acord-1, GPC-15 and RHS-335. The locations for all wells can be found on Figure 3. Productive wells tapping the Roosevelt hydrothermal system lie east of the Opal Mound fault with near-surface temperature profiles that follow boiling-point-for-depth conditions. The hydrothermal well profiles represent pre-development conditions; development of the reservoir has lowered these profiles by more than 300 m.

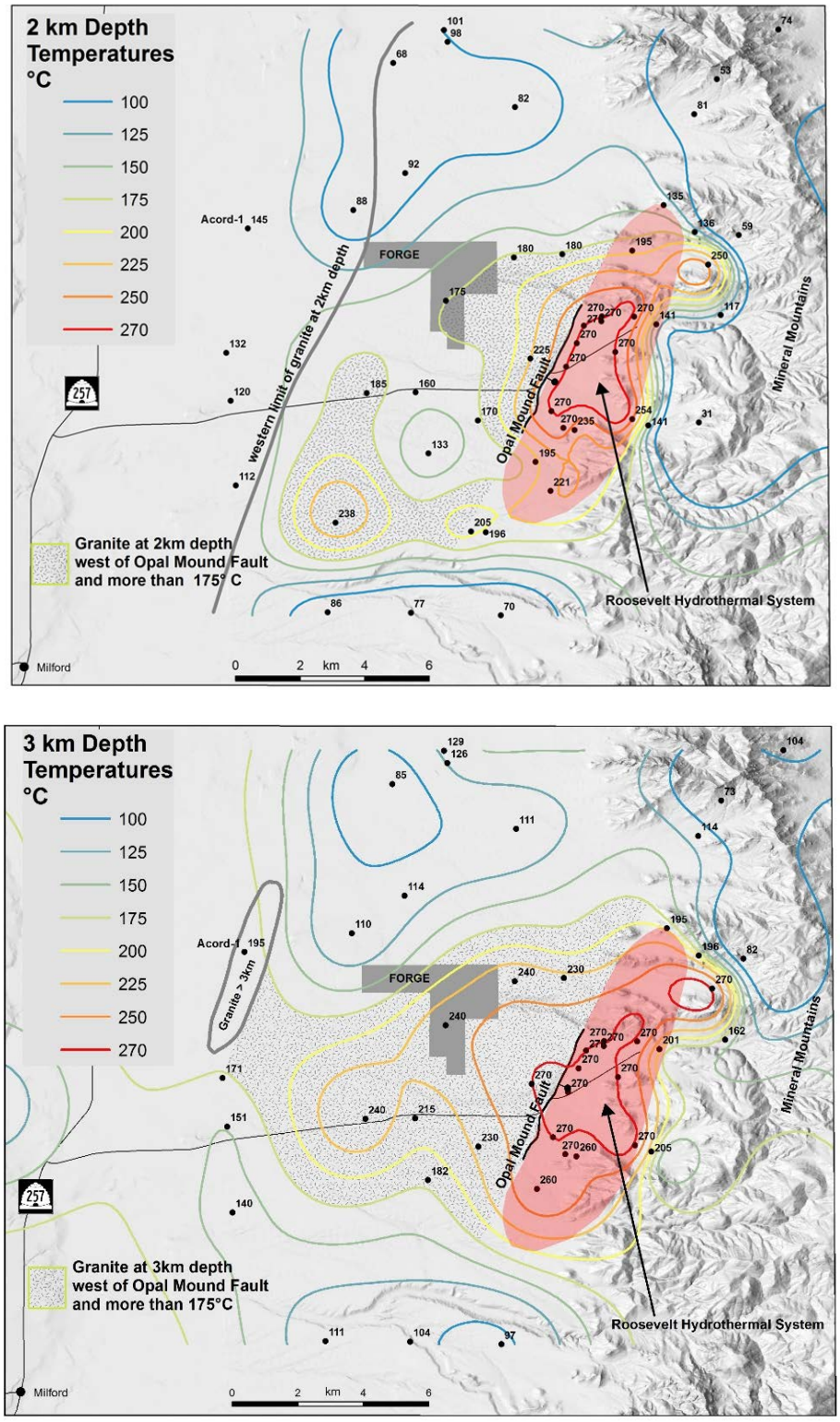

Figure 9. Contours of temperature at 2 and 3 km depth derived from observations in deep wells and geotherms fitted to thermal gradient wells. Temperature contours have been smoothed using kriging options in ESRI's ArcMap software, and typically have an uncertainty of ± 10°C depending on adjacent well data. The appropriate contour for the granite surface has been superimposed from Figure 4. The stipple highlights where granite at that depth is hotter than the minimum reservoir temperature constraint of 175ºC. On the 3 km map, granite hotter than 175ºC extends significantly west and north of Acord-1, but has not been shown because of poor well control.

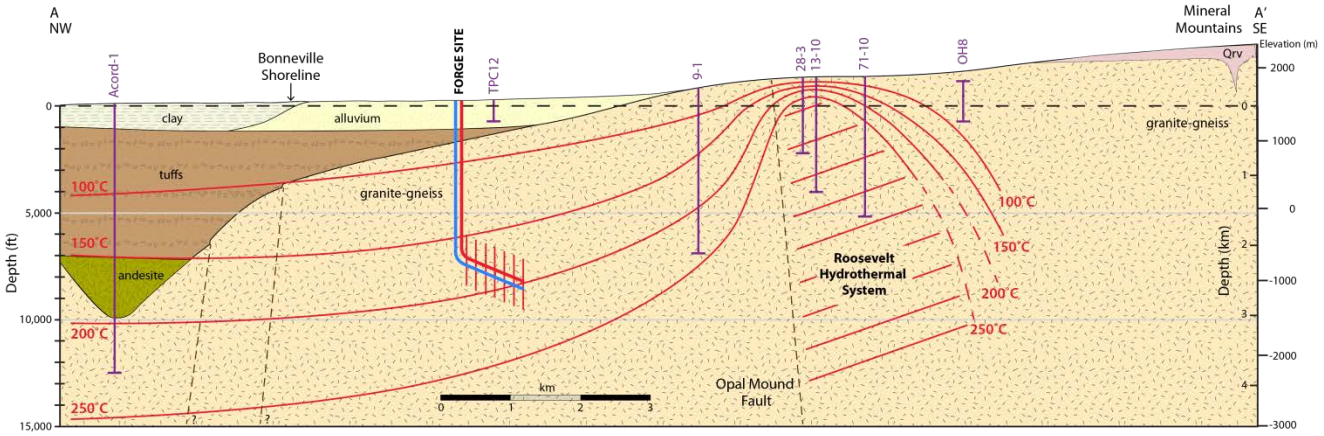

Figure 10. Cross-section showing granite with a temperature of more than 175°C extends at least 10 km west of the Opal Mound fault. The Roosevelt Hot Springs hydrothermal system appears to be about 2 km in width east of the Opal Mound fault. The zero datum for the depth axes is at 1525 m asl (5000 ft asl). The line of cross-section is shown on Figure 4. The isotherms between Acord-1 and the FORGE site cross the granite surface without major deflection because the change in heat flow compensates for the thermal conductivity contrast.

5. FLUID PRESSURE TRENDS

Deep wells east of the Opal Mound fault had a uniform pressure profile consistent with hot water with a density of 800 kg/m^3 prior to significant production (Allis and Larsen, 2012; Figure 11). The one deep well west of the Opal Mound fault with reliable pressure data, 82-33, had a pressure profile about 3 MPa lower than wells in the hydrothermal system. The primary pressure control point in 82-33 is at a major loss zone in granite at 600 m. The two pressure points in Faulder (1994) are consistent with cold water with a density of 1000 kg/m^3. The potentiometric head for 82-33 is at about 1600 m asl. This compares to the elevation of the Roosevelt Hot Spring at 1800 m asl, and the potentiometric head of the hydrothermal wells at about 1900 m asl.

There is one other intermediate-depth well west of the Opal Mound fault, GPC-15, with a water level at 165 m depth, implying a head at 1525 m asl (5000 ft asl; Glenn and Hulen, 1979). Several other shallower water wells on the alluvial fan and the central Milford Valley also show water levels of around 1500 m asl. When the information is compiled on a pressure-depth graph, two pressure trends are evident: the hydrothermal system trend east of the Opal Mound fault, and the rest of the Milford Valley west of the fault (Figure 11). There appears to be a major pressure boundary coinciding with the Opal Mound fault, with well 9-1 being unproductive but located on that boundary. This well was recommended by Los Alamos National Laboratory as a candidate for hot dry rock technology testing (Goff and Decker, 1983). PacifiCorp Energy currently has a pressure monitor in the well, and although unproductive, it now provides a long-term monitor of reservoir pressure trends in the hydrothermal system.

We anticipate that naturally fractured granite underlies the FORGE deep well site, and that it may have a pressure regime similar to that shown for the Milford basin west of the Opal Mound fault. For a reservoir centered at 2.5 km depth, the pressure should be at 23 MPa (3300 psi). Although no pressure measurements were recorded during the drilling of Acord-1, based on its depth and temperature profile, the bottom hole pressure should be about 35 MPa (5000 psi) assuming it is successfully cleaned out.

6. SEISMICITY AND STRESS DIRECTION

The University of Utah Seismograph Stations (UUSS) installed a seismic station (NMU) 3 km (2 mi) north of the RHS in 1987. Improved resolution of the station network occurred in 2009, and in late 2015, a three-component broadband seismometer was installed 3 km south of the RHS (UFOR, Figure 12) and incorporated into the network. The estimated minimum magnitude of complete recording for the study area is M 1.5 (Pankow *et al.*, 2004). The new station is expected to lower the detection threshold for future events in the FORGE area, and will allow for better understanding of source mechanisms. Preliminary analysis of the seismicity (occurring from 1988 - 2015) shows no events locate near the FORGE site and that seismicity rates are low in this region.

Seismic events in the UUSS catalog in the Milford region have been relocated using an improved velocity model. Two clusters of events are evident: one near Milford, and the second 10 km NW of Milford (Figure 12). More diffuse seismicity occurs beneath the Mineral Mountains. Waveform analysis and event timing indicates that events in the NW cluster (outlined by the blue ellipse in Figure 12) are the result of quarry blasts, from the quarry mines in the area, not tectonic earthquakes. Evidence for this conclusion includes the limited and small magnitudes (M 0.49 to 2.05), the shallow depths (above 2.5 km below sea level), the restricted timing (all events occur during daylight hours) (Figure 12), and the highly correlated waveforms implying a similar location and source mechanism. The second cluster outlined by the green ellipse (Figure 12) is located near the Milford airport and not far from the M_W 4.1 1908 Milford earthquake (the largest recorded earthquake in the study area). The magnitudes in this cluster range from 0.46 to 3.87, and the events occur throughout the day (without a time bias). This cluster is interpreted as tectonic in origin.

The direction of minimum horizontal stress (T-axis, or SHmin) based on the moment tensor from an M_W 3.8 earthquake (depth 6 km) is NW-SE (Whidden and Pankow, 2012). This is close to the extension direction inferred from structural development of the Milford basin mentioned earlier. Interestingly, the focal mechanism for this event is strike-slip. A compilation of evidence from borehole

breakouts from multi-arm caliper logs, the attitude of fractures, dikes and young normal faults all indicate the horizontal compressive stress (SHmax) is primarily directed N-S (170–180º) to NNE-SSW (035º) at Roosevelt Hot Springs.

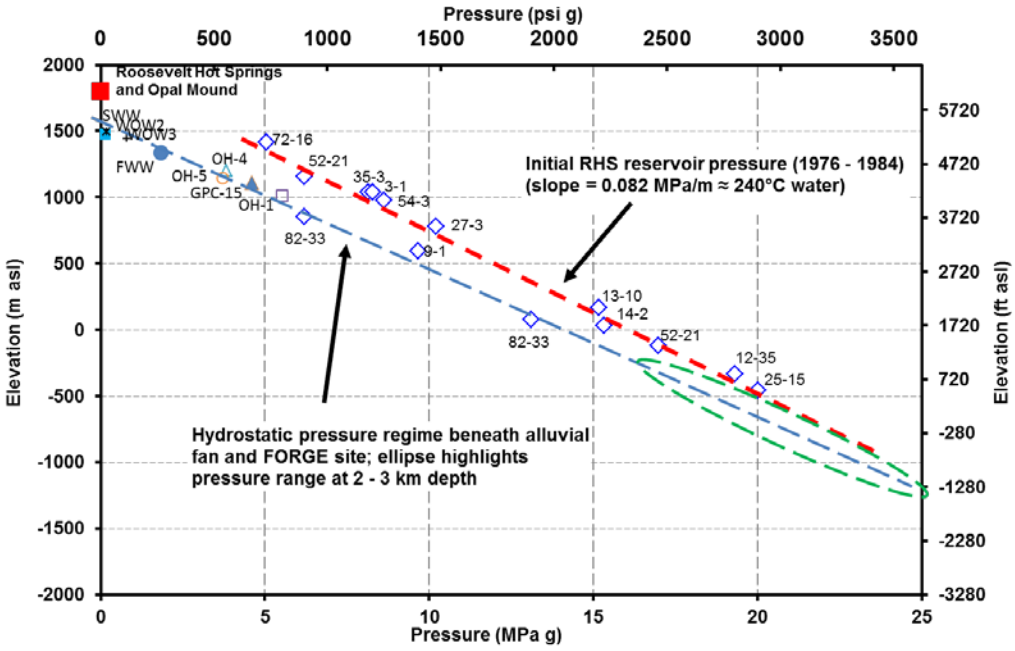

Figure 11. Pressure trends derived from wells in the Roosevelt Hydrothermal System, and in wells west of the Opal Mound fault. Pressure in the hydrothermal wells is from Faulder (1994) and represents pre-production conditions. The cold hydrostatic trend west of the fault is derived from groundwater wells and several geothermal exploration wells. Where no other data exists, the pressure control point is assumed to be at the mid-screen depth (elevation) or at total depth. Well locations are shown in Figure 3.

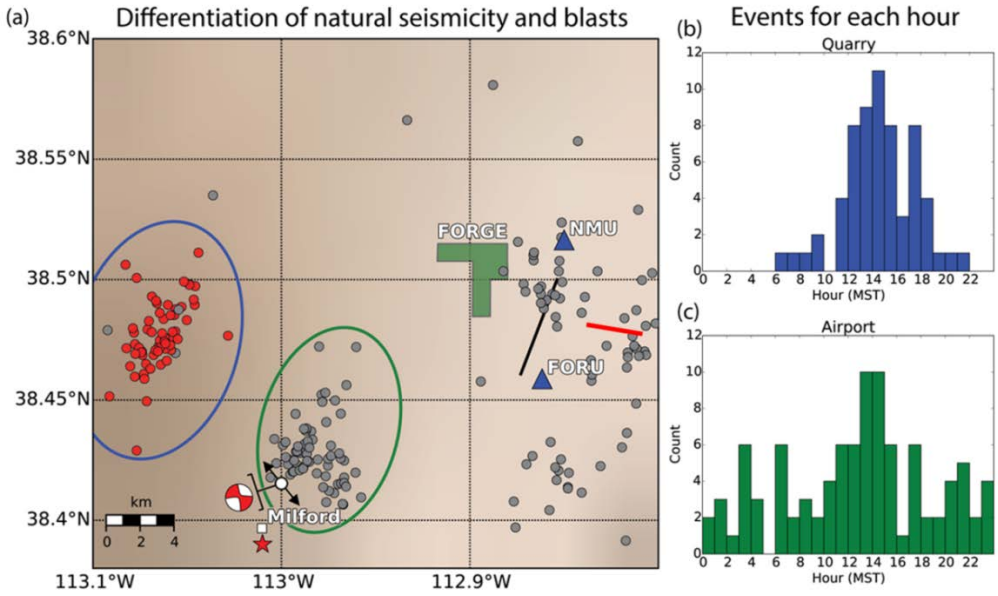

Figure 12 (a) Differentiation between natural seismic events and quarry blasts. Red and gray circles represent blasts and natural seismicity, respectively. The ellipses refer to the events within the histograms. The blue triangles are seismic stations; the green polygon represents the proposed FORGE area. The white square represents the center of Milford, UT and the red star is the epicenter of the 1908 earthquake, magnitude 4.1. The white circle represents the April 10, 1998M_W 3.8 earthquake with T-axis and focal mechanism (displayed offset from T-axis). The red line between NMU and FORU is the earthquake swarm detected by Zandt et al. (1982). This swarm was oriented approximately west-east. (b) shows the blasts as a function of time of day (these events occurring during daylight hours) and (c) shows that the natural seismicity occurs during all hours of the day. 62 of the 201 events displayed are blasts. Point data represents years 1965 – 2012.

6. CONCLUSIONS

The Milford FORGE site in central Utah offers an ideal field laboratory to develop next-generation technologies capable of generating geothermal power from tight crystalline rock. The site is easily accessible year round, with the local infrastructure 16 km away in Milford providing a comfortable base for visiting researchers. The preferred deep drilling location is a 5 km^2 area on non-federal land about 4 km from the hydrothermal system tapped by the Blundell power plants. Required temperatures of 175 to 225ºC exist at 2 - 3 km depth in granite, which occurs at 400 ± 200 m depth below the ground surface at the site. Groundwater rights for the project have been acquired, allowing use of over 600 million L (150 million gallons) for the duration of the project. Pump tests on a groundwater well near the proposed project office site 3 km from the deep well site demonstrate that two wells should be sufficient to supply water at the required rates. Groundwater in north Milford Valley is not potable and has not been extensively used because it has geothermal components that make it unsuitable for agriculture. The deep drill site is largely surrounded by BLM land. Environmental Impact Statements at neighboring wind, solar and transmission sites indicate no threatened or endangered species, and minimal risk of cultural/historic sites. Casual use permits for geophysical surveying around the deep well site during Phase 2 should also be straightforward. An unproductive, 3.8 km well (Acord-1), 5 km from the deep well site can likely cleaned out for testing tools up to temperatures of 230ºC and pressures up to 35 MPa (5000 psi).

The site is in an area of low natural seismicity. There has now been over 30 years of production of hot water and injection of cool water in deep wells tapping the adjacent Roosevelt Hydrothermal System. The circulation rates for most of the time has been in the range 250 - 300 L/s (Allis and Larsen, 2012), with no obvious induced seismicity. At the FORGE deep well site we anticipate the flow rate experiments to be carried out at about one tenth this rate, so the induced seismicity risk should be minimal.

Analysis of the extent of the low-permeability thermal anomaly adjacent to the Roosevelt Hot Springs hydrothermal system demonstrates why developing techniques to extract the heat is so important to future geothermal power development. The area of apparently tight rock with a temperature of over 150ºC could be about 100 km^2, and is more than 10 times the area of the hydrothermal system. The volume of this rock at less than 4 km depth is at least 100 km^3. The power potential here could be as high as 1 GW if this rock can be successfully fractured.

ACKNOWLEDGMENTS

Funding for this work was provided by DOE grants DE-EE0005128 and DE-EE0007080. We thank the many stakeholders who are supporting this project, including Smithfield, Utah School and Institutional Trust Lands Administration, Beaver County, and PacifiCorp Energy. The Bureau of Land Management and the Utah State Engineer's Office have been very helpful in guiding the project through the permitting processes. Jay Hill and John Good (UGS) assisted with many of the figures used in this paper.

REFERENCES

Allis R. G. and Larsen, G.: Roosevelt Hot Springs Geothermal field, Utah – reservoir response after more than 25 years of power production. *Proceedings*, 37th Workshop on Geothermal Reservoir Engineering, Stanford University, Stanford, CA, (2012).

Allis, R.G., Gwynn, M., Hardwick, C., Kirby, S., Moore, J., and Chapman, D.: Re-evaluation of the pre-development thermal regime of Roosevelt Hot Springs geothermal system, Utah. *Proceedings*, 40th Workshop on Geothermal Reservoir Engineering, Stanford University, Stanford, CA, (2015).

Boyd, L., Vagnetti, V., Metcalfe, E., Vandermeer, W., Porse, S., Henry, S., Frone, Z., and Tew, A.: The U.S. Department of Energy's Frontier Observatory for Research in Geothermal Energy (FORGE); New Directions in Subsurface Research and Development. *Proceedings*, 41st Workshop on Geothermal Reservoir Engineering, Stanford University, Stanford, CA, (2016).

Capuano, R., and Cole, D.R.: Fluid-mineral equilibria in a hydrothermal system, Roosevelt Hot Springs, Utah. *Geochimica et Cosmochemica Acta*, **46**, 1353–1364, (1982).

Faulder, D.D.: Long-term flow test #1, Roosevelt Hot Springs, Utah. *Transactions*, Geothermal Resources Council Transactions, **18**, 583–590, (1994).

Glenn, W, E., and Hulen, J.B.: Interpretation of well log data from four drill holes at Roosevelt Hot Springs KGRA. Univ. Utah Research Inst., Earth Science Lab. *Report* **28**, 74 p., (1979).

Goff F., and Decker, E.R.: Candidate sites for future hot dry rock development in the United States, *Jl. Volcanol. Geothermal. Research*, **15**, 187–221, (1983).

Hardwick C.L., Gwynn, M., Allis, R., Wannamaker, P., and Moore, J.: Geophysical Signatures of the Milford, Utah FORGE Site. *Proceedings*, 41st Workshop on Geothermal Reservoir Engineering, Stanford University, Stanford, CA, (2016).

Moore, J.N. and Nielson, D.L.: An overview of the geology and geochemistry of the Roosevelt Hot Springs geothermal system, Utah. *Utah Geological Association Publication*, **23**, 25–36, (1994).

Pankow, K. L., Arabasz, W.J., Nava, S.J., and Pechmann, J.C.: Triggered seismicity in Utah from the 3 November 2002 Denali fault earthquake, *Bull. Seism. Soc. Am*. **94**, S332–S347, (2004).

Robinson, R. and Iyer. H.M.: Delineation of a low-velocity body under the Roosevelt Hot Springs geothermal area, Utah, using teleseismic P-wave data, *Geophysics*, **46**, 1456-1466, (1981).

Ross, H.P., Nielson, D.L., Moore, J.N.: Roosevelt Hot Springs geothermal system, Utah – case study. *Amer. Assoc. Petroleum Geologists*, **66**, 879–902, (1982).

Shannon S.S., Goff, F., Rowley, J.C., Pettitt, R.A., Vituaz, F.D.: Roosevelt Hot Springs/Hot Dry Rock prospect and evaluation of the Acord 1-26 well. *Transactions*, Geothermal Resources Council, **7**, 541–544, (1983).

Simmons, S., Kirby, S., Jones, C., Moore, J., and Allis, R.: The Geology, Geochemistry, and Hydrology of the EGS FORGE Site, Milford Utah. *Proceedings*, 41st Workshop on Geothermal Reservoir Engineering, Stanford University, Stanford, CA, (2016).

Ward, S.H., Parry, W.R., Nash, W.P., Sill, W.R., Cook, K.L., Smith, R.B., Chapman, D.S., Brown, F.H., Whelan, J.A., and Bowman, J.R.: A summary of the geology, geochemistry, and geophysics of the Roosevelt Hot Springs thermal area, Utah. *Geophysics*, **43**, 1515–1542, (1978).

Whidden K.M. and Pankow, K.R.: A catalog of Regional Moment Tensors in Utah from 1998 to 2011, *Seismological Research Letters*, **83**, p. 775–783. doi: 10.1785/0220120046, (2012).

Zandt, G., McPherson, L., Schaff, S., and Olsen, S.: Seismic baseline and induction studies: Roosevelt Hot Springs, Utah, and Raft River, Idaho, U.S. Dept. of Energy Report DOE/ID/01821-T1, 58 pp., (1982).

APPENDIX 1.1B

Triaxial Compression and Permeability

Triaxial Compression:

Six samples were evaluated in unconfined and triaxial compression. The triaxial loading frame is shown in Figure 1. Figure 2 shows a sample and affiliated instrumentation for measuring axial force as well as strains (axial and in two radial orthogonal directions. Three samples were plugged along the axis of the core (presumed to be nominally vertical) and three samples were plugged perpendicular to the axis of the core. A designation of "V" indicates vertical or the long axis of the plugged sample is aligned with the axis of the core. Similarly, "H" indicates a sample that is nominally horizontal and cut orthogonal to the axis of the core.

Figure 1: Triaxial compression loading frame use to measure the mechanical properties described subsequently.

Stress-strain curves and photographs from before and after the testing are included in Appendix A. Measurements were made under three confining pressure conditions (0, 2800 and 8000 psi). Typical data are shown in Figures 3 and for Sample GNS-1H. The confining pressure for this test was 2800 psi. A series of tests are being carried out on to define a failure envelope, to provide representative hydraulic fracture design parameters and for future geomechanical assessments. Figure 3 shows the 1.5-inch nominal diameter sample before and after triaxial testing. Figure 4 shows the stress strain data for this sample, indicating that this is an ideal and representative reservoir for effectively testing drilling, stimulation and production protocols in an environment that embodies strong, crystalline rock.

Figure 2: The left hand panel shows a sample encapsulated in a shrink-fit Teflon jacket to prevent penetration of confining fluid. These measurements were made at ambient temperature. Also visible are cantilever devices to determine average axial strain and radial strain in two orthogonal directions. The panel at right shows the same sample configuration mounted on a base plug and a load cell, immediately before being raised into the confining pressure vessel (at top of photograph) prior to testing.

The triaxial compression data are summarized in Table 1. Acoustic measurements have also been made and dynamic values of Young's Modulus and Poisson's ratio are being determined.[1]

Table 1: Summary of Triaxial Compression Testing

Sample	Depth (ft)	Confining Pressure (psi)	Compressive Strength (psi)	Residual Strength (psi)	Young's Modulus (10^6 psi)	Poisson's Ratio
1-H		2800	59,400	55,400	10.49	0.21
2-H		8000	90,000	-	10.70	0.22
4-H		0	27,000	-	7.94	0.12
5-V		2800	61,200	51,500	9.49	0.24
6-V		8000	90,400	82,400	10.50	0.25
7-V		0	29,100	-	7.36	0.18

The data show no obvious directional dependency for any of the measured mechanical properties. This is further evident from the Mohr's failure envelopes shown in Figures 5 and 6.

[1] The data are being analyzed further and the values for Young's Modulus and Poisson's ratio could change slightly.

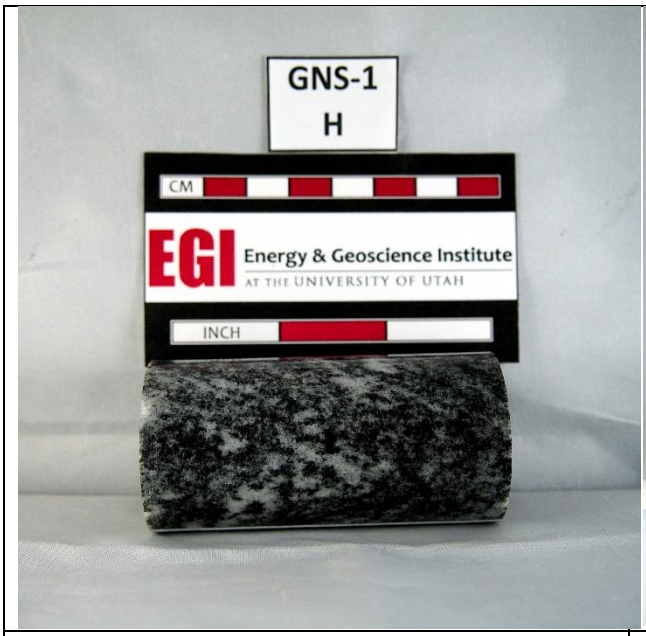

Figure 3a. This is a pre-test view of sample GNS-1H. The H designates an orientation normal to the axis of the core (horizontal).

Figure 3b. This is a post-test view of sample GNS-1H. The H designates an orientation normal to the axis of the core (horizontal).

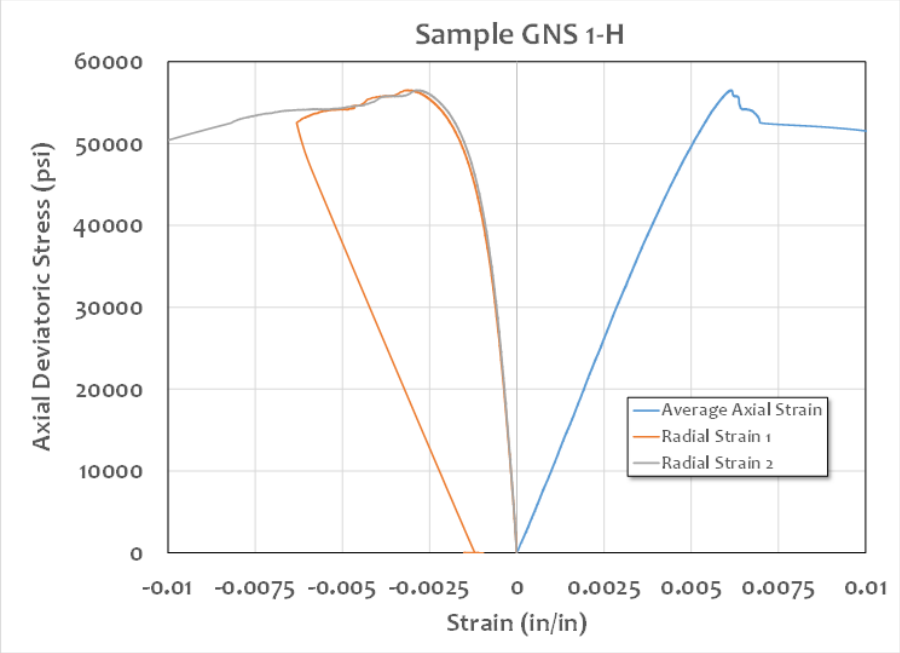

Figure 4. Axial and radial strain recorded as a function of the axial deviatoric stress (axial stress minus confining pressure). The sample failed at an axial deviatoric stress of approximately 56,000 psig. Young's modulus, Poisson's ratio and compressive strength are among the properties that are determined.

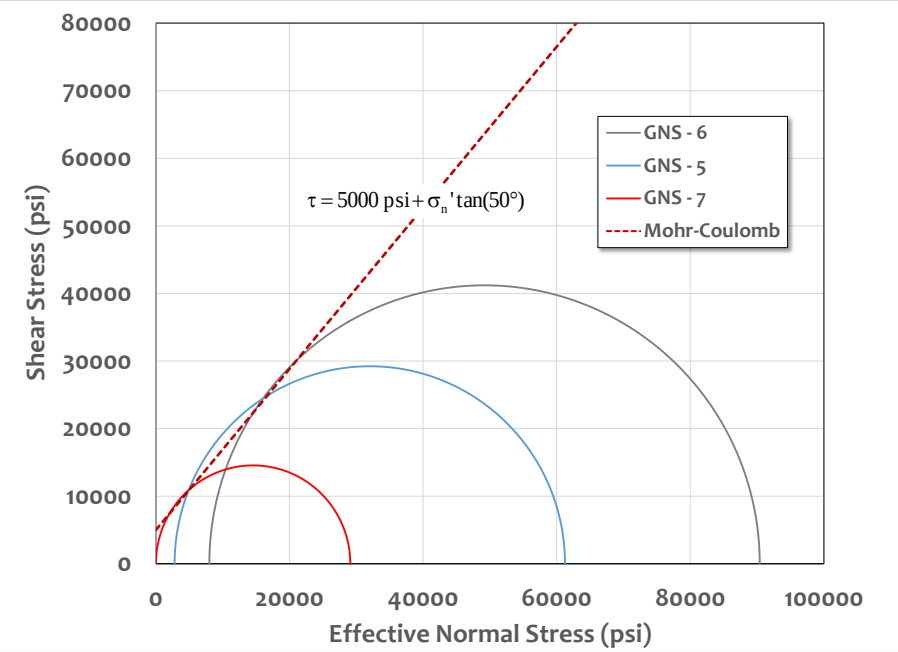

Figure 5. Mohr-Coulomb Failure envelope for vertically oriented samples.

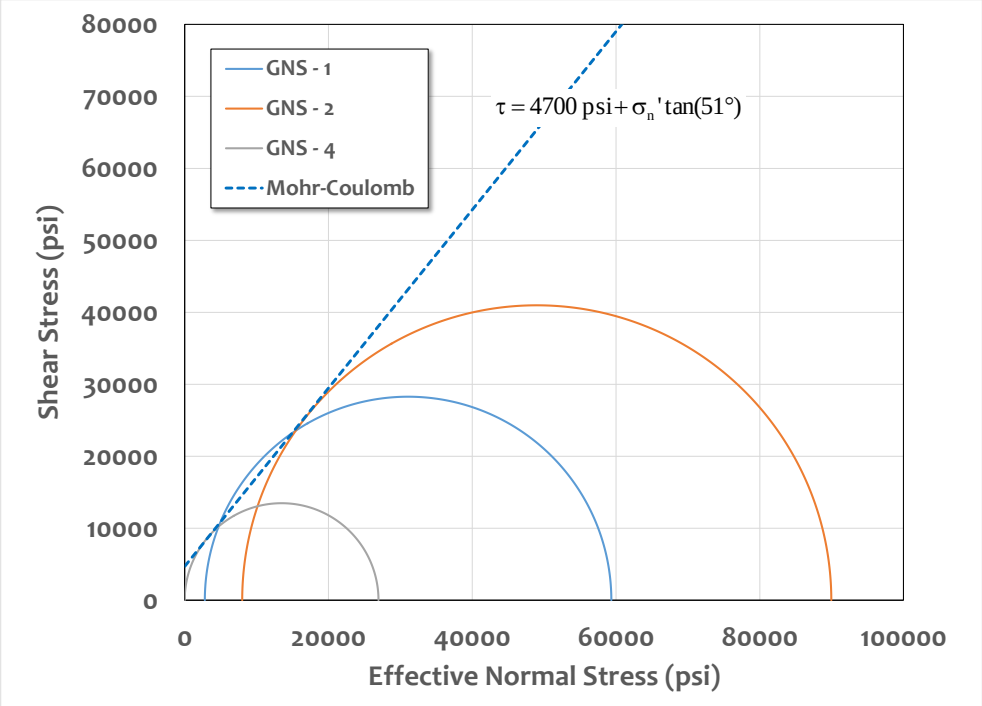

Figure 6. Mohr-Coulomb Failure envelope for horizontally oriented samples.

Permeability and Porosity:

Porosity was measured on Sample GNS 3-H. The porosity and bulk density measured were:

Porosity 0.13%

Bulk Density ..... 2623 kg/m^3

Absolute permeability to water was determined using the apparatus shown in Figure 7. The testing chronology is shown in Figure 8, suggesting for this sample, a relatively high permeability of 0.3± microdarcies (300 nanodarcies), at a confining pressure of 2800 psi. This permeability is attributed to partially healed microcracks evident visually.

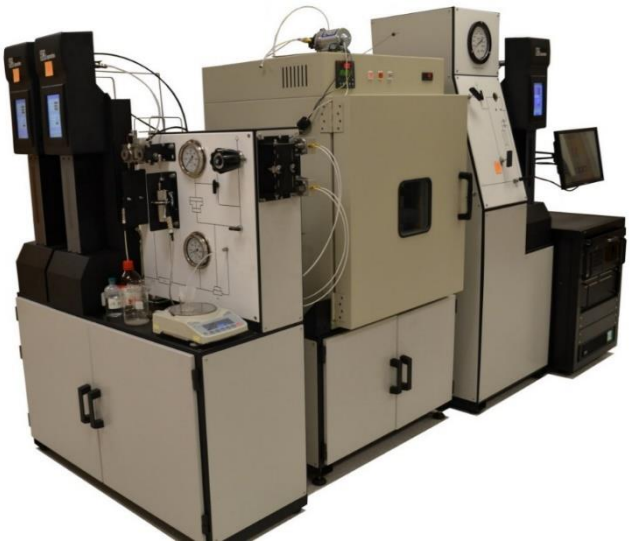

Figure 7. Permeability apparatus for steady state (one- or two-phase) liquid permeability measurements.

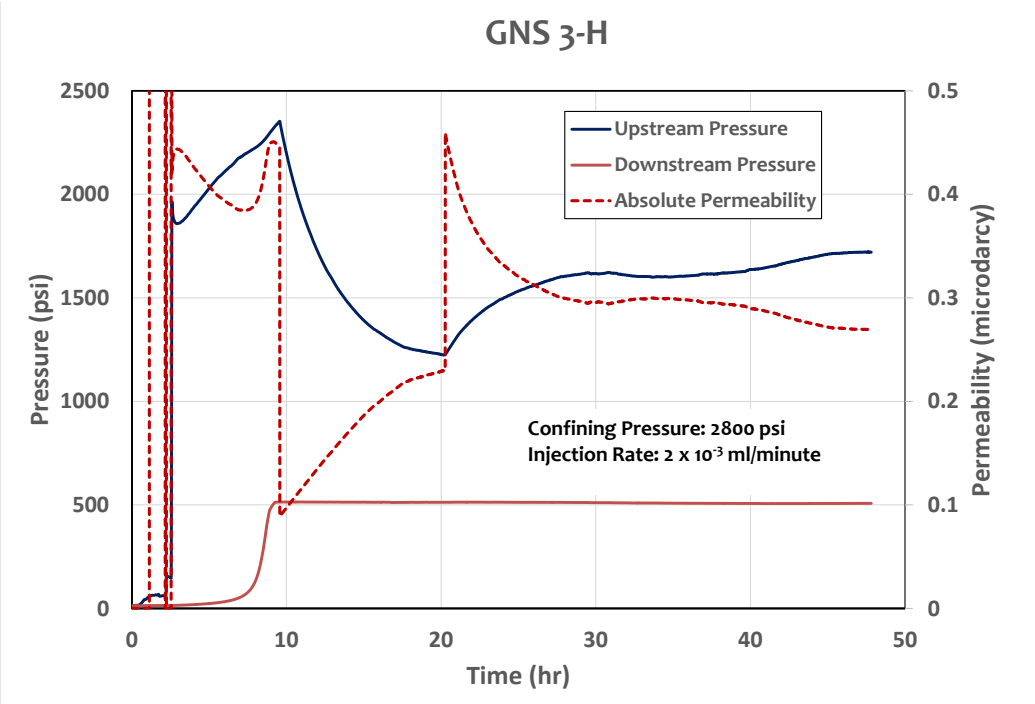

Figure 8. Upstream and downstream pressure and absolute permeability (ambient temperature) a 500 psi backpressure and a flow rate of 0.002 ml/minute

Sample GNS 1-H

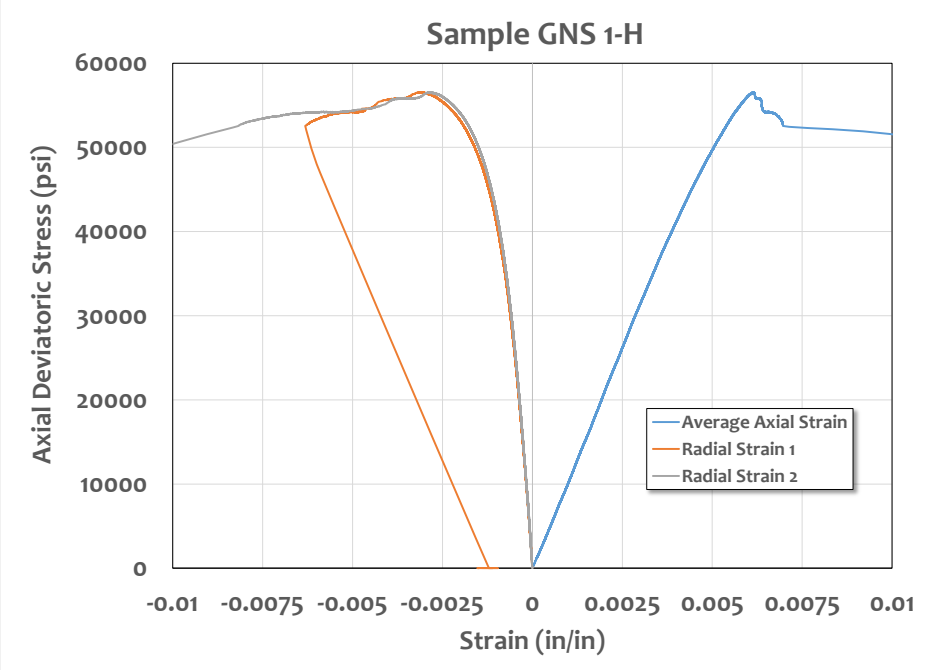

Pre-Testing	Post-Testing
	

Pre-Testing	Post-Testing
	

Sample GNS 2-H

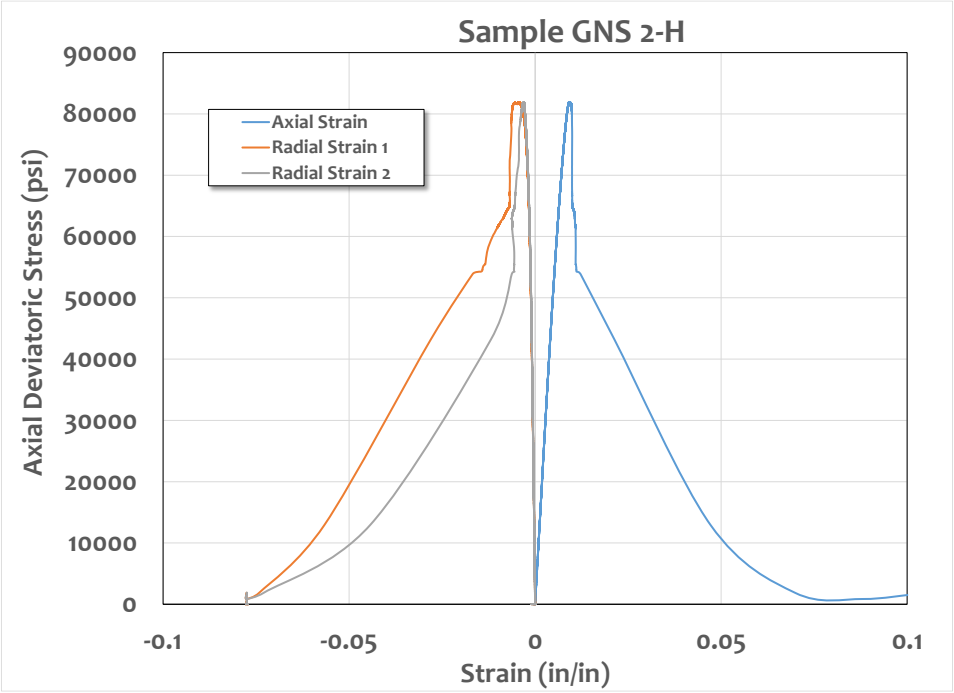

Pre-Testing	Post-Testing
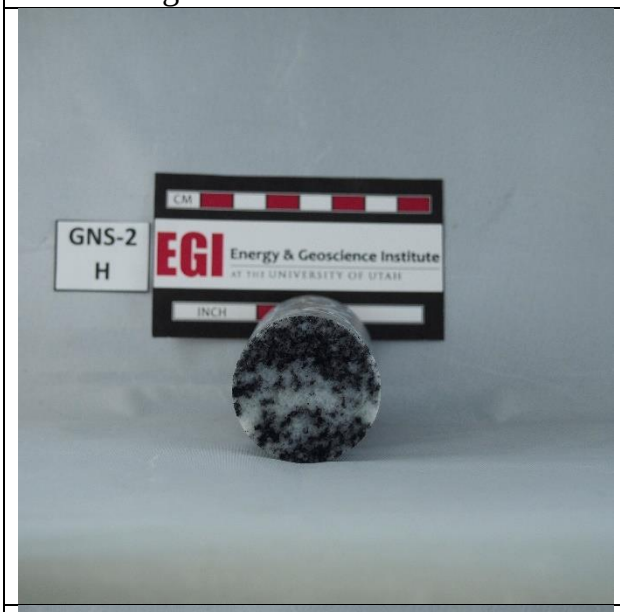	
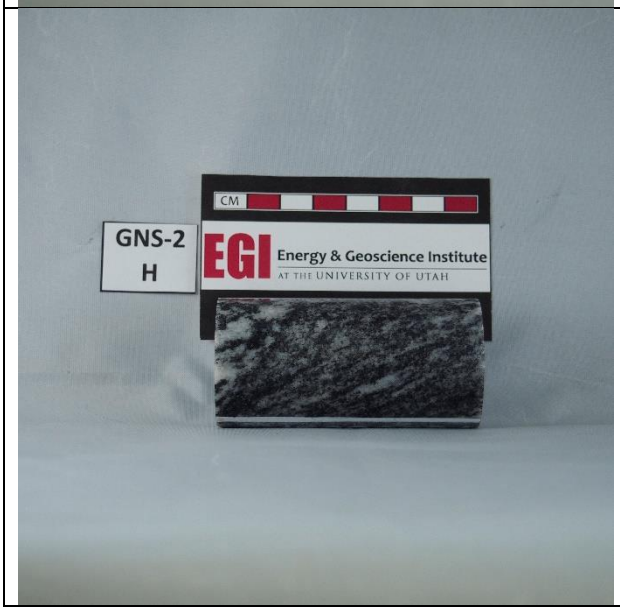	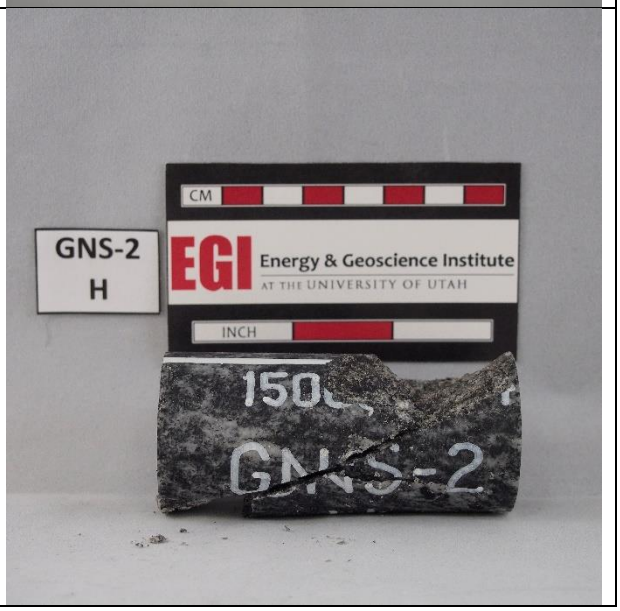

Sample GNS 4-H

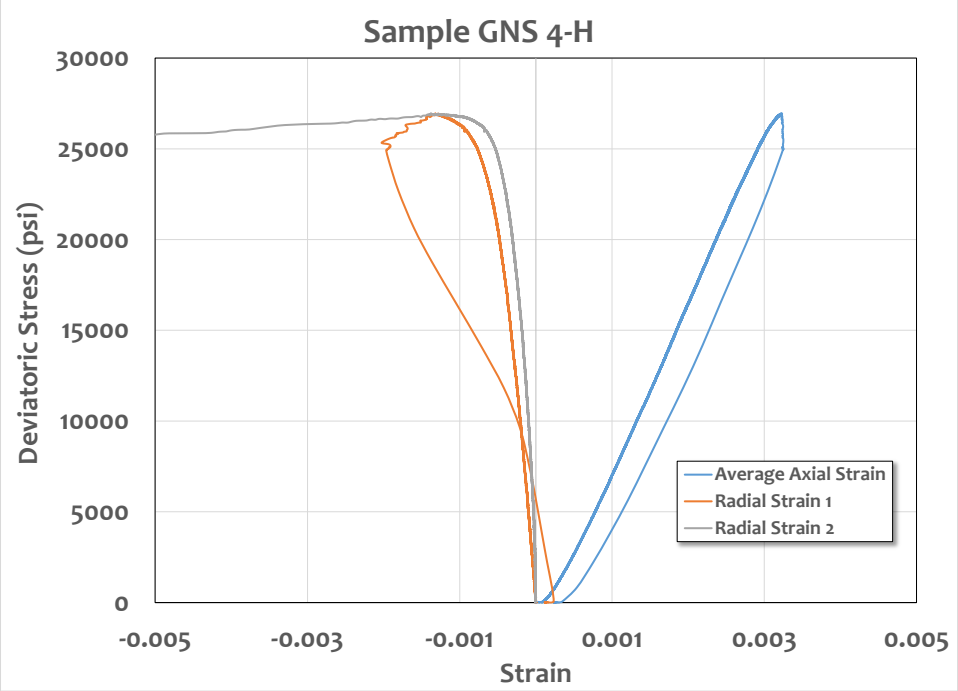

Pre-Testing	Post-Testing
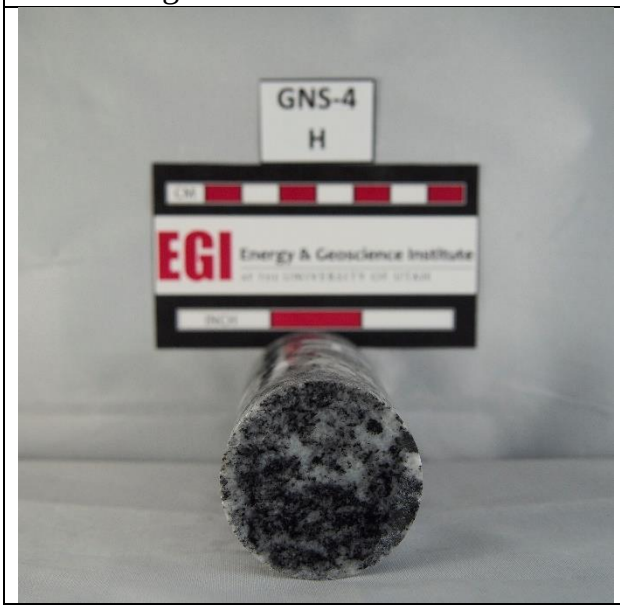	

Pre-Testing	Post-Testing
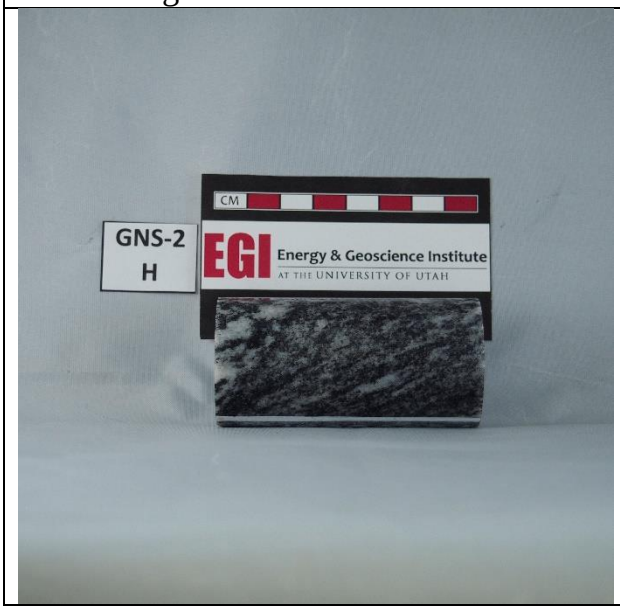	

Sample GNS 5-V

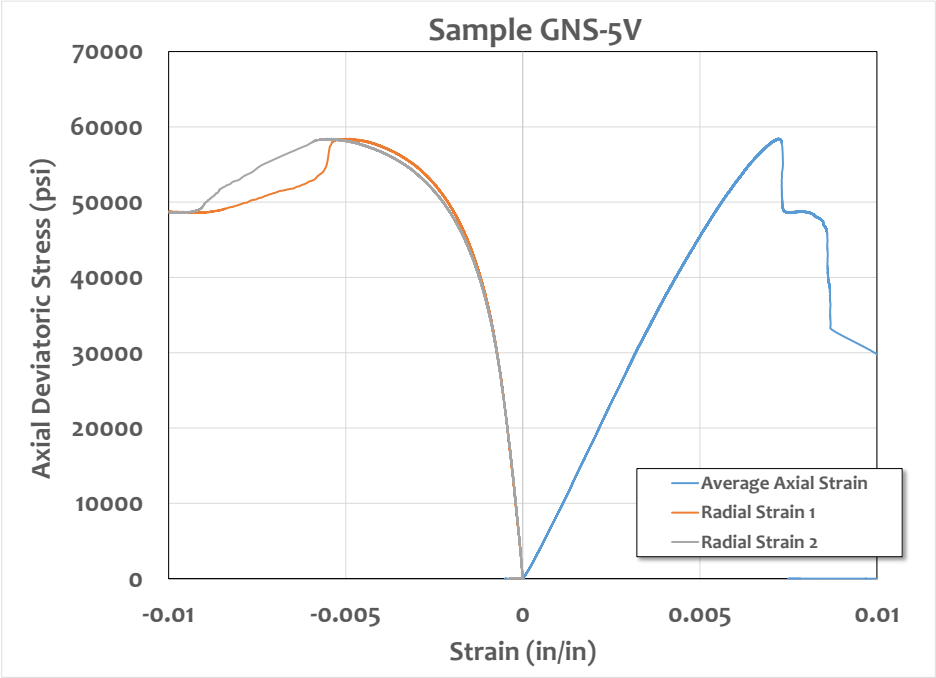

Pre-Testing	Post-Testing
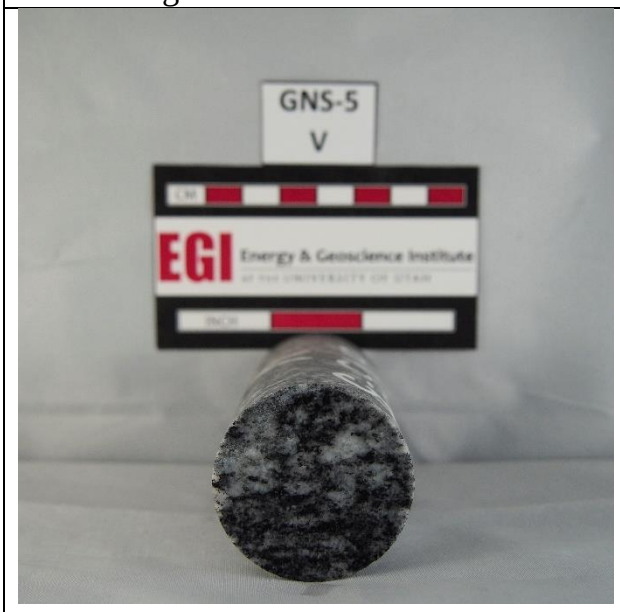	
	

Sample GNS 6-V

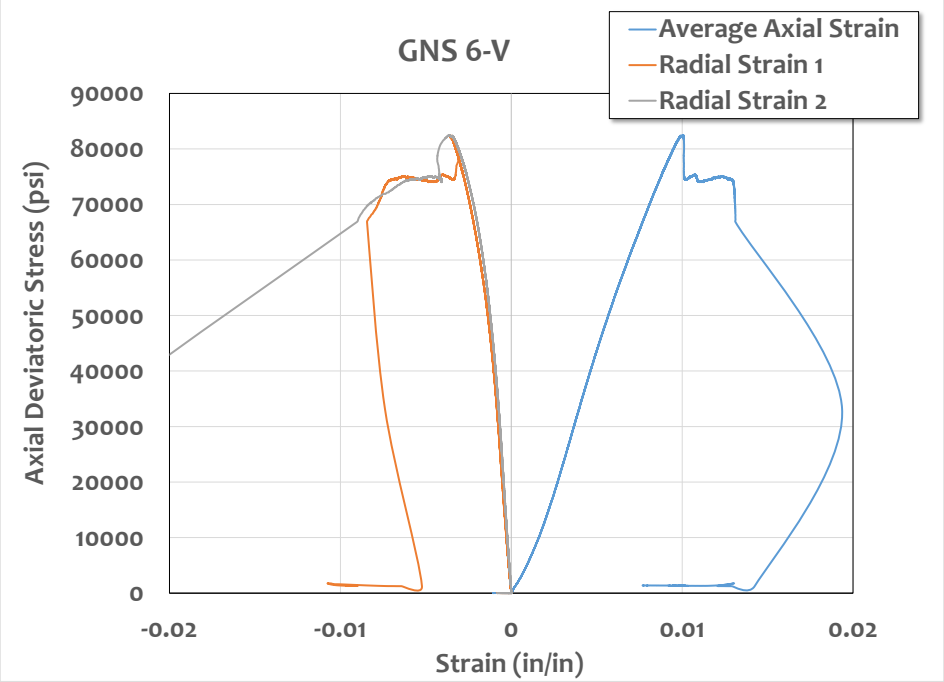

Pre-Testing	Post-Testing
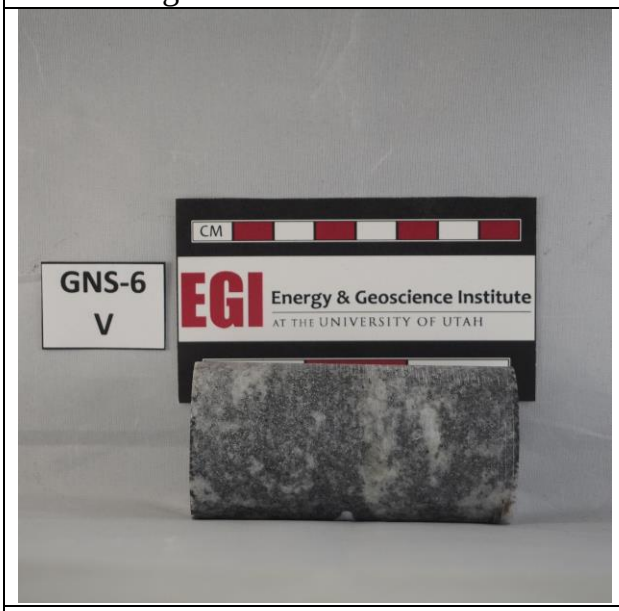	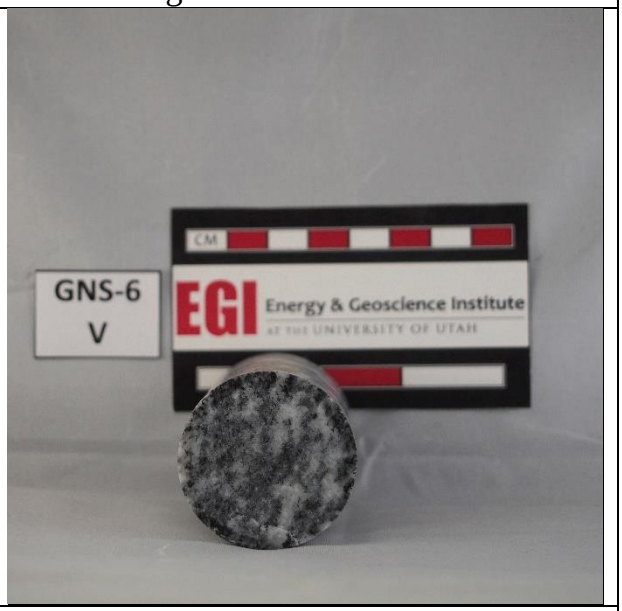

Sample GNS 7-V

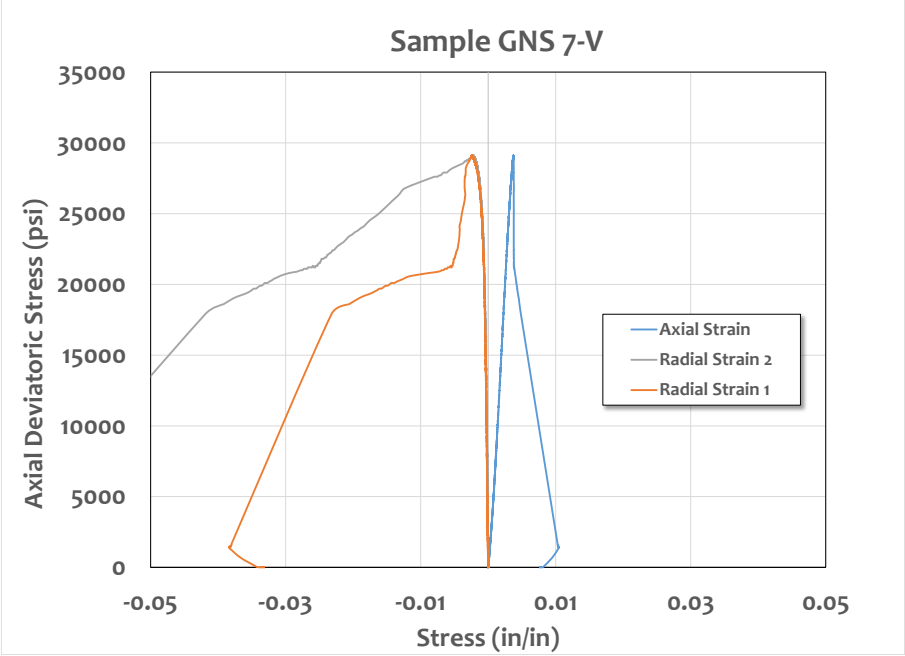

Pre-Testing	Post-Testing
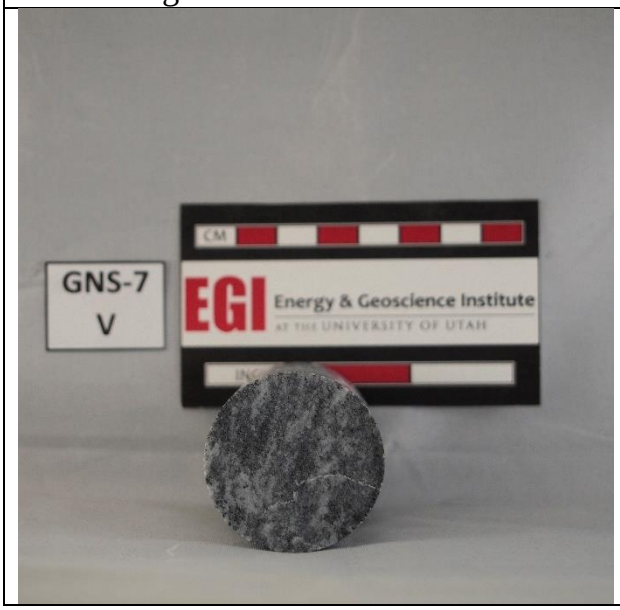	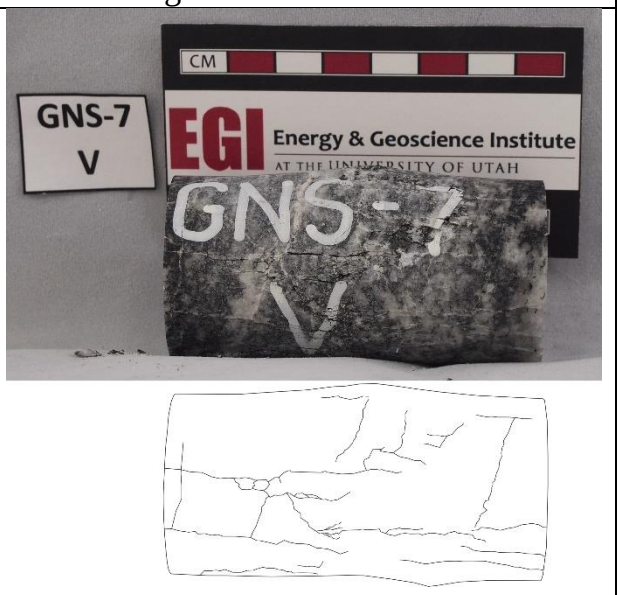

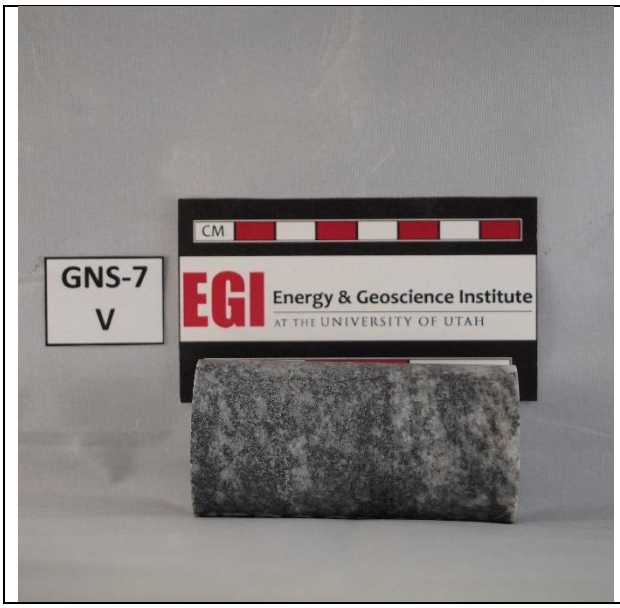
GNS-7
V
CM
EGI
Energy & Geoscience Institute
AT THE UNIVERSITY OF UTAH


1500023